Title
The Regulation of Pre-mRNA Splicing in Response to Environmental Stress in Budding Yeast

Author
Bergkessel, Megan

Publication Date
2010

Peer reviewed|Thesis/dissertation

The Regulation of Pre-mRNA Splicing in Response to Environmental Stress in Budding Yeast

by

Megan Bergkessel

DISSERTATION

Submitted in partial satisfaction of the requirements for the degree of

DOCTOR OF PHILOSOPHY

in

Biochemistry and Molecular Biology

in the

GRADUATE DIVISION

of the

UNIVERSITY OF CALIFORNIA, SAN FRANCISCO

Acknowledgments

The work described here is the product of a graduate school adventure that has been occasionally very uncertain and occasionally very difficult, but mostly just fascinating and fun, and I have many people to thank for helping to make it that way. Firstly, I never thank Christine Guthrie enough for being such an ideal mentor in so many ways. I really respect and appreciate the way in which she approaches science. I enjoyed having her support in pursuing the questions I found interesting, even when it wasn't clear where those paths would lead, and her knowledge and insight were impressive and helpful. I also learned a lot about the communication of science. But perhaps most of all, I deeply respect and appreciate her ability to lead a group of amazing individuals who all in a way that fosters community – the Guthrie lab has been the most amazing work environment imaginable for all of my time in graduate school, even though it has been composed of different individuals at different times.

Several of those individuals have been extremely close collaborators and friends. Jeff Pleiss and Gregg Whitworth developed the splicing microarray technique which was the basis for much of the work described here. Gregg in particular has been a close collaborator on the work described in the first three chapters, and also a close friend. I can't thank him enough – his rare gift for both computer programming and biological insight make him an incredible collaborator for large microarray studies such as the ones described here. More importantly, his friendship has been an invaluable source of support during the most difficult and uncertain times. Gwen Wilmes was also a close

collaborator on much of the work described here. Gwen's meticulous attention to detail and unique sense of humor were both much appreciated.

Many other graduate students and post-docs have contributed greatly to making the Guthrie lab the amazing place that it is. Wendy Gilbert has been a close friend and an inspiration to me throughout grad school, even though we only overlapped in the lab for less than a year. Her intelligence and drive are amazing, and I excited to see what fascinating discoveries she will make as she continues in her career. We have shared many adventures together, both scientific and outdoors, and I hope we will share more in the future. Maki Inada's positive outlook and warm smile and laugh are a source of inspiration to me. Tamara Brenner and Alex Plocik were great lab mates, and I particularly appreciate Alex's help with strain construction for the intron swap strains described in chapter 4. I love the energy and enthusiasm of Bellos Hadjivasiliou. Finally, Erica Moehle and Argenta Price were a pleasure to have as rotation students in the lab, and I couldn't have been more pleased when they decided to join. It will be fun to see where their fascinating projects go!

The post-docs in the Guthrie lab have also been really great people to work with. Alan Kutach's hard work and generosity was much appreciated, and Tommaso Villa and Pascal Preker were fun and interesting people to have around. Tracy Kress, Quinn Mitrovich, Corina Maeder, Rebecca Holmes, and Sarah Ledoux have all contributed greatly to the exciting intellectual environment and the friendly community of the lab, and I will miss them! I appreciate Jaci Greimann's brave willingness to take on some

unfinished aspects of this work, and take the project in new and exciting directions. I wish her the best of luck and I can't imagine a more capable person to whom to hand off this torch! Finally, I want to thank John Abelson and Anne de Bruyn-Kops for their contributions to the lab dynamic – it's been really amazing having John's depth of knowledge and enthusiasm at group meetings and in my bay, and I appreciated all Anne does to keep things running smoothly.

My committee members, Joe DeRisi and Peter Walter, have been very helpful. I have appreciated their insight and good suggestions, and also technical assistance. I also really enjoyed collaborating with Nevan Krogan, and appreciate his encyclopedic knowledge of yeast genes, and his willingness to share that knowledge. I appreciated the generosity of Rob Singer in allowing me to come to his lab for a week to learn more about single molecule FISH.

Outside the lab, several of my classmates have been close friends. I have had the pleasure of being roommates and/or co-conspirators in adventure with Jenny Shock, Julia Kardon, Niels Bradshaw, and Brad Zuchero, and I hope these adventures will be the seeds of lifelong friendship.

As a parallel adventure to my scientific one throughout grad school, climbing has been a great source of friendships and community for me as well. Sarah Elson, Stephanie Dohar, Aaron Hernday, Clarissa Nobile, Phyllis Ponte, Molly Martin, Sean O'Toole, Sam McGeehan, and Scott Johnston have all been great friends and a huge source of moral support.

Most importantly, I met my wonderful boyfriend Phil Esra through climbing, and I can't thank him enough for all his love and support, especially through the insanity of the last few months of finishing up. Whether it was by bringing dinners to me or copy-editing manuscripts or helping me move out of my apartment, he has risen far above and beyond the call of duty, and he has kept my spirits up when things have been difficult. We have shared lots of great adventures, and we look forward to sharing many more!

Finally, I want to thank my family – my parents Marge and Ernie and my sister Kelly – for their unconditional love and support. My parents have always supported and encouraged me in everything I have done, and my sister has been a great partner in many adventures, and a great friend. Their love has meant more to me than I can express in words, and I really thank them for it.

Published Work

Introduction

Figure 1 in the Introduction was previously published as referenced below, and was done in collaboration with Gwen Wilmes.

Bergkessel M, Wilmes GM, Guthrie C (2009) SnapShot: Formation of mRNPs. Cell 136: 794, 794.e1.

Chapter 1

Chapter 1 was previously published as referenced below, and was work done in collaboration with Jeff Pleiss and Gregg Whitworth.

Pleiss JA, Whitworth GB, Bergkessel M, Guthrie C (2007) Rapid, transcript-specific changes in splicing in response to environmental stress. Mol Cell 27: 928-937.

Chapter 2

Chapter 2 was previously published as referenced below, and was done in collaboration with Gwen Wilmes, Gregg Whitworth, and Tracy Kress; and Nevan Krogan's, Jonathan Weissman's and Trey Ideker's laboratories

Wilmes GM, Bergkessel M, Bandyopadhyay S, Shales M, Braberg H et al. (2008) A genetic interaction map of RNA-processing factors reveals links between Sem1/Dss1-containing complexes and mRNA export and splicing. Mol Cell 32: 735-746.

Unpublished Work

Chapter 3

Chapter 3 has been submitted to PLoS Biology, and was done in collaboration with Gregg Whitworth.

Chapter 4

The work described in chapter 4 is being carried on by Jaclyn Greimann, and is being prepared for publication.

Appendix 1

Appendix 1 describes various genetic results, which are included in case of future usefulness.

Appendix 2

Appendix 2 contains cover art for the journal issues in which chapters 1 and 2 were published.

Abstract

Cells must respond to a wide range of external stimuli by altering their gene expression programs. The contribution to these responses of changes to transcription initiation has been studied extensively, but subsequent mRNA processing steps can also be regulated. In this work, we have investigated the potential for regulation at the level of pre-mRNA splicing. We found that the pre-mRNAs for a majority of the ribosomal protein genes (RPGs) rapidly accumulated in response to amino acid starvation. By contrast, most RPG pre-mRNAs were rapidly degraded by the nuclear exosome in response to a variety of stresses that inactivated TORC1. These responses required casein kinase 2. In the case of amino acid starvation, the native promoter of an RPG, but not its native intron, was also required for the response. This suggested that the mechanism of splicing inhibition following amino acid starvation involved modulation of the co-transcriptional dynamics of spliceosome recruitment. Consistent with this model, we found that the inhibition of pre-mRNA splicing was accompanied by a rapid accumulation of both U1 snRNP and RNA polymerase II at the 3' ends of many ribosomal protein genes, suggesting that U1 release was inhibited. This inhibition of U1 release was insufficient to fully commit the RPG pre-mRNAs to eventual splicing however, as single molecule RNA FISH revealed that the accumulating pre-mRNAs localized to the cytoplasm during amino acid starvation. These results suggested a high degree of interaction among transcription, splicing, 3' end processing, and mRNA export, and we carried out a high throughput genetic screen to identify interactions among factors and complexes involved in mRNA processing. This screen revealed previously unknown

connections between a proteasome component (Sem1) and mRNA export, and between a component of the COP9 signalosome and pre-mRNA splicing. We hope this dataset will also continue to be useful as we and others continue efforts to elucidate the interconnected regulatory mechanisms that contribute to control of gene expression at the level of mRNA processing.

Table of Contents

List of Tables

Chapter 4

Appendix 1

List of Figures

Introduction

Chapter 1

Chapter 2

Introduction

Post-transcriptional Regulation of Gene Expression

The post-transcriptional processing that occurs to every mRNA transcribed in a eukaryotic cell is absolutely critical in order for the message to be usable by the cell, and extremely complex (Fig.1). Presumably all this complexity affords opportunities to fine-tune regulation of gene expression to the extent that is needed in a system as exquisitely robust, responsive, and adaptable as even the simplest eukaryote. Indeed, hundreds of examples of post-transcriptional regulation have been described, but it seems that these findings barely scratch the surface in their progress toward a deep and comprehensive understanding of how post-transcriptional processing is integrated into the regulation of gene expression. This project arose from a desire to better understand not only the mechanisms that control one of these processing steps, pre-mRNA splicing, but also the cellular and evolutionary context for this complexity. In other words, I wished to gain some insight not only into how splicing is controlled, but why it exists in the way that it does.

Splicing is a ubiquitous and highly conserved process throughout the eukaryotic kingdom. In higher eukaryotes, nearly every gene is spliced, and the presence of multiple introns in most genes means that alternative splicing of the exons in a single gene can lead to multiple protein products. The high potential for splicing to contribute to both the regulation and diversity of protein production seems clear in this system, and there are many examples of perturbations of splicing leading to disease states. In the budding yeast *Saccharomyces cerevisiae,* on the other hand, introns have been retained in only about 5% of the genes, and nearly all of these genes contain only a single intron. The bias of the distribution of introns in the *S. cerevisiae* genome – more

than one third of them are found in ribosomal protein genes (RPGs), and more than two thirds of ribosomal protein genes contain introns – suggested that an important function of splicing in this organism might be contributing to the regulation of this extremely highly expressed and tightly regulated group of transcripts.

Asking the question of whether splicing could contribute to the regulation of a large group of transcripts required the ability to simultaneously assay the splicing efficiency for each member of that large group of transcripts. In this respect, the simplicity of the *Saccharomyces cerevisiae* genome with respect to splicing was a major advantage. The small number of intron-containing genes and the lack of alternative splicing meant that microarray probes could be designed to specifically detect pre-mRNA using a probe to the intron, mature mRNA using a probe to the splice junction, and total mRNA using a probe to the second exon, for each intron containing gene. Relative splicing efficiency between two mutants or conditions could then be estimated by comparing the relative changes for each probe type for each intron containing gene.

Investigating the contribution of splicing to the regulation of RPG expression also required finding a condition in which splicing of the RPGs changed in a detectable way. Again, the use of *Saccharomyces cerevisiae* as a model organism for this question provided many advantages. A rich literature of responses to environmental stresses showed that expression of the RPGs changed in many stresses, thus providing many opportunities to ask whether regulation at the level of splicing contributed to regulation of RPG expression in many different contexts.

While the question of how splicing might contribute to the regulation of ribosomal protein gene expression was interesting in its own right, we also hoped that studying this question might offer a unique perspective into the underlying architecture of the transcription and splicing system. We hoped that pushing the system to change might offer insight into how the system is put together in the first place. The mechanisms by which transcription and splicing are coordinated are still poorly understood, and observing different coordinated behaviors in different stress conditions has allowed us to begin to understand some of the range of dynamic interactions that are possible.

The dynamic and complex nature of the interaction between the spliceosome and a pre-mRNA substrate affords nearly limitless potential opportunities for regulation. The spliceosome is not a static enzymatic complex, but rather assembles dynamically on each pre-mRNA substrate via a stepwise assembly of spliceosomal sub-complexes (Staley & Guthrie, 1998; Wahl *et al.*, 2009). Following recruitment of five snRNP complexes, massive rearrangements of the RNA and protein interactions within the megadalton complex lead to formation of the active spliceosome and splicing catalysis by a two-step trans-esterification reaction. The U1 snRNP is the first sub-complex to be recruited to the nascent pre-mRNA, and recognizes the 5' splice site. Subsequently, the U2 snRNP recognizes the branch point within the pre-mRNA intron. The U4/U6·U5 tri-snRNP is then recruited, and the assembling RNP machine undergoes massive rearrangements leading to the release of the U1 and U4 snRNAs (along with many of their associated proteins) and the establishment of the catalytically active spliceosome. At this point the first catalytic step takes place, in which the adenosine at the branch

point attacks the 5' splice, cleaving the 5' exon and generating the lariat intermediate. In the second catalytic step, the 5' splice site attacks the 3' splice site, resulting in the ligation of the 5' and 3' exons and the release of the intron (Fabrizio *et al.*, 2009).

The many dynamic rearrangements of the spliceosome are orchestrated by the activities of several RNA-dependent ATP helicases, and it is becoming clear that the activities of these proteins are delicately regulated by post-translational modifications, protein-protein interactions within spliceosomal sub-complexes, and interactions with GTP (Bellare *et al.,* 2008; Maeder & Guthrie, 2008; Maeder *et al.*, 2009; Small *et al.*, 2006). Furthermore, it is becoming clear that the assembly of the spliceosome, and in many cases, splicing catalysis itself, occurs co-transcriptionally, affording the opportunity for regulatory interactions between the spliceosome, RNA polymerase II, and the chromatin environment (Perales & Bentley, 2009). It had been thought that the short terminal exons of the ribosomal protein genes would be too short to allow splicing catalysis to be completed co-transcriptionally, but recent studies by the Beggs and Neugebauer labs have suggested that the rate of elongation of RNA polymerase II may be modulated in a splicing dependent way, such that splicing is allowed to finish co-transcriptionally. (Alexander *et al.,* 2010; Carrillo Oesterreich *et al.*, 2010). This suggests a high degree of coordination between splicing and transcription, and in this context, chromatin modifications, transcription factors, and 3' end processing factors could all contribute significantly to the regulation of splicing.

In higher eukaryotes, a host of accessory splicing factors, most notably of the SR and hnRNP family of proteins, have been shown to influence alternative splicing decisions. While yeast lack many of these proteins, a role in splicing has been demonstrated for one of the three yeast SR proteins, Npl3 (Kress *et al.*, 2008), and preliminary evidence suggests that the hnRNP protein Nab2 may also influence splicing (unpublished results). Thus, a role for accessory factors in splicing regulation in yeast may yet be uncovered.

Regulation of splicing in response to an environmental stress also implies the existence of a signaling pathway leading from an external stimulus to the splicing machinery. Here, again, the potential for complex signaling from a stimulus to the nuclear milieu where splicing takes place seems nearly limitless (for example, as reviewed in (Zaman *et al.*, 2008)). Many stresses are known to influence expression of ribosomal protein genes (Gasch *et al.*, 2000), acting through several interconnected signaling pathways, and it seemed possible that any of these pathways could also influence the splicing of the RPGs.

To begin, we focused on examining splicing in response to the amino acid starvation-mimicking drug, 3-AT. Chapter 1 describes work that was carried out in collaboration with Gregg Whitworth and Jeffrey Pleiss. Here we showed that the splicing of a large subset of RPGs is inhibited following 3-AT treatment. The subsequent chapters describe work that was carried out in an effort to better understand the mechanism by which this splicing inhibition takes place, and how it is integrated into the larger systems of mRNA processing and overall cellular metabolism. Chapter 2 describes a high-throughput

genetic interaction study (an Epistasis Mini-Array Profile, or EMAP), focused on factors involved in RNA processing, that was carried out in collaboration with Gwedolyn Wilmes and the laboratories of Nevan Krogan, Jonathan Weissman, and Trey Ideker. Chapter 3 describes a survey of a broad range of translation-inhibitory stresses with respect to their influences on processing of the RPG pre-mRNAs, and shows that the kinase complex CK2, or casein kinase 2, is important for some of observed stress-induced changes. Chapter 4 describes efforts to elucidate the mechanism by which splicing is inhibited in response to amino acid starvation by interrogating the contributions of *cis*-elements, the changes to association of RNA polymerase and U1 with RPG genomic loci, and the subcellular localization of the accumulating unspliced pre-mRNA. This work has raised many new questions, and future directions are outlined in the epilogue. Appendix 1 describes the results of genetic screens to uncover factors that contribute to the splicing response to amino acid starvation, which may be of use in the future.

References

Alexander RD, Innocente SA, Barrass JD, Beggs JD (2010) Splicing-dependent RNA polymerase pausing in yeast. Mol Cell 40: 582-593.

Bellare P, Small EC, Huang X, Wohlschlegel JA, Staley JP et al. (2008) A role for ubiquitin in the spliceosome assembly pathway. Nat Struct Mol Biol 15: 444-451.

Bergkessel M, Wilmes GM, Guthrie C (2009) SnapShot: Formation of mRNPs. Cell 136: 794, 794.e1.

Carrillo Oesterreich F, Preibisch S, Neugebauer KM (2010) Global analysis of nascent RNA reveals transcriptional pausing in terminal exons. Mol Cell 40: 571-581.

Cheng, H., Dufu, K., Lee, C. S., Hsu, J. L., Dias, A., and Reed, R. (2006). Human mRNA export machinery recruited to the 5' end of mRNA. Cell *127*, 1389-1400.

Egloff, S., and Murphy, S. (2008). Cracking the RNA polymerase II CTD code. Trends Genet *24*, 280-288.

Fabrizio P, Dannenberg J, Dube P, Kastner B, Stark H et al. (2009) The evolutionarily conserved core design of the catalytic activation step of the yeast spliceosome. Mol Cell 36: 593-608.

Gasch AP, Spellman PT, Kao CM, Carmel-Harel O, Eisen MB et al. (2000) Genomic expression programs in the response of yeast cells to environmental changes. Mol Biol Cell 11: 4241-4257.

Jurica, M. S., and Moore, M. J. (2003). Pre-mRNA splicing: awash in a sea of proteins. Mol Cell *12*, 5-14.

Kohler, A., and Hurt, E. (2007). Exporting RNA from the nucleus to the cytoplasm. Nat Rev Mol Cell Biol *8*, 761-773.

Kress TL, Krogan NJ, Guthrie C (2008) A single SR-like protein, Npl3, promotes pre-mRNA splicing in budding yeast. Mol Cell 32: 727-734.

Maeder C, Guthrie C (2008) Modifications target spliceosome dynamics. Nat Struct Mol Biol 15: 426-428.

Maeder C, Kutach AK, Guthrie C (2009) ATP-dependent unwinding of U4/U6 snRNAs by the Brr2 helicase requires the C terminus of Prp8. Nat Struct Mol Biol 16: 42-48.

Mandel, C. R., Bai, Y., and Tong, L. (2008). Protein factors in pre-mRNA 3'-end processing. Cell Mol Life Sci *65*, 1099-1122.

Moore, M. J. (2005). From birth to death: the complex lives of eukaryotic mRNAs. Science *309*, 1514-1518.

Perales R, Bentley D (2009) "Cotranscriptionality": the transcription elongation complex as a nexus for nuclear transactions. Mol Cell 36: 178-191.

Pleiss JA, Whitworth GB, Bergkessel M, Guthrie C (2007) Rapid, transcript-specific changes in splicing in response to environmental stress. Mol Cell 27: 928-937.

Rougemaille, M., Villa, T., Gudipati, R. K., and Libri, D. (2008). mRNA journey to the cytoplasm: attire required. Biol Cell *100*, 327-342.

Sanford, J. R., Ellis, J., and Caceres, J. F. (2005). Multiple roles of arginine/serine-rich splicing factors in RNA processing. Biochem Soc Trans *33*, 443-446.

Shatkin, A. J., and Manley, J. L. (2000). The ends of the affair: capping and polyadenylation. Nat Struct Biol *7*, 838-842.

Small EC, Leggett SR, Winans AA, Staley JP (2006) The EF-G-like GTPase Snu114p regulates spliceosome dynamics mediated by Brr2p, a DExD/H box ATPase. Mol Cell 23: 389-399.

Staley JP, Guthrie C (1998) Mechanical devices of the spliceosome: motors, clocks, springs, and things. Cell 92: 315-326.

Wahl MC, Will CL, Luhrmann R (2009) The spliceosome: design principles of a dynamic RNP machine. Cell 136: 701-718.

Wang, Z., and Burge, C. B. (2008). Splicing regulation: from a parts list of regulatory elements to an integrated splicing code. Rna *14*, 802-813.

Wilmes GM, Bergkessel M, Bandyopadhyay S, Shales M, Braberg H et al. (2008) A genetic interaction map of RNA-processing factors reveals links between Sem1/Dss1-containing complexes and mRNA export and splicing. Mol Cell 32: 735-746.

Zaman S, Lippman SI, Zhao X, Broach JR (2008) How Saccharomyces responds to nutrients. Annu Rev Genet 42: 27-81.

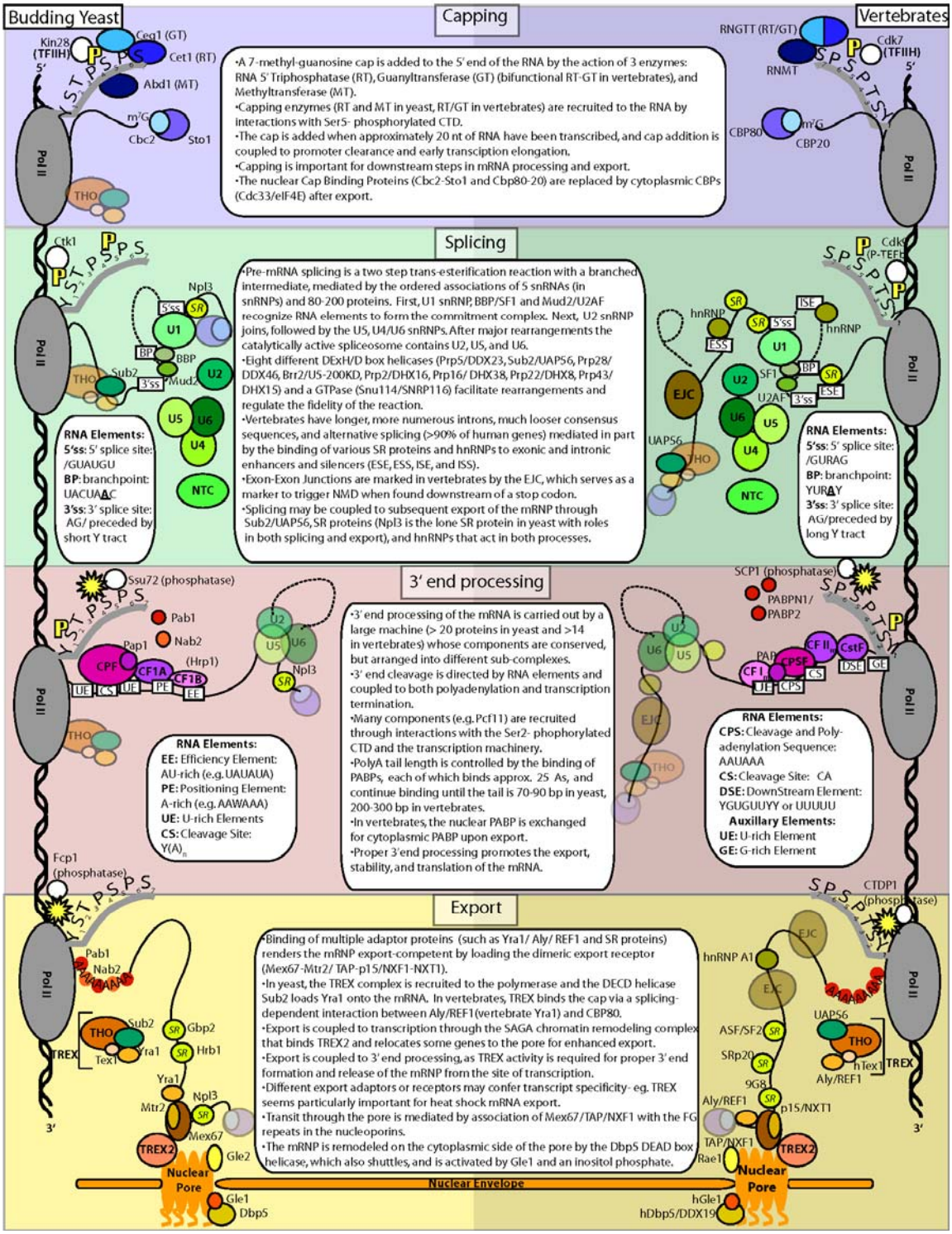

Figure 1. mRNP Formation: RNA Processing and Export. The biosynthesis of a functional mRNA requires multiple covalent modifications to the nascent transcript, including 5' capping, splicing, and generation of a polyadenylated 3' end. These steps are collectively termed RNA processing. The correctly processed mRNA must then be

delivered to the nuclear pore, where it is exported to the cytoplasm for translation. The goal of this Snapshot is to provide a broad overview of these nuclear steps in gene expression. For ease of presentation we have partitioned these steps into 4 sets of reactions but it is important to note that these processes are generally tightly coupled physically, temporally and often functionally. Thus, for example, the addition of the m7G cap to the 5' end of the transcript occurs early but is required for most of the downstream steps. Importantly, although they can be uncoupled in vitro, most of the processing reactions occur co-transcriptionally in vivo. Consistent with this, the phosphorylation state of the heptad repeats (YSTPSPS, repeated 26 times in yeast and 52 times in metazoans) of the carboxy-terminal domain (CTD) of the largest subunit of RNA polymerase II seems to play an important role in recruiting and coordinating the activities of the various RNA processing machineries. We have depicted the major characterized kinases, phosphatases, and phosphorylations of the CTD, but additional modifications and modifying enzymes have been shown to act in specific cases. Likewise, we have depicted the major splicing and export pathways, but alternative or additional pathways have also been described. For example, in the case of splicing, an alternative minor spliceosome has been described in metazoans, which recognizes different consensus splice sites than the major spliceosome, and although chromatin immunoprecipitation data supports the stepwise assembly of the spliceosome in a co-transcriptional context, a fully assembled "penta-snRNP" complex containing all five snRNAs has been also been purified in yeast. In the case of export, an alternative Crm1-dependent pathway can be used to transport mRNPs out of the nucleus, under some circumstances.

Because the nascent mRNAs exist as complex ribonucleoprotein particles (RNPs) and the constellation of associated proteins is highly dynamic, the precise composition of a biological substrate for a given processing reaction is difficult to define. Regardless, the complex interplay between emerging RNA structure, multiple RNA binding proteins, and the large splicing and 3' end processing machineries provides rich opportunities for regulation. It has been estimated that >80% of human genes are

alternatively spliced and >50% have alternative 3' ends; this arises from competition, both between weak and strong binding sites on the nascent RNA transcripts and between the splicing and polyA machineries with one another. Additionally, recent genome-wide datasets are beginning to suggest significant transcript specificity for many of the RNA binding proteins that are involved in the processes described here. Finally, the RNA processing steps described here afford opportunities for additional quality control. Although we have only depicted the proper completion of each processing step, it is important to note that improperly processed mRNPs can be selectively retained and degraded in the nucleus by the nuclear exosome. Thus, the emerging picture of mRNP formation is one of a dynamic, regulated, and coordinated series of processing steps capable of contributing significantly to the overall control of gene expression.

Abbreviations/Definitions:

BBP Branchpoint binding protein

CF Cleavage factor

CPSF Cleavage and polyadenylation specificity factor

CStF Cleavage stimulation factor

CTD Carboxy-terminal domain (of the largest subunit of RNA polymerase II)

DExD/H-box helicase – a member of a family of ATP-dependent, RNA-stimulated helicases characterized by a DExD/H motif

EJC Exon junction complex

ESE Exonic splicing enhancer

ESS Exonic splicing silencer

hnRNP heterogeneous ribonucleoprotein particle

NMD nonsense mediated decay

NTC Prp **N**ine**T**een-associated **C**omplex

PABP poly A binding protein

Pol II RNA polymerase II

snRNP small nuclear ribonucleoprotein particle

SR Serine-Arginine rich

Chapter 1

Rapid, transcript-specific changes in splicing in response to environmental stress

Abstract

While the core splicing machinery is highly conserved between budding yeast and mammals, the absence of alternative splicing in Saccharomyces cerevisiae raises the fundamental question of why introns have been retained in only 5% of the 6000 genes. Because ribosomal protein-encoding genes (RPGs) are highly overrepresented in the set of intron-containing genes, we tested the hypothesis that splicing of these transcripts would be regulated under conditions in which translation is impaired. Using a microarray-based strategy, we find that, within minutes after the induction of amino acid starvation, the splicing of the majority of RPGs is specifically inhibited. In response to an unrelated stress, exposure to toxic levels of ethanol, splicing of a different group of transcripts is inhibited, while the splicing of a third set is actually improved. We propose that regulation of splicing, like transcription, can afford rapid and specific changes in gene expression in response to the environment.

Introduction

Messenger RNA splicing is an essential part of eukaryotic gene expression as the coding regions of most eukaryotic genes are interrupted by noncoding introns. In higher eukaryotes, the process of splicing is utilized to regulate both qualitative and quantitative aspects of gene expression (reviewed in Black, 2000 and Blencowe, 2006). Alterations in the pattern of splice site usage in multi-intronic transcripts can produce a spectrum of protein isoforms from a single genomic locus, greatly expanding the genetic repertoire of an organism. Furthermore, when coupled to nonsense-mediated decay, alternative splicing can function as an "on/off" switch by introducing premature termination codons, thereby directing mRNA degradation (Lewis et al., 2003 and Mitrovich and Anderson, 2000).

By contrast, only 5% of genes in the budding yeast Saccharomyces cerevisiae are intron containing, and with few exceptions these genes have only a single intron (Spingola et al., 1999). Splice site sequences in yeast introns generally conform to a strict consensus, and documented instances of alternative splicing are rare (Davis et al., 2000). Nonetheless, a number of examples of regulated splicing have been demonstrated in yeast, including a set of transcripts that are constitutively transcribed but are efficiently spliced only during meiosis (Davis et al., 2000, Juneau et al., 2007 and Nandabalan et al., 1993). These introns, as well as the autoregulated introns in Rpl30 and Yra1, all contain nonconsensus splice sites, which are required for regulation (Eng and Warner, 1991 and Preker et al., 2002). However, because most yeast introns contain consensus splice site

sequences, it has remained unknown whether splicing could function as a more general regulator of gene expression.

Interestingly, the set of intron-containing genes in yeast includes many metabolic regulators and is highly enriched for ribosomal protein genes (RPGs). Of the 139 RPGs encoded in the yeast genome, 102 are interrupted by at least one intron, making this by far the largest functional category. It has been previously established that starvation for amino acids leads to transcriptional repression of RPG synthesis, repression of rRNA synthesis, a general repression of translation, and an upregulation of enzymes involved in amino acid biosynthesis through a process controlled by the nonessential kinase Gcn2 (Chen and Powers, 2006, Cherkasova and Hinnebusch, 2003, Dever et al., 1992 and Hinnebusch, 2005). Because of the overrepresentation of translational components among the intron-containing genes, we hypothesized that the splicing of these transcripts might also be regulated in response to amino acid starvation.

Here we have taken a microarray-based strategy to examine the transcript-specific splicing changes resulting from exposure to two unrelated but environmentally relevant stresses: amino acid starvation and ethanol toxicity. We find that the splicing of the majority of RPGs is inhibited within minutes of inducing amino acid starvation. By comparison, exposure to toxic levels of ethanol, which is not known to induce a global repression of translation, has little effect on the splicing of the RPG transcripts. Rather, in response to the latter stress, the splicing of a different set of transcripts is downregulated, while the splicing efficiency of a third group of transcripts is improved. The specificity of these responses and the speed of their onset argue that splicing

provides an important opportunity for regulation of gene expression in response to environmental stress. Furthermore, the capacity for transcription-independent regulation may explain the evolutionary retention of introns in these genes.

Results

A Genome-wide Approach to Examining Pre-mRNA Splicing

We have employed a microarray-based strategy to monitor quantitative changes in the splicing of ~250 intron-containing yeast transcripts in response to alterations in the environment. The microarrays contain three different oligonucleotide probes targeting each intron-containing gene, as described previously (Clark et al., 2002 and Pleiss et al., 2007). These probes allow for the independent determination of differences in the levels of the precursor mRNA species (probe P), mature mRNA species (probe M), and total transcript (probe T) between two samples (Figure 1). Whereas analysis of a traditional expression array hinges upon a single measurement of the relative abundance of a transcript in an experimental and reference sample, analysis of changes in the splicing behavior of a transcript requires the simultaneous consideration of the relative behaviors of all three types of probes. By examining the behavior of both the precursor species and the mature species against the background of changes in the total level of transcript, splicing efficiency can be distinguished from overall changes in transcript levels (Pleiss et al., 2007). Thus, a splicing profile can be generated and used to identify transcripts whose splicing is affected by an experimental treatment.

Changes in Pre-mRNA Splicing in Response to Amino Acid Starvation

We began by examining the cellular response to amino acid starvation. Amino acid starvation was induced by addition of the histidine-mimic 3-aminotriazole (3AT) (Hinnebusch, 2005). Cells were collected at several short times after either a mock treatment or exposure to 50 mM 3AT. Figure 2 shows the time-resolved splicing profiles for each intron-containing gene obtained from microarray experiments comparing RNA isolated from cells exposed to these two treatments. Genes have been divided into two groups: RPGs and non-RPGs. Within these groups, the genes are ordered based on the similarity of the behavior of their three feature types across the amino acid starvation time course. Notably, the splicing of the majority of RPG transcripts is rapidly reduced, as evidenced by the increased abundance of precursor mRNA in starved relative to unstarved cells. Not surprisingly, because RPG transcripts exhibit a strong partitioning toward their spliced form (Pleiss et al., 2007), little decrease is seen in the level of mature mRNA for these species during the short time course of 3AT exposure. By comparison, little change is seen in the level of pre-mRNA for any of the non-RPG transcripts. Interestingly, several non-RPG transcripts do show a rapid decrease in the level of total mRNA and mature mRNA present, suggesting that the mature forms of these transcripts may be rapidly destabilized in response to amino acid starvation.

Quantitative RT-PCR Validation of Splicing Inhibition

To validate the observed response to amino acid starvation, quantitative RT-PCR

experiments using both intron- and exon-specific primers were employed. As seen in Figure 3, results from the quantitative PCR assay are in good agreement with the microarray data. Both methods show accumulation of the RPG pre-mRNAs corresponding to Rpl21a and Rpl17b at very short time points after induction of amino acid starvation. As seen in Supplemental Figure 1, nearly equal levels of accumulation are detected when using primers that include the intron and the entire second exon, demonstrating that the accumulating product is in fact an unspliced species. By contrast, no defect is detected in the splicing of either the U3 pre-snRNA or the Tef4 pre-mRNA.

Comparison with a General Inhibition of Splicing

Because ribosomal proteins are highly transcribed (Holstege et al., 1998), it was important to demonstrate that the observed RPG-specific phenotype truly results from an RPG-specific change in splicing and does not simply suggest that these pre-mRNAs are more likely to show accumulation given their high level of transcription. Thus, we compared the splicing profile derived from amino acid starvation to that seen after inactivation of a core spliceosomal factor. Figure 2B shows the splicing profile resulting from shifting a strain containing the temperature-sensitive prp8-1 mutant to the nonpermissive temperature. PRP8 encodes a stable component of the U5 small nuclear RNP, and mutations in Prp8 are expected to result in defects in the splicing of most actively transcribed pre-mRNAs. In response to inactivation of prp8-1, the fold increases in pre-mRNA levels are nearly equal for RPG and non-RPG transcripts alike. This strongly suggests that amino acid starvation does not impart a global defect in splicing

but instead that the splicing of RPG transcripts is specifically downregulated. Importantly, these experiments also demonstrate the relative stability of the mature forms of the RPG mRNAs in response to defects in splicing; whereas the decreases in mature levels for many non-RPG transcripts are apparent within minutes of inactivation of Prp8, very little decrease in the level of mature RPG transcripts can be observed during the prp8-1 time course.

Reduced RNA Turnover Is Unlikely to Account for the Increased Pre-mRNA Levels

Considered a priori, two different mechanisms could account for the observed accumulation of RPG transcript pre-mRNA during amino acid starvation. First, a reduction in the splicing efficiency of these transcripts could lead to an increase in their pre-mRNA levels. Alternatively, some fraction of these pre-mRNAs may normally be targeted to a decay pathway prior to their processing by the spliceosome. In this case, the specific inhibition of their decay could result in an increase in pre-mRNA levels. To discriminate between these possibilities, we asked whether RPG pre-mRNAs as a class are specifically stabilized in the absence of any one of a number of different components involved in RNA turnover. Figure 2C shows the splicing profiles resulting from deletion of the following: RRP6, a component of the nuclear exosome (Houseley et al., 2006); RAI1 and RTT103, two components of the Rat1 nuclear decay pathway (Kim et al., 2004); SKI2, a regulator of 3′ to 5′ decay (Frischmeyer et al., 2002 and van Hoof et al., 2002); UPF1, a component of the nonsense-mediated degradation pathway (Leeds et al., 1991); or XRN1, a cytoplasmic 5′ to 3′ exonuclease (Fillman and Lykke-Andersen,

2005). Notably, while the genome-wide changes in mRNA levels resulting from deletion of many of these factors have previously been reported (He et al., 2003, Lelivelt and Culbertson, 1999 and Wyers et al., 2005), our experiments specifically address the behavior of the pre-mRNA species.

Importantly, there is no evidence from these experiments that RPG pre-mRNAs as a class are constitutively degraded at significant levels under normal growth conditions. By contrast, our data validate several pre-mRNAs that were previously shown to be stabilized in response to mutations in these decay pathways. For example, the RPL28 pre-mRNA is strongly stabilized in the absence of UPF1 (He et al., 1993). Also, as we had previously shown (Preker and Guthrie, 2006), the YRA1 pre-mRNA is strongly stabilized in the absence of XRN1. Several additional pre-mRNAs are also stabilized in response to each of these mutations. While we cannot formally rule out the possibility that a different, completely nonoverlapping degradation pathway may contribute to the phenotype observed in response to amino acid starvation, our results strongly suggest that the increased levels of pre-mRNA result from a failure of these transcripts to be efficiently spliced.

Gcn2 Is Not Required for the Spliceosomal Response to Amino Acid Starvation

Given the well-defined role of Gcn2 in regulating the response to amino acid starvation, it was important to determine whether the observed splicing changes were also dependent upon the activity of this nonessential kinase. The accumulation of uncharged tRNAs resulting from amino acid starvation is known to activate Gcn2, which

subsequently phosphorylates the initiation factor eIF-2α, causing a general decrease in translation initiation (Dong et al., 2000). By a mechanism that is now well understood, this results in the paradoxical increase in translation of the transcription factor Gcn4 (Hinnebusch, 1997), which leads to the transcriptional upregulation of numerous genes involved in amino acid biosynthesis (Natarajan et al., 2001). Interestingly, as seen in Figure 3, the onset of the splicing response appears to precede the transcriptional upregulation of one Gcn4 target, HIS4, suggesting that the changes in splicing are independent of the Gcn4-mediated transcriptional response.

Using a strain deleted for GCN2, we repeated our experiment by comparing an untreated sample with one exposed to 3AT. As expected, the Δgcn2 strain is largely unable to effect the upregulation of the biosynthetic genes in response to amino acid starvation (Figure 4A and B). Nonetheless, the capacity of this strain to downregulate RPG splicing is nearly unchanged. Indeed, a direct experimental comparison of the amino acid starvation responses of a wild-type and a Δgcn2 strain both treated with 3AT demonstrates their highly divergent transcriptional responses but nearly identical splicing responses (Figure 4C). Interestingly, slight differences are apparent between the two strains at the longer time points, with more pre-mRNA accumulation apparent in the Δgcn2 strain. We presume this difference reflects the Gcn2-dependent global downregulation of RPG transcription known to accompany amino acid starvation. The onset of this transcriptional program presumably limits pre-mRNA accumulation in the wild-type cells.

Distinct Splicing Regulation Is Observed in Response to Ethanol Toxicity

To determine whether splicing changes affecting the RPG transcripts are specific to the cellular response to amino acid starvation or reflect a more general response to unfavorable growth conditions, we examined the effects of exposure to toxic levels of ethanol. Figure 5A shows the kinetic response of wild-type cells to ethanol toxicity. Interestingly, in response to ethanol exposure, a small number of transcripts decrease in splicing efficiency (marked with a red bar in Figure 5A and highlighted in the top of Figure 5B). As seen in Figure 5C, these transcripts show no splicing defect in response to amino acid starvation. Notably, the splicing efficiency of a second small subset of transcripts actually increases in response to ethanol (marked with a green bar in Figure 5A and highlighted at the bottom of Figure 5B). These transcripts likewise showed no change in splicing efficiency in response to amino acid starvation. A full comparison of the responses to amino acid starvation and toxic ethanol shown in Figure 6 reveals their nonoverlapping nature, demonstrating that the splicing changes are specifically tailored to each of these particular environmental stresses.

Discussion

Here we have taken a microarray-based approach to examine the capacity of pre-mRNA splicing in the budding yeast, S. cerevisiae, to be regulated in response to changes in environment. In response to amino acid starvation, the splicing efficiency of nearly all RPG transcripts is rapidly downregulated. Interestingly, these changes in splicing

efficiency, unlike previously described responses to amino acid starvation, are not dependent upon the activity of the Gcn2 kinase. Furthermore, this response appears specific to amino acid starvation, as a different environmental stress, exposure to toxic levels of ethanol, does not globally repress RPG splicing. Instead, ethanol toxicity induces a unique spliceosomal response wherein the splicing efficiency of a different set of transcripts is downregulated while the splicing efficiency of another group of transcripts is improved.

The splicing architecture present in yeast is simple relative to higher eukaryotes. Very few genes in yeast contain multiple introns, and yeast introns tend to conform to tight consensus sequences at their splice sites, precluding the process of alternative splicing so rampant in metazoans. As such, it has been unclear whether yeast has retained the capacity to extensively regulate the activity of this step in gene expression. However, our experiments demonstrate that the splicing efficiency of distinct sets of transcripts can be rapidly and specifically modulated in response to changing environmental conditions. We have recently reported that mutations in core spliceosomal components can lead to transcript-specific defects in splicing (Pleiss et al., 2007), demonstrating that the yeast splicing architecture exhibits the physical capacity to differentiate among transcripts. Importantly, the results of our current experiments suggest that there must exist in yeast mechanisms to differentiate splicing activity even among the many transcripts that contain strong consensus splice sites.

The Biology of Splicing Regulation

The splicing changes observed in response to amino acid starvation can be readily rationalized: under conditions in which translational resources are limiting, the spliceosome can rapidly downregulate the synthesis of new ribosomal components. Under normal growth conditions, wild-type yeast devote a significant fraction of their metabolic resources to the synthesis of new ribosomes. Many steps in this pathway are known to be tightly regulated, presumably reflecting the importance of optimizing the process of ribosome production (Warner, 1999). Our results suggest an explanation for the prevalence of introns in RPGs in that they may offer an additional level at which translational capacity can be coordinately regulated.

Moreover, the provocative result that the splicing of certain transcripts can be rapidly upregulated in response to ethanol toxicity suggests that not all yeast transcripts are processed by the spliceosome at maximal efficiency at all times. Indeed, upregulation of the splicing of these genes potentially allows for a rapid increase in protein expression without the need for de novo transcription. An analogy can be drawn with the unfolded protein response, in which induction of splicing of the Hac1 transcription factor, in this case by a nonspliceosomal mechanism, allows for a rapid response to the stress in the absence of new transcription (Sidrauski and Walter, 1997). Remarkably, one of the transcripts whose splicing is improved after ethanol exposure encodes Srb2, a nonessential component of the Mediator complex of transcription factors. Our results suggest that expression of this conserved coactivator of transcription can also be

regulated at the level of splicing and that splicing can in turn act to regulate transcription.

Mechanisms of Splicing Regulation

While it is true that yeast splice sites generally adhere to a strict consensus, all previously documented cases of regulated splicing in yeast rely on the presence of suboptimal splice site sequences. For example, a nonconsensus 5′ splice site in the Rpl30 transcript is necessary to maintain a splicing-based autoregulatory feedback loop (Eng and Warner, 1991). Likewise, nonconsensus 5′ splice sites in the transcripts of MER2 and MER3 are necessary for their positive regulation during meiosis (Nandabalan et al., 1993). However, splice site sequences alone are insufficient to explain the transcript-specific changes we have observed during amino acid starvation, as no unique sequences have been identified within this group of transcripts (Figure 23). Another potential explanation is based on the observation that, as a class, RPG introns tend to be significantly larger in size than introns in other yeast genes: the median RPG intron is ~400 nucleotides in length, whereas the median non-RPG intron is only ~130 nucleotides. Nevertheless, size alone is also insufficient to explain the specificity, as the splicing of non-RPGs such as Act1, whose intron contains 308 nucleotides, is unaffected during amino acid starvation. Thus, other currently unknown cis-acting features must contribute to the observed specificity.

In higher eukaryotes, members of the large SR and hnRNP families of regulatory proteins are known to play major roles in regulating alternative splicing decisions. By

comparison, the spectrum of yeast proteins belonging to these families is reduced, and it remains unknown whether these proteins play any role in regulating splicing activity in yeast. Instead, recent evidence suggests that “specificity” factors will include core components of the spliceosome itself. RNAi-mediated knockdowns in flies of several essential splicing factors have been shown to have differential effects on the splicing of alternative exons (Park et al., 2004). Likewise, our recent microarray analyses of point mutations in conserved, core splicing components (Pleiss et al., 2007) also revealed remarkably transcript-specific effects that were not readily accounted for by splice site sequences per se. In particular, we previously demonstrated that the spliceosome interacts with RPG transcripts in a fundamentally different way than it does with non-RPG transcripts. The similar behavior of RPG pre-mRNAs in response to perturbations in essential, core spliceosomal components may well underlie the behavior of these premRNAs in response to amino acid starvation.

We previously proposed that the rate of co-transcriptional loading of spliceosomal components would be higher for RPG transcripts than for non-RPG transcripts (Pleiss et al., 2007). Consistent with this proposal, recent genome-wide chromatin immunoprecipitation experiments demonstrated a higher density of the U1 snRNP on RPGs than nonribosomal protein genes (Tardiff et al., 2006). Conceivably, modification of a common spliceosomal factor that affects the cotranscriptional engagement of the spliceosome could be responsible for the RPG-specific reduction of splicing efficiency seen in response to amino acid starvation. By comparison, a separate genome-wide experiment (Moore et al., 2006) showed that the transcript encoding Srb2 is one of a

small number of intron-containing transcripts that fails to engage with the spliceosome cotranscriptionally. The improved splicing seen for this transcript in response to toxic ethanol may therefore also depend upon its ability to efficiently recruit active spliceosomes. For example, these data suggest that under normal growth conditions the Srb2 transcript is inefficiently engaged by the spliceosome but that under conditions of ethanol toxicity spliceosomal recruitment is increased, allowing for more efficient splicing. Further characterization of the behavior of this transcript will likely provide important insights into the general mechanism by which transcripts engage spliceosomes.

Connecting the Spliceosome to Cellular Environment

An important question for the future regards the mechanisms by which environmental signals are transduced to the splicing machinery. The unique molecular profiles observed in response to two unrelated physiological stresses suggest that at least two independent pathways connect the spliceosome with the cellular environment. The rapid onset of the molecular defects in response to amino acid starvation suggests that posttranslational modifications of spliceosomal components might likely be involved in this regulation. Interestingly, recent evidence suggests a potential role for ubiquitin in regulating the splicing cycle (Bellare et al., 2006). Alternatively, phosphorylation and methylation of regulatory proteins play an important role in regulating splicing in higher eukaryotes and would be obvious candidates in yeast as well (Shin and Manley, 2004). Nevertheless, the candidate most likely to control such a signaling pathway in response

to amino acid starvation, the Gcn2 kinase, is not essential for the spliceosomal response. Rather, our results imply the existence of a previously uncharacterized signaling pathway linking amino acid starvation with transcript-specific changes in premRNA splicing.

Implications

The findings presented here argue strongly that pre-mRNA splicing can play an important role in regulating gene expression even in a system that lacks the infrastructure necessary for alternative splicing. Further, these results argue against the notion that most transcripts interact equally with the spliceosome, suggesting instead that transcript identity is an important factor in determining splicing activity. Given the high level of conservation of the basic splicing machinery, we predict that the mechanisms utilized by yeast to regulate pre-mRNA splicing will also be important in higher eukaryotes, where they likely underlie or augment the regulation of alternative splice site choices.

Experimental Procedures

Sample Collection and Preparation

Amino acid starvation experiments utilized either the wild-type strain (yMB1) or the Δgcn2 strain (yMB2). The strain yMB1 was constructed by repairing the HIS3 locus in the BY4742 strain (Brachmann et al., 1998) using standard methods. The strain yMB2 was constructed by disrupting the GCN2 locus of yMB1 with LEU2. A single master

culture of these strains was grown at 30°C in 250 ml of minimal medium lacking histidine (Guthrie and Fink, 2002) until its optical density was between A600 = 0.5 and A600 = 0.7. An initial 15 ml sample was collected by filtration using Millipore HAWP0025 filters (http://www.millipore.com) prior to initiation of the time course. The filters were immediately frozen in N2(l). Experiments were initiated by splitting the master culture into two 100 ml aliquots and adding either 5 ml of water or 1 M 3AT. At the appropriate times, 15 ml of cells were collected.

For experiments examining ethanol toxicity, a single master culture of the strain BY4742 was grown at 30°C in 300 ml of YEPD (Guthrie and Fink, 2002) until its optical density was between A600 = 0.5 and A600 = 0.7. Samples were then collected in a 96-well format as previously described (Pleiss et al., 2007). Briefly, 180 µl of water or 100% ethanol was added to each well of a 96-well plate. A reverse time course was initiated by addition of 1.6 ml aliquots of culture to the appropriate wells at the appropriate times. At the completion of the time course, cells were collected by centrifugation at 5000 × g for 5 min.

For experiments examining inactivation of Prp8, master cultures of both the wild-type (yEJS1) and prp8-1 (yEJS17) strain were grown at 25°C in 100 ml of complete minimal medium until their optical densities were between A600 = 0.5 and A600 = 0.7. Cells were shifted from 25°C to 37°C, and 15 ml samples were collected by filtration (as above) at the indicated times.

For experiments examining the nonessential RNA turnover mutants, samples of each mutant strain (all derivatives of BY4741 Brachmann et al., 1998) and the wild-type strain

(BY4742) were grown at 30°C in 50 ml of complete minimal medium until their optical densities were between A600 = 0.5 and A600 = 0.7. Cells were then collected by centrifugation at 3000 × g for 5 min.

Samples for microarray analysis were isolated and prepared as previously described (Pleiss et al., 2007). Briefly, 25 µg of total cellular RNA was collected from each sample and converted into cDNA for each individual microarray. Data presented as figures are derived from independent biological replicates, which were utilized to perform dyeflipped microarray replicates. Additional experiments examining distinct biological replicates have been performed and yield similar results. Microarray images were collected and analyzed as previously described (Pleiss et al., 2007).

Quantitative PCR

Total cellular RNA for quantitative RT-PCR experiments was treated with DNase I (Fermentas, http://www.fermentas.com) according to the manufacturer's protocol prior to use. The cDNA was then produced as previously described (Pleiss et al., 2007). Quantitative PCR was then performed using an Opticon from MJ Research (http://www.mjresearch.com). Error bars in Figure 19 are the result of triplicate measurements from a single biological sample. Standard deviations were only slightly higher when comparing biological replicates. A series of 10-fold dilutions of genomic DNA covering a total range of 106 molecules was used to generate the standard curves. Genomic DNA was purified using a ZR Fungal DNA kit (Zymo Research) according to the manufacturer's protocol.

Acknowledgements

We thank J. DeRisi, A. Carroll, and M. Ares for technical assistance with the microarrays; J. Abelson, J. Steitz, A. Johnson, H. Madhani, M. McMahon, M. Inada, and members of the C.G. lab for helpful discussions and critical comments on the manuscript. This work was supported by funds from the Damon Runyon Cancer Research Foundation (J.A.P.), N.I.H. and N.S.F. (G.B.W.), HHMI (M.B.), and N.I.H. grant GM21119 (C.G.). C.G. is an American Cancer Society Research Professor of Molecular Genetics.

References

Bellare, P., Kutach, A. K., Rines, A. K., Guthrie, C., and Sontheimer, E. J. (2006). Ubiquitin binding by a variant Jab1/MPN domain in the essential pre-mRNA splicing factor Prp8p. Rna 12, 292-302.

Black, D. L. (2000). Protein diversity from alternative splicing: a challenge for bioinformatics and post-genome biology. Cell 103, 367-370.

Blencowe, B. J. (2006). Alternative Splicing: New Insights from Global Analyses. Cell 126, 37-47.

Brachmann, C. B., Davies, A., Cost, G. J., Caputo, E., Li, J., Hieter, P., and Boeke, J. D. (1998). Designer deletion strains derived from Saccharomyces cerevisiae S288C: a useful set of strains and plasmids for PCR-mediated gene disruption and other applications. Yeast 14, 115-132.

Chen, J. C., and Powers, T. (2006). Coordinate regulation of multiple and distinct

biosynthetic pathways by TOR and PKA kinases in S. cerevisiae. Curr Genet 49, 281-293.

Cherkasova, V. A., and Hinnebusch, A. G. (2003). Translational control by TOR and TAP42 through dephosphorylation of eIF2alpha kinase GCN2. Genes Dev 17, 859-872. 104

Clark, T. A., Sugnet, C. W., and Ares, M., Jr. (2002). Genomewide analysis of mRNA processing in yeast using splicing-specific microarrays. Science 296, 907-910.

Davis, C. A., Grate, L., Spingola, M., and Ares, M., Jr. (2000). Test of intron predictions reveals novel splice sites, alternatively spliced mRNAs and new introns in meiotically regulated genes of yeast. Nucleic Acids Res 28, 1700-1706.

Dever, T. E., Feng, L., Wek, R. C., Cigan, A. M., Donahue, T. F., and Hinnebusch, A. G. (1992). Phosphorylation of initiation factor 2 alpha by protein kinase GCN2 mediates gene-specific translational control of GCN4 in yeast. Cell 68, 585-596.

Dong, J., Qiu, H., Garcia-Barrio, M., Anderson, J., and Hinnebusch, A. G. (2000). Uncharged tRNA activates GCN2 by displacing the protein kinase moiety from a bipartite tRNA-binding domain. Mol Cell 6, 269-279.

Eng, F. J., and Warner, J. R. (1991). Structural basis for the regulation of splicing of a yeast messenger RNA. Cell 65, 797-804.

Fillman, C., and Lykke-Andersen, J. (2005). RNA decapping inside and outside of processing bodies. Curr Opin Cell Biol 17, 326-331.

Frischmeyer, P. A., van Hoof, A., O'Donnell, K., Guerrerio, A. L., Parker, R., and Dietz, H. C. (2002). An mRNA surveillance mechanism that eliminates transcripts lacking

termination codons. Science 295, 2258-2261.

Guthrie, C., and Fink, G. R. (2002). Guide to yeast genetics and molecular and cell biology (Amsterdam ; Boston ; London, Academic Press).

He, F., Li, X., Spatrick, P., Casillo, R., Dong, S., and Jacobson, A. (2003). Genome-wide analysis of mRNAs regulated by the nonsense-mediated and 5' to 3' mRNA decay pathways in yeast. Mol Cell 12, 1439-1452.

He, F., Peltz, S. W., Donahue, J. L., Rosbash, M., and Jacobson, A. (1993). Stabilization and ribosome association of unspliced pre-mRNAs in a yeast upf1- mutant. Proc Natl Acad Sci U S A 90, 7034-7038.

Hinnebusch, A. G. (1997). Translational regulation of yeast GCN4. A window on factors that control initiator-trna binding to the ribosome. J Biol Chem 272, 21661-21664.

Hinnebusch, A. G. (2005). Translational regulation of GCN4 and the general amino acid control of yeast. Annu Rev Microbiol 59, 407-450.

Holstege, F. C., Jennings, E. G., Wyrick, J. J., Lee, T. I., Hengartner, C. J., Green, M. R., Golub, T. R., Lander, E. S., and Young, R. A. (1998). Dissecting the regulatory circuitry of a eukaryotic genome. Cell 95, 717-728.

Houseley, J., LaCava, J., and Tollervey, D. (2006). RNA-quality control by the exosome. Nat Rev Mol Cell Biol 7, 529-539.

Juneau, K., Palm, C., Miranda, M., and Davis, R. W. (2007). High-density yeast-tiling array reveals previously undiscovered introns and extensive regulation of meiotic splicing. Proc Natl Acad Sci U S A 104, 1522-1527.

Kim, M., Krogan, N. J., Vasiljeva, L., Rando, O. J., Nedea, E., Greenblatt, J. F., and

Buratowski, S. (2004). The yeast Rat1 exonuclease promotes transcription termination by RNA polymerase II. Nature 432, 517-522.

Leeds, P., Peltz, S. W., Jacobson, A., and Culbertson, M. R. (1991). The product of the yeast UPF1 gene is required for rapid turnover of mRNAs containing a premature translational termination codon. Genes Dev 5, 2303-2314.

Lelivelt, M. J., and Culbertson, M. R. (1999). Yeast Upf proteins required for RNA surveillance affect global expression of the yeast transcriptome. Mol Cell Biol 19, 6710-6719.

Lewis, B. P., Green, R. E., and Brenner, S. E. (2003). Evidence for the widespread coupling of alternative splicing and nonsense-mediated mRNA decay in humans. Proc Natl Acad Sci U S A 100, 189-192.

Mitrovich, Q. M., and Anderson, P. (2000). Unproductively spliced ribosomal protein mRNAs are natural targets of mRNA surveillance in C. elegans. Genes Dev 14, 2173-2184.

Moore, M. J., Schwartzfarb, E. M., Silver, P. A., and Yu, M. C. (2006). Differential recruitment of the splicing machinery during transcription predicts genome-wide patterns

of mRNA splicing. Mol Cell 24, 903-915.

Nandabalan, K., Price, L., and Roeder, G. S. (1993). Mutations in U1 snRNA bypass the requirement for a cell type-specific RNA splicing factor. Cell 73, 407-415.

Natarajan, K., Meyer, M. R., Jackson, B. M., Slade, D., Roberts, C., Hinnebusch, A. G., and Marton, M. J. (2001). Transcriptional profiling shows that Gcn4p is a master

regulator of gene expression during amino acid starvation in yeast. Mol Cell Biol 21, 4347-4368.

Park, J. W., Parisky, K., Celotto, A. M., Reenan, R. A., and Graveley, B. R. (2004). Identification of alternative splicing regulators by RNA interference in Drosophila. Proc Natl Acad Sci U S A 101, 15974-15979.

Pleiss, J. A., Whitworth, G. B., Bergkessel, M., and Guthrie, C. (2007). Transcript Specificity in Yeast Pre-mRNA Splicing Revealed by Mutations in Core Spliceosomal Components. PLoS Biol 5, e90.

Preker, P. J., and Guthrie, C. (2006). Autoregulation of the mRNA export factor Yra1p requires inefficient splicing of its pre-mRNA. Rna 12, 994-1006.

Preker, P. J., Kim, K. S., and Guthrie, C. (2002). Expression of the essential mRNA export factor Yra1p is autoregulated by a splicing-dependent mechanism. Rna 8, 969-980.

Shin, C., and Manley, J. L. (2004). Cell signalling and the control of pre-mRNA splicing. Nat Rev Mol Cell Biol 5, 727-738.

Sidrauski, C., and Walter, P. (1997). The transmembrane kinase Ire1p is a site-specific endonuclease that initiates mRNA splicing in the unfolded protein response. Cell 90, 1031-1039.

Spingola, M., Grate, L., Haussler, D., and Ares, M., Jr. (1999). Genome-wide bioinformatic and molecular analysis of introns in Saccharomyces cerevisiae. Rna 5, 221-234.

Tardiff, D. F., Lacadie, S. A., and Rosbash, M. (2006). A genome-wide analysis indicates

that yeast pre-mRNA splicing is predominantly posttranscriptional. Mol Cell 24, 917-929.

van Hoof, A., Frischmeyer, P. A., Dietz, H. C., and Parker, R. (2002). Exosomemediated recognition and degradation of mRNAs lacking a termination codon. Science 295, 2262-2264.

Warner, J. R. (1999). The economics of ribosome biosynthesis in yeast. Trends Biochem Sci 24, 437-440.

Wyers, F., Rougemaille, M., Badis, G., Rousselle, J. C., Dufour, M. E., Boulay, J., Regnault, B., Devaux, F., Namane, A., Seraphin, B., et al. (2005). Cryptic pol II transcripts are degraded by a nuclear quality control pathway involving a new poly(A) polymerase. Cell 121, 725-737.

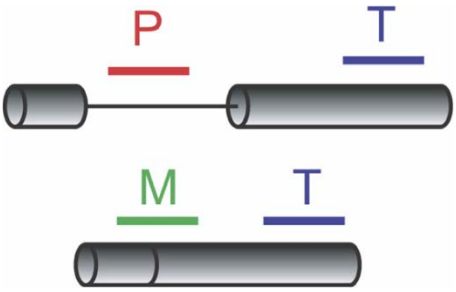

Figure 1. Splicing-specific microarrays. Probes targeting intron-containing genes are designed to detect the precursor species (P), the mature species (M), or the total transcript (T).

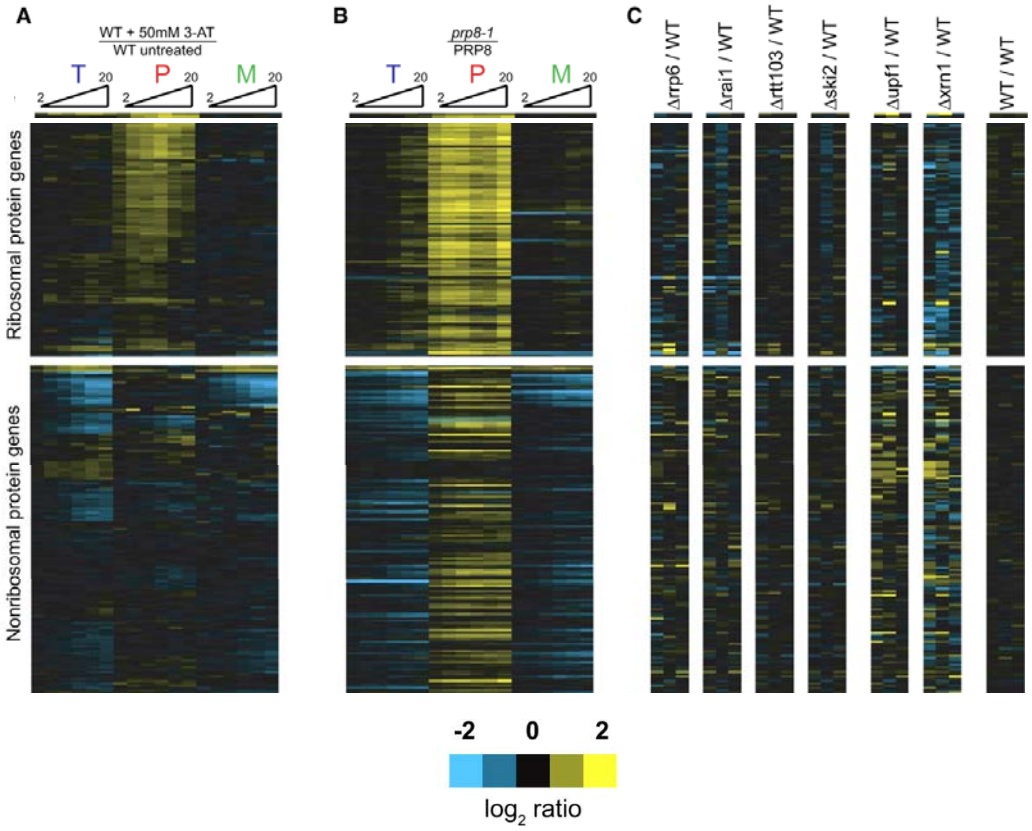

Figure 2. Regulation of pre-mRNA splicing in repsonse to amino acid starvation. Time-resolved splicing profiles resulting from comparisons of (A) wild-type cells either treated with 50 mM 3AT or mock treated for 2, 4, 6, 10, 15, and 20 min; (B) *prp8-1* and wild-type cells shifted from 25°C to 37°C for 5, 10, 15, 20, 25, and 30 min; and (C) wild-type cells compared to cells deleted for either *RRP6*, *RAI1*, *RTT103*, *SKI2*, *UPF1*, or *XRN1*. Also included is a comparison of two wild-type strains. The transcripts are ordered identically in all images.

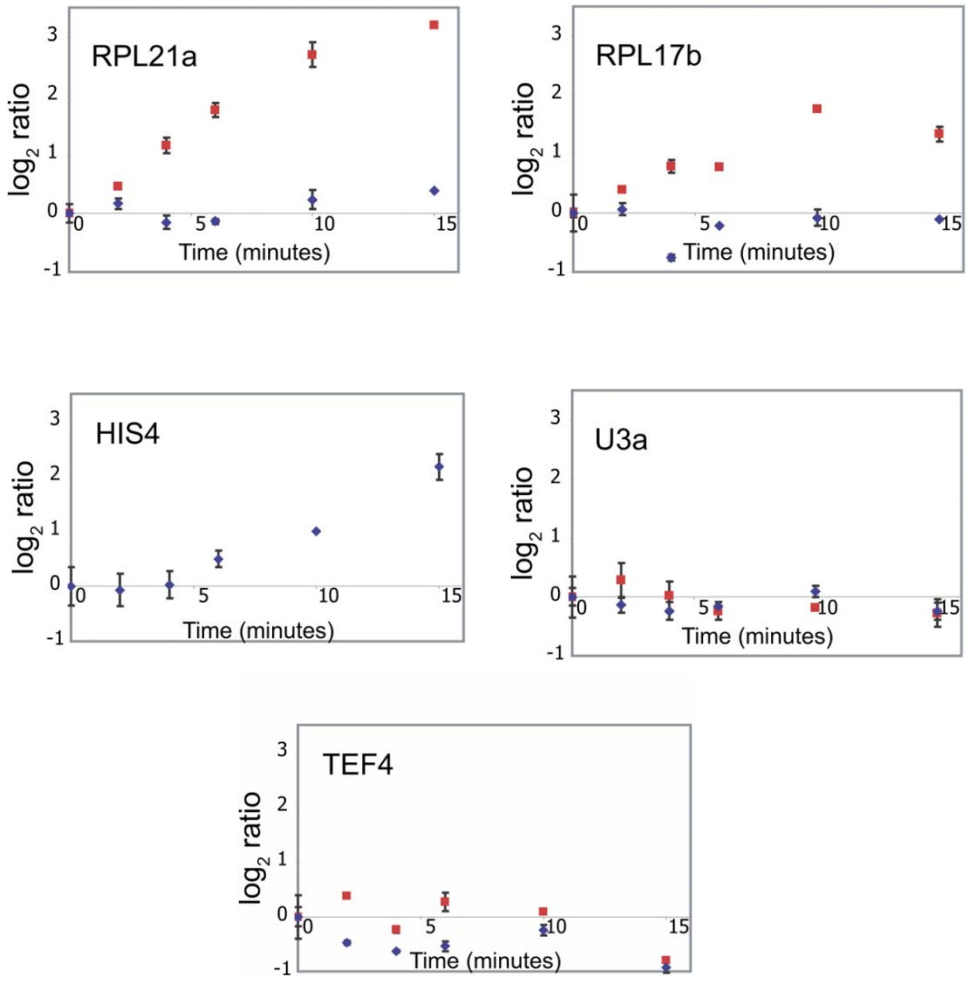

Figure 3. Quantitative RT-PCR validates the rapid, transcript-specific downregulation of splicing in response to amino acid starvation. The behaviors of RPL21a, RPL17b, HIS4, U3 snRNA, and TEF4 were examined using primers specific to intron regions (red squares) or exon regions (blue diamonds). Error bars are the result of triplicate measurements from a single biological sample.

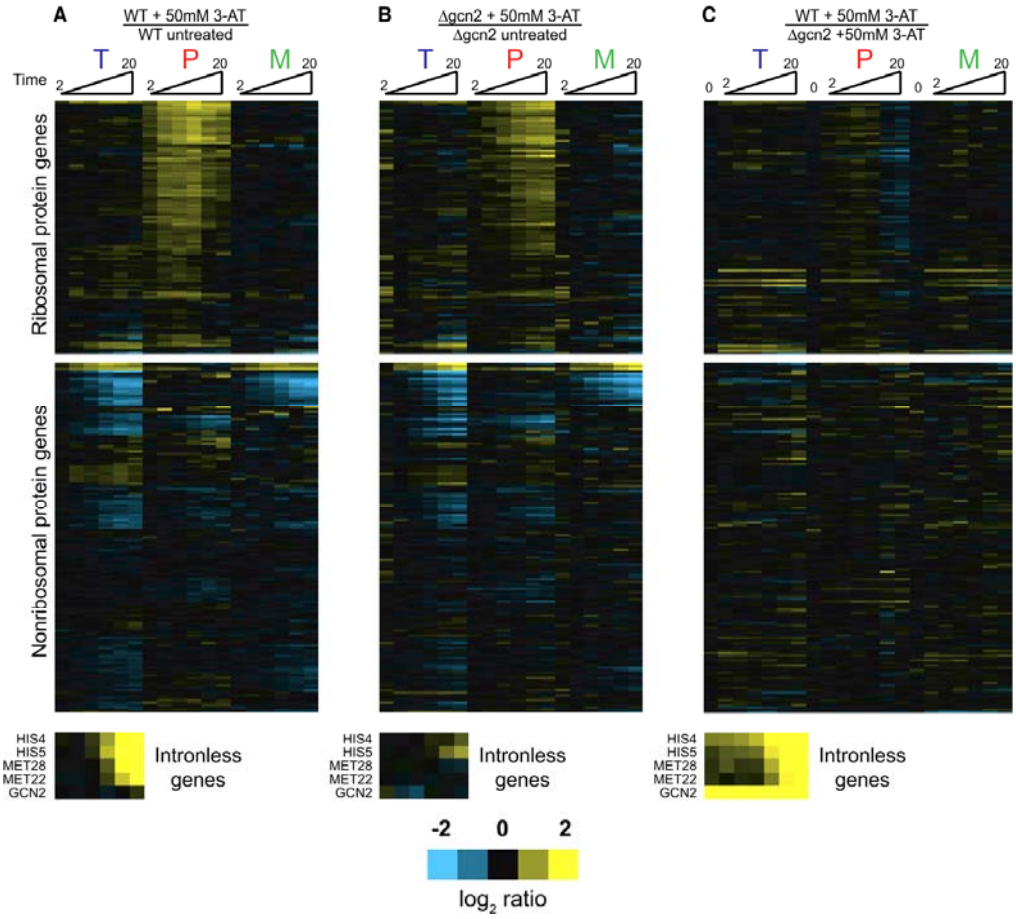

Figure 4. The splicing response to amino acid starvation does not require the activity of Gcn2. Time-resolved splicing profiles resulting from (A) wild-type cells treated with 50 mM 3AT compared to mock-treated, (B) cells deleted for *GCN2* treated with 50 mM 3AT compared to mock-treated, or (C) wild-type cells treated with 50 mM 3AT compared to cells deleted for *GCN2* treated with 50 mM 3AT. Included in the final set is a comparison of the wild-type strain with the *GCN2*-deleted strain in the absence of 3AT

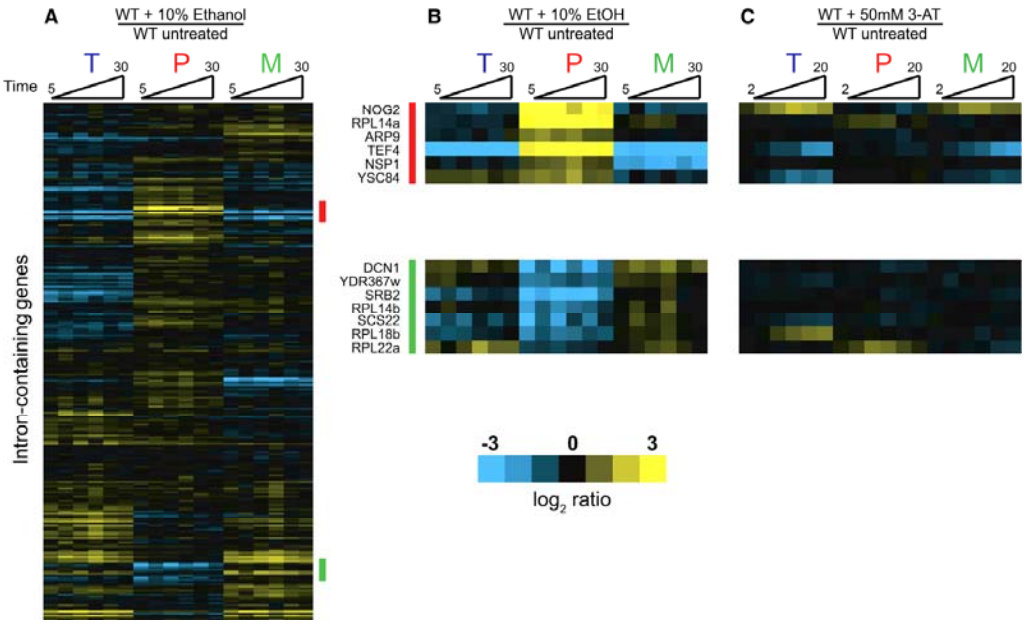

Figure 5. Regulation of pre-mRNA splicing in response to Ethanol Toxicity. A) Time-resolved splicing profiles resulting from comparisons of wild-type cells either treated with 10% ethanol or mock treated for 5, 10, 15, 20, 25, and 30 min. (B) Genes whose splicing is downregulated (top panel, also highlighted with a red bar in [A]) or upregulated (bottom panel, also highlighted with a green bar in [A]). (C) Behavior of genes highlighted in (B) in response to amino acid starvation.

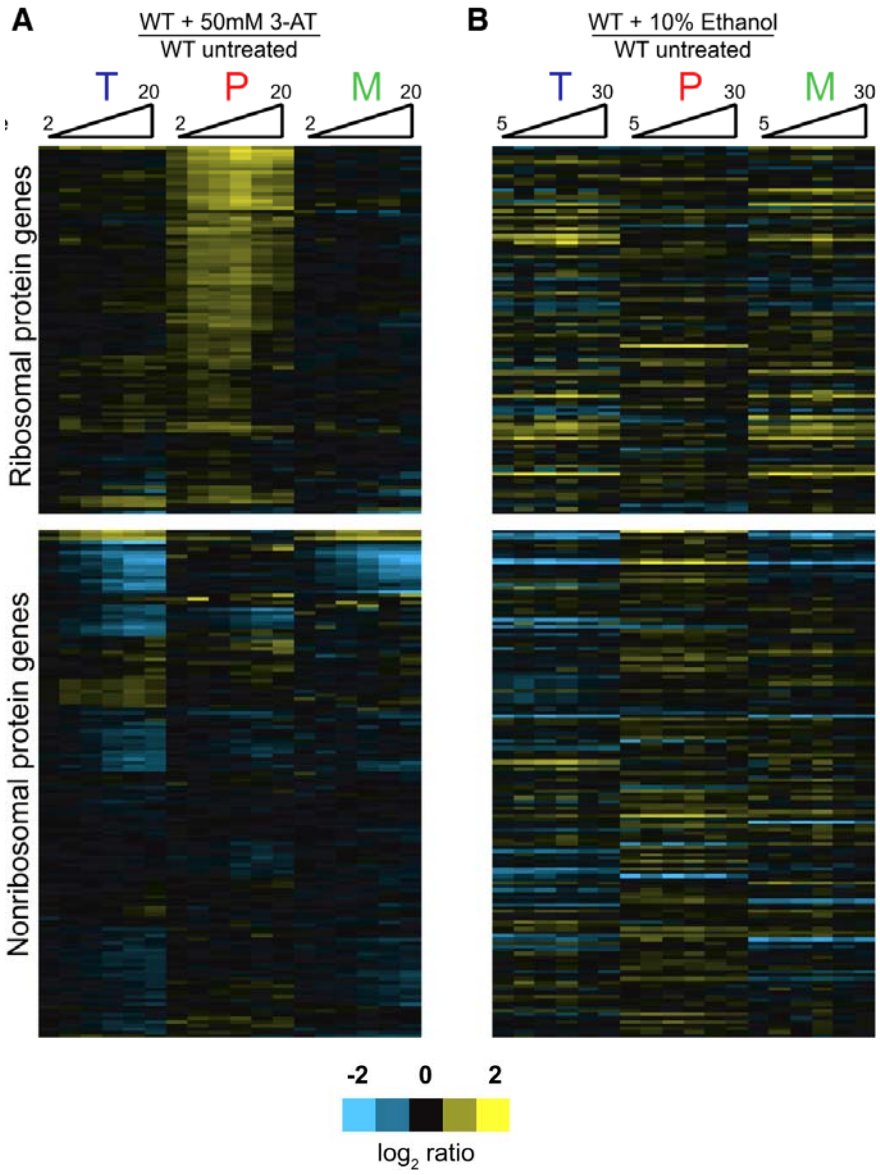

Figure 6. Comparison of splicing responses to amino acid starvation and ethanol toxcity. The order of genes is identical to that shown in Figure 2.

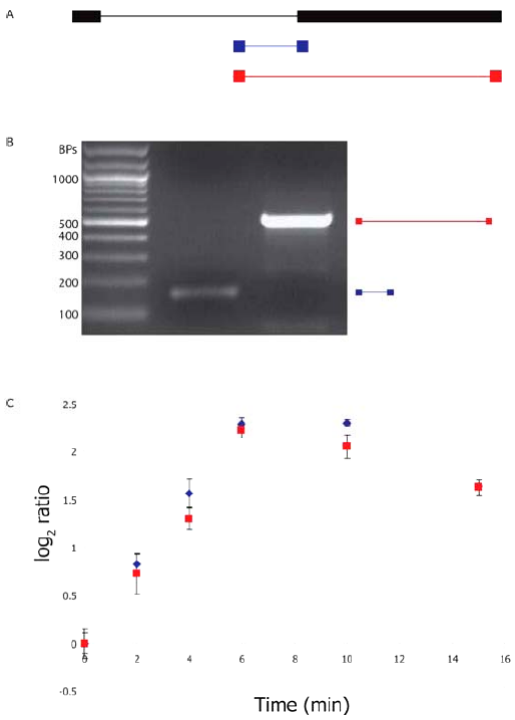

Supplemental Figure 1. Accumulation of pre-mRNAs as measured using different primers. (A) A scaled drawing of the architecture of the Rpl26a transcript is shown in black with exons denoted as boxes and the intron as a thin line. The locations of PCR primers are shown as boxes (blue and red), along with their products of amplification. (B) PCR products resulting from amplification using the primers depicted in (A). Expected product sizes are listed to the right of the gel. (C) Results of QPCR using the primers depicted in (A). Error bars are the result of duplicate measurements from a single biological sample.

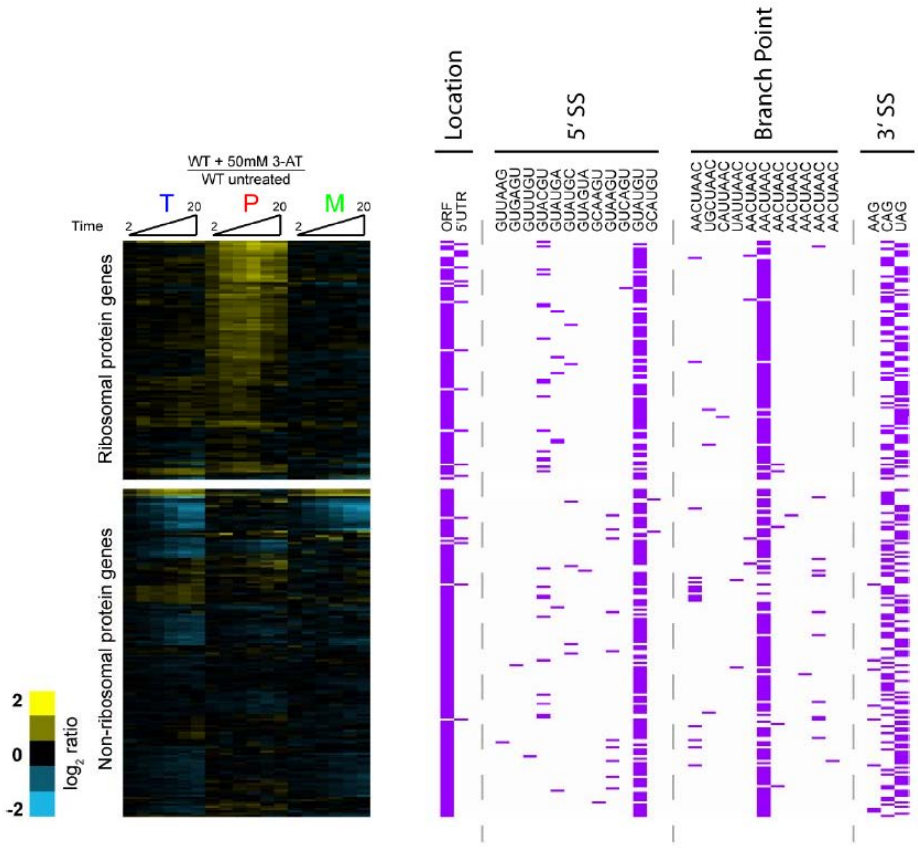

Supplemental Figure 2. Analysis of splice site sequences and transcript behavior following amino acid starvation. Purple hashes denote the locations of introns and the sequences present at their 5’ and 3’ splice sites and branch points.

Chapter 2

A Genetic Interaction Map of RNA Processing Factors Reveals Links Between Sem1/Dss1-Containing Complexes and mRNA Export and Splicing

Summary

We have used a quantitative, high-density genetic interaction map to interrogate functional relationships within and between RNA processing pathways. Due to their complexity, and the essential roles of many of the components, these pathways have previously been difficult to dissect. Here we report the results for 107,155 individual interactions involving 552 mutations, 166 of which are hypomorphic alleles of essential genes. Our data allowed for the discovery of links between components of the mRNA export and splicing machineries and Sem1/Dss1, a component of the 19S proteasome. In particular, we demonstrate that Sem1 has a proteasome-independent role in mRNA export as a functional component of the Sac3-Thp1 complex. We further show that Sem1 interacts with Csn12, a component of the COP9 signalosome. Finally, we show that Csn12 plays an unexpected role in pre-mRNA splicing, and that this role is independent of other signalosome components. Thus Sem1 is involved in three separate and functionally distinct complexes.

Introduction

Following the initial identification of yeast genes by the genome sequencing project (Goffeau et al., 1996), the phenotypic analysis of gene deletion mutations (Giaever et al., 2002), and the characterization of cellular protein complexes (Gavin et al., 2006; Krogan et al., 2006), an important next step toward a comprehensive understanding of cellular function is to place these complexes within specific *in vivo* pathways. Genetic interactions, which measure the extent to which the function of one protein depends on the presence of a second, can not only help place complexes in pathways but also provide information about the functional cross-talk between pathways and processes. Two approaches, synthetic genetic array (SGA) (Tong et al., 2001) and diploid based synthetic lethality analysis on microarrays (dSLAM) (Pan et al., 2004), have been developed to identify synthetic sickness/lethal (SSL) relationships on a genome-wide scale in *S. cerevisiae.* These approaches systematically reveal cases where two mutations in combination cause a more severe growth defect than that due to either mutation alone.

However, SSL interactions only represent a subset of the total possible genetic interactions. We recently exploited the SGA methodology to develop the E-MAP (epistatic miniarray profile) approach, which uses colony size of double mutants as a quantitative read-out. This allows for the characterization of the entire range of epistatic relationships, including both negative (i.e. SSL) and positive genetic interactions (Collins et al., 2007b; Schuldiner et al., 2005) (Roguev et al., 2008). Positive interactions

include cases where the double mutant is inferred to be either no sicker or actually healthier than the expected fitness of the sicker single mutant. The E-MAP method highlights the broad effects of perturbing biochemically distinct processes, and so gives a picture of how these cellular processes interact, while also resolving functional interactions at the level of the protein complex or pathway. It is ideally suited for analysis of RNA processing functions, which are biochemically complex, being separated temporally and compartmentally within the cell, but linked by many physically interacting protein complexes.

In this study, we used the E-MAP approach to generate a high density genetic interaction map for a large set of genes (~10% of the genome) that are collectively involved in virtually all aspects of RNA metabolism, including regulating and/or processing rRNAs, mRNAs, snoRNAs, snRNAs and tRNAs. Since many of the factors we genetically analyzed are required for cell viability, we created hypomorphic alleles, which allowed for an unprecedented view of the epistatic architecture of essential genes. We employed recently developed analytical tools for visualization of the quantitative genetic interaction data. This analysis provides a global view of the epistatic behavior within and between RNA-related processes as well as the genetic “cross-talk” between individual protein complexes that function within these processes. The network view allowed for the discovery of a number of previously uncharacterized functional connections. For example, this E-MAP allowed us to place the 19S proteasome subunit Sem1/Dss1 into two other functionally and physically distinct complexes: one involved in mRNA export and the other linked to mRNA splicing. We

fully anticipate that this dataset will be a useful resource to the RNA community both on its own and in conjunction with previously published E-MAP datasets (Collins et al., 2007b; Schuldiner et al., 2005) and protein-protein interaction datasets (Gavin et al., 2006; Ho et al., 2002; Krogan et al., 2006; Collins et al., 2007a) (http://interactome-cmp.ucsf.edu).

Results and Discussion

Generation of an RNA Processing Genetic Interaction Map

To genetically interrogate RNA processing in *Saccharomyces cerevisiae*, we created an E-MAP comprised of 552 mutations, each within a different gene involved in one of various RNA-related processes, including mRNA splicing and export, tRNA modification, translation, rRNA processing and RNA degradation (Figure 1A, Supplemental Figure 1). To facilitate comparison with other EMAPs, we also included sets of genes involved in other processes that indirectly impinge on RNA metabolism, including transcription, chromatin remodelling, and ubiquitin/protein degradation. Finally, we included a number of previously uncharacterized genes that have been functionally linked to RNA-related processes through unbiased, large-scale screens (Gavin et al., 2006; Krogan et al., 2006; Krogan et al., 2004; Tong et al., 2004). Since a large fraction of genes involved in these processes are essential for viability, we employed the DAmP (decreased abundance by mRNA perturbation) strategy (Schuldiner et al., 2005) to create 166 hypomorphic (partial loss of function) alleles of essential

genes (Figure 1A). In all, this genetic map contains 107,155 distinct, pair-wise genetic interaction measurements (http://interactome-cmp.ucsf.edu).

We subjected the entire dataset to hierarchical clustering, an approach that groups genes with similar patterns of genetic interactions. Several known protein complexes, such as the nuclear pore, Prefoldin, and a complex involved in nonsense mediated mRNA decay (NMD) are represented by distinct clusters (Supplemental Figure 1). Similarly, all six known components of the Elongator complex, which was initially linked to transcriptional elongation (Otero et al., 1999), cluster together. Furthermore, components of Elongator also cluster next to *TRM10*, a tRNA methyltransferase (Jackman et al., 2003), and display strong negative interactions with several other tRNA modifying enzymes (e.g. *ARC1* and *DEG1*), consistent with work implicating this complex in the regulation of tRNA modification (Esberg et al., 2006). Interestingly, the ubiquitin-like modifier *URM1* (Furukawa et al., 2000) also clusters with the components of Elongator, and recent work has suggested that Urm1p functions as a thiol group carrier important for thiol modification of tRNAs (Nakai et al., 2008; Schmitz et al., 2008) (Supplemental Figure 1).

Components of known spliceosomal subcomplexes, including the U1 snRNP (*MUD1*, *NAM8*, *PRP42* and *SNU56*) (Gottschalk et al., 1998; Neubauer et al., 1997) and the Prp19 associated Nineteen Complex (NTC) (*NTC20*, *ISY1*, *SYF2*, *PRP19*) (Chen et al., 2002) satisfyingly cluster together (Supplemental Figure 1). Two largely uncharacterized factors, *CWC21* and *CWC27*, also cluster with the NTC, consistent with work demonstrating that they physically associate with the NTC component Cef1 (Ohi

and Gould, 2002). Additionally, we identified many positive genetic interactions between the NTC and the U1 snRNP (Supplemental Figure 1), perhaps reflecting the fact that the U1 snRNP departs the spliceosome approximately when the NTC joins (Chan et al., 2003). Further investigation will be required to understand the implications of these and the many other genetic interactions contained within this E-MAP (http://interactome-cmp.ucsf.edu).

Global Analysis of Genetic and Physical Interaction Data

While inspection of the E-MAP genetic interaction datasets in isolation have already yielded many interesting observations, analysis of these data in conjunction with published high throughput protein-protein interaction datasets promises to be especially powerful. We have shown in other E-MAPs that genes exhibiting positive genetic interactions are more likely than expected by chance to encode proteins that have physical interactions (Collins et al., 2007b; Roguev et al., 2007), and inspection of the data from the RNA processing E-MAP revealed a similar overrepresentation of factors with protein-protein interactions (PPIs) among pairs of factors with positive genetic interactions. Protein-protein interactions were defined by tandem affinity purification (TAP)-derived purification enrichment (PE) scores of > 1.0, as described previously (Collins et al., 2007a). However, in contrast to what has been observed in other EMAPS, there is also an enrichment of PPIs among factors displaying negative genetic interactions (Figure 1B). Notably, the RNA processing E-MAP greatly expands the

number of components of essential complexes that have been interrogated by the E-MAP technique, both by including many non-essential factors that participate in several large essential complexes, and by including a large number of hypomorphic alleles of essential factors. This difference from previous E-MAPs may at least in part account for the more prevalent negative genetic interactions observed among physically interacting factors. Indeed, a recent analysis of a previously published E-MAP focused on chromosome biology showed that complexes dominated by negative genetic interactions are more likely to contain at least one essential gene (Bandyopadhyay et al., 2008).

Interestingly, the hypomorphic alleles of essential genes that are included in this E-MAP do not generally have more negative genetic interactions than the non-essential genes when each of these subsets is considered as a whole. We compared the ratio of negative ($S \leq -2.5$) to positive ($S \geq 2.0$) genetic interactions (N to P) involving either pairs of non-essential genes or pairs where at least one gene is essential (Figure 1C, see Experimental Procedures). In the entire dataset, we found an N to P ratio of ~1, regardless of whether the mutant pairs contained at least one essential gene (1.00) or not (1.29). However, when we restricted the analyses to genes whose corresponding proteins are physically associated (as defined above), we found that the genetic interactions observed with essential genes are over three times as likely to be negative (N to P =2.84, p=.0003) (Figure 1C; Supplemental Table 2) compared to interactions between null mutations of non-essential genes (N to P =0.93).

These observations suggest that the introduction of two mutations in the same

essential complex is very likely to have a synthetic negative effect on growth, whereas a second mutation in a non-essential complex is unlikely to have a further detrimental effect above that caused by the first mutation, and may indeed improve growth. Thus, a positive interaction observed between two factors that physically interact within an essential complex may suggest that these factors form a non-essential module within the complex. One example of this is the positive interaction between IST3 and BUD13, which have been suggested to physically interact with both the non-essential RES complex and with the essential SF3b complex of the spliceosome (Dziembowski et al., 2004; Wang et al., 2005). Our data support the model that IST3 and BUD13 function as a non-essential module in these complexes.

While factors with protein-protein interactions are overrepresented among the strong genetic interactions observed in the RNA processing E-MAP, there are also certainly many genetic interactions between factors that have functional, but not physical, interactions. Indeed, these interactions comprise a powerful tool for discovering previously uncharacterized pathways connecting protein complexes. However, visualizing the relative contributions of within-complex and between-complex genetic interactions to the overall interaction landscape is a complicated problem. To address this, we used an approach we have recently described (Bandyopadhyay et al., 2008) that classifies protein pairs as either operating within the same module or between functionally related modules given their genetic and physical interactions (see Experimental Procedures for a more detailed description of the analyses). In the resulting representation, blue and yellow denote a statistically significant enrichment of

negative and positive interactions, respectively, whereas green corresponds to cases where there are significant enrichments in total interactions, but the numbers of positives and negatives are roughly equal. Nodes (boxes) correspond to complexes and edges (lines), the genetic cross-talk between the complexes (Figure 2A).

Several interesting connections become evident when the data are analyzed in this way. For example, there are negative genetic interactions (blue line) between the chromatin remodeling complex, SWR-C, which incorporates the histone H2A variant, Htz1, into chromatin (Kobor et al., 2004; Krogan et al., 2003; Mizuguchi et al., 2004), and the nuclear pore factors Mex67-Nup120, consistent with recent work demonstrating that Htz1 is involved in tethering genes to the nuclear periphery (Brickner et al., 2007). Also, we found positive genetic interactions (yellow line) between the complex containing both casein kinase II (CKII) and the chromodomain-containing protein Chd1, and the spliceosome. Consistent with this finding, Reinberg and colleagues found a physical and functional connection in human cells between Chd1 and the spliceosome (Sims et al., 2007). There are many testable hypotheses that can be extracted from this data set in this format and we have created an interactive website that allows for searching of individual interactions as well as the connections between complexes (http://www.cellcircuits.org/complexes/RNAProcessing/html/).

In an effort to gain insight into the functional organization of RNA-related processes at an even broader level, we created a map that highlights strong genetic trends both within and between these processes, without respect to known physical interactions (Figure 2B). Nodes (boxes) now correspond to the interactions within

distinct functional processes (defined by a combination of GO term analysis and manual annotation) whereas edges (lines) represent the genetic cross-talk between processes.

A striking finding is that several sets of genes that are known to function in the same biochemical processes contain predominantly positive or predominantly negative interactions, as was also observed in an analysis of the computed epistatic behavior among yeast metabolic genes (Segre et al., 2005). For example, genes classed as involved in cytoplasmic rRNA biogenesis and mitochondrial rRNA biogenesis are significantly enriched in positive genetic interactions (Figure 2B yellow nodes). In contrast, factors involved in mRNA splicing, mRNA export and the nuclear pore have strongly negative interactions (blue nodes). Finally, not all groups show consistent patterns of interactions; for instance, RNA degradation, tRNA biogenesis and transcription show mixed but still significant genetic interactions (green nodes). The broad trends that emerge when the data are viewed in this way suggest that the patterns of genetic interactions are influenced not only by direct physical interactions between factors and direct functional interactions between complexes, but also probably by higher-level interactions within and between processes.

The Sem1/Dss1 Component of the Proteasome is Involved in mRNA Export Via the Sac3-Thp1 Complex

Our E-MAP uncovered positive genetic interactions between the proteasome and the Sac3-Thp1 (TREX-2) complex involved in mRNA export (Figure 2A), suggesting that a direct functional relationship may exist between these two complexes. We

confirmed that these positive interactions represented suppressive relationships through tetrad analysis and dilution growth assays at 16°C (Supplemental Figure 2). The proteasome is a large molecular machine that degrades ubiquitylated substrates (Collins and Tansey, 2006) and is concentrated at the nuclear periphery in yeast (Enenkel et al., 1998; Wilkinson et al., 1998). During the process of mRNA export, multiple components of the Mex67-mediated export pathway interact with the nuclear pore basket via the Sac3-Thp1 complex (Luna et al., 2008).

To investigate the significance of the genetic connections between the proteasome and the Sac3-Thp1 mRNA export complex, we compared their global genetic interaction patterns from the E-MAP. The genetic interaction profiles we obtained for *SAC3* and *THP1* are extremely similar (correlation coefficient = 0.7), consistent with their known biochemical and functional interactions (Fischer et al., 2002; Gallardo et al., 2003). After each other, the genetic interactions of *SAC3* and *THP1* are most similar to those of the nuclear pore components *NUP60* and *NUP120*, *THP2* (a component of the THO/TREX complex that co-transcriptionally associates with the mRNP), and, interestingly, the proteasome lid component *SEM1* (Figure 3A and http://interactome-cmp.ucsf.edu/). In contrast, the genetic profiles of other components of the proteasome (e.g. *RPN10*, *PRE9* and *RPN4*) do not correlate with these export factors. *SEM1* differs from other proteasome mutants in sharing many genetic interactions with *THP1-SAC3*, including negative ones with the exosome (*LRP1*, *RRP6*), nuclear pore (*NUP100*, *NUP120*, *NUP60*, *NUP57*) and other factors implicated in mRNA export (such as *MEX67*, *APQ12*, *DBP5*) (Figure 3B and Supplemental Figure 1).

These genetic data suggest that Sem1 may act as an export factor in *S. cerevisiae,* and so we directly tested whether deleting *SEM1* affected mRNA export. Deletion of either *SAC3* or *THP1* results in a substantial increase of polyadenylated mRNA in the nucleus (Fischer et al., 2002; Gallardo et al., 2003; Lei et al., 2003). We found that deletion of *SEM1* also results in a moderate mRNA export defect at 25°C, 30°C and 37°C (Figure 3C and data not shown), suggesting a direct role for Sem1 in mRNA export. This is consistent with previous work in fission yeast (Mannen et al., 2008; Thakurta et al., 2005). Interestingly, we found that deletion of *SEM1* in the *thp1*Δ background not only partially suppresses its growth defect at 16°C (Supplemental Figure 2) but also reduces the intensity of the mRNA export phenotype compared to *thp1*Δ alone (Figure 3C).

However, deletion of proteasome factors other than *SEM1* (*RPN10*, *PRE9*, *UBP6*, *DOA1*, *RPN4*), or inhibition of the proteasome by the drug MG132 in a *pdr5Δ* background (which allowed for more efficient uptake of the drug), do not cause an mRNA export defect in this assay (Figure 3C and data not shown). Furthermore, although *RPN10* deletion exacerbates the growth, proteasome integrity and DNA damage response defects of a *sem1Δ* strain (Funakoshi et al., 2004; Sone et al., 2004), we found no significant effect on *sem1Δ*'s moderate mRNA export defect (Figure 3C). Together, these data argue that Sem1 is directly involved in mRNA export, but other components of the proteasome are not.

We next asked whether Sem1 is physically associated with the Sac3-Thp1 complex. Since we found that introducing a tag on the C-terminus of Sem1 results in a

defect in mRNA export (data not shown), we used a polyclonal antibody (Funakoshi et al., 2004) to immunoprecipitate or detect Sem1 from cellular extracts of a panel of GFP-tagged strains. Both Thp1-GFP and Sac3-GFP reciprocally co-immunoprecipitate with Sem1 (Figure 3D and Supplemental Figure 3). Consistent with previous results, GFP-tagged Rpt4, a 19S proteasome component, co-immunoprecipitates both Sem1 and Rpt6, another known component of the proteasome (Funakoshi et al., 2004; Krogan et al., 2004; Sone et al., 2004). In contrast, Sac3-GFP and Thp1-GFP are not associated with Rpt6 (Figure 3D), strongly suggesting that Sem1 interacts with Sac3-Thp1 independent of the rest of the proteasome. Previous work in *S. pombe* suggested physical associations between Dss1 (*S. cerevisiae* Sem1) and other mRNA export factors, including Nup159, Rae1 (*S. cerevisiae* Gle2), and Mlo3 (*S. cerevisiae* Yra1) (Thakurta et al., 2005); however, we do not detect these physical connections in budding yeast (Figure 3E and data not shown). We also do not find Sem1 associated with TREX (e.g. Thp2) or the transcriptional activation complex SAGA (e.g. Ada2), both of which are complexes that have been reported to interact with Sac3-Thp1 (Fischer et al., 2002; Rodriguez-Navarro et al., 2004). Finally, the physical interaction between Sac3-Thp1 and Sem1 is insensitive to RNAse A treatment (Figure 3D and data not shown), suggesting that this interaction is not mediated by RNA.

To gain further insight into the physically interacting partners of Sem1, we analyzed data from our earlier large-scale protein-protein interaction project that used a systematic affinity tagging, purification and mass spectrometry approach to identify protein complexes (Krogan et al., 2006). After components of the proteasome, the

proteins that most significantly immunoprecipitated Sem1 as prey were Csn12, a component of the CSN (COP Nine Signalosome, another large complex with structural similarity to the proteasome lid), and Ypr045c, an uncharacterized protein, both of which also co-purified with each other (http://tap.med.utoronto.ca/). We confirmed the Sem1-Csn12 and Sem1-Ypr045C interactions by co-immunoprecipitation (Figure 3D). Together with our Sac3-Thp1-Sem1 results, these physical interactions suggest that Sem1 may be part of at least three functionally distinct complexes in *S. cerevisiae*: the 19S proteasome (Funakoshi et al., 2004; Krogan et al., 2004; Sone et al., 2004), Sac3-Thp1, and a complex containing Csn12 and Ypr045c (see Figure 5). This is consistent with previous glycerol gradient fractionation data showing that a significant fraction of the Sem1 in the cell is contained in complexes smaller than the proteasome (Funakoshi et al., 2004). These complexes are all likely to be conserved, as a purification of protein complexes associated with human Dss1 identified two metazoan-specific complexes and components of all three *S. cerevisiae* complexes that we describe here (Baillat et al., 2005). Furthermore, *S. cerevisiae* or human Sem1/Dss1 can complement a *dss1Δ* strain for mRNA export in *S. pombe* (Thakurta et al., 2005).

Examining the domain structure of Sem1-interacting proteins suggests a model for how Sem1 associates with each of these complexes. Rpn3, Thp1, and Csn12 are the only three proteins in *S. cerevisiae* that harbor the PAM (PCI-Associated Module) domain (Ciccarelli et al., 2003), a highly conserved region upstream of a subset of PCI domains (protein interaction domains named after three complexes rich in these domains: the proteasome, the CSN, and eIF3) (Hofmann and Bucher, 1998; Scheel and

Hofmann, 2005). Similarly, Rpn12, Sac3, and Ypr045c are the only three proteins in *S. cerevisiae* that contain a highly conserved variant of the PCI domain, called the SAC3 domain (PFAM database (Finn et al., 2006) # PF03399) (Figure 5). Indeed, the region of Sac3 that interacts with Thp1 was mapped to a small section containing the SAC3 domain (Fischer et al., 2002). Furthermore, a number of studies have placed Rpn3, Rpn12, and Sem1 in a subcomplex within the proteasome lid (Fu et al., 2001; Isono et al., 2005; Sharon et al., 2006). Sem1 crosslinks directly to Rpn3 *in vivo* (Sharon et al., 2006), and binds to Rpn3 *in vitro* (Wei et al., 2008). Thus, these domains suggest a model that Sem1 may be interacting with PAM and/or SAC3 domains in multiple large protein complexes.

Indeed, our results raise the intriguing possibility that the SAC3 and PAM domains may in fact bind to one another, and in turn, recruit Sem1. Consistent with this notion, we found that both Sac3 and Thp1 are required for the other to interact with Sem1 (Figure 3D and Supplemental Figure 3). Previous studies have suggested that Sem1 is involved in stabilizing protein complexes. One of the metazoan-specific Sem1/Dss1 containing complexes, that containing BRCA2, is unstable unless Dss1 is co-purified (Li et al., 2006; Yang et al., 2002). The proteasome is also unstable in cells lacking Sem1 (Funakoshi et al., 2004; Sone et al., 2004), although a recent study suggests that this instability does not stem from abrogation of the PAM-domain (Rpn3)-SAC3-domain (Rpn12) interaction (Wei et al., 2008). In the presence of 1M salt, the proteasome falls apart in a *sem1Δ* strain (Sone et al., 2004). In contrast, we find that in the absence of Sem1, Sac3-GFP still remains associated with immunoprecipitated Thp1-

HA in the presence of at least 1 M NaCl (Figure 3E). Consistent with these data, we find that the localization of Thp1 to the nuclear envelope is not strongly affected by *sem1Δ*, in contrast to *sac3Δ* , which results in its complete mislocalization ((Fischer et al., 2002) and data not shown). Thus, these data suggest that Sem1 has roles other than simply stabilizing protein complexes.

The Sac3-Thp1 mRNA export complex is implicated in the pathway that loads the export receptor Mex67 (or TAP in higher eukaryotes) onto mRNAs, and our genetic, functional, and physical data suggest that Sem1 may act as part of the Sac3-Thp1 complex. Sub2 and Yra1 are co-transcriptionally loaded onto mRNAs as part of the THO/TREX complex, and Yra1 acts as an adaptor protein to load Mex67 onto the mRNP to making it competent for export (Luna et al., 2008). Because Yra1 can interact with either Sub2 or Mex67, but not both simultaneously, Sub2 may be exchanged for Mex67 (Strasser and Hurt, 2001) (Figure 3G). To investigate the role of Sac3-Thp1-Sem1 in RNP formation, we UV crosslinked proteins to RNA *in vivo*, made cell extracts, purified the poly(A) RNA over an oligo dT cellulose column, and then examined protein components in the resulting poly(A) eluates in wild-type and mutant backgrounds. In a wild-type strain, low levels of Sub2, Yra1, and Mex67 can be detected crosslinked to poly(A) mRNA in a UV-dependent manner (Figure 3F). Deletion of *SEM1*, *THP1* or *SAC3* all result in a significant accumulation of Sub2 and Yra1 on polyA mRNA, whereas Mex67 binding increases only modestly in all three cases (Figure 3F and data not shown). In contrast, large quantities of Mex67, but not Yra1, accumulate on mRNA when it is blocked at the nuclear periphery in a *dbp5,rrp6* double mutant (Lund and

Guthrie, 2005). These data suggest that the Thp1-Sac3-Sem1 complex facilitates the exchange of Sub2 for Mex67 (Figure 3G). The modest increase in Mex67 association may reflect a partial block during Mex67 loading, or may reflect aberrant binding of Mex67 to the particularly large amounts of Yra1 that appear to be accumulating on the mRNA. Although further work will be required to identify the exact role that this complex plays in the export pathway, our data argue that Sem1 is acting in concert with Sac3-Thp1 to load Mex67 onto mRNA.

The Csn12 Component of the COP9 Signalosome is Involved in mRNA Splicing

The functions of two of the three Sem1-containing complexes (the proteasome and Sac3-Thp1) were known, so we used the E-MAP, in conjunction with physical interaction data, to gain insight into the function of the Csn12-Ypr045c complex. Csn12 was previously described as a subunit of the COP9 signalosome (CSN), a complex responsible for the removal of the Rub1 modifier (known as Nedd8 in higher eukaryotes) from cullin proteins, which are components of various E3 ubiquitin ligase complexes (Maytal-Kivity et al., 2003). However, deletion of *CSN12* fails to cause accumulation of neddylated Cdc53p, a phenotype observed in all other mutants of CSN subunits (Wee et al., 2002). Inspection of the quantitative genetic interaction data revealed that *CSN12* is most similar genetically to components of the spliceosome. For example, the profile of genetic interactions of *csn12*Δ is highly correlated with that of *isy1*Δ and also several other mRNA splicing factor mutants, including *syf2*Δ, *prp11*-DAmP, *ist3*Δ, *snu66*Δ and *prp19-DAmP*, whereas deletions of other components of the

CSN display very different genetic interaction profiles (Figure 4A). Consistent with a functional link between Csn12 and the spliceosome, large-scale protein TAP studies identified a physical link between only this component of the CSN and many factors involved in mRNA splicing (Collins et al., 2007a; Gavin et al., 2006; Krogan et al., 2006).

To test whether Csn12 plays a functional role in mRNA splicing, we used a splicing-specific microarray to measure the levels of pre-mRNA, mature mRNA, and total mRNA for most of the intron-containing genes in the yeast genome (Pleiss et al., 2007). In general, a decrease in splicing efficiency for a given transcript results in an accumulation of its pre-mRNA, and often in a measurable loss of mature mRNA (Clark et al., 2002; Pleiss et al., 2007). We examined the splicing efficiencies of *isy1*Δ, *csn12*Δ, and *ypr045c*Δ (the SAC3 domain-containing protein that physically interacts with Csn12) as well as deletions of *CSN9* and *PCI8*, two other components of the CSN. As expected, deletion of *ISY1* causes a substantial accumulation of pre-mRNA for many intron-containing genes (Figure 4B). Interestingly, deletion of either *CSN12* or *YPR045c* causes a pre-mRNA accumulation in many of the same transcripts adversely affected in the *isy1*Δ strain (Figure 4B). In contrast, *csn9*Δ and *pci8*Δ strains fail to show a splicing defect (Figure 4B). We also failed to detect a splicing defect in the *sem1*Δ strain (data not shown). It may be that under the conditions tested, the loss of Sem1p does not significantly impair the function of the Csn12-Ypr045c complex in splicing.

In order to more quantitatively assess the similarity of the splicing microarray profiles observed with *csn12*Δ and *ypr045c*Δ to those obtained from well characterized splicing factors, we calculated pairwise Pearson correlation coefficients between a

number of mutant pairs using the ratios from all of the microarray features reporting on intron-containing genes (Figure 4C). As previously reported, various splicing factor mutations result in a wide range of splicing phenotypes (Pleiss et al., 2007). The splicing microarray profiles of the *csn12*Δ and *ypr045c*Δ strains are highly correlated with each other as well as with the profiles of a number of well-characterized splicing factor mutants (e.g. *prp2-1*, *prp16-302*, *prp8-1*, *ist3*Δ, *isy1*Δ), whereas *csn9*Δ and *pci8*Δ exhibit distinct behavior on the splicing array (Figure 4C). Thus, Csn12 and Ypr045c, but not other components of the CSN, are involved in maintaining normal levels of mRNA splicing.

Perspective

In this study, we generated a quantitative genetic interaction map in budding yeast that is focused on virtually all aspects of RNA processing and includes factors implicated in the generation and regulation of tRNAs, mRNAs, rRNAs, snoRNAs and snRNAs. We have applied novel analytical tools that allow for the visualization of the genetic crosstalk between the different RNA-related processes and the protein complexes that function within these processes. Using these representations and other data exploration tools such as hierarchical clustering and searchable databases, we predicted and experimentally verified several novel biological connections as examples of how this data can be mined. Along with the examples explored here, we also found a strong link between Npl3, an SR domain-containing protein involved in mRNA export, and mRNA splicing (see Kress etal., in press).

The large amount of genetic data from the E-MAP is even more useful when analyzed in combination with other large data sets, including other E-MAPs (Collins et al., 2007b; Schuldiner et al., 2005) and physical interaction data sets such as the TAP database (Collins et al., 2007a; Gavin et al., 2006; Ho et al., 2002; Krogan et al., 2006) (http://interactome-cmp.ucsf.edu). This approach allowed us to identify two novel protein complexes containing the 19S proteasome component Sem1, one of which (Sac3-Thp1) acts in mRNA export, and one of which (Csn12-Ypr045c) acts in mRNA splicing (Figure 4). We failed to detect an mRNA export defect in both *csn12*Δ and *ypr045c*Δ, and we failed to detect a splicing defect in both *sac3*Δ and *thp1*Δ (data not shown), suggesting that these two complexes are functionally distinct despite sharing Sem1 as a common component.

SEM1 has positive genetic interactions with *SAC3*, *THP1*, *CSN12*, and *YPR045C*, consistent with the global pattern observed when we interrogated the entire data set, whereby factors that share physical interactions in non-essential complexes tend to have positive genetic interactions. By contrast, *SEM1* has mainly negative genetic interactions with components of the proteasome, which is essential. *SAC3* and *THP1* have positive genetic interactions with each other, as do *CSN12* and *YPR045C*, again consistent with the observed pattern. Interestingly, the interactions between components of different Sem1-containing complexes were largely positive, possibly reflecting crosstalk mediated by the shared Sem1 component (Supplemental Figure 1). Both the genetic and functional data confirmed a role for Sem1 in mRNA export, but we did not observe a splicing defect in the *sem1Δ* strain (data not shown). The

genetic interactions of *SEM1* with *CSN12* and *YPR045C* are weaker than those observed with *SAC3* and *THP1*, and the splicing defect caused by deletion of *CSN12* or *YPR045C* is mild compared to the dramatic export defect caused by deletion of *SAC3* or *THP1*. It may be that the rich growth conditions under which these studies were performed do not strongly necessitate the function of the Csn12-Ypr045c-Sem1 complex. Alternatively, Sem1's function in this complex may be related to a still undiscovered splicing-independent role. Further studies will be required to better understand the role of this complex in splicing, and the conditions under which its function is most relevant.

The links reported here between Sem1 and multiple mRNA processes suggest a model for Sem1 action in multiple distinct complexes. We favor a model in which Sem1/Dss1 acts as a nucleic acid analog, modulating access between nucleic acids and the protein complexes with which they interact. The proteasome has been suggested to play roles in transcription activation, DNA repair, and RNA degradation (Ezhkova and Tansey, 2004; Ferdous et al., 2001; Gautier-Bert et al., 2003; Gonzalez et al., 2002), all of which would involve interactions with nucleic acids, which could be facilitated at least in part by Sem1. Indeed, inspection of a co-crystal of human Dss1 with the metazoan22 specific breast cancer protein BRCA2 and ssDNA led to a similar model, in which Dss1 might modulate access of ssDNA to BRCA2 during double strand break repair.

Sem1/Dss1 is a small (10 kD) extremely acidic protein, with physical characteristics strikingly similar to those of nucleic acids (Yang et al., 2002). It has recently been shown that a small patch of conserved very acidic residues in Sem1 is necessary and sufficient to mediate interaction with a PAM domain-containing protein

(Rpn3) (Wei et al., 2008). Therefore, it is tempting to speculate that it could act as both an RNA and DNA chaperone, facilitating the association of nucleic acid with several complexes. Further work will be required to elucidate the biophysical details of such interactions.

Finally, combining the unbiased genetic map with physical interaction data suggests functions for several previously uncharacterized proteins. For example, *YNR004W* encodes a small protein that has no identifiable domains or homology, but deletion of this non-essential gene causes a similar genetic interaction profile to that seen with *tgs1*Δ, a protein that trimethylates snoRNA and spliceosomal snRNA caps (Mouaikel et al., 2002). Both *TGS1* and *YNR004W* cluster with components of the spliceosome (Supplemental Figure 1), and a two-hybrid interaction has been reported for the corresponding pair of proteins (Uetz et al., 2000). Strikingly, we have found that deletion of *YNR004W* causes a nearly identical splicing defect to that observed with *tgs1*Δ (Supplemental Figure 4). These data suggest that Ynr004w functions directly with Tgs1 to ensure proper tri-methylation of snRNA caps. A number of other currently unnamed open reading frames included in the E-MAP display strong patterns of genetic interactions suggestive of roles in specific processes, providing numerous directions for further experimentation.

In order to facilitate further data-mining by the RNA community, we have developed an interactive and searchable web-based database (http://interactome-cmp.ucsf.edu). One can query single mutants for individual genetic interactions or for other factors that share similar genetic interaction profiles. This database is integrated

with the results from previous E-MAPs, allowing a wealth of information from different fields to be cross-referenced. Additionally, an interface for navigating the higher-level analysis of interactions between complexes has been developed, and is linked to from within the database (http://www.cellcircuits.org/complexes/RNAProcessing/html/). We anticipate that this dataset will be used as a resource by others to launch more detailed investigations into the biology of RNA processing.

Experimental Procedures

E-MAP analysis

Strains were constructed and E-MAP experiments were performed as previously described (Collins et al., 2007b; Collins et al., 2006; Schuldiner et al., 2005).

Functional connections between processes and complexes

For analysis of connections between related processes, 446 genes were classified with one of 12 functions, using a combination of GO annotations and manual curation. The median genetic interaction score of protein pairs spanning two processes or within the same process was compared to equal sized random samples of genetic interactions. A cutoff of $p<0.001$ was used for the between-process connections and a cutoff of $p<0.05$ was used for connections within a process. Enrichments for strong (both positive and negative) interactions were computed by comparison of the median of the absolute values of the S-scores to the absolute value of a random distribution with a $p<0.001$. Complexes involved in RNA processing were identified using previously described

methods (Bandyopadhyay et al., 2008). This analysis categorizes interactions supported by both strong genetic and physical evidence as operating within a module, or complex. Interactions with a strong genetic but weak physical signal are better characterized as operating between two functionally related modules. Given within- and between-module likelihoods for individual interactions, an agglomerative clustering procedure seeks to merge these interactions into increasingly larger modules and to identify pairs of modules interconnected by many strong genetic interactions. Pairs of functionally related complexes and genetic interactions within a complex were then categorized through analysis of their pairwise genetic interaction distributions as described above.

Yeast Genetics

Yeast were grown and double deletions made according to standard methods (Guthrie and Fink, 2002). For serial dilution growth tests, cells were grown to log phase and diluted to OD 0.1, and then serially diluted by one fifth. Serial dilutions were transferred onto YPD and incubated at 16°C for 7 days.

In Situ Hybridizations and Microscopy

In situ hybridizations were performed as described previously with a few modifications (Duncan et al., 2000). Briefly, cells were grown to OD 0.15-0.25 in YEPD, and fixed for one hour in 5% formaldehyde, spheroplasted with zymolyase 100T (Seikagaku Corporation), fixed briefly with paraformaldehyde and permeabilized with cold methanol. Bulk polyadenylated RNA was detected by in situ hybridization with approximately 10 ng of digoxigenin-11-dUTP (Roche) labeled oligo dT50 probe followed by staining with anti-digoxigenin-fluroescein Fab fragments (Roche) (1:25). In

parallel, cells were treated with secondary antibody and no probe. Cells were mounted in SlowFade Gold antifade reagent with DAPI (Invitrogen). Images were collected on an Olympus BX-60 microscope with a 100x Olympus UPlanFI NA 1.30 objective and appropriate filters with a Sensys CCD camera (Photometrics) and analyzed using iVision imaging Software (Biovision Technologies). All strains were analyzed at least three times, and all images within a set were treated identically.

Immunoprecipitations

Twenty-five mLs log phase cultures of cells from the GFP tagged collection (Huh et al., 2003) were washed and resuspended in lysis buffer containing 50 mM Tris HCl pH 7.5, 150 mM NaCl, 0.1 % NP40, and protease inhibitors, and lysed by vigorous shaking with glass beads. Immunoprecipitations between Sem1 and Thp1GFP were stable in buffer containing up to at least 1 M NaCl. Extracts were clarified by centrifugation at 10,000 g for 8 minutes, an input sample was removed and the extracts were immunoprecipitated overnight with 1 µL polyclonal antibody to Sem1 (Funakoshi et al., 2004) (generous gift of Hideki Kobayashi), or 2 µg monoclonal antibody to GFP (Roche) followed by a one hour incubation with 30 µL of a 50% slurry of IgG beads (Amersham). The beads were washed 5 times with lysis buffer and resuspended in 1X SDS sample buffer. Western blots were then probed for Sem1 (1:1000), GFP (1:2000), and Rpt6/Sug1 (1:1000) (generous gift of Thomas Kodadek), or HA (12CA5 Roche). For RNAse A treatment, either 25 µg of RNAse A was added to extracts for 10 min at room temperature, or the extracts were mock treated, and a total RNA sample was analyzed by agarose gel electrophoresis to check degradation of total RNA. All immunoprecipitations were

performed at least three times.

UV Crosslinking Assay

Cells were grown to OD 0.8 and subjected to UV crosslinking, extract preparation, and poly(A) RNA purification performed as in (Gilbert et al., 2001). Western blots were then probed for Mex67 (1:10000, generous gift of Catherine Dargement), Sub2 (1:2000, polyclonal antisera specific to Sub2 produced in the lab), and Yra1 (1:2000, generous gift of Douglas Kellogg).

Splicing Microarrays

Splicing microarray sample collection, data analysis, and arrays are as previously described with the following modifications (Pleiss et al., 2007). Briefly, total RNA was purified from wild type and mutant yeast cultures growing in log phase at 30° C, and converted to animo-allyl labeled cDNA, which was then coupled to dyes and competitively hybridized to splicing microarrays. Values represent averaged data collected from dye-flipped technical replicates performed on two biological replicates for the *csn12Δ*, *ypr045cΔ*, *csn9Δ*, and *pci8Δ* arrays. The *isy1Δ* values are derived from a single representative biological replicate. Similarities between splicing microarray profiles were measured by Pearson correlation, calculated on the complete observations (Becker et al., 1988). Experimental factors were then symmetrically arranged along the X- and Y-axis of Figure 4C using hierarchical clustering (de Hoon et al., 2004) of euclidean distances between correlation values with unweighted centroid linkages. Array data has been deposited in the GEO database (http://www.ncbi.nlm.nih.gov/geo/), accession number GSE11634.

Acknowledgements

We would like to thank H. Kobayashi, T. Kodadek, D. Kellogg, and Catherine Dargement for antibodies, D. Cameron for strains, M. Dinglasin for technical assistance, M. Schuldiner for help with the screens, P. Kemmerman for help with the website, L. Booth for work on *ynr004w*Δ, and V. Panse for sharing unpublished data. We would like to thank members of the Guthrie lab, A. Frankel and J. Gross for reading and advice on the manuscript. G.M.W. was supported by postdoctoral fellowships from the American Cancer Society and the Sandler Foundation. M.B. was supported by an HHMI predoctoral fellowship. C.G. is an American Cancer Society Research Professor of Molecular Genetics. This research was funded by NIH grant GM21119 (C.G.) and from Sandler Family Funding (N.J.K.).

References

Baillat, D., Hakimi, M. A., Naar, A. M., Shilatifard, A., Cooch, N., and Shiekhattar, R. (2005). Integrator, a multiprotein mediator of small nuclear RNA processing, associates with the C-terminal repeat of RNA polymerase II. Cell *123*, 265-276.

Bandyopadhyay, S., Kelley, R., Krogan, N. J., and Ideker, T. (2008). Functional maps of protein complexes from quantitative genetic interaction data. PLoS Comput Biol *4*, e1000065.

Becker, R. A., Chambers, J. M., and Wilks, A. R. (1988). The new S language : a programming environment for data analysis and graphics (Pacific Grove, Calif., Wadsworth & Brooks/Cole Advanced Books & Software).

Brickner, D. G., Cajigas, I., Fondufe-Mittendorf, Y., Ahmed, S., Lee, P. C., Widom, J., and Brickner, J. H. (2007). H2A.Z-mediated localization of genes at the nuclear periphery confers epigenetic memory of previous transcriptional state. PLoS Biol *5*, e81.

Chan, S. P., Kao, D. I., Tsai, W. Y., and Cheng, S. C. (2003). The Prp19p-associated complex in spliceosome activation. Science *302*, 279-282.

Chen, C. H., Yu, W. C., Tsao, T. Y., Wang, L. Y., Chen, H. R., Lin, J. Y., Tsai, W. Y., and Cheng, S. C. (2002). Functional and physical interactions between components of the Prp19p-associated complex. Nucleic Acids Res *30*, 1029-1037.

Ciccarelli, F. D., Izaurralde, E., and Bork, P. (2003). The PAM domain, a multi-protein complex-associated module with an all-alpha-helix fold. BMC Bioinformatics *4*, 64.

Clark, T. A., Sugnet, C. W., and Ares, M., Jr. (2002). Genomewide analysis of mRNA processing in yeast using splicing-specific microarrays. Science *296*, 907-910.

Collins, G. A., and Tansey, W. P. (2006). The proteasome: a utility tool for transcription? Curr Opin Genet Dev *16*, 197-202.

Collins, S. R., Kemmeren, P., Zhao, X. C., Greenblatt, J. F., Spencer, F., Holstege, F. C., Weissman, J. S., and Krogan, N. J. (2007a). Toward a comprehensive atlas of the physical interactome of Saccharomyces cerevisiae. Mol Cell Proteomics *6*, 439-450.

Collins, S. R., Miller, K. M., Maas, N. L., Roguev, A., Fillingham, J., Chu, C. S., Schuldiner, M., Gebbia, M., Recht, J., Shales, M*., et al.* (2007b). Functional dissection of protein complexes involved in yeast chromosome biology using a genetic interaction map. Nature *446*, 806-810.

Collins, S. R., Schuldiner, M., Krogan, N. J., and Weissman, J. S. (2006). A strategy for extracting and analyzing large-scale quantitative epistatic interaction data. Genome Biol *7*, R63.

de Hoon, M. J., Imoto, S., Nolan, J., and Miyano, S. (2004). Open source clustering software. Bioinformatics *20*, 1453-1454.

Duncan, K., Umen, J. G., and Guthrie, C. (2000). A putative ubiquitin ligase required for efficient mRNA export differentially affects hnRNP transport. Curr Biol *10*, 687-696.

Dziembowski, A., Ventura, A. P., Rutz, B., Caspary, F., Faux, C., Halgand, F., Laprevote, O., and Seraphin, B. (2004). Proteomic analysis identifies a new complex required for nuclear pre-mRNA retention and splicing. Embo J *23*, 4847-4856.

Enenkel, C., Lehmann, A., and Kloetzel, P. M. (1998). Subcellular distribution of proteasomes implicates a major location of protein degradation in the nuclear envelope-ER network in yeast. Embo J *17*, 6144-6154.

Esberg, A., Huang, B., Johansson, M. J., and Bystrom, A. S. (2006). Elevated levels of two tRNA species bypass the requirement for elongator complex in transcription and exocytosis. Mol Cell *24*, 139-148.

Ezhkova, E., and Tansey, W. P. (2004). Proteasomal ATPases link ubiquitylation of histone H2B to methylation of histone H3. Mol Cell *13*, 435-442.

Ferdous, A., Gonzalez, F., Sun, L., Kodadek, T., and Johnston, S. A. (2001). The 19S regulatory particle of the proteasome is required for efficient transcription elongation by RNA polymerase II. Mol Cell *7*, 981-991.

Finn, R. D., Mistry, J., Schuster-Bockler, B., Griffiths-Jones, S., Hollich, V., Lassmann, T., Moxon, S., Marshall, M., Khanna, A., Durbin, R.*, et al.* (2006). Pfam: clans, web tools and services. Nucleic Acids Res *34*, D247-251.

Fischer, T., Strasser, K., Racz, A., Rodriguez-Navarro, S., Oppizzi, M., Ihrig, P., Lechner, J., and Hurt, E. (2002). The mRNA export machinery requires the novel Sac3p- Thp1p complex to dock at the nucleoplasmic entrance of the nuclear pores. Embo J *21*, 5843 5852.

Fu, H., Reis, N., Lee, Y., Glickman, M. H., and Vierstra, R. D. (2001). Subunit interaction maps for the regulatory particle of the 26S proteasome and the COP9 signalosome. Embo J *20*, 7096-7107.

Funakoshi, M., Li, X., Velichutina, I., Hochstrasser, M., and Kobayashi, H. (2004). Sem1, the yeast ortholog of a human BRCA2-binding protein, is a component of the proteasome regulatory particle that enhances proteasome stability. J Cell Sci *117*, 6447-6454.

Furukawa, K., Mizushima, N., Noda, T., and Ohsumi, Y. (2000). A protein conjugation system in yeast with homology to biosynthetic enzyme reaction of prokaryotes. J Biol Chem *275*, 7462-7465.

Gallardo, M., Luna, R., Erdjument-Bromage, H., Tempst, P., and Aguilera, A. (2003). Nab2p and the Thp1p-Sac3p complex functionally interact at the interface between transcription and mRNA metabolism. J Biol Chem *278*, 24225-24232.

Gautier-Bert, K., Murol, B., Jarrousse, A. S., Ballut, L., Badaoui, S., Petit, F., and Schmid, H. P. (2003). Substrate affinity and substrate specificity of proteasomes with RNase activity. Mol Biol Rep *30*, 1-7.

Gavin, A. C., Aloy, P., Grandi, P., Krause, R., Boesche, M., Marzioch, M., Rau, C., Jensen, L. J., Bastuck, S., Dumpelfeld, B*., et al.* (2006). Proteome survey reveals modularity of the yeast cell machinery. Nature *440*, 631-636.

Giaever, G., Chu, A. M., Ni, L., Connelly, C., Riles, L., Veronneau, S., Dow, S., Lucau-Danila, A., Anderson, K., Andre, B*., et al.* (2002). Functional profiling of the Saccharomyces cerevisiae genome. Nature *418*, 387-391.

Gilbert, W., Siebel, C. W., and Guthrie, C. (2001). Phosphorylation by Sky1p promotes Npl3p shuttling and mRNA dissociation. Rna *7*, 302-313.

Goffeau, A., Barrell, B. G., Bussey, H., Davis, R. W., Dujon, B., Feldmann, H., Galibert, F., Hoheisel, J. D., Jacq, C., Johnston, M*., et al.* (1996). Life with 6000 genes. Science *274*, 546, 563-547.

Gonzalez, F., Delahodde, A., Kodadek, T., and Johnston, S. A. (2002). Recruitment of a 19S proteasome subcomplex to an activated promoter. Science *296*, 548-550.

Gottschalk, A., Tang, J., Puig, O., Salgado, J., Neubauer, G., Colot, H. V., Mann, M., Seraphin, B., Rosbash, M., Luhrmann, R., and Fabrizio, P. (1998). A comprehensive biochemical and genetic analysis of the yeast U1 snRNP reveals five novel proteins. Rna *4*, 374-393.

Guthrie, C., and Fink, G. R. (2002). Guide to yeast genetics and molecular and cell biology. Part B (San Diego, Calif., Academic Press).

Ho, Y., Gruhler, A., Heilbut, A., Bader, G. D., Moore, L., Adams, S. L., Millar, A., Taylor, P., Bennett, K., Boutilier, K.*, et al.* (2002). Systematic identification of protein complexes in Saccharomyces cerevisiae by mass spectrometry. Nature *415*, 180-183.

Hofmann, K., and Bucher, P. (1998). The PCI domain: a common theme in three multiprotein complexes. Trends Biochem Sci *23*, 204-205.

Huh, W. K., Falvo, J. V., Gerke, L. C., Carroll, A. S., Howson, R. W., Weissman, J. S., and O'Shea, E. K. (2003). Global analysis of protein localization in budding yeast. Nature *425*, 686-691.

Isono, E., Saito, N., Kamata, N., Saeki, Y., and Toh, E. A. (2005). Functional analysis of Rpn6p, a lid component of the 26 S proteasome, using temperature-sensitive rpn6 mutants of the yeast Saccharomyces cerevisiae. J Biol Chem *280*, 6537-6547.

Jackman, J. E., Montange, R. K., Malik, H. S., and Phizicky, E. M. (2003). Identification of the yeast gene encoding the tRNA m1G methyltransferase responsible for modification at position 9. Rna *9*, 574-585.

Kobor, M. S., Venkatasubrahmanyam, S., Meneghini, M. D., Gin, J. W., Jennings, J. L., Link, A. J., Madhani, H. D., and Rine, J. (2004). A protein complex containing the conserved Swi2/Snf2-related ATPase Swr1p deposits histone variant H2A.Z into euchromatin. PLoS Biol *2*, E131.

Krogan, N. J., Cagney, G., Yu, H., Zhong, G., Guo, X., Ignatchenko, A., Li, J., Pu, S., Datta, N., Tikuisis, A. P.*, et al.* (2006). Global landscape of protein complexes in the yeast Saccharomyces cerevisiae. Nature *440*, 637-643.

Krogan, N. J., Keogh, M. C., Datta, N., Sawa, C., Ryan, O. W., Ding, H., Haw, R. A., Pootoolal, J., Tong, A., Canadien, V.*, et al.* (2003). A Snf2 family ATPase complex required for recruitment of the histone H2A variant Htz1. Mol Cell *12*, 1565-1576.

Krogan, N. J., Lam, M. H., Fillingham, J., Keogh, M. C., Gebbia, M., Li, J., Datta, N., Cagney, G., Buratowski, S., Emili, A., and Greenblatt, J. F. (2004). Proteasome involvement in the repair of DNA double-strand breaks. Mol Cell *16*, 1027-1034.

Lei, E. P., Stern, C. A., Fahrenkrog, B., Krebber, H., Moy, T. I., Aebi, U., and Silver, P. A. (2003). Sac3 is an mRNA export factor that localizes to cytoplasmic fibrils of nuclear pore complex. Mol Biol Cell *14*, 836-847.

Li, J., Zou, C., Bai, Y., Wazer, D. E., Band, V., and Gao, Q. (2006). DSS1 is required for the stability of BRCA2. Oncogene *25*, 1186-1194.

Luna, R., Gaillard, H., Gonzalez-Aguilera, C., and Aguilera, A. (2008). Biogenesis of mRNPs: integrating different processes in the eukaryotic nucleus. Chromosoma.

Lund, M. K., and Guthrie, C. (2005). The DEAD-box protein Dbp5p is required to dissociate Mex67p from exported mRNPs at the nuclear rim. Mol Cell *20*, 645-651.

Mannen, T., Andoh, T., and Tani, T. (2008). Dss1 associating with the proteasome functions in selective nuclear mRNA export in yeast. Biochem Biophys Res Commun *365*, 664-671.

Maytal-Kivity, V., Pick, E., Piran, R., Hofmann, K., and Glickman, M. H. (2003). The COP9 signalosome-like complex in S. cerevisiae and links to other PCI complexes. Int J Biochem Cell Biol *35*, 706-715.

Mizuguchi, G., Shen, X., Landry, J., Wu, W. H., Sen, S., and Wu, C. (2004). ATP-driven exchange of histone H2AZ variant catalyzed by SWR1 chromatin remodeling complex. Science *303*, 343-348.

Mouaikel, J., Verheggen, C., Bertrand, E., Tazi, J., and Bordonne, R. (2002). Hypermethylation of the cap structure of both yeast snRNAs and snoRNAs requires a conserved methyltransferase that is localized to the nucleolus. Mol Cell *9*, 891-901.

Nakai, Y., Nakai, M., and Hayashi, H. (2008). Thio-modification of Yeast Cytosolic tRNA Requires a Ubiquitin-related System That Resembles Bacterial Sulfur Transfer Systems. J Biol Chem *283*, 27469-27476.

Neubauer, G., Gottschalk, A., Fabrizio, P., Seraphin, B., Luhrmann, R., and Mann, M. (1997). Identification of the proteins of the yeast U1 small nuclear ribonucleoprotein complex by mass spectrometry. Proc Natl Acad Sci U S A *94*, 385-390.

Ohi, M. D., and Gould, K. L. (2002). Characterization of interactions among the Cef1p-Prp19p-associated splicing complex. Rna *8*, 798-815.

Otero, G., Fellows, J., Li, Y., de Bizemont, T., Dirac, A. M., Gustafsson, C. M., Erdjument-Bromage, H., Tempst, P., and Svejstrup, J. Q. (1999). Elongator, a multisubunit component of a novel RNA polymerase II holoenzyme for transcriptional elongation. Mol Cell *3*, 109-118.

Pan, X., Yuan, D. S., Xiang, D., Wang, X., Sookhai-Mahadeo, S., Bader, J. S., Hieter, P., Spencer, F., and Boeke, J. D. (2004). A robust toolkit for functional profiling of the yeast genome. Mol Cell *16*, 487-496.

Pleiss, J. A., Whitworth, G. B., Bergkessel, M., and Guthrie, C. (2007). Transcript specificity in yeast pre-mRNA splicing revealed by mutations in core spliceosomal components. PLoS Biol *5*, e90.

Rodriguez-Navarro, S., Fischer, T., Luo, M. J., Antunez, O., Brettschneider, S., Lechner, J., Perez-Ortin, J. E., Reed, R., and Hurt, E. (2004). Sus1, a functional component of the

SAGA histone acetylase complex and the nuclear pore-associated mRNA export machinery. Cell *116*, 75-86.

Roguev, A., Bandyopadhyay, S., Zofall, M., Zhang, K., Fischer, T., Collins, S. R., Qu, H., Shales, M., Park, H. O., Hayles, J.*, et al.* (2008). Conservation and Rewiring of Functional Modules Revealed by an Epistasis Map in Fission Yeast. Science.

Roguev, A., Wiren, M., Weissman, J. S., and Krogan, N. J. (2007). High-throughput genetic interaction mapping in the fission yeast Schizosaccharomyces pombe. Nat Methods *4*, 861-866.

Scheel, H., and Hofmann, K. (2005). Prediction of a common structural scaffold for proteasome lid, COP9-signalosome and eIF3 complexes. BMC Bioinformatics *6*, 71.

Schmitz, J., Chowdhury, M. M., Hanzelmann, P., Nimtz, M., Lee, E. Y., Schindelin, H., and Leimkuhler, S. (2008). The sulfurtransferase activity of Uba4 presents a link between ubiquitin-like protein conjugation and activation of sulfur carrier proteins. Biochemistry *47*, 6479-6489.

Schuldiner, M., Collins, S. R., Thompson, N. J., Denic, V., Bhamidipati, A., Punna, T., Ihmels, J., Andrews, B., Boone, C., Greenblatt, J. F.*, et al.* (2005). Exploration of the function and organization of the yeast early secretory pathway through an epistatic miniarray profile. Cell *123*, 507-519.

Segre, D., Deluna, A., Church, G. M., and Kishony, R. (2005). Modular epistasis in yeast metabolism. Nat Genet *37*, 77-83.

Sharon, M., Taverner, T., Ambroggio, X. I., Deshaies, R. J., and Robinson, C. V. (2006). Structural organization of the 19S proteasome lid: insights from MS of intact complexes. PLoS Biol *4*, e267.

Sims, R. J., 3rd, Millhouse, S., Chen, C. F., Lewis, B. A., Erdjument-Bromage, H., Tempst, P., Manley, J. L., and Reinberg, D. (2007). Recognition of trimethylated histone H3 lysine 4 facilitates the recruitment of transcription postinitiation factors and premRNA splicing. Mol Cell *28*, 665-676.

Sone, T., Saeki, Y., Toh-e, A., and Yokosawa, H. (2004). Sem1p is a novel subunit of the 26 S proteasome from Saccharomyces cerevisiae. J Biol Chem *279*, 28807-28816.

Strasser, K., and Hurt, E. (2001). Splicing factor Sub2p is required for nuclear mRNA export through its interaction with Yra1p. Nature *413*, 648-652.

Thakurta, A. G., Gopal, G., Yoon, J. H., Kozak, L., and Dhar, R. (2005). Homolog of BRCA2-interacting Dss1p and Uap56p link Mlo3p and Rae1p for mRNA export in fission yeast. Embo J *24*, 2512-2523.

Tong, A. H., Evangelista, M., Parsons, A. B., Xu, H., Bader, G. D., Page, N., Robinson, M., Raghibizadeh, S., Hogue, C. W., Bussey, H.*, et al.* (2001). Systematic genetic analysis with ordered arrays of yeast deletion mutants. Science *294*, 2364-2368.

Tong, A. H., Lesage, G., Bader, G. D., Ding, H., Xu, H., Xin, X., Young, J., Berriz, G. F., Brost, R. L., Chang, M.*, et al.* (2004). Global mapping of the yeast genetic interaction network. Science *303*, 808-813.

Uetz, P., Giot, L., Cagney, G., Mansfield, T. A., Judson, R. S., Knight, J. R., Lockshon, D., Narayan, V., Srinivasan, M., Pochart, P*., et al.* (2000). A comprehensive analysis of protein-protein interactions in Saccharomyces cerevisiae. Nature *403*, 623-627.

Wang, Q., He, J., Lynn, B., and Rymond, B. C. (2005). Interactions of the yeast SF3b splicing factor. Mol Cell Biol *25*, 10745-10754.

Wee, S., Hetfeld, B., Dubiel, W., and Wolf, D. A. (2002). Conservation of the COP9/signalosome in budding yeast. BMC Genet *3*, 15.

Wei, S. J., Williams, J. G., Dang, H., Darden, T. A., Betz, B. L., Humble, M. M., Chang, F. M., Trempus, C. S., Johnson, K., Cannon, R. E., and Tennant, R. W. (2008). Identification of a Specific Motif of the DSS1 Protein Required for Proteasome Interaction and p53 Protein Degradation. J Mol Biol.

Wilkinson, C. R., Wallace, M., Morphew, M., Perry, P., Allshire, R., Javerzat, J. P., McIntosh, J. R., and Gordon, C. (1998). Localization of the 26S proteasome during mitosis and meiosis in fission yeast. Embo J *17*, 6465-6476.

Yang, H., Jeffrey, P. D., Miller, J., Kinnucan, E., Sun, Y., Thoma, N. H., Zheng, N., Chen, P. L., Lee, W. H., and Pavletich, N. P. (2002). BRCA2 function in DNA binding and recombination from a BRCA2-DSS1-ssDNA structure. Science *297*, 1837-1848.

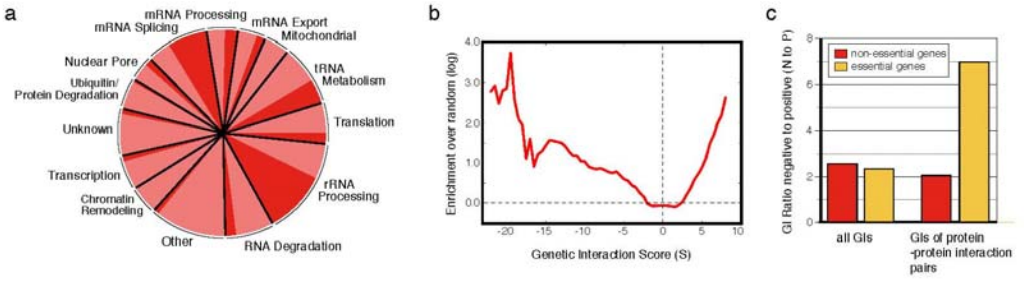

Figure 1. Description of the RNA processing E-MAP. A) Composition of the RNA processing E-MAP. The genetic map is comprised of 552 genes (166 of which are essential) and represents virtually all processes involved in RNA metabolism, including rRNA, tRNA, snoRNA, snRNA and mRNA processing. The dark red portions of the pie chart represent the proportions of the processes that correspond to essential genes. **B)** Comparison of genetic and physical interactions. The graph compares pairs of proteins that are physically associated (PE > 1.0, (Collins et al., 2007a)) and the genetic interaction scores from the corresponding mutants (S-score, (Collins et al., 2006)). Based on a comparison to randomized genetic interaction scores, protein pairs with strong positive and negative genetic interactions are more likely to be physically associated. **C**) Comparisons of ratios of negative (S ≤ -2.5) to positive (S ≥ 2.0) (N to P) genetic interactions. The graph is divided into two parts: 1) all genetic interactions from the RNA processing E-MAP and 2) only those from pairs of genes whose corresponding proteins are physically associated (PE > 1.0, (Collins et al., 2007a)). Red bars correspond to genetic interactions derived entirely from deletions of pairs of non-essential genes (n= 88,879 total (left), 110 physically interacting (right)), while yellow bars are derived from pairs including one (n=49,380 total ,73 physically interacting) or two (n= 639 total, 4 physically interacting) DAmP alleles of essential genes. The overrepresentation of negative genetic interactions among pairs of genes that include an essential gene and have physical interactions was found to be highly significant using Fisher's exact test, with a two-tailed p-value of 3x10-4. The trend was not strongly dependent on using various different thresholds for defining negative and positive interactions (data not shown). GIs, genetic interactions.

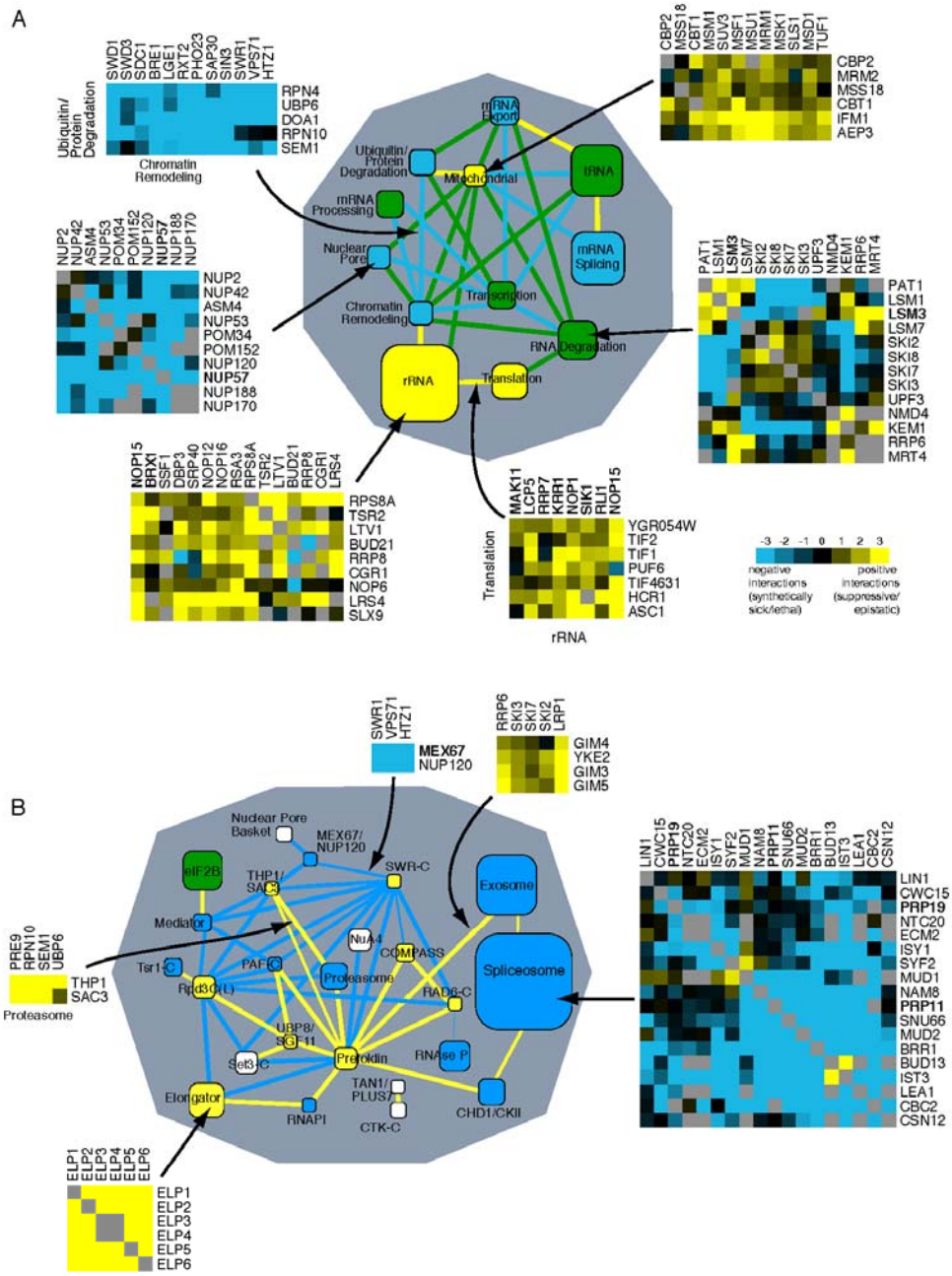
A
Ubiquitin/ Protein Degradation
Chromatin Remodeling
mRNA Export
Mitochondrial
tRNA
mRNA Splicing
Transcription
RNA Degradation
Translation
rRNA
Nuclear Pore
mRNA Processing
Chromatin Remodeling
Translation
rRNA
-3 -2 -1 0 1 2 3
negative interactions (synthetically sick/lethal)
positive interactions (suppressive/ epistatic)
B
MEX67 NUP120
Nuclear Pore Basket
MEX67/ NUP120
SWR-C
THP1/ SAC3
eIF2B
Exosome
Mediator
NuA4
COMPASS
Tsr1-C
PAF-C
Proteasome
Spliceosome
Rpd3(L)
RAD6-C
UBP8/ SGF11
Prefoldin
RNAse P
Set3C
TAN1/ PLUS7
Elongator
RNAP I
CTK-C
CHD1/CKII
Proteasome
THP1
SAC3
ELP1
ELP2
ELP3
ELP4
ELP5
ELP6

Figure 2. Functional cross-talk between biological processes and protein complexes. Global views of the genetic cross-talk between different RNA-related protein complexes (**A**) and processes (**B**). Blue and yellow represent a statistically significant enrichment of negative and positive interactions, respectively, whereas green corresponds to cases where there are roughly equal numbers of positive and negative genetic interactions. White corresponds to a lack of significant interactions or lack of data. Nodes (boxes) correspond to distinct protein complexes (**A**) or functional processes (**B**) whereas edges (lines) represent how the complexes and processes are genetically connected. Line thickness represents the significance of the connection. Node size is proportional to the number of genes in the process or complex. Essential genes (DAmP alleles) are in bold. Representative genetic interactions which contributed to the overall enrichment for interactions are shown for sample nodes and edges, according to the scale shown, with grey boxes representing missing data points. See Experimental Procedures for a description of how the networks are generated.

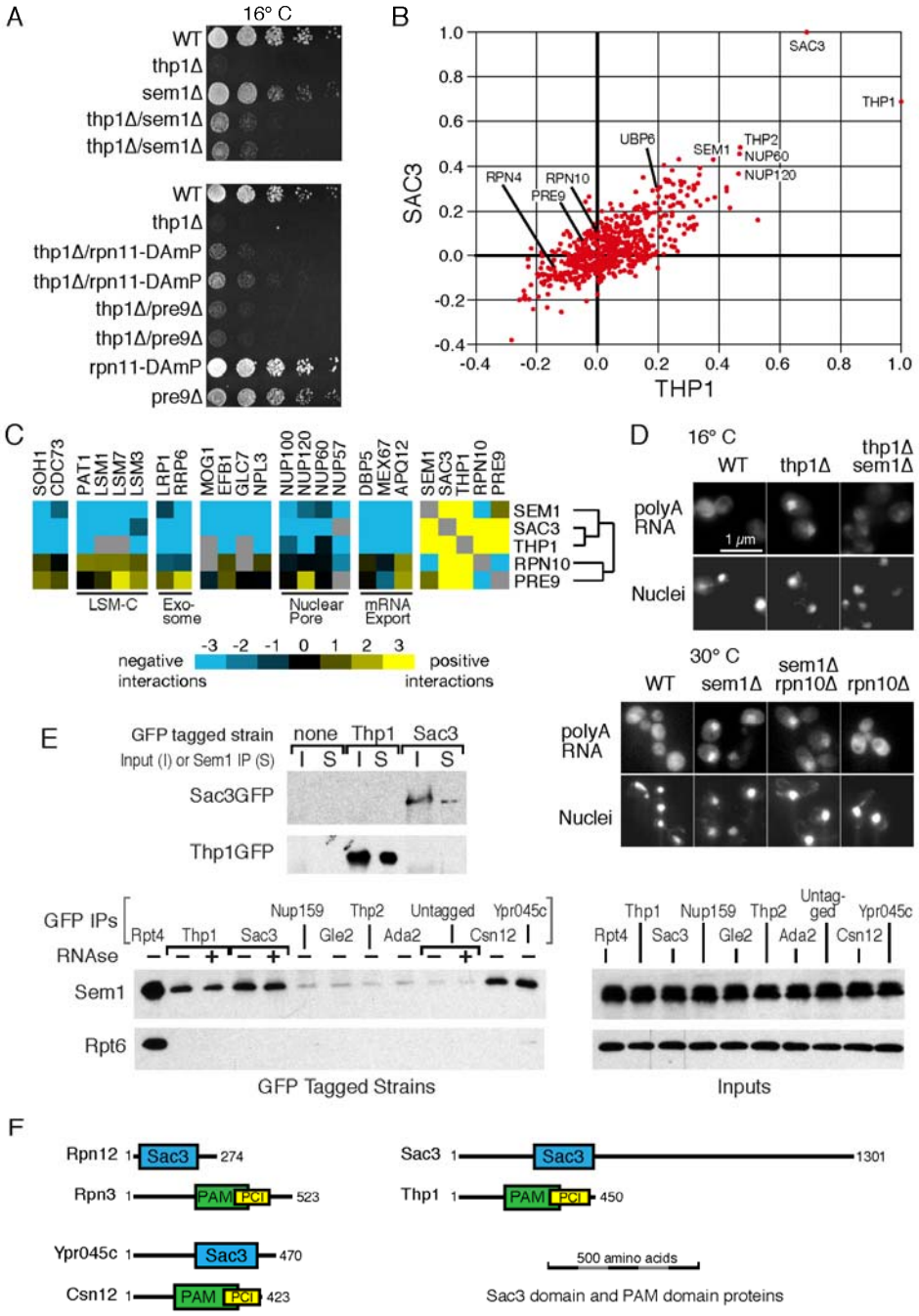

Figure 3. Sem1 is involved in mRNA export via the Sac3-Thp1 complex. A) Scatter plot of correlation coefficients for each mutant compared to the profiles generated from *SAC3* (y-axis) and *THP1* (x-axis). **B)** Representative genetic interactions from the EMAP that

differentiate *SEM1*, *SAC3*, and *THP1* from *RPN10* and *PRE9*. Blue and yellow indicate negative and positive genetic interactions, respectively. **C)** In situ hybridizations with a dT50 probe to detect accumulation of poly(A) RNA (top row). The bottom row is DAPI staining to detect nuclei. Cells were either kept at permissive temperature (30°C, right) or shifted to 16°C for 2 hours before fixation (left). **D)** Co-immunoprecipitations (IPs) of Sem1 and Rpt6 with GFP-tagged proteins. The indicated strains were IPed with a monoclonal GFP antibody, either with or without prior RNAse A treatment of the extract, and the blot was cut and probed with polyclonal antibodies against Sem1 or Rpt6. The right panel is 1/200th of the sample for the GFP IPs exposed identically to the left. **E)** Co- IPs of Thp1-6HA with Sac3GFP in a *sem1Δ* background. The IPs were performed in buffer with 150 mM NaCl, and then washed 4 times at room temperature for 10 minutes each wash in buffers containing the indicated amount of salt. The right panel represents1/20th the sample for the GFP IPS. **F)** In vivo UV crosslinking of proteins to poly(A) RNA. Each lane of the poly(A) eluates contains equal amounts of purified poly(A) RNA. The "no UV" strain contains Thp1-6HA. The * in the Sub2 blot represents a nonspecific cross-reacting band. The left and right panels were exposed differently, and the Yra1 poly(A) blot was overexposed to allow visualization of the Yra1 band in the wild-type strain. **G)** Depiction of the export block identified by the poly(A) crosslinking in part F. Sac3-Thp1-Sem1 could facilitate an exchange of Sub2 for Mex67. See text for more details.

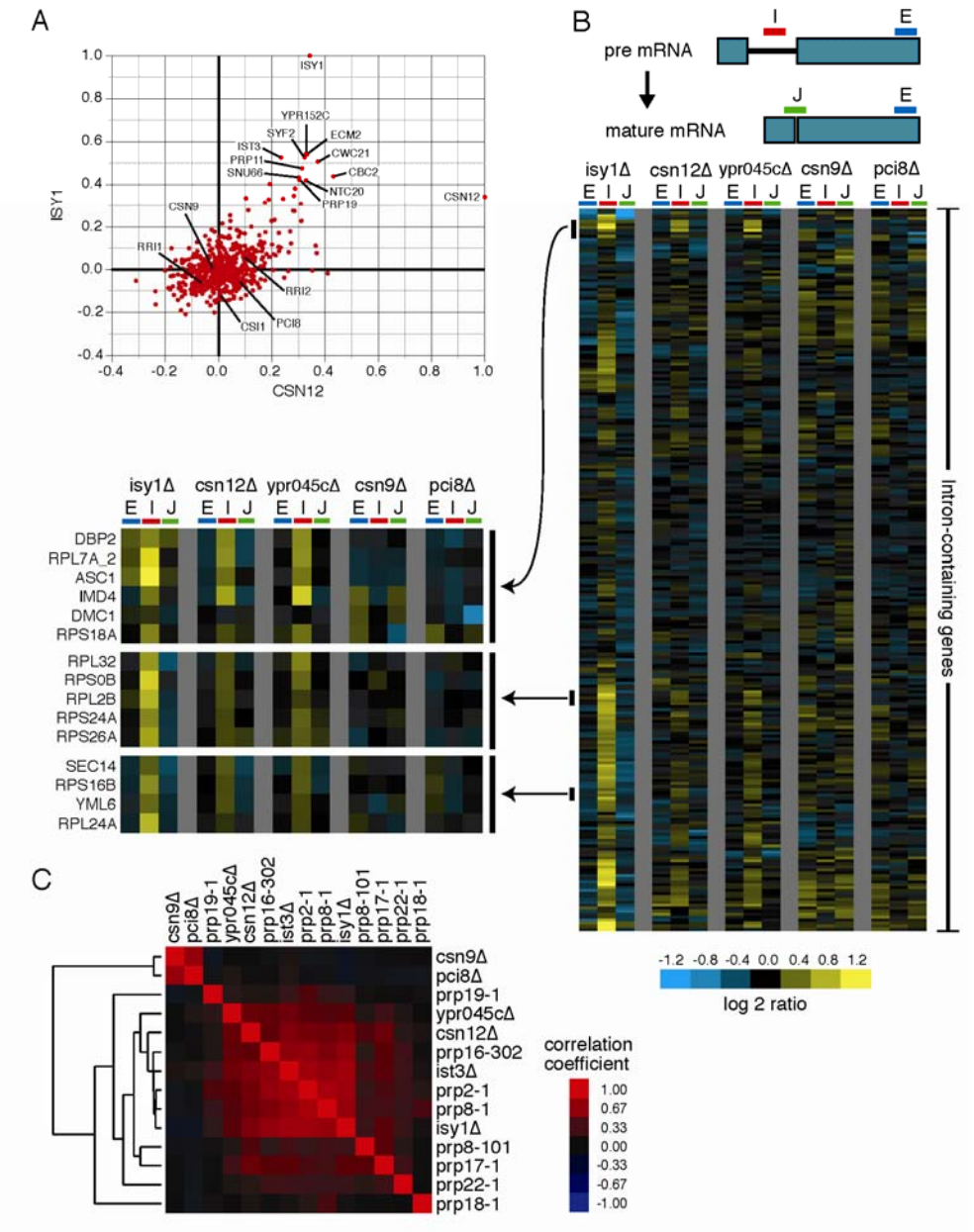
A
B
C
pre mRNA
mature mRNA
I
E
J
ISY1
CSN12
YPR152C
SYF2
ECM2
IST3
CWC21
PRP11
CBC2
SNU66
NTC20
PRP19
CSN9
RRI1
RRI2
CSI1
PCI8
isy1Δ
csn12Δ
ypr045cΔ
csn9Δ
pci8Δ
E I J
DBP2
RPL7A_2
ASC1
IMD4
DMC1
RPS18A
RPL32
RPS0B
RPL2B
RPS24A
RPS26A
SEC14
RPS16B
YML6
RPL24A
Intron-containing genes
-1.2 -0.8 -0.4 0.0 0.4 0.8 1.2
log 2 ratio
correlation coefficient
1.00
0.67
0.33
0.00
-0.33
-0.67
-1.00
prp16-302
ist3Δ
prp2-1
prp8-1
prp8-101
prp17-1
prp22-1
prp18-1
prp19-1

Figure 4) Csn12 is involved in mRNA splicing. (**A**) Plot of correlation coefficients generated from comparison of the genetic interaction profiles from *csn12*Δ or *isy1*Δ to all other profiles in the E-MAP. **B**) Splicing-specific microarray profiles for several mutant strains. The schematic displays the positions of the microarray probes that report specifically on the levels of pre-mRNA (in the Intron), mature mRNA (at the Junction), and total mRNA (in the second Exon) for each intron-containing transcript. The relative levels of exon, intron, and junction for a single intron-containing gene are displayed as log2 ratios for the indicated mutant strains compared to a wild type strain, across each row. The ordering of genes was determined by hierarchical clustering. For selected clusters of genes, the splicing profiles across the mutants tested are displayed at higher resolution to the left of the full splicing profiles. **C**) Pairwise Pearson correlation coefficients were calculated between each of the mutants tested, as well as between these mutants and several previously characterized splicing mutants. The matrix of correlations was subjected to hierarchical clustering.

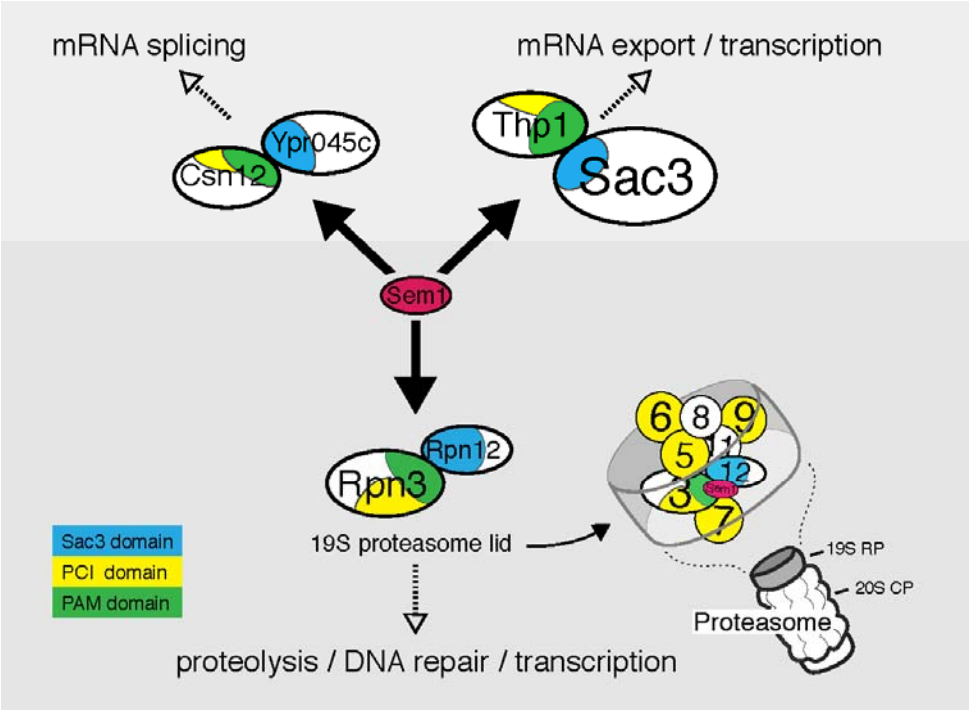

Figure 5. Model for three Sem1-containing complexes. 19S RP= Regulatory Particle of the proteasome, which includes both the lid (diagrammed here), and the base. 20S CP=Core Particle of the proteasome. The schematic of protein organization in the proteasome lid is based on the model from Sharon et al (Sharon et al., 2006). The "SAC3" domains (PFAM PF03399) are amino acids: Rpn12 20-211, Ypr045c 205-408, and Sac3 248-443, and the PAM domains (Ciccarelli et al., 2003): Rpn3 204-378, Csn12 136-343, and Thp1 151-332. Also shown are the PCI domains (PFAM PF01399) associated with the PAM domains: Rpn3 343-447, Csn12 298-415, and Thp1 300-430.

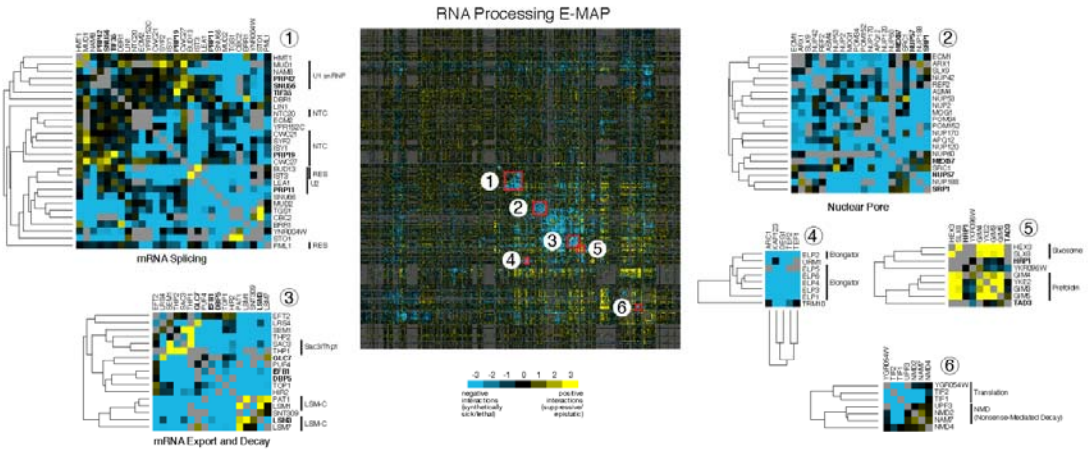

Supplemental Figure 1. Hierarchical clustergram of all 552 genes in the RNA Processing E-MAP. Numbered pullouts represent subclusters with processes and protein complexes labeled. Essential genes are in bold. Blue and yellow represent negative and positive genetic interactions, respectively, whereas grey corresponds to data that was not collected.

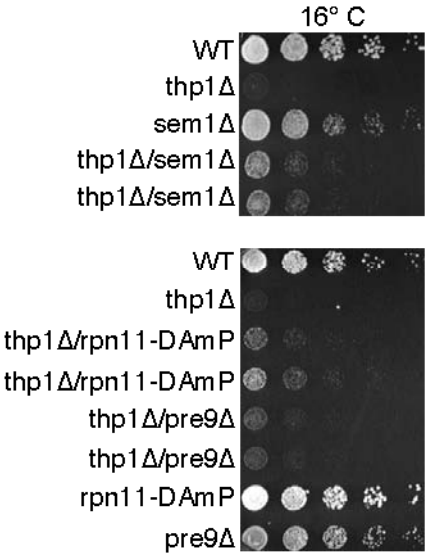

Supplemental Figure 2. Verification of positive genetic interactions derived from the E-MAP. Five-fold serial dilutions of wild-type, single and double deletion cells spotted onto YPD and grown at 16°C for 7 days.

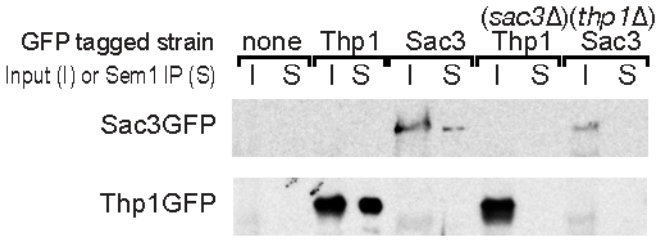

Supplemental Figure 3. Sac3GFP and Thp1GFP co-immunoprecipitate with Sem1 if both Sac3 and Thp1 are present in the strain. Sem1 was immunoprecipitated with a polyclonal antibody in the indicated strains and the blots were probed for GFP. Inputs represent 1/20th of the IP sample.

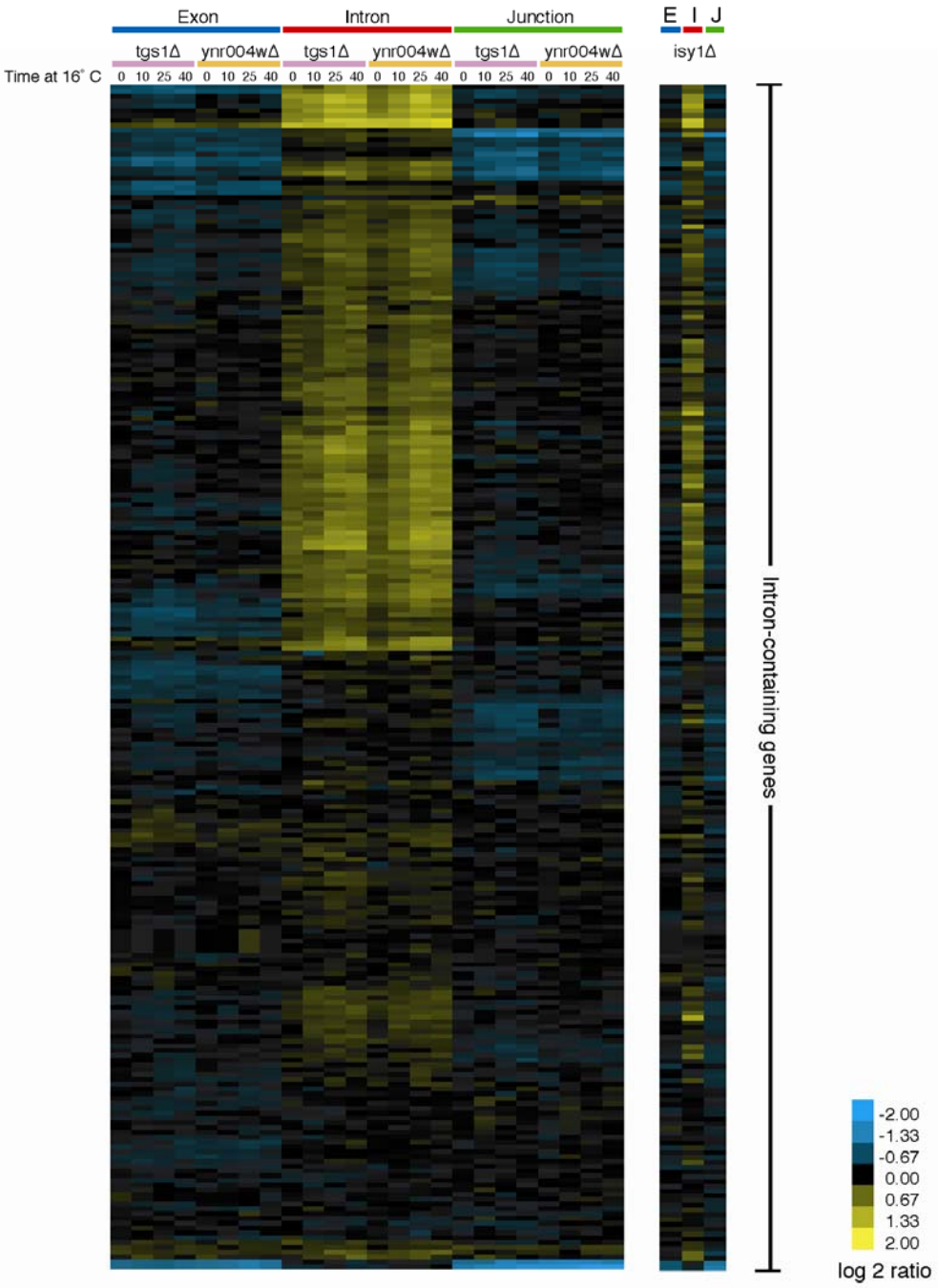
Exon
Intron
Junction
E I J
tgs1Δ
ynr004wΔ
tgs1Δ
ynr004wΔ
tgs1Δ
ynr004wΔ
isy1Δ
Time at 16° C
0 10 25 40 0 10 25 40 0 10 25 40 0 10 25 40 0 10 25 40 0 10 25 40
Intron-containing genes
-2.00
-1.33
-0.67
0.00
0.67
1.33
2.00
log 2 ratio

Supplemental Figure 4. Tgs1 and Ynr004w are required for normal mRNA splicing. Splicing-specific microarray profiles were generated for *tgs1*Δ and *ynr004w*Δ, as described in figure 4 and Experimental Procedures, with the exception that this experiment involves a temperature shift. *tgs1*Δ and *ynr004w*Δ cultures grown at 30° C were shifted to 16°C and samples were collected at the indicated times (in minutes) and hybridized against samples collected from a wild type strain also shifted to 16°C. Genes are ordered by hierarchical clustering of this dataset. The splicing profile for the splicing mutant *isy1*Δ strain in log phase at 30°C (as described in figure 4) is included here for reference, with the genes ordered to match the order in the *tgs1*Δ and *ynr004w*Δ profile.

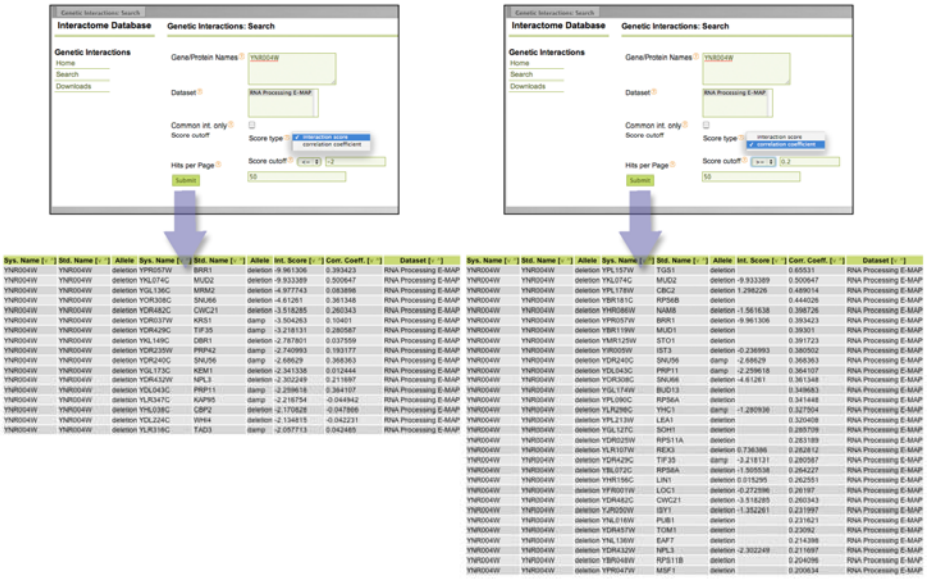

Supplemental Figure 5. Representative screenshots from the web-based database that allows for the query of individual genetic interactions and/or profiles from specific mutants derived from the genetic data from the RNA Processing E-MAP.

Chapter 3

Diverse Environmental Stresses Elicit Distinct Responses at the Level of Pre-mRNA Processing in Yeast

Abstract

We find that diverse stresses cause distinct patterns of changes at the level of pre-mRNA processing. The responses we observed are most dramatic for the RPGs and can be categorized into three major classes. The first is characterized by accumulation of RPG pre-mRNA and is seen in multiple types of amino acid starvation regimes; the magnitude of splicing inhibition correlates with the severity of the stress. The second class is characterized by a rapid decrease in both pre- and mature RPG mRNA and is seen in many stresses that inactivate the TOR C1 kinase complex. These decreases depend on nuclear turn-over of the intron-containing pre-RNAs. The third class is characterized by a decrease in RPG pre-mRNA with only a modest reduction in the mature species; this response is observed in hyperosmotic and cation-toxic stresses. We show that casein kinase 2 (CK2) makes important contributions to the changes in pre-mRNA processing, particularly for the first two classes of stress responses. In total, our data suggest that complex post-transcriptional programs cooperate to fine-tune expression of intron-containing transcripts in budding yeast.

Introduction

Regulation of ribosomal protein gene (RPG) expression is of great importance to overall cellular metabolism; up to 50% of all RNA polymerase II transcription in budding yeast is dedicated to making RPG mRNAs in nutrient-rich conditions [1]. Accordingly, RPG expression is known to be tightly regulated both transcriptionally and post-transcriptionally. Transcriptional regulation involves multiple transcription factors, kinases, and chromatin modifications [2-5]. Measurements of mRNA half-lives for all yeast transcripts reveal that the half lives of the RPGs are strikingly similar to one another, suggesting that this is a regulated property [6]. Moreover, RPGs generally have shorter than average 5' UTRs, which is believed to contribute to their high translational efficiency, and longer than average poly A tails, which is believed to contribute to their stability [7, 8]. Despite widespread intron loss from the *Saccharomyces cerevisiae* genome, introns have been retained in a majority of ribosomal protein genes and RPGs contain over one third of the remaining *S. cerevisiae* introns [9, 10]. This bias in intron distribution suggests that the presence of introns in ribosomal protein genes could also contribute to their regulation. Indeed, we showed previously that pre-mRNAs for the RPGs accumulate in response to treatment with the amino acid starvation mimicking drug, 3-amino 1,2,4-triazole (3-AT) [11].

Translation initiation is inhibited in response to 3-AT, and prolonged treatment leads eventually to a decrease in ribosomal protein gene expression [12, 13]. Many other stresses that down-regulate translation are also known to cause a decrease in ribosomal protein gene expression, presumably because the vast energy resources normally

directed toward ribosome biogenesis under favorable growth conditions must be re-directed toward the relevant stress response [14, 15]. While it has been suggested that the stability of the RPG transcripts is specifically altered in response to some stresses [16-18], the best-characterized stress-responsive regulation of RPG expression occurs at the level of transcription. A central nutrient- and stress-sensitive regulator of RPG transcription is the TORC1 (**T**arget **O**f **R**apamycin Complex 1) kinase complex, which phosphorylates multiple substrates in favorable conditions to promote RPG expression (reviewed in [19, 20]). Under a variety of stressful conditions, including depletion of glucose, nitrogen, or phosphorus, heat shock, and hyperosmotic stress, the TORC1 complex is inactivated, leading to a strong decrease in RPG expression [21]. Additional signaling pathways are known to contribute to the responses to these translation-inhibitory stresses. Protein kinase A, Ire1, Hog1, Pho85, and Gcn2 contribute to unique aspects of the responses to glucose starvation, endoplasmic reticulum stress, hyperosmotic stress, phosphate starvation, and amino acid starvation, respectively, and in many cases, examples of crosstalk among these pathways, and between these pathways and the TORC1 pathway, have also been identified [22-27]. In addition to inhibiting RPG expression, inactivation of TORC1 leads to entry into a G1-like quiescent state, referred to as G0 or stationary phase [28]. Entry into G0 is protective under stressful conditions – mutations or conditions that prevent it cause decreased long term survival [29-31]. In short, a complex network of stress-responsive signaling mediates appropriate responses to many stresses, which are characterized by some common

features, such as transcriptional down-regulation of ribosomal protein genes and entry into G0, and some features unique to each individual stress.

In addition to TORC1 there are other, less well-characterized signaling complexes that are likely to contribute to regulation under stressful conditions. One such kinase complex with proposed roles in nutrient sensing is casein kinase 2 (CK2). In yeast, CK2 consists of two regulatory subunits (Ckb1 and Ckb2) and two catalytic subunits (Cka1 and Cka2), and appears to be highly promiscuous within the cell, with dozens of reported substrates [32, 33]. They include subunits of all three RNA polymerases, chromatin remodeling ATPases, splicing factors, transcription factors, ribosome biogenesis factors, mRNA binding proteins, tRNA synthetases, ribosomal proteins, and translation factors [34-37], (and others). Unlike many other kinases involved in stress signaling pathways, CK2 has no known direct interactions with the TORC1 complex. In general, its regulation is very poorly understood – the catalytic subunits have high constitutive activity *in vitro*, and the roles of the regulatory subunits in directing this activity toward appropriate substrates are unknown [38]. That CK2 appears to have substrates involved in many aspects of regulating protein biosynthetic capacity places it in a unique position to contribute to translation-inhibitory stress responses.

We wished to determine the contribution of the presence of introns in stress-regulated transcripts to the overall integrated stress response of the cell. We used a custom microarray platform (previously described in[39]) to specifically measure changes in the amounts of pre-mRNA, mature mRNA, and total mRNA for the majority of intron-

containing genes in yeast, following exposure to a wide range of translation-inhibitory stresses. This dataset allowed us to contextualize the role of regulation at the level of pre-mRNA processing, including both splicing and turnover, within a large arena of growth conditions and responses, and offered novel insights into mechanisms by which this regulation is imposed and integrated with other stress response pathways.

Results

A microarray platform for analyzing pre-mRNA processing in response to stress

We used a previously described splicing-sensitive microarray platform that allowed for specific measurements of pre-mRNA (using a probe against the intron sequence), mature mRNA (using a probe across the junction sequence), and total mRNA (using a probe against the second exon sequence) to assay changes in relative levels of these species during stress [39]. Yeast were exposed to a range of stresses and culture aliquots were collected at 5-, 10-, 20-, and 40-minute time points after the induction of the stress. Total RNA was extracted, cDNA was synthesized and labeled with fluorophores, and samples were competitively hybridized to microarrays, all as previously described. In stress treatments in which media was exchanged, each sample was hybridized against a mock-treated sample. For heat shock and stress treatments involving the addition of a drug, samples were hybridized against a pre-treatment sample.

The relative abundances of the pre-mRNA, mature mRNA, and total mRNA species for each intron-containing gene over each stress time course were measured by dye-flipped replicate microarrays (full dataset available online, GEO accession#). To visualize the results, the total, pre-mRNA, and mature mRNA values for all of the time points for each transcript were plotted on the same row of a heat map, colored according to the log2-transformed ratio values from the microarrays, and the rows of the heat map were ordered by a hierarchical clustering algorithm (Supplemental Figs. S1-S15). In order to analyze the relationships between each of the different stress responses, as determined by changes in pre-mRNA and mature mRNA levels, the time course data for each stress response were first summarized by taking the time point exhibiting the greatest overall change in the intron and junction feature responses. These values were then clustered, using both hierarchical and k-means clustering (see Materials and Methods for more details) (Fig. 1). Hierarchical clustering assesses the similarity of each stress to every other stress in the dataset, and was used to construct a dendogram displaying these relationships. K-means clustering, on the other hand, fits the stresses to a predefined number of classes, minimizing within-class variability. In all k-means analyses presented below, solutions were calculated for the full range of possible numbers of classes and the data shown represent the solutions with the smallest number of classes that provided meaningful subdivisions of the data.

We focused on stresses previously reported to affect translation, RNA processing, or both. Following our earlier demonstration that treatment with 3-AT induces the accumulation of RPG pre-mRNA, we wanted to test other formats of amino acid

starvation. 3-AT induces an amino acid starvation response when cells are grown in synthetic media lacking histidine by inhibiting an enzyme in the histidine biosynthetic pathway. In addition to repeating the 3-AT treatment using the same time course and cell collection protocol used for the rest of the stress treatments in this study, we also simply removed histidine by filtering a culture growing in synthetic complete media, washing the cells with synthetic media lacking only histidine, and resuspending them in that media. To create a situation in which this stress would be more stringent, we repeated the histidine depletion using a strain that was auxotrophic for histidine. We also examined the response when all amino acids, uracil, and adenine were removed by replacing synthetic complete media with media containing only yeast nitrogen base, ammonium sulfate, and glucose. Finally, we used another drug, sulfometuron methyl (SMM), that like 3-AT inhibits an amino acid biosynthetic pathway and induces the general amino acid control pathway. SMM inhibits an enzyme in the biosynthetic pathways for leucine, isoleucine and valine, and thus elicits an amino acid starvation response when added to a culture growing in media lacking isoleucine and valine [40, 41].

We tested two additional starvation stresses that have been shown to at least transiently inactivate TORC1. We starved cells for phosphate by replacing synthetic complete media with media lacking potassium phosphate, and for a carbon source by replacing rich media with rich media lacking glucose. We also tested the effects of TORC1 inactivation directly by treating cells with two drugs that inhibit this complex: rapamycin and wortmannin [42].

Conditions leading to the accumulation of unfolded or misfolded proteins in the endoplasmic reticulum are also known to down-regulate translation and to induce the unfolded protein response (UPR) [22]. We tested two stresses that induce the UPR: treatment with dithiothreitol (DTT), a strong reducing agent, and a temperature shift from 30°C to 42°C (heat shock). Heat shock has also previously been suggested to broadly inhibit pre-mRNA splicing [43-45] .

Salt stress is also known to strongly down-regulate translation [15]. Treatment with 500 mM sodium chloride (NaCl), commonly used to elicit a hyperosmotic stress response, is both a hyperosmotic stress and a cation-toxic stress. We tested this concentration of NaCl, and also used lithium chloride (LiCl) at a concentration that is primarily cation toxic (300 mM) and potassium chloride (KCl) at a concentration that is primarily hyperosmotic-stress-inducing (1M). We also treated cells with 1M sorbitol, a hyperosmotic stress but not a salt [46].

Stress responses cluster into three groups

The first class defined by clustering analysis (blue bars in k-means classes in Fig. 1) shows behavior similar to that previously described as the pre-mRNA processing response to amino acid starvation – accumulation of the pre-mRNA for a majority of the RPGs [11]. 3-AT treatment, SMM treatment, and depletion of all amino acids form one branch within this group, and depletion of just histidine, in both wild-type and histidine auxotroph strains, forms another branch. Closer inspection of the full time courses for

each of these stresses shows that accumulation of RPG pre-mRNA at the earliest (5- and 10-minute) time points is a common characteristic of all of the amino acid starvation responses (Fig. 2). Furthermore, the magnitude of the accumulation seems to scale with the severity of the stress. Depletion of just histidine from the growth media elicits a much more subtle response than the other treatments. Washing histidine away likely fails to completely remove all histidine from the cell, and instead causes a slow decrease in the available pools of histidine. In the wild-type strain, up-regulation of the histidine biosynthetic pathway may be nearly able to keep up with the depletion of histidine from environmental sources. The perturbation to translation is thus mild and transient. Accumulation of the RPG pre-mRNA is barely discernible in the heat map representation of the data, but plotting the average log2-transformed ratio for each feature type (RPG pre-, mature, and total mRNA and non-RPG pre-, mature, and total mRNA) (Fig. 2B) shows that the RPG pre-mRNA levels are in fact modestly elevated while the other features are essentially unchanged.

When histidine is depleted from a histidine auxotroph, the response is somewhat more pronounced, presumably because the histidine shortage caused by washing histidine out of the media cannot be successfully relieved by up-regulation of the histidine biosynthetic pathway in this strain. Treatments with 3-AT or SMM cause inhibition of biosynthetic pathways that are already engaged as the sole sources of histidine or isoleucine and valine, respectively, and are expected to cause a sudden sharp drop in the available pools of those amino acids. The perturbation to translation is thus more dramatic, and a strong accumulation of RPG pre-mRNAs is observed throughout the

early portion of the time course, while amino acid biosynthetic genes are being up-regulated.

Depletion of all amino acids (plus uracil and adenine) causes a degree of accumulation of RPG pre-mRNA similar to that observed for histidine depletion in a histidine auxotroph in the early time points of the time course. The wild-type strain used in this experiment is in fact auxotrophic for leucine, uracil, and lysine, so the similarity of the magnitude and kinetics of the RPG pre-mRNA accumulation in this treatment to that seen when a histidine auxotroph is depleted for histidine is perhaps unsurprising. However, the behaviors of the mature and total mRNA species diverge significantly in the later time points of the time course, as these species decrease significantly in abundance following depletion of all amino acids. The loss of RPG mature mRNA at later time points is a pronounced feature of the responses that lead to inactivation of TORC1 (see Fig. 3 and results below), and may reflect cross-talk between the amino acid starvation and TORC1 pathways [47]. Amino acids can also be utilized as a nitrogen source, so depletion of all amino acids may also trigger some activation of nitrogen starvation pathways that lead to TORC1 inactivation (reviewed in [20]).

The second class of responses identified by clustering analysis is characterized by decreases in all three species of RPG transcripts, and includes glucose and phosphate depletion, drugs that inhibit TORC1, heat shock, and DTT treatment (green bars in Fig. 1). The pre-mRNAs decrease more rapidly than the mature and total mRNA species, with significant decreases apparent at the first time point, while the mature and total

only show significant decreases at the 20- and 40-minute time points (Fig. 3). Interestingly, heat shock appears to induce the most rapid and dramatic loss of RPG mRNA transcripts. Previous work had suggested that heat shock leads to inhibition of all pre-mRNA splicing and widespread accumulation of pre-mRNAs [43-45]. However, this conclusion was made based on the behavior of a small number of transcripts. Our results show that while a few transcripts do indeed accumulate pre-mRNA in response to heat shock (Fig. 3A and Fig. 8C), the majority of RPG pre-mRNAs are rapidly degraded. The magnitudes of the changes observed in response to phosphate starvation were small, but the patterns of changes were similar enough to those observed in other TORC1-inactivating stresses for it to cluster with this group.

The third class of response identified by the clustering analysis included the ionic and hyperosmotic stresses (red bars in Fig. 1). These responses are characterized by a rapid loss of RPG pre-mRNA, but relatively smaller decreases in the mature mRNAs than in the second class (Fig. 4). For the cation-toxic stresses (NaCl and LiCl), the loss of RPG pre-mRNA is more dramatic than for the hyperosmotic stresses. In the KCl treatment, the levels of total and mature mRNAs for the RPGs actually increase over the time course. A sample taken at 60 minutes showed that the total and mature mRNAs for the RPGs did eventually decrease below the level at which they started. The response to sorbitol is milder in magnitude than the responses to the salt stresses, but still shows a decrease in RPG pre-mRNAs at the early time points, coupled with very small decreases in the mature and total mRNAs only late in the time course. Hyperosmotic stresses lead to transient inactivation of TORC1 [21], and the expected concomitant downregulation of

RPG transcription is reflected by the loss of RPG pre-mRNA. The persistence of the mature and total mRNA species for the RPGs, relative to the other TORC1-inactivating stresses in the previous class of responses, could reflect an increase in the stability of the cytoplasmic pool of mature mRNAs for these genes, or a higher proportion of the pre-mRNAs being spliced to mature transcripts rather than going directly to decay, or both.

We wanted to pursue further the question of whether the mechanisms contributing to the loss of RPG pre-mRNA are distinct for the second and third classes of stress. Changes in three rates contribute to changes in the steady state levels of pre-mRNAs: the rate of appearance of new pre-mRNAs due to transcription, the rate of disappearance of pre-mRNAs due to splicing, and the rate of disappearance of pre-mRNAs due to degradation. To determine the contribution of active nuclear degradation to the loss of RPG pre-mRNAs in these two classes of stress, we repeated the rapamycin and KCl treatments in a *Δrrp6* strain, and competitively hybridized these samples directly against samples from the wild-type strain (Fig. 5). Rrp6 is a nucleus-specific component of the exosome that contributes to nuclear decay of aberrant mRNAs [48, 49]. At steady state, levels of many pre-mRNAs are mildly elevated in a *Δrrp6* strain compared to a wild-type strain (see the time 0 column in fig. 5). However, upon rapamycin treatment, the levels of most RPG pre-mRNAs become dramatically higher in the *Δrrp6* strain compared to the wild-type subjected to the same treatment. At later time points, the levels of mature RPG transcripts are also higher in the *Δrrp6* strain, suggesting that, in the wild type strain, the nuclear degradation of pre-mRNAs at early

points in the time course contributes substantially to the decrease in mature transcript observed at later time points. By contrast, in the KCl treatment, most transcripts show little additional accumulation over the time course, although a small subset of RPG pre-mRNAs show mild increases in at the 20- and 40-minute time points. Thus it appears that nuclear degradation of RPG pre-mRNAs does not account for most of the decreases observed during KCl treatment, especially at early time points. Instead, the decreases in this stress could be due to a decreased rate of new transcription, or an increased rate of pre-mRNA splicing. Previous work has suggested that RPG transcription is in fact down-regulated during hyperosmotic stress [15] and that the RPG transcripts are extremely efficiently co-transcriptionally spliced in non-stress conditions [50]. Based on these findings, we believe it most likely that the decreases observed in the RPG pre-mRNA in the KCl treatment are due to decreased transcription with little change in splicing efficiency, and not due to increased splicing efficiency.

Although quantitative analysis of the behavior of the splicing isoform-specific species in various stresses yields three distinct classes of response, it is also clear that each response has some unique characteristics, and that some characteristics are shared across classes of response. The hierarchical clustering algorithm defined two major branches in a dendogram representing all of the stresses (Fig. 1, right side): one that contained stresses causing increases in the pre-mRNAs for at least some RPGs, and another that contained all of the stresses that displayed decreases in the pre-mRNAs for the RPGs. The stresses in the first branch are not known to lead directly to TORC1 inactivation or cell cycle arrest, while the second branch included the stresses expected

to inactivate TORC1. The classification of the responses by both clustering algorithms is largely driven by the behavior of the RPGs, as they represent approximately 40% of the transcripts analyzed, and their abundances were generally coordinately and dramatically affected by the stresses we tested. We were interested in gaining further insight into which additional signaling pathways might contribute to the observed changes in RPG pre-mRNA processing. Our previous work had shown that Gcn2, the kinase canonically responsible for sensing amino acid starvation and signaling to the translation machinery (reviewed in [41]), was not required for the RPG pre-mRNA accumulation response to amino acid starvation [11]. We undertook a candidate screening approach to find other kinases that might be involved in mediating responses to stress at the level of pre-mRNA splicing.

CK2 is involved in mediating stress responses at the level of pre-mRNA processing

We focused initially on identifying factors that were required for the accumulation of pre-mRNA in response to amino acid starvation. Because direct inactivation of TORC1 by rapamycin or wortmannin clustered with a variety of stresses known to cause TORC1 inactivation, and away from amino acid starvation stresses, we sought a candidate that did not have known direct interactions with TORC1 signaling. CK2 (CK2) satisfied this condition, and additionally was shown to genetically interact with several splicing factors in yeast [51].

CK2 consists of two catalytic subunits (Cka1 and Cka2) and two regulatory subunits (Ckb1 and Ckb2). Deletion of any single subunit does not cause an obvious growth

phenotype, and deletion of both regulatory subunits yields an epistatic genetic interaction in a quantitative epistasis mini-array profile [52]. We thus started by testing the ability of a *Δckb1Δckb2* double regulatory subunit mutant to respond at the level of pre-mRNA splicing to amino acid starvation. Strikingly, we found that the accumulation of RPG pre-mRNA following 3-AT treatment was almost completely abolished in this mutant (fig. 6A). We next looked at the effects of deleting each of the two regulatory subunits individually, and found that while each of the deletions diminished the accumulation of RPG pre-mRNA following 3-AT treatment relative to the wild type, the *Δckb2* mutant had a stronger effect than did the *Δckb1* mutant.

We also examined the effects of pre-treating cells with a drug that inhibits CK2 activity, 4,5,6,7-Tetrabromo-2-azabenzimidazole (TBB) [53]. Inhibiting the catalytic activity of CK2 strongly abrogates the accumulation of RPG pre-mRNAs in response to 3-AT as well (fig. 6B). Deletion of the CK2 regulatory subunits and treatment with TBB both cause some mild changes to steady state levels of pre-mRNA, mature mRNA, and total mRNA for the RPGs, but these changes do not phenocopy the changes observed in response to 3-AT (fig. 6A and 6B). This suggests that normal CK2 activity constitutively influences transcription, splicing, and/or turnover of the RPG transcripts, but that the loss of 3-AT response observed when CK2 is perturbed is not because the perturbation itself causes cells to be in an amino acid starvation response state constitutively.

Finally, we asked whether the contribution made by CK2 to the amino acid starvation response at the level of pre-mRNA processing might correlate with a fitness phenotype

under amino acid starvation conditions. We spotted serial dilutions of strains carrying mutations for each of the CK2 subunits, plus the regulatory subunit double mutant, onto plates containing 50 mM 3-AT. For reference, a strain carrying a deletion of Gcn2, the kinase involved in the translational response to amino acid starvation, was also plated. The *Δckb2* strain showed a strong fitness defect under conditions of exposure to 3-AT. Interestingly, the *Δckb1* strain showed a milder fitness defect, and the double regulatory subunit delete showed a defect similar to the milder *Δckb1* defect. The *Δcka1* strain also showed an intermediate fitness defect, while the *Δcka2* strain grew as well as the wild type (fig. 6C). The fitness defect of the catalytic subunit delete is perhaps consistent with the pre-mRNA processing defect caused by inhibiting the catalytic activity of CK2 with TBB. These results suggest that the CK2 subunits may have specialized functions with regard to the amino acid starvation response.

Because the response to rapamycin also involves a change in processing of the RPG pre-mRNAs, leading to their Rrp6-mediated degradation, we asked whether CK2 contributes to this response as well. We subjected the *Δckb1Δckb2* double mutant to the rapamycin stress time course, and found that the loss of RPG pre-mRNA was diminished in this mutant compared to the wild type (Fig. 7A). We also pretreated the wild-type strain with TBB before subjecting it to rapamycin treatment, and in contrast to the result with the regulatory subunit double mutant, found that inhibiting the catalytic activity of CK2 had little effect on the response to rapamycin treatment (fig. 7A). We also assayed each of the CK2 subunit deletes for fitness defects by spotting the strains onto plates containing rapamycin. Interestingly, the pattern of sensitivity to rapamycin

was distinct from that observed for 3-AT. Deletion of *CKB2* caused extreme sensitivity that was not suppressed by deletion of *CKB1* in the double mutant. No other subunit deletion caused substantial sensitivity to rapamycin, consistent with the observation that deletion of both regulatory subunits but not inhibition of the catalytic activity of CK2 diminished the response to rapamycin at the level of RPG pre-mRNA processing.

To determine which signaling pathways might contribute to the loss of RPG pre-mRNA in hyperosmotic stress, we started by exposing *Δhog1* cells to a KCl treatment time course. Hog1 is the mitogen-activated kinase known to be responsible for transcriptional induction of several genes involved in the response to high osmolarity. However, we found the response to KCl at the level of RPG pre-mRNA processing to be virtually unperturbed by deletion of this kinase (fig. 7B), reminiscent of the lack of requirement for Gcn2 in the pre-mRNA processing response to amino acid starvation. We also tested whether CK2 contributes to this stress response by measuring the response in the *Δckb1Δckb2* strain and in cells pre-treated with TBB, and found that neither perturbation of CK2 function affected the behavior of the RPG transcripts during KCl treatment (fig. 7B). Consistent with this observation, none of the CK2 subunit deletions caused a substantial fitness defect when grown on plates containing 1 M KCl (fig. 7C).

Several groups of transcripts are differentially regulated at the level of pre-mRNA processing

Thus far we have focused on the behavior of the RPG transcripts as a group, because a majority of these transcripts behave coordinately across most of the stresses we tested,

and these behaviors dominate quantitative analysis of stress-induced changes to pre-mRNA processing as a whole. In order to look for subgroups of RPGs behaving distinctly under stress, as well as for groups of non-RPG transcripts that might be coordinately regulated at the level of pre-mRNA processing, we again used hierarchical and k-means clustering. This time, instead of analyzing the behavior of each stress across all transcripts, we subjected to clustering the behavior of each transcript across all stresses. Hierarchical clustering produced a complex dendogram (Fig. 8, right), and k-means clustering produced five groups of transcripts (Fig. 8, left). Two of these (orange and blue) comprised sub-groups of RPGs, two other small groups (purple and green) contained primarily non-RPG transcripts, and the fifth group contained the rest of the transcripts (white). The larger RPG subgroup (blue) contains most of the RPG transcripts that show strong pre-mRNA accumulation in response to the amino acid starvation stresses and strong loss of pre-mRNA in response to TORC1-inactivating stresses. Interestingly, chi-squared analysis of paralog pairs of the RPGs revealed that both members of a paralog pair were less likely than expected by chance to be present in the same sub-group of RPGs ($p<10^{-4}$). Examples of paralog pairs that separate into the two different RPG subgroups include *RPL14A* (blue) and *B* (orange), and *RPS11A* (orange) and *B* (blue) (Fig. 8B). By contrast, one of the small clusters (purple) contains both paralogous copies of the U3 snoRNA. These transcripts seem to behave oppositely to the majority of the RPG transcripts in many of the stresses tested (Fig. 8B). While the RPGs are largely being degraded in stringent stresses, the levels of mature and total U3 snoRNA go up, and the levels of the pre-RNA for these transcripts go down.

The other non-RPG cluster, represented by green in figure 8A, contains several transcripts whose pre-mRNA and mature mRNA levels change dramatically in some stresses, but are not easily classified as having a coherent set of biological functions. Nonetheless, some interesting patterns can be observed. The *ACT1* gene, which has traditionally been used as a splicing reporter, shows increased levels of both the pre-mRNA and the mature mRNA in many stresses. For example, heat shock, which has previously been reported to cause accumulation of the *ACT1* pre-mRNA, does indeed do so in our hands, but it also leads to an increase in the mature message. *TUB1* and *TUB3* are paralogs encoding alpha-tubulin. Like many of the RPG paralogs, they fall into different k-means clusters on the basis of their behavior in stress (fig. 8B). *HNT1* and *HNT2* belong to the histidine triad family of nucleotide binding proteins. They both fall into the green cluster of transcripts in this analysis, and interestingly, show strong pre-mRNA accumulation in some of the stresses where RPG pre-mRNAs are rapidly lost. This further illustrates that regulation at the level of pre-mRNA processing is dynamic and transcript-specific, with a range of behaviors observed for different transcripts under the same stress condition.

Discussion

We present here a broad survey of pre-mRNA processing changes in response to stress. All of the types of amino acid starvation that we tested led to a transient accumulation of RPG pre-mRNA, and the magnitude of the accumulation scaled with the severity of

the stress. Unlike amino acid starvation, stresses that led to TORC1 inactivation caused a rapid loss of RPG pre-mRNA, and could be further sub-divided into two categories: one category that is characterized by a strong decrease in the mature mRNAs for the RPGs following a decrease in the RPG pre-mRNAs, and another category that is characterized by relative stabilization of the mature RPG mRNAs despite decreases in the pre-mRNAs. We showed that the nuclear exosome component Rrp6 was required for the RPG mRNA decreases seen in response to rapamycin, which fell into the first class of stresses leading to TORC1 inactivation, but not for the decreases seen in response to KCl, a member of the second class. We also showed that perturbation of CK2 has different effects on different stress responses. Finally, we can observe different patterns of change for a variety of non-RPG transcripts. In total, these results suggest that regulation at the level of pre-mRNA processing contributes to the regulation of the gene expression program in the face of a wide range of environmental challenges.

Fine-tuning regulation of ribosomal protein gene expression and ribosome biogenesis

By far the most striking effects observed in this study were on ribosomal protein gene transcripts, suggesting that changes to pre-mRNA processing can contribute to regulation of these transcripts in the context of stresses that inhibit translation at different levels and over different periods of time. It seems likely that changes to pre-mRNA processing could allow for modulation of both the initial kinetics of the down-regulation and also the kinetics of the recovery from the stress response.

In the case of amino acid starvation, translation is at least transiently down-regulated at the level of initiation, which contributes to the Gcn4-dependent induction of amino acid biosynthetic genes and also presumably conserves cellular energy resources while amino acid biosynthesis is being up-regulated [41]. It has been shown, however, that amino acid starvation does not induce a protracted growth arrest. Even starvation of an auxotroph for the amino acid it cannot make fails to induce a G0 arrest, despite a long-term loss of viability, while starvation of the same strain for glucose, nitrogen, or phosphate does induce a protective G0 growth arrest [30]. For a wild-type yeast strain, a decrease in the environmental availability of one or several specific amino acids in the presence of sufficient carbon, nitrogen, sulfate, and phosphate sources should not require a growth arrest, as the missing amino acids can be synthesized. The regulation at the level of pre-mRNA processing of the RPGs that we have observed, in which splicing is inhibited and pre-mRNAs transiently accumulate, could provide a transient inhibition of ribosomal protein biogenesis consistent with the transient translational inhibition caused by amino acid starvation. The increasing accumulation of RPG pre-mRNA during the first 10 minutes of the stress suggests that transcription of the RPGs is ongoing. In the mildest form of this stress, histidine depletion, the RPG pre-mRNA accumulation was very modest and transient indeed, and no decreases in the mature pools of RPG mRNA were detected, suggesting that transcription of the RPGs was largely unperturbed. The capacity to transiently down-regulate RPG expression by a mechanism that allows RPG promoters to remain active could allow for a faster resumption of maximal growth rate following alleviation of the amino acid shortage.

By contrast, the common characteristic of the other two groups of stresses was a decrease in the pre-mRNAs for the RPGs. In the second class of stress responses (including heat shock, rapamycin, wortmannin, and glucose starvation), a rapid decrease in pre-mRNA levels for the RPGs was followed by a strong decrease in the mature mRNA levels. The requirement for Rrp6 in this response suggests that active degradation of the pre-mRNA contributes substantially, both to the early loss of pre-mRNA and the later loss of mature mRNA. Interestingly, when rapamycin treatment is combined with 3-AT treatment, the response closely approximates the response to rapamycin alone, suggesting that this more stringent response at the level of RPG pre-mRNA processing (leading to nuclear turnover of nascent transcripts) is dominant over the transient amino acid starvation response (Supplemental Fig. S22). This epistatic behavior suggests that the two responses, although very different, impinge on the same process, and is perhaps consistent with the observation that both responses require the Ckb2 subunit of CK2. The pattern of RPG pre-mRNA loss observed for this class of stresses is indicative of preparation for a protracted arrest, and also a very rapid downshift in ribosome production, which may be appropriate when energy resources are at a premium, or when protein folding resources are overtaxed.

For all of the hyperosmotic and ionic stresses, the loss of mature mRNAs is mild compared to the loss of pre-mRNAs for the RPGs, over a wide range of magnitudes of pre-mRNA loss. This may be due to stabilization of the cytoplasmic pools of mature mRNA, and is consistent with recent studies that have showed decreased decay rates specifically for RPG mRNAs in hyperosmotic and ionic stresses, even as these messages

were being transcriptionally repressed [16, 17]. Neither Rrp6 nor CK2 was required for the response to KCl, suggesting that the response does not involve active turnover of the RPG pre-mRNA, and that the regulation of this response is distinct from the regulation of the amino acid starvation and rapamycin responses. We also find that combining the KCl and 3-AT stresses yields a response that is distinct from the responses to either individual stress (Supplemental Fig. S22). This non-epistatic behavior supports the model that amino acid starvation and KCl affect RPG transcripts via distinct pathways. In any case, a mechanism of RPG repression whereby new transcription is halted but the messages that have already been transcribed continue to be processed and/or stabilized to varying degrees could allow the cell to prepare for a protracted growth arrest, while still transiently maintaining needed translational capacity for adapting to the stress.

Consistent with the idea that regulation at the level of pre-mRNA processing may contribute to both induction of and recovery from a stress response, we also observe interesting behavior in the pre- and mature RNA species for the two copies of U3, the spliced snoRNA that helps direct rRNA cleavage and is therefore essential in ribosome biogenesis. In the stresses that most strongly down-regulate the RPGs at both the pre- and mature mRNA levels, the U3 transcripts show increases for the total and mature species and decreases for the pre-RNA. Thus, U3 appears to be up-regulated at the same time the cell is broadly down-regulating ribosome biogenesis. While the requirement for new ribosomes is much diminished during a G0 arrest, translation does not stop completely. It has been shown that after the initial rapid and dramatic

polysome collapse during glucose starvation, translation can in fact resume [54]. The cell may need to up-regulate U3 in preparation for resumed protein synthesis. Interestingly, the salt stresses just show a decrease of the unspliced U3 message, without a corresponding increase in the mature message, and the amino acid starvation stresses show little change in the abundance of the U3 transcript species. Thus it appears that regulation at the level of pre-mRNA processing may also differentially influence the levels of a ribosome biogenesis factor in different stresses.

Another observation potentially consistent with ongoing but differentially regulated synthesis of ribosomes under stress conditions is the tendency of paralogous pairs of ribosomal protein genes to show differential behavior across stress treatments. Different regulatory elements governing expression of the RPG paralogs could allow for ongoing expression of each required ribosomal protein under very different regulatory regimes. For example, in some cases it is known that one of the paralogs is more highly expressed under rich nutrient conditions [55], and it may be that expression of the other paralog is important under less optimal conditions, when expression of the normally more highly expressed paralog is shut down. Notably, we also observed distinct behavior across the stress treatments for the *TUB1* and *TUB3* transcripts (paralogous copies of the gene encoding alpha tubulin). This suggests that maintaining paralogous copies of highly expressed genes, which can be differentially regulated both at the level of transcription and at the level of pre-mRNA processing, may be a broadly utilized strategy.

CK2 plays has stress-specific effects on pre-mRNA processing

We have shown here that perturbing CK2 in various ways alters the response at the level of pre-mRNA processing to some stresses, and causes sensitivity to those same stresses. Given the host of reported CK2 substrates with roles in transcription, mRNA processing, ribosome biogenesis, and translation, it is tempting to speculate that our results reflect a role for CK2 in coordinating translational down-regulation in response to some stresses. While its large number of relevant substrates makes CK2 a good candidate for contributing to this regulation, they also make it very difficult to determine the precise mechanistic roles. Nevertheless, our data may suggest new insight into possible stress-responsive roles for CK2.

The Ckb2 regulatory subunit appears to have a distinct role in the responses to both amino acid starvation and rapamycin. Deletion of *CKB2* caused significantly more sensitivity to these stresses than deletion of any of the other subunits. This is consistent with the recent finding that *CKB2*, but not any other CK2 subunit, was among a cluster of genes that, when deleted, decreased competitive fitness under both phosphate and leucine starvation conditions [56]. It has been suggested that, in mammalian cells, the CK2 β regulatory subunit is capable of associating with and regulating other kinases besides CK2 – it has been reported to activate A-Raf, Chk1, and Wee1, while it appears to inhibit c-Mos (reviewed in [57]). Alternate kinase associations for either of the regulatory subunits have not yet been identified in yeast, but our results suggest that, at

least under some stress conditions, Ckb2 may have an important independent function in yeast.

The pattern of sensitivity observed for 3-AT is intriguing – deletion of *CKB2* alone causes the strongest growth inhibition, while deletion of *CKB1* on top of the *CKB2* deletion suppresses some of that sensitivity. Deletion of *CKB1* alone or *CKA1* alone causes a similar degree of sensitivity as the *Δckb1Δckb2* double delete. This is distinct from the pattern observed with rapamycin, where deletion of *CKB2* caused a high degree of sensitivity whether or not *CKB1* was also deleted. This pattern of sensitivity may suggest that Ckb1 can also function independently of the CK2 holoenzyme, and possibly antagonistically to Ckb2 in the 3-AT response. The fact that the *Δckb1Δckb2* double delete and the *Δcka1* delete show some sensitivity suggests that the CK2 holoenzyme likely also plays some role in the 3-AT response.

The multi-subunit nature of CK2, and the apparent ability of its four subunits to act both independently and also as a heterotetrameric holoenzyme, makes it an intriguing candidate for a factor that helps integrate stress signals to coordinate ribosome biogenesis. Currently, the mechanism of regulation of CK2 activity is unknown, but the possibility that different functional roles may compete for CK2 subunits is intriguing. Such a model is reminiscent of previous work suggesting that CK2 might participate in coordinating synthesis of RPG mRNA and rRNA, such that excess rRNA processing factors could compete the RPG transcription factor Ifh1 away from active transcription

complexes containing Rap1 and Fhl1. The complex containing Ifh1 and the rRNA processing factors Utp22 and Rrp7 also contained at least some subunits of CK2 [58].

Regulation of non-RPG transcripts at the level of pre-mRNA processing

One motivation for measuring pre-mRNA and mature mRNA species for a majority of the intron-containing genes across a wide variety of stresses was to determine whether other groups of transcripts might show clear co-regulation at the level of pre-mRNA processing. The behavior of the RPGs dominated the patterns of change to pre-mRNA processing in all stresses tested, but clustering analysis of transcript behavior across all stresses did identify some additional transcripts whose levels of pre-mRNA and mature mRNA change in a variety of stresses. These transcripts did not fall into easily identifiable biological categories.

Since we intentionally chose stresses known to down-regulate translation, it is not surprising that most of the effects we observed were on ribosomal protein genes. Thus there may well be functionally coherent groups of transcripts that are coordinately regulated at the level of pre-mRNA splicing in response to other types of stress. For example, meiotic genes are also overrepresented among the intron-containing genes in yeast, and have been shown to be regulated both at the level of transcription and at the level of splicing [59]. It is interesting to note that the conditions that induce meiosis in *S. cerevisiae* involve extreme nutrient deprivation – depletion of both carbon and nitrogen sources for a long period of time. Regulation at the level of pre-mRNA

processing may in fact play a role at multiple stages in a response to ongoing nutrient deprivation of varying degrees of severity – inhibition of RPG splicing in response to a transient and mild starvation, active degradation of RPG pre-mRNAs in response to a more severe or more protracted starvation, and induction and splicing of meiotic genes when a diploid is exposed to protracted, severe starvation. In each case, the capacity to regulate expression of the relevant genes at the level of pre-mRNA processing may contribute to fine-tuning the kinetics of changes to gene expression.

Another potential function for regulation at the level of pre-mRNA processing may be to dampen changes in expression levels, which would be difficult to detect using the measurements in this study. Some intron-containing genes, such as *GLC7*, *ACT1* and *YRA1*, are known to be toxic when over-expressed, and the presence of an intron in these genes may help prevent excess transcripts from being expressed [60, 61]. In the case of *YRA1*, the intron is required for an autoregulatory mechanism by which excess Yra1 protein prevents splicing of the *YRA1* transcript [62, 63]. For the *ACT1* transcript, we see that many stresses lead to increases in both the pre-mRNA and the mature transcript. One explanation for this pattern could be that under conditions of transcriptional up-regulation, splicing can become rate-limiting, thus dampening the increase in expression of a protein for which dosage is sensitively regulated.

While there are still many unanswered questions with regard to mechanism, our work has demonstrated that the presence of introns in RPGs provides distinct opportunities for fine-tuning the regulation of gene expression under a wide range of stress

conditions. We observed distinct patterns of change in different stresses, and showed that CK2 plays important and distinct roles in these stress responses. This work provides an important context for understanding the role of regulation at the level of pre-mRNA processing in the overall architecture of yeast responses to the environment, and sheds some light on the ways in which this regulation may be integrated with other stress signaling pathways.

Materials and Methods

Strains and growth conditions: The strain yMB1 [11] was used as the wild type strain in all stress experiments, and was constructed by repairing the *HIS3* locus in the BY4742 strain [64] by homologous recombination of the full *HIS3* open reading frame into the partially deleted locus. The BY4742 strain is isogenic except for the *HIS3* locus, and was used as the histidine auxotroph in the histidine depletion experiments. The *Δckb1 Δckb2* strain was constructed by crossing the *MAT a Δckb1::KAN* strain from the deletion collection [65] to the *MATα Δckb2::NAT* strain carrying SGA markers [66]. From this cross, spores carrying both deletions but none of the SGA markers were selected, and the *HIS3* locus was subsequently repaired as in yMB1, yielding the following genotype: *Mat a Δckb1::KAN Δckb2::NAT leu2Δ0 ura3Δ0*. The *Δrrp6, Δcka1, Δcka2, Δckb1*, and *Δckb2* strains were BY4741 strains from the deletion collection in which the *HIS3* locus was repaired as described above, and the *Δhog1* strain was a BY4741 strain from the deletion collection [65]. In general, for each stress condition, a 50 ml culture was grown

to mid-log phase (OD_{600} 0.3-0.7) in the appropriate starting media at 30°C, and then the stress was applied as described below. Synthetic complete media is defined as: 6.7 g/L yeast nitrogen base (containing 5 g/L ammonium sulfate, 1g/L monopotassium phosphate, and 0.2 g/L inositol, among other vitamins and nutrients, from Difco unless otherwise noted), the following supplemented amino acids and purines (all from Sigma): 15 mg/L valine; 20mg/L arginine, adenine, histidine, methionine, tryptophan, and uracil; 30mg/L lysine, tyrosine, and isoleucine; 50 mg/L phenylalanine; 60 mg/L leucine; and 200 mg/L threonine, and 20g/L glucose. Rich media is defined as 10g/L bacto yeast extract (Difco), 20 g/L bacto peptone (Difco), and 20g/L glucose. Except in the case of heat shock, growth after the stress application was also at 30°C. 10-15 ml aliquots of culture were collected by centrifugation at 5, 10, 20, and 40 minutes after application of the stress, and cell pellets were immediately frozen in liquid nitrogen.

3-Amino-1,2,4-triazole (3-AT) treatment: Yeast were grown to mid-log phase in synthetic media lacking histidine and then 3-AT (Sigma) was added to a final concentration of 50 mM.

Amino acid depletion: Yeast were grown to mid-log phase in synthetic complete media and then collected on a 95 mm nitrocellulose filter (Whatmann) by vacuum filtration. Cells were washed with 500 ml media containing only yeast nitrogen base plus ammonium sulfate and glucose, and were then resuspended in 50 ml of this media.

Histidine depletion: Yeast were grown to mid-log phase in synthetic complete media and then collected on a 95 mm nitrocellulose filter by vacuum filtration. Cells were

washed with 500 ml synthetic media lacking histidine and were then resuspended in 50 ml of this media.

Sulfometuron methyl (SMM) treatment: Yeast were grown to mid-log phase in synthetic media lacking isoleucine and valine and then SMM (Sigma), from a stock solution of 1 mg/ml SMM in acetone, was added to a final concentration of 5 ug/ml.

Phosphate depletion: Yeast were grown to mid-log phase in synthetic complete media and then collected on a 95 mm nitrocellulose filter by vacuum filtration. Cells were washed with 500 ml synthetic media made using yeast nitrogen base that lacked monopotassium phosphate (MP Biomedicals) and were then resuspended in 500 ml of this media.

Glucose depletion: Yeast were grown to mid-log phase in rich media and then collected on a 95 mm nitrocellulose filter by vacuum filtration. Cells were washed with 500 ml rich media lacking glucose and were then resuspended in 50 ml of this media.

Rapamycin treatment: Yeast were grown to mid-log phase in rich media and then rapamycin (Calbiochem), from a stock solution of 1 mg/ml in 90% ethanol, 10% Tween-20, was added to a final concentration of 200 ng/ml.

Wortmannin treatment: Yeast were grown to mid-log phase in rich media and then wortmannin (Sigma), from a stock solution of 1 mg/ml in DMSO, was added to a final concentration of 10 ug/ml.

Dithiothreitol (DTT) treatment: Yeast were grown to mid-log phase in rich media and then DTT (Sigma), from a stock solution of 1 M in water, was added to a final concentration of 10 mM.

Heat shock: Yeast were grown to mid-log phase in rich media and then were shifted to a 42°C water bath for 5 minutes with manual shaking. Following the collection of the aliquot for the 5 minute time point, the culture was incubated on a rotary shaker at 42°C for the remainder of the time course.

Lithium chloride (LiCl) treatment: Yeast were grown to mid-log phase in rich media and then collected on a 95 mm nitrocellulose filter by vacuum filtration. Cells were washed with 500 ml rich media containing 300 mM LiCl and were then resuspended in 50 ml of this media.

Potassium chloride (KCl) treatment: Yeast were grown to mid-log phase in rich media and then collected on a 95 mm nitrocellulose filter by vacuum filtration. Cells were washed with 500 ml rich media containing 1 M KCl and were then resuspended in 50 ml of this media.

Sodium chloride (NaCl) treatment: Yeast were grown to mid-log phase in rich media and then collected on a 95 mm nitrocellulose filter by vacuum filtration. Cells were washed with 500 ml rich media containing 500 mM NaCl and were then resuspended in 50 ml of this media.

Sorbitol treatment: Yeast were grown to mid-log phase in rich media and then collected on a 95 mm nitrocellulose filter by vacuum filtration. Cells were washed with 500 ml rich media containing 1 M sorbitol and were then resuspended in 50 ml of this media.

4,5,6,7-Tetrabromo-2-azabenzimidazole (TBB) treatment: For TBB treatment alone, yeast were grown to mid-log phase in rich media and then TBB (Sigma), from a stock solution of 10mM in DMSO, was added to a final concentration of 20uM. For pre-treatment with TBB, yeast were grown and stress was applied as described above, but TBB was added to a final concentration of 20 uM 20 minutes prior to the application of the stress.

Growth assays: Yeast were grown to mid-log phase and were then diluted to an OD_{600nm} of 0.1. From this, four-fold serial dilutions were made and spotted on agar plates containing the indicated nutrients and/or drugs. Plates were incubated at 30°C for 2-4 days.

Microarrays: RNA was isolated from the frozen cell pellets by hot acid phenol extraction, as has been described previously [67]. Briefly, pellets were resuspended and mixed vigorously in equal volumes of acid phenol and aqueous buffer, then incubated for 15 minutes at 65°C, mixing vigorously every 2-3 minutes. An equal volume of chloroform was added and the mixture transferred to a 2 ml phase-lock tube (eppendorf). The mixture was additionally extracted with an equal volume of phenol:chloroform:isoamyl alcohol and then an equal volume of chloroform. The aqueous phase was transferred to a new microcentrifuge tube and sodium acetate was

added to a final concentration of 300 mM. An equal volume of isopropyl alcohol was added and the RNA was allowed to precipitate for at least 2 hours at -20°C. The precipitated RNA was washed once with 70% ethanol, dried, and resuspended in water. 50 ug RNA was used for each cDNA synthesis reaction, to generate cDNA for dye-flipped replicate arrays. cDNA synthesis, clean-up, and labeling was carried out in 96-well plate format, and hybridization to a custom splicing microarray platform was performed as described previously [39].

Microarray image analysis and preprocessing. Microarray images were acquired using an Axon Instruments GenePix 4000B scanner, reading at wavelengths of 635 nm and 532 nm (Axon Instruments, http://www.axon.com). Image analysis was performed using Axon Instruments GenePix Pro version 6.0. Ratio values derived from the median pixel intensities for the 635 nm and 532 nm images of each spot were used to represent probe behaviors in data preprocessing analysis. A standardized qualitative assessment of array quality was performed using the Bioconductor arrayQuality package, version 1.4.0 s [68, 69]. Spot ratio data were log2 transformed and normalized within each array using print-tip-based loess regression implemented in the Bioconductor marray package [6]. As all experimental contrasts are represented in the dataset at least twice (as dye-flipped replicates) and as many as 6 times for biological replicates, both within-array and between-array data replication were analyzed for data quality. Array pairs with lower than 80% correlation values were discarded from any further analysis. Additionally, arrays showing exceptional within-array variability (measured by mean replicate variance > 2 standard deviations above average across dataset) were discarded from

further analysis. The final microarray dataset represents 554 unique hybridizations covering each experimental contrast with between 2- and 6-fold replication. Prior to higher-order analysis, within- and between-array replicates on high-quality arrays were averaged.

Clustering. Hierarchical clustering was performed using the R standard library distance matrix computation [70, 71]. After preprocessing, data were clustered without centering or filtering. Unless otherwise noted, distance calculations were performed using Euclidean distance and clustering was performed among centroids. Clustering heatmaps were drawn using the R standard library 'heatmap' function, without scaling and with color saturation values at fold changes of $2^{(-2.5)}$ shown as blue and $2^{(2.5)}$ shown as yellow. Row and column annotations, including RPG transcript location and k-means clustering classes, were also drawn using this package. K-means clustering was performed using the C Clustering Library (v. 1.49) implementation [72], using Euclidean distance to classify transcript behaviors (Fig. 8A) and Kendall's tau to classify environmental treatments (Fig. 1). For k-means clustering, solutions were calculated for all possible response class numbers (k = 2 – (n-1)), and models failing to show robust solutions over 10^3 independent runs were discarded. For pair-wise transcript distance matrix calculations, experimental time points were chosen from each stress dataset representing the largest average absolute transcript level change between experimental and control samples. Similarity in transcript behaviors across all stresses was calculated using Euclidean distance. This similarity matrix was then clustered using hierarchical clustering and k-means clustering (both as described above).

Acknowledgments

We would like to thank Quinn Mitrovitch, Alex Plocik, Rebecca Holmes, Jaclyn Greimann, Phil Esra, and Wendy Gilbert for helpful suggestions and critical reading of this manuscript, and Wendy Gilbert for sharing unpublished data. We would also like to thank Joe DeRisi and Jeff Pleiss for technical assistance, and members of the Guthrie lab for useful discussion.

References

1. Warner JR (1999) The economics of ribosome biosynthesis in yeast. Trends Biochem Sci 24: 437-440.

2. Marion RM, Regev A, Segal E, Barash Y, Koller D et al. (2004) Sfp1 is a stress- and nutrient-sensitive regulator of ribosomal protein gene expression. Proc Natl Acad Sci U S A 101: 14315-14322.

3. Martin DE, Soulard A, Hall MN (2004) TOR regulates ribosomal protein gene expression via PKA and the Forkhead transcription factor FHL1. Cell 119: 969-979.

4. Zhao Y, McIntosh KB, Rudra D, Schawalder S, Shore D et al. (2006) Fine-structure analysis of ribosomal protein gene transcription. Mol Cell Biol 26: 4853-4862.

5. Rohde JR, Cardenas ME (2003) The tor pathway regulates gene expression by linking nutrient sensing to histone acetylation. Mol Cell Biol 23: 629-635.

6. Wang J, Nygaard V, Smith-Sørensen B, Hovig E, Myklebost O (2002) MArray: analysing single, replicated or reversed microarray experiments. Bioinformatics 18: 1139-1140.

7. David L, Huber W, Granovskaia M, Toedling J, Palm CJ et al. (2006) A high-resolution map of transcription in the yeast genome. Proc Natl Acad Sci U S A 103: 5320-5325.

8. Beilharz TH, Preiss T (2007) Widespread use of poly(A) tail length control to accentuate expression of the yeast transcriptome. RNA 13: 982-997.

9. Stajich JE, Dietrich FS, Roy SW (2007) Comparative genomic analysis of fungal genomes reveals intron-rich ancestors. Genome Biol 8: R223.

10. Fisk DG, Ball CA, Dolinski K, Engel SR, Hong EL et al. (2006) Saccharomyces cerevisiae S288C genome annotation: a working hypothesis. Yeast 23: 857-865.

11. Pleiss JA, Whitworth GB, Bergkessel M, Guthrie C (2007) Rapid, transcript-specific changes in splicing in response to environmental stress. Mol Cell 27: 928-937.

12. Moehle CM, Hinnebusch AG (1991) Association of RAP1 binding sites with stringent control of ribosomal protein gene transcription in Saccharomyces cerevisiae. Mol Cell Biol 11: 2723-2735.

13. Natarajan K, Meyer MR, Jackson BM, Slade D, Roberts C et al. (2001) Transcriptional profiling shows that Gcn4p is a master regulator of gene expression during amino acid starvation in yeast. Mol Cell Biol 21: 4347-4368.

14. Li B, Nierras CR, Warner JR (1999) Transcriptional elements involved in the repression of ribosomal protein synthesis. Mol Cell Biol 19: 5393-5404.

15. Gasch AP, Spellman PT, Kao CM, Carmel-Harel O, Eisen MB et al. (2000) Genomic expression programs in the response of yeast cells to environmental changes. Mol Biol Cell 11: 4241-4257.

16. Molin C, Jauhiainen A, Warringer J, Nerman O, Sunnerhagen P (2009) mRNA stability changes precede changes in steady-state mRNA amounts during hyperosmotic stress. RNA 15: 600-614.

17. Romero-Santacreu L, Moreno J, Perez-Ortin JE, Alepuz P (2009) Specific and global regulation of mRNA stability during osmotic stress in Saccharomyces cerevisiae. RNA 15: 1110-1120.

18. Grigull J, Mnaimneh S, Pootoolal J, Robinson MD, Hughes TR (2004) Genome-wide analysis of mRNA stability using transcription inhibitors and microarrays reveals posttranscriptional control of ribosome biogenesis factors. Mol Cell Biol 24: 5534-5547.

19. Wullschleger S, Loewith R, Hall MN (2006) TOR signaling in growth and metabolism. Cell 124: 471-484.

20. Zaman S, Lippman SI, Zhao X, Broach JR (2008) How Saccharomyces responds to nutrients. Annu Rev Genet 42: 27-81.

21. Urban J, Soulard A, Huber A, Lippman S, Mukhopadhyay D et al. (2007) Sch9 is a major target of TORC1 in Saccharomyces cerevisiae. Mol Cell 26: 663-674.

22. Patil C, Walter P (2001) Intracellular signaling from the endoplasmic reticulum to the nucleus: the unfolded protein response in yeast and mammals. Curr Opin Cell Biol 13: 349-355.

23. Wykoff DD, O'Shea EK (2001) Phosphate transport and sensing in Saccharomyces cerevisiae. Genetics 159: 1491-1499.

24. Wilson WA, Roach PJ (2002) Nutrient-regulated protein kinases in budding yeast. Cell 111: 155-158.

25. Cherkasova VA, Hinnebusch AG (2003) Translational control by TOR and TAP42 through dephosphorylation of eIF2alpha kinase GCN2. Genes Dev 17: 859-872.

26. Schroder M, Clark R, Liu CY, Kaufman RJ (2004) The unfolded protein response represses differentiation through the RPD3-SIN3 histone deacetylase. EMBO J 23: 2281-2292.

27. Hohmann S (2009) Control of high osmolarity signalling in the yeast Saccharomyces cerevisiae. FEBS Lett 583: 4025-4029.

28. Pedruzzi I, Dubouloz F, Cameroni E, Wanke V, Roosen J et al. (2003) TOR and PKA signaling pathways converge on the protein kinase Rim15 to control entry into G0. Mol Cell 12: 1607-1613.

29. Swinnen E, Wanke V, Roosen J, Smets B, Dubouloz F et al. (2006) Rim15 and the crossroads of nutrient signalling pathways in Saccharomyces cerevisiae. Cell Div 1: 3.

30. Boer VM, Amini S, Botstein D (2008) Influence of genotype and nutrition on survival and metabolism of starving yeast. Proc Natl Acad Sci U S A 105: 6930-6935.

31. Talarek N, Cameroni E, Jaquenoud M, Luo X, Bontron S et al. (2010) Initiation of the TORC1-regulated G0 program requires Igo1/2, which license specific mRNAs to evade degradation via the 5'-3' mRNA decay pathway. Mol Cell 38: 345-355.

32. Bidwai AP, Reed JC, Glover CV (1994) Casein kinase II of Saccharomyces cerevisiae contains two distinct regulatory subunits, beta and beta'. Arch Biochem Biophys 309: 348-355.

33. Olsten MEK, Litchfield DW (2004) Order or chaos? An evaluation of the regulation of protein kinase CK2. Biochem Cell Biol 82: 681-693.

34. Sawa C, Nedea E, Krogan N, Wada T, Handa H et al. (2004) Bromodomain factor 1 (Bdf1) is phosphorylated by protein kinase CK2. Mol Cell Biol 24: 4734-4742.

35. Dermody JL, Dreyfuss JM, Villen J, Ogundipe B, Gygi SP et al. (2008) Unphosphorylated SR-like protein Npl3 stimulates RNA polymerase II elongation. PLoS One 3: e3273.

36. Deng Y, Singer RH, Gu W (2008) Translation of ASH1 mRNA is repressed by Puf6p-Fun12p/eIF5B interaction and released by CK2 phosphorylation. Genes Dev 22: 1037-1050.

37. Allen JJ (2008) Development and Application of Technologies to Study Individual Kinase Substrate Relationships. PhD Thesis, University of California, San Francisco.

38. Prudent R, Sautel CF, Moucadel V, Laudet B, Filhol O et al. (2010) In vitro and in vivo assays of protein kinase CK2 activity. Methods Enzymol 485: 597-610.

39. Pleiss JA, Whitworth GB, Bergkessel M, Guthrie C (2007) Transcript specificity in yeast pre-mRNA splicing revealed by mutations in core spliceosomal components. PLoS Biol 5: e90.

40. Jia MH, Larossa RA, Lee JM, Rafalski A, Derose E et al. (2000) Global expression profiling of yeast treated with an inhibitor of amino acid biosynthesis, sulfometuron methyl. Physiol Genomics 3: 83-92.

41. Hinnebusch AG (2005) Translational regulation of GCN4 and the general amino acid control of yeast. Annu Rev Microbiol 59: 407-450.

42. Alarcon CM, Heitman J, Cardenas ME (1999) Protein kinase activity and identification of a toxic effector domain of the target of rapamycin TOR proteins in yeast. Mol Biol Cell 10: 2531-2546.

43. Bracken AP, Bond U (1999) Reassembly and protection of small nuclear ribonucleoprotein particles by heat shock proteins in yeast cells. RNA 5: 1586-1596.

44. Yost HJ, Lindquist S (1991) Heat shock proteins affect RNA processing during the heat shock response of Saccharomyces cerevisiae. Mol Cell Biol 11: 1062-1068.

45. Vogel JL, Parsell DA, Lindquist S (1995) Heat-shock proteins Hsp104 and Hsp70 reactivate mRNA splicing after heat inactivation. Curr Biol 5: 306-317.

46. Garcia MJ, Rios G, Ali R, Belles JM, Serrano R (1997) Comparative physiology of salt tolerance in Candida tropicalis and Saccharomyces cerevisiae. Microbiology 143 (Pt 4): 1125-1131.

47. Staschke KA, Dey S, Zaborske JM, Palam LR, McClintick JN et al. (2010) Integration of general amino acid control and target of rapamycin (TOR) regulatory pathways in nitrogen assimilation in yeast. J Biol Chem 285: 16893-16911.

48. Honorine R, Mosrin-Huaman C, Hervouet-Coste N, Libri D, Rahmouni A (2010) Nuclear mRNA quality control in yeast is mediated by Nrd1 co-transcriptional recruitment, as revealed by the targeting of Rho-induced aberrant transcripts. Nucleic Acids Res : .

49. Schmid M, Jensen TH (2008) Quality control of mRNP in the nucleus. Chromosoma 117: 419-429.

50. Carrillo Oesterreich F, Preibisch S, Neugebauer KM (2010) Global analysis of nascent RNA reveals transcriptional pausing in terminal exons. Mol Cell 40: 571-581.

51. Wilmes GM, Bergkessel M, Bandyopadhyay S, Shales M, Braberg H et al. (2008) A genetic interaction map of RNA-processing factors reveals links between Sem1/Dss1-containing complexes and mRNA export and splicing. Mol Cell 32: 735-746.

52. Collins SR, Miller KM, Maas NL, Roguev A, Fillingham J et al. (2007) Functional dissection of protein complexes involved in yeast chromosome biology using a genetic interaction map. Nature 446: 806-810.

53. Pagano MA, Bain J, Kazimierczuk Z, Sarno S, Ruzzene M et al. (2008) The selectivity of inhibitors of protein kinase CK2: an update. Biochem J 415: 353-365.

54. Ashe MP, De Long SK, Sachs AB (2000) Glucose depletion rapidly inhibits translation initiation in yeast. Mol Biol Cell 11: 833-848.

55. Komili S, Farny NG, Roth FP, Silver PA (2007) Functional specificity among ribosomal proteins regulates gene expression. Cell 131: 557-571.

56. Gresham D, Boer V, Caudy A, Ziv N, Brandt N et al. (2010) System-Level Analysis of Genes and Functions Affecting Survival During Nutrient Starvation in Saccharomyces cerevisiae. Genetics : .

57. Bibby AC, Litchfield DW (2005) The multiple personalities of the regulatory subunit of protein kinase CK2: CK2 dependent and CK2 independent roles reveal a secret identity for CK2beta. Int J Biol Sci 1: 67-79.

58. Rudra D, Mallick J, Zhao Y, Warner JR (2007) Potential interface between ribosomal protein production and pre-rRNA processing. Mol Cell Biol 27: 4815-4824.

59. Munding EM, Igel AH, Shiue L, Dorighi KM, Trevino LR et al. (2010) Integration of a splicing regulatory network within the meiotic gene expression program of Saccharomyces cerevisiae. Genes Dev 24: 2693-2704.

60. Liu H, Krizek J, Bretscher A (1992) Construction of a GAL1-regulated yeast cDNA expression library and its application to the identification of genes whose overexpression causes lethality in yeast. Genetics 132: 665-673.

61. Rodriguez-Navarro S, Strasser K, Hurt E (2002) An intron in the YRA1 gene is required to control Yra1 protein expression and mRNA export in yeast. EMBO Rep 3: 438-442.

62. Preker PJ, Kim KS, Guthrie C (2002) Expression of the essential mRNA export factor Yra1p is autoregulated by a splicing-dependent mechanism. RNA 8: 969-980.

63. Preker PJ, Guthrie C (2006) Autoregulation of the mRNA export factor Yra1p requires inefficient splicing of its pre-mRNA. RNA 12: 994-1006.

64. Brachmann CB, Davies A, Cost GJ, Caputo E, Li J et al. (1998) Designer deletion strains derived from Saccharomyces cerevisiae S288C: a useful set of strains and plasmids for PCR-mediated gene disruption and other applications. Yeast 14: 115-132.

65. Giaever G, Chu AM, Ni L, Connelly C, Riles L et al. (2002) Functional profiling of the Saccharomyces cerevisiae genome. Nature 418: 387-391.

66. Fiedler D, Braberg H, Mehta M, Chechik G, Cagney G et al. (2009) Functional organization of the S. cerevisiae phosphorylation network. Cell 136: 952-963.

67. Schmitt ME, Brown TA, Trumpower BL (1990) A rapid and simple method for preparation of RNA from Saccharomyces cerevisiae. Nucleic Acids Res 18: 3091-3092.

68. Paquet AC YY arrayQuality: Assessing array quality on spotted arrays.

69. Gentleman RC, Carey VJ, Bates DM, Bolstad B, Dettling M et al. (2004) Bioconductor: open software development for computational biology and bioinformatics. Genome Biol 5: R80.

70. Becker RA, Chambers JM, Wilks AR (1988) The new s language. Chapman & Hall, New York. p.

71. Borg I, Groenen P (1997) Modern multidimensonal scaling. theory and applications. Springer. p.

72. de Hoon MJL, Imoto S, Nolan J, Miyano S (2004) Open source clustering software. Bioinformatics 20: 1453-1454.

Financial Disclosure

This work was supported by NIH grant GM21119. MB was supported by an HHMI pre-doctoral fellowship. GBW received funding from the Committee for the Support of Faculty Scholarship at Grinnell College. CG is an American Cancer Society Research Professor of Molecular Genetics. The funders had no role in study design, data collection and analysis, decision to publish, or preparation of the manuscript.

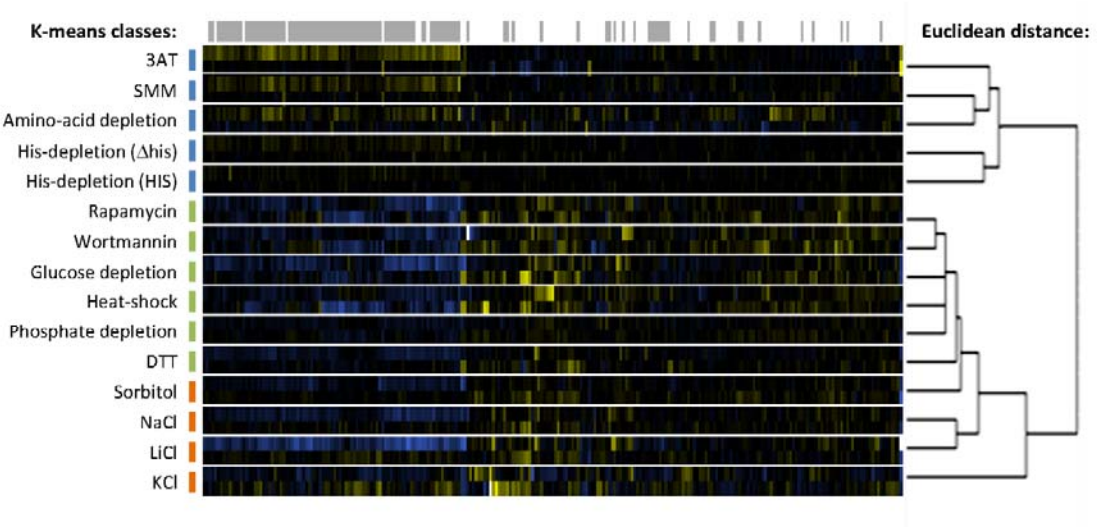

Figure 1. **Comparison of mature mRNA and pre-mRNA level changes across diverse environmental stresses by clustering analysis**. Stress treatments, named in the left-hand column, are ordered vertically by hierarchical clustering using Euclidean distance (dendogram shown at the right of the figure). K-means clustering was also used to group responses into three distinct subclasses, highlighted by colored bars. For each stress response, changes in total mRNA levels (top row) and pre-mRNA levels (bottom row) are shown in the central heatmap (saturated blue indicates at least a 5.7-fold ($2^{2.5}$) decrease in abundance, saturated yellow at least a 5.7-fold increase). Grey bars across the top of the heatmap mark the locations of RPG transcripts.

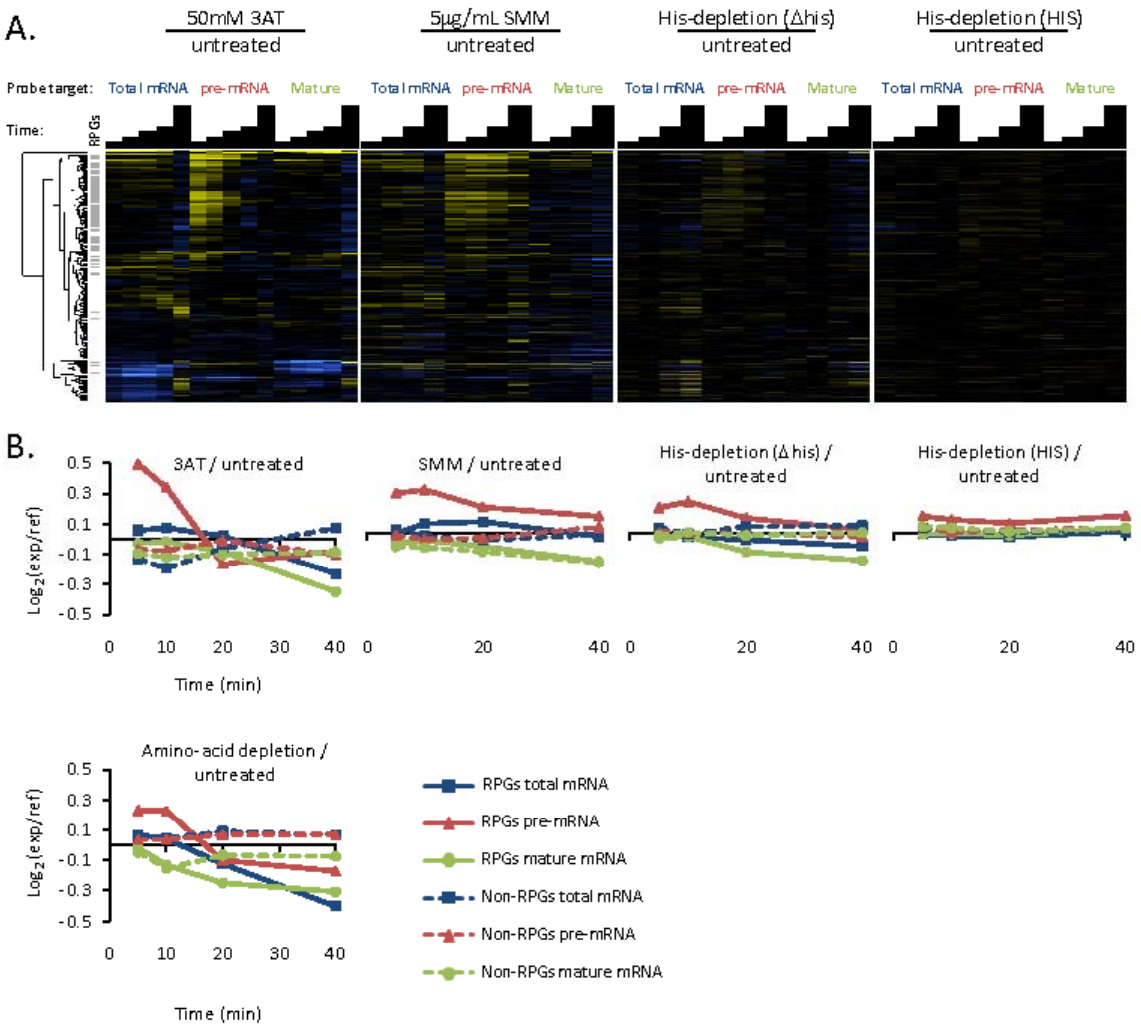

Figure 2. Accumulation of RPG pre-mRNAs under amino acid starvation conditions. (A) Time resolved splicing profiles resulting from comparison of wild-type cells treated with amino acid biosynthesis inhibitors or shifted into amino acid-depleted media, compared to a mock treatment. Samples were collected at 5, 10, 15, 20, and 40 minutes (3-AT) or at 5, 10, 20, 40 minutes (all others) following treatment. Transcripts are arranged on the vertical axis by hierarchical clustering (dendogram shown at left), and grey bars highlight the positions of RPGs within this cluster. In the heatmap, saturated blue indicates at least a 5.7-fold decrease and saturated yellow at least a 5.7-fold increase in transcript abundance. (B) Averaged RPG and non-RPG transcript behaviors across datasets shown in (A).

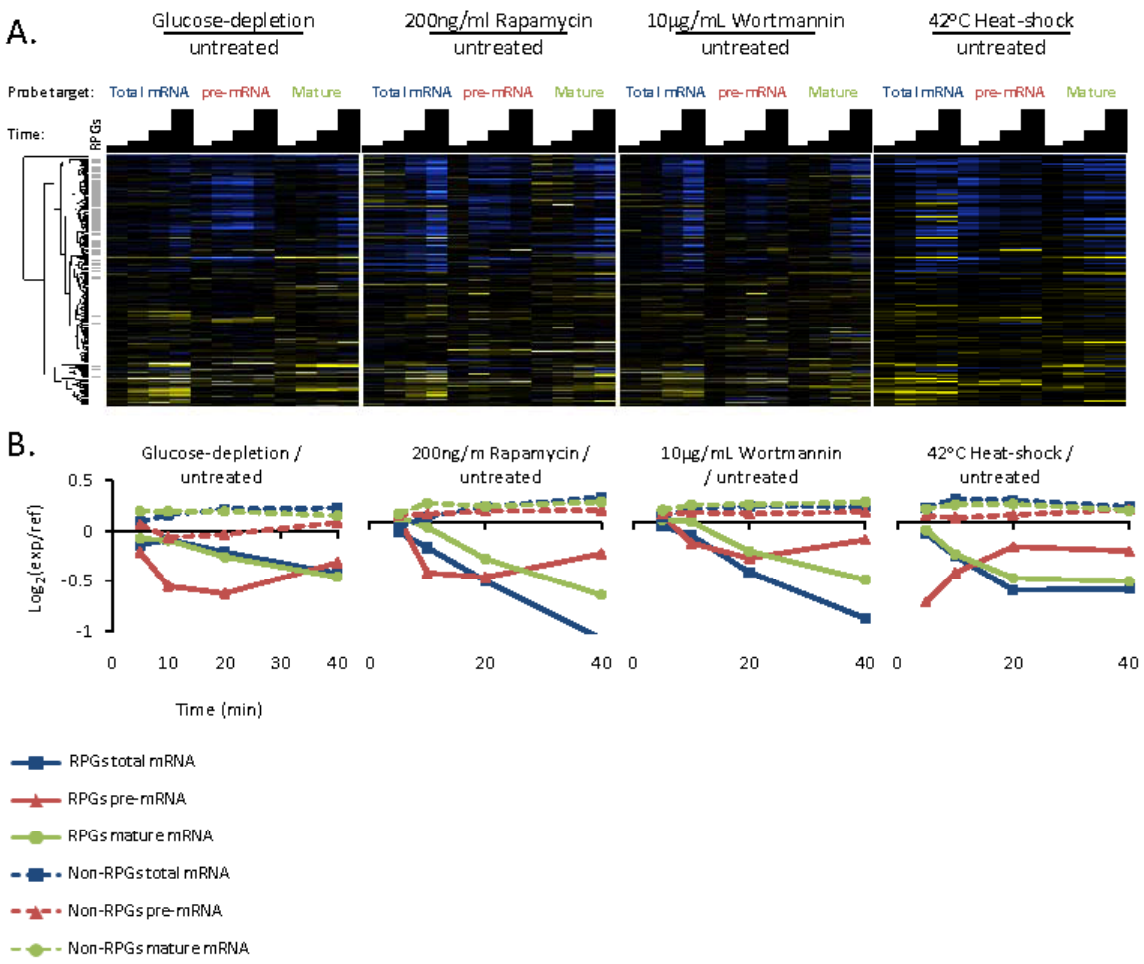

Figure 3. Rapid loss of RPG pre-mRNAs and mature mRNAs levels following glucose starvation, heatshock and direct TORC1 inhibition. (A) Time resolved splicing profiles are shown from comparisons of wild-type cells in treated and untreated samples across a time course of 5, 10, 20, 40 minutes. Transcripts are arranged on the vertical axis by hierarchical clustering (dendrogram shown at left), and grey bars highlight the positions of RPGs within this cluster. In the heatmap, saturated blue indicates at least a 5.7-fold decrease and saturated yellow at least a 5.7-fold increase in transcript abundance. (B) Averaged RPG and non-RPG transcript behaviors across datasets shown in (A).

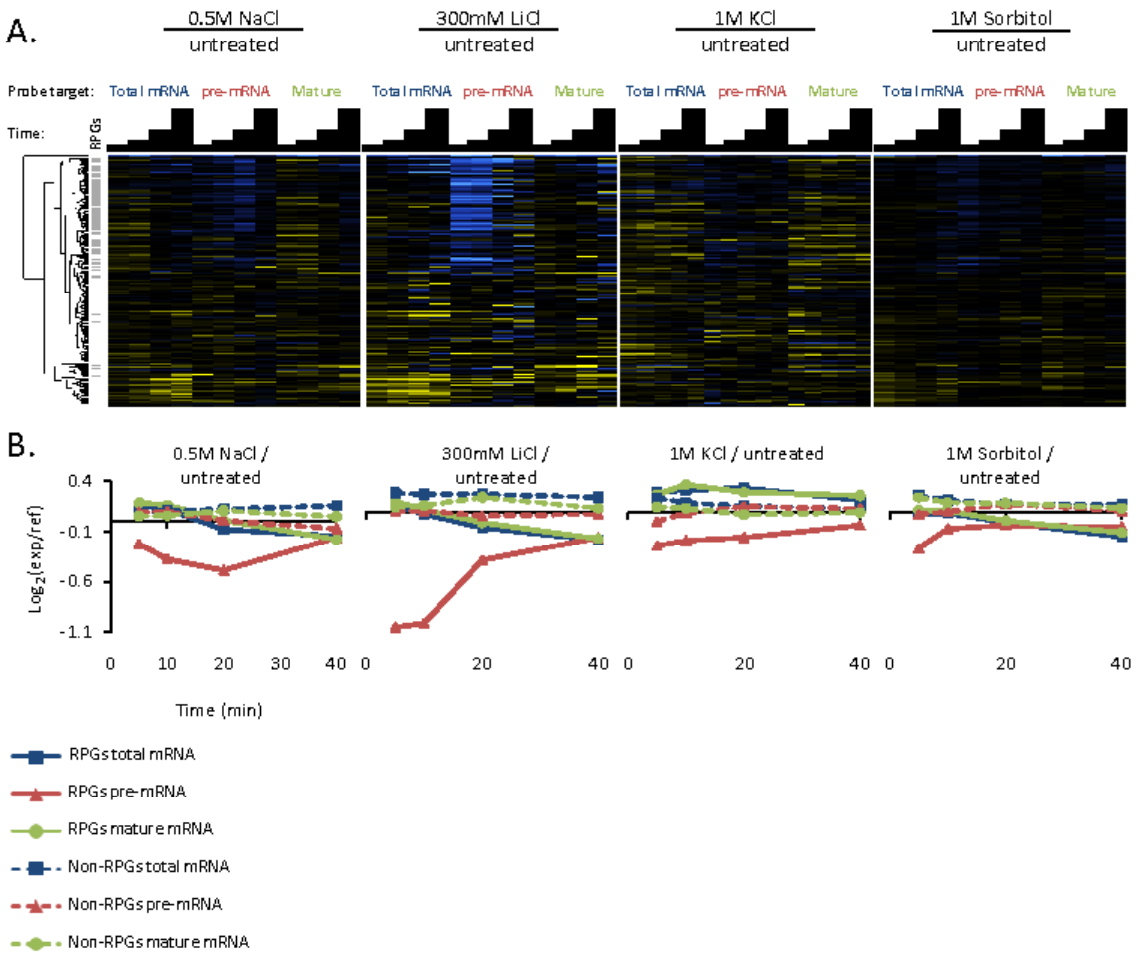

Figure 4. **Rapid loss of RPG pre-mRNAs in response to cation toxicity and hyperosmotic stresses.** (A) Time resolved splicing profiles are shown from comparisons of wild-type cells in treated and untreated samples across a time course of 5, 10, 20, 40 minutes. Transcripts are arranged on the vertical axis by hierarchical clustering (dendogram shown at left), and grey bars highlight the positions of RPGs within this cluster. In the heatmap, saturated blue indicates at least a 5.7-fold decrease and saturated yellow at least a 5.7-fold increase in transcript abundance. (B) Averaged RPG and non-RPG transcript behaviors across datasets shown in (A).

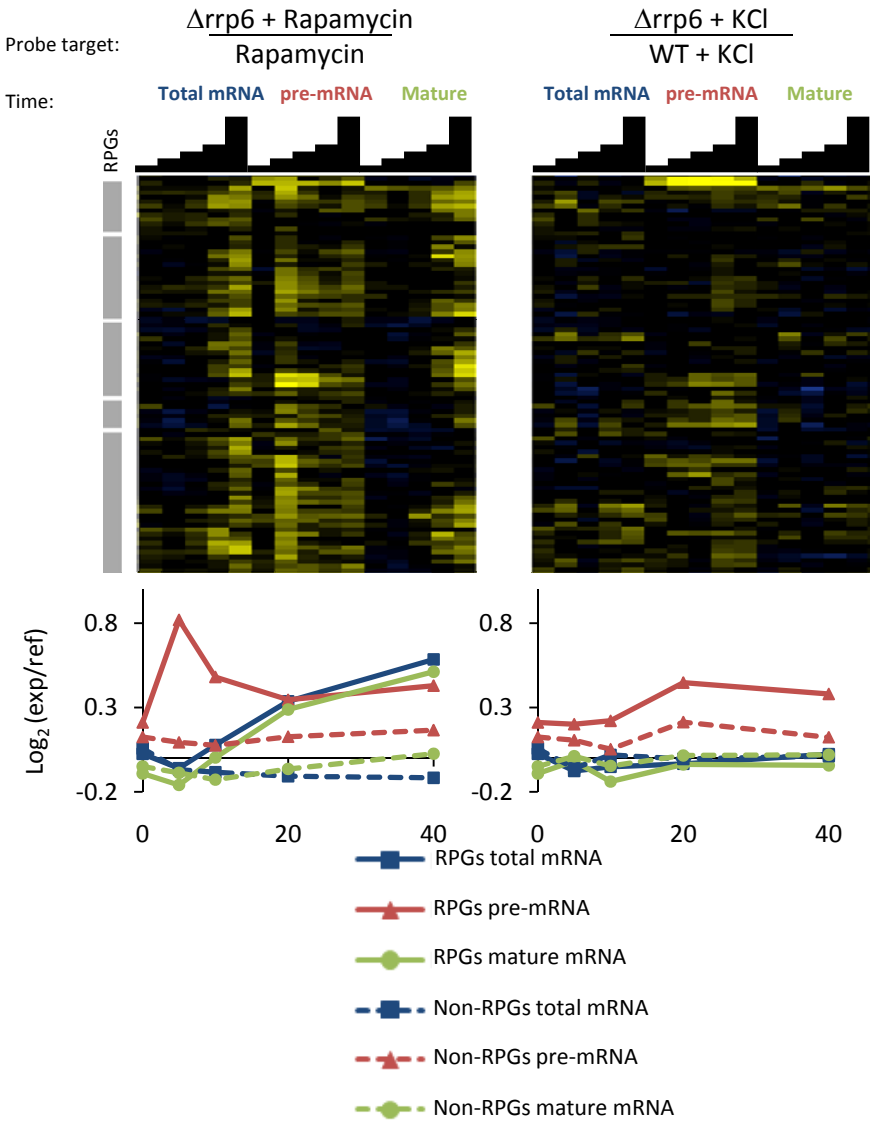

Figure 5. **The nuclear exosome component Rrp6 contributes substantially to the decrease in RPG transcripts caused by rapamycin treatment, but not by KCl treatment.** (A) Time resolved splicing profiles are shown from comparisons of *Δrrp6* cells to wild type cells both treated with either rapamycin or KCl, with samples across a time course of 0, 5, 10, 20, 40 minutes after the beginning of the treatment. Transcripts are arranged on the vertical axis by hierarchical clustering, and grey bars highlight the positions of RPGs within this cluster. In the heatmap, saturated blue indicates at least a 5.7-fold decrease and saturated yellow at least a 5.7-fold increase in transcript abundance. (B) Averaged RPG and non-RPG transcript behaviors across datasets shown in (A).

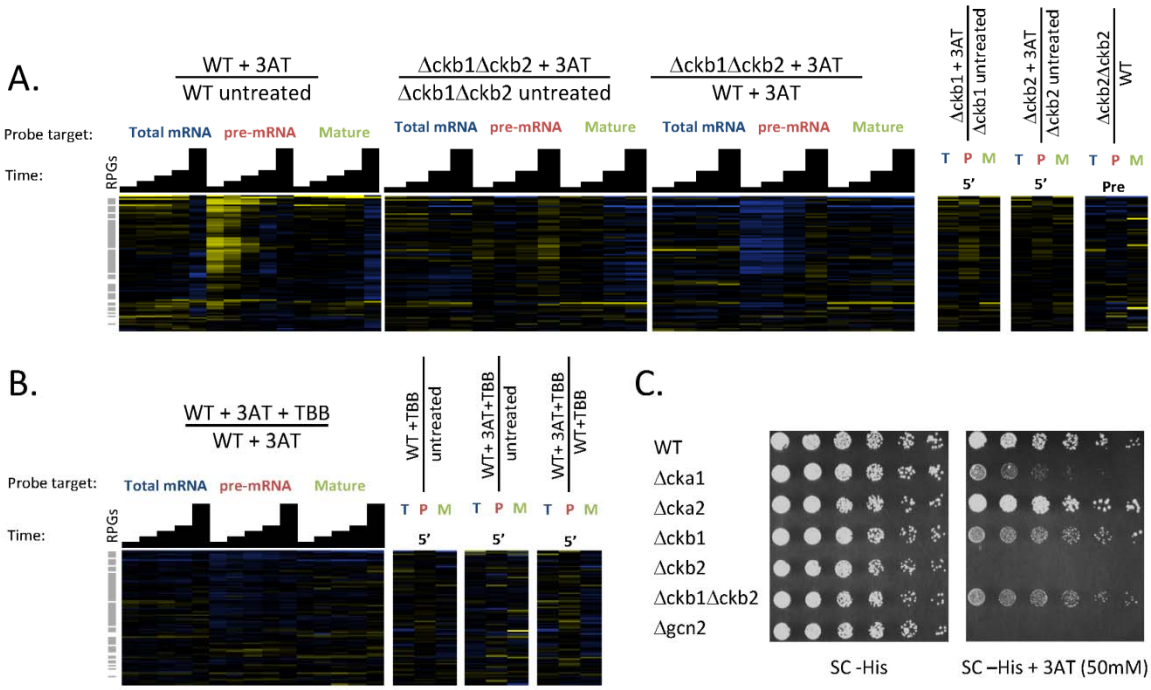

Figure 6. **CK2 is required for inhibition of RPG pre-mRNA splicing following amino acid starvation. (**A) Splicing profiles are shown for wild-type or CK2 deficient cells (*Δckb1Δckb2*) undergoing amino acid starvation induced by 3-AT compared to an untreated control. (B) Splicing profiles are shown for wild-type cells undergoing amino acid starvation induced by 3-AT in either the presence or absence of a CK2 inhibitor, TBB. In both (A) and (B), transcripts are arranged on the vertical axis by hierarchical clustering, grey bars highlight the positions of RPGs, and in the heatmap saturated blue indicates at least a 5.7-fold decrease in transcript abundance and saturated yellow at least a 5.7-fold increase. (C) Growth phenotypes for CK2 mutants under control (SC-HIS) and amino acid starvation conditions (SC-HIS + 3AT).

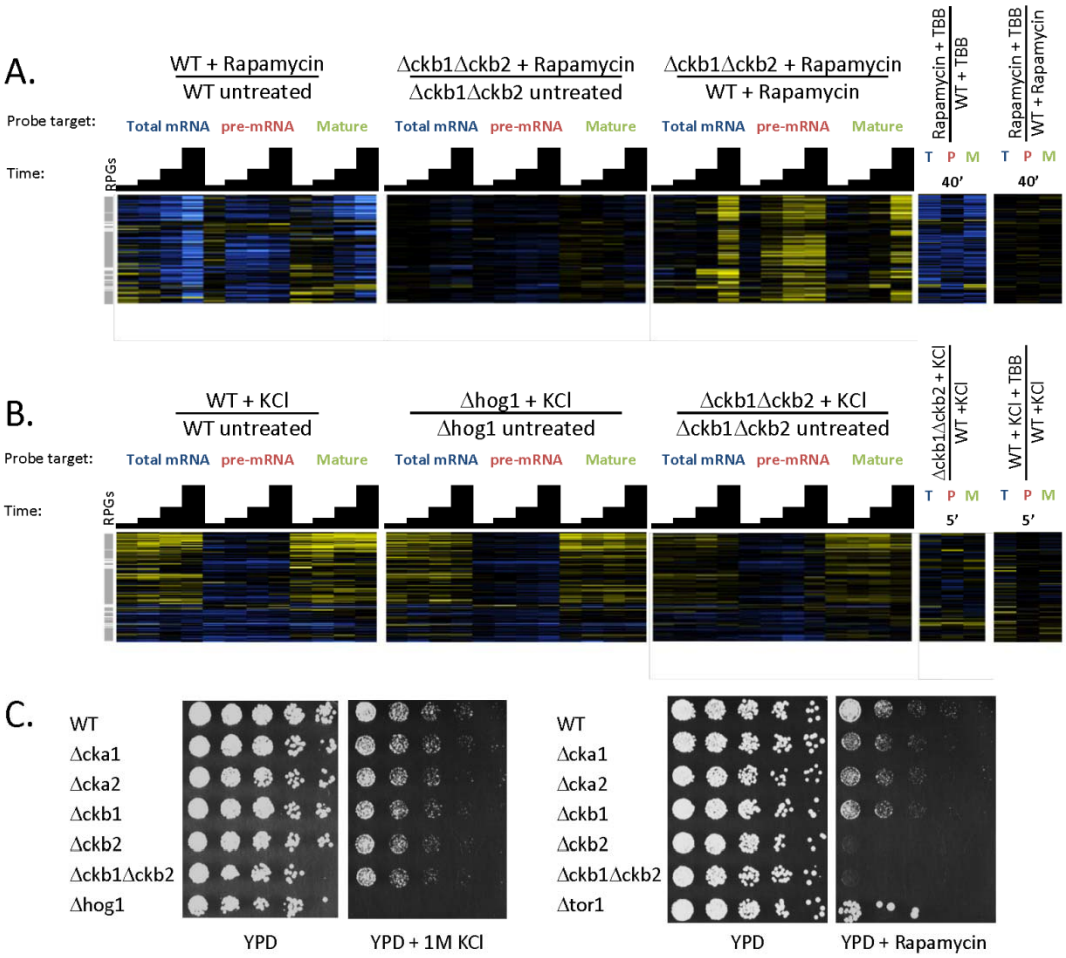

Figure 7. **Effects of CK2 inhibiton on other stress response classes.** (A) Splicing profiles of cells in control or rapamycin treatment carrying caseine kinase 2 deletion mutations or treated with a CK2 inhibitor (TBB). (B) Splicing profiles of cells undergoing osmotic stress induced by KCl, carrying deletions in *HOG1* or CK2, or treated with the CK2 inhibitor TBB. In both (A) and (B), transcripts are arranged on the vertical axis by hierarchical clustering , grey bars highlight the positions of RPGs, and in the heatmap saturated blue indicates at least a 5.7-fold decrease in transcript abundance and saturated yellow at least a 5.7-fold increase. (C) Growth phenotypes for CK2 mutants under control (YPD) and KCl or rapamycin treatment conditions.

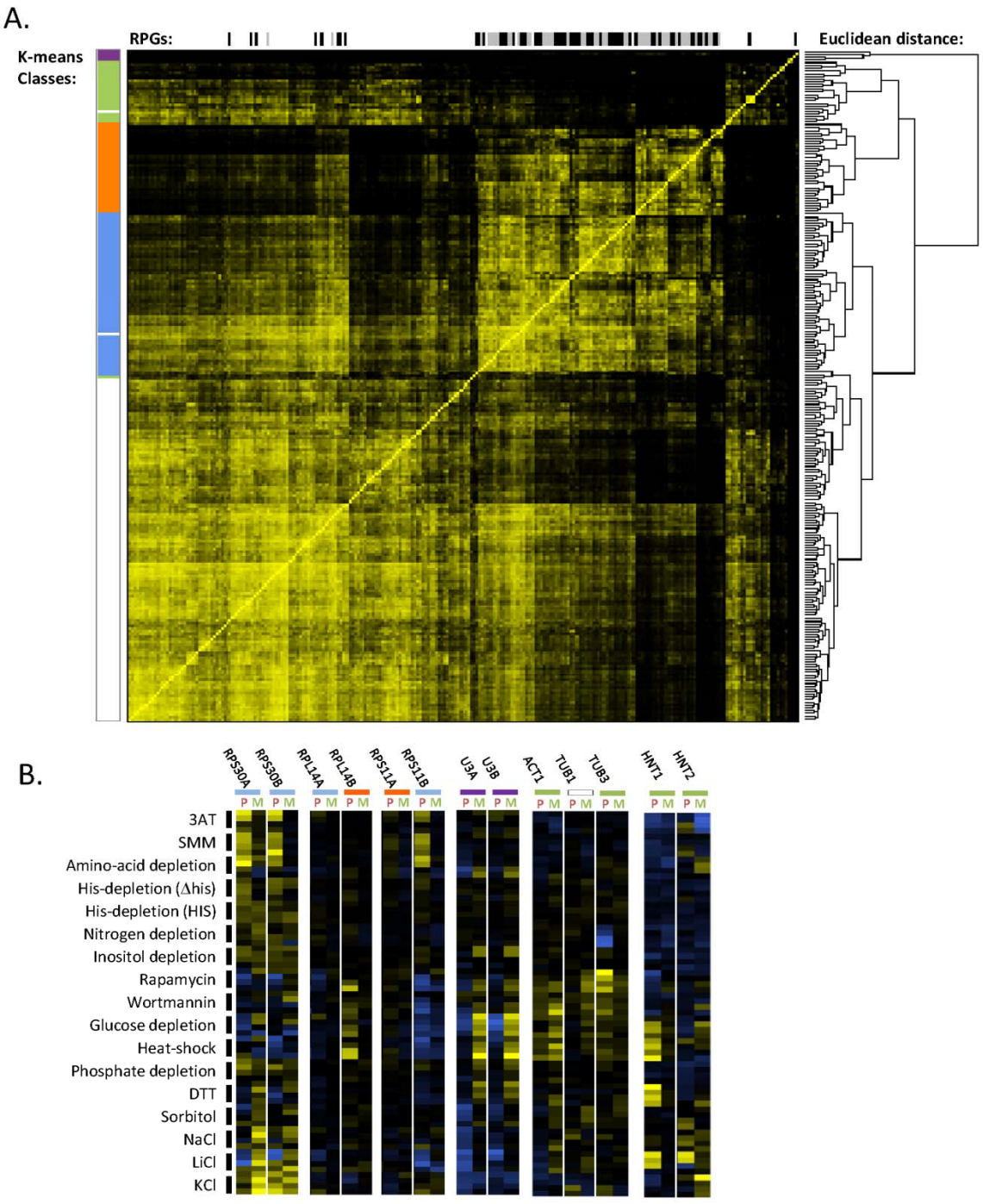
A.
RPGs:
K-means Classes:
Euclidean distance:
B.
RPS30A
RPS30B
RPL14A
RPL14B
RPS11A
RPS11B
U3A
U3B
ACT1
TUB1
TUB3
HNT1
HNT2
P M
3AT
SMM
Amino-acid depletion
His-depletion (Δhis)
His-depletion (HIS)
Nitrogen depletion
Inositol depletion
Rapamycin
Wortmannin
Glucose depletion
Heat-shock
Phosphate depletion
DTT
Sorbitol
NaCl
LiCl
KCl

Figure 8. **Analysis of relatedness of transcript behaviors across all environmental stress conditions.** (A) Pair-wise distance analysis was used to cluster transcripts symmetrically across the horizontal and vertical axes. In the central heatmap, brighter yellows represents greater degrees of correlation in transcript behaviors across the stress response dataset (small Euclidean distances). The dendogram to the right of the heatmap shows hierarchical clustering of transcript correlations. The colored bars to the left of the heatmap highlight transcripts that fall into each of the five transcript subclasses identified by k-means clustering. Across the top of the heatmap, light grey bars show the location of small ribosomal subunit transcripts and black bars show the location of large ribosomal subunit transcripts. (B) Stress response profiles of select transcripts.

S1. 3AT / untreated

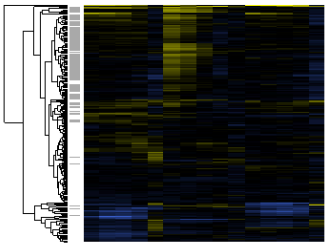

S2. Amino-acid depletion / untreated

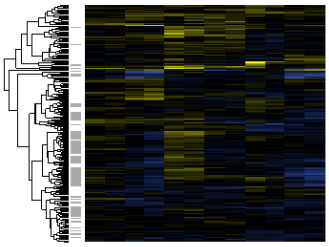

S3. Wortmannin / untreated

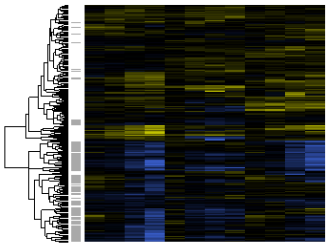

S4. His depletion (HIS4) / untreated

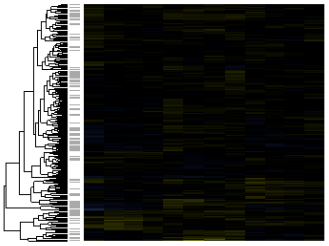

S5. His depletion (Δhis3) / untreated

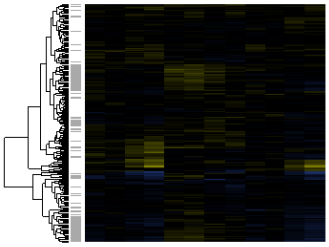

S6. Rapamycin / untreated

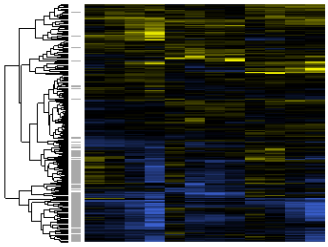

S7. Glucose depletion / untreated

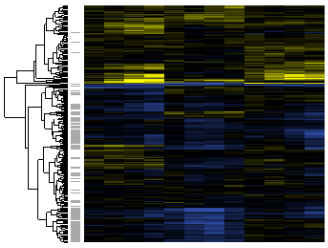

S8. Phosphate depletion/ untreated

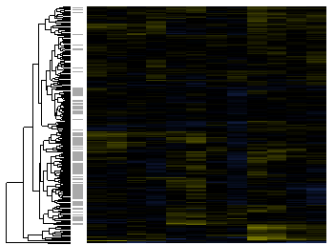

S9. Heat-shock (42°C) / untreated

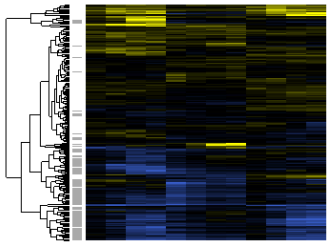

S10. DTT (1mM) / untreated

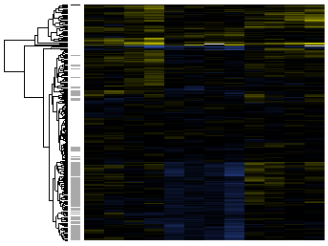

S11. DTT (10mM) / untreated

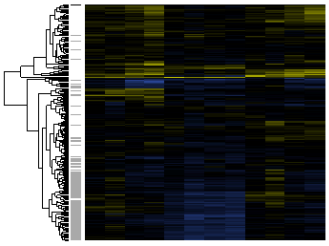

S12. Sorbitol / untreated

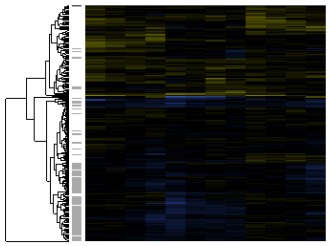

S13. NaCl / untreated

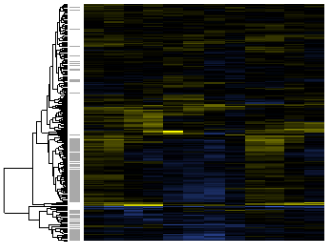

S14. LiCl / untreated

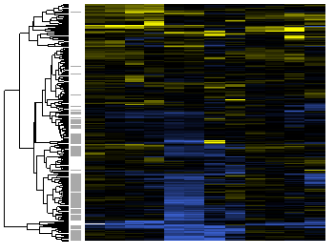

S15. KCl / untreated

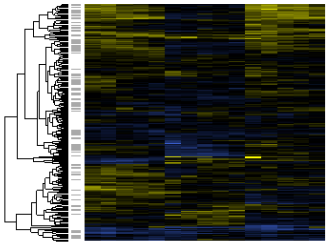

Supplemental Figure 1. Independent Wild-Type Clusters. Changes in total (left columns), pre- (middle columns), and mature mRNA (right columns) over the time course following each stress and subjected to hierarchical clustering independently of other stresses. Grey bars mark the ribosomal protein genes, and saturated blue and yellow indicate 5.7-fold decreases and increases respectively.

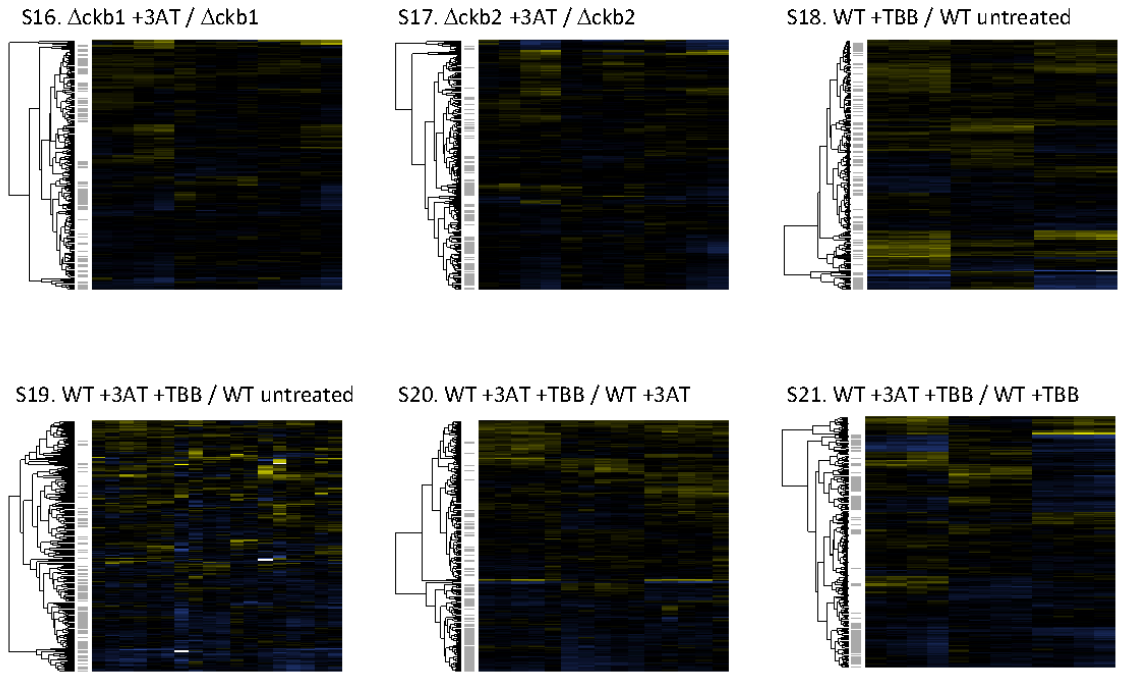

Supplemental Figure 2. Full CK2 mutant and TBB-treated clusters aligned to the 3-AT cluster. Changes in total (left columns), pre- (middle columns), and mature mRNA (right columns) over the time course following each stress and aligned to the gene order established by hierarchical clustering of the data from the 3-AT stress. Grey bars mark the ribosomal protein genes, and saturated blue and yellow indicate 5.7-fold decreases and increases respectively.

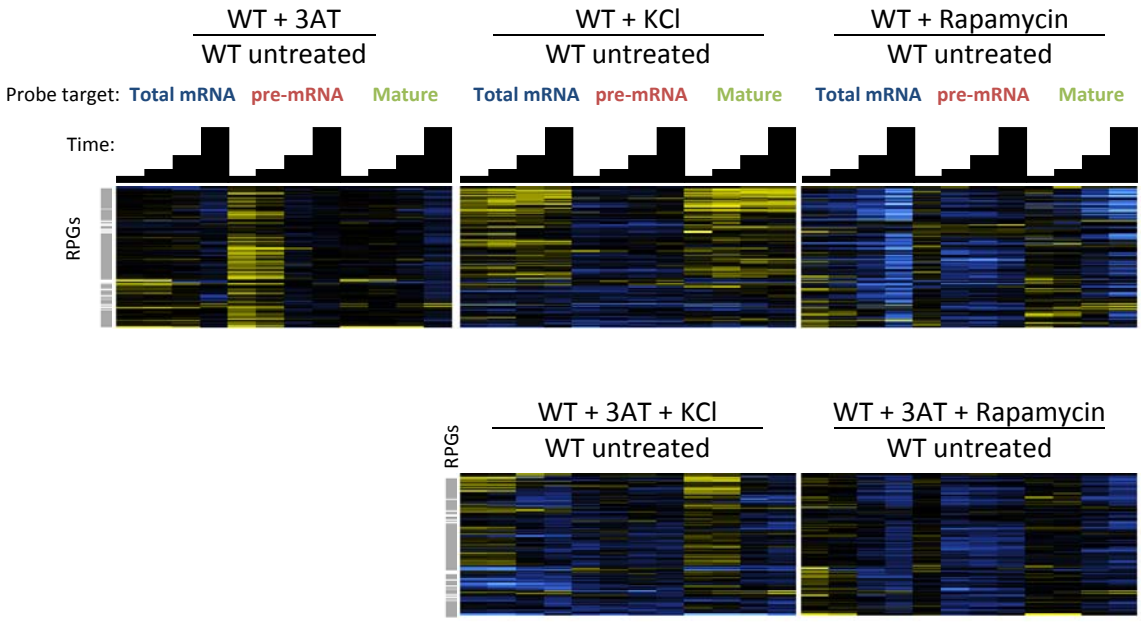

Supplemental Figure 3 Combinations of Stresses. Cells were simulatneously treated with two stresses as indicated. Changes in total (left columns), pre- (middle columns), and mature mRNA (right columns) for a cluster including the ribosomal protein genes are displayed. Grey bars mark the ribosomal protein genes, and saturated blue and yellow indicate 5.7-fold decreases and increases respectively.

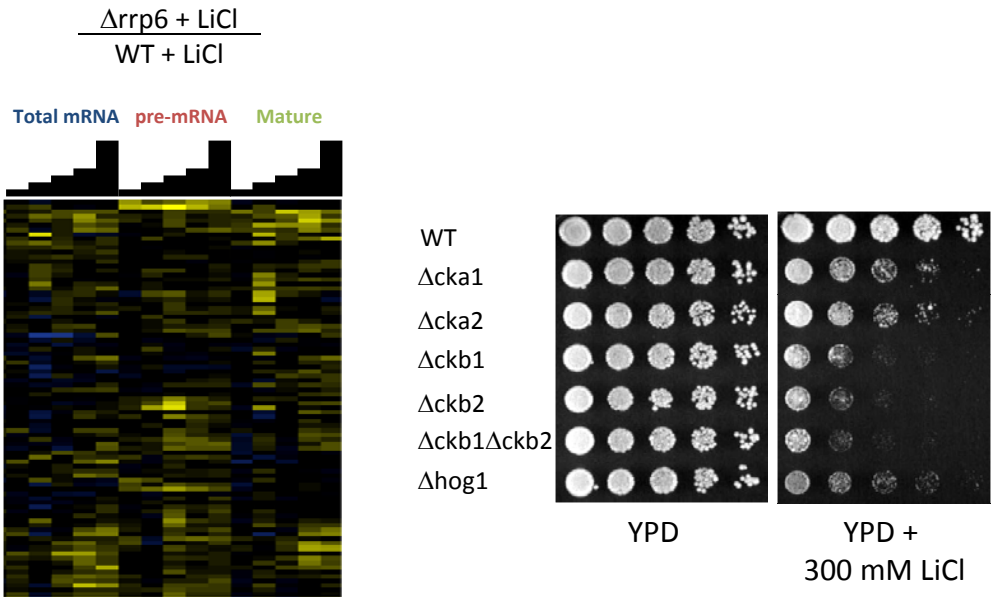

Supplemental Figure 4. The response to lithium in Δrrp6 and lithium sensitivity of CK2 deletes. A. The strain carrying the deletion of *RRP6* was subjected to LiCl treatment and compared to the wild-type strain subjected to LiCl treatment as described in Fig. 5. **B.** Serial dilutions of strains carrying deletions in CK2 subunits were spotted on YPD plates, or YPD plates containing 300 mM LiCl.

Chapter 4

The Inhibition of Ribosomal Protein Gene Splicing in Response to Amino Acid Starvation Is Achieved Through Modulation of Co-Transcriptional Splicing Dynamics

Abstract

We showed previously that pre-mRNAs for most of the ribosomal protein genes (RPGs) accumulate rapidly following the induction of an amino acid starvation stress by treatment with 3-amino-1,2,4-triazole (3-AT), indicating a block to their normally very efficient splicing. To interrogate the mechanism by which this occurs, we generated strains carrying chimeric spliced genes, integrated at their endogenous loci in the yeast genome. By swapping introns and promoters between RPGs and non-RPGs, we found that the identity of the intron is not important for mediating 3-AT-induced splicing inhibition, but that an element in the promoter is required both for constitutive efficient splicing, and for the splicing response to 3-AT. The promoter dependence of the splicing response suggested an intimate connection between the response and transcription, so we examined the distributions of both RNA polymerase II and an early splicing factor along intron-containing genes during the 3-AT response, using chromatin immunoprecipitations followed by microarray analysis. We found that RNA polymerase II accumulates to high levels at the 3' ends of the RPGs during amino acid starvation stress, consistent with a dramatic slowing or pausing of the polymerase in response to the stress. Prp42, a component of the U1 snRNP, briefly decreases its association with the 5' ends of RPGs, but then also accumulates to high levels at the 3' ends of these genes, possibly indicating that both recruitment and release of U1 are decreased. Finally we show, using single molecule RNA fluorescence in-situ hybridization (FISH) against two RPG introns, that a majority of the accumulated unspliced pre-mRNAs escape into the cytoplasm, suggesting that they have failed to productively engage the

spliceosome. Our results suggest that the promoters of intron-containing RPGs contain elements that promote the efficient co-transcriptional splicing of their transcripts, and that this is abrogated in response to amino acid starvation.

Introduction

Splicing is a complex and energetically expensive process, and in the budding yeast, *Saccharomyces cerevisiae*, introns have been retained in only about five percent of genes. However, the distribution of introns in the genome is highly biased. Of 296 currently annotated introns, 101 are found in ribosomal protein genes (RPGs). This prompted the hypothesis that introns could contribute to the regulation of RPGs, which are extremely highly expressed and tightly regulated in response to environmental conditions. We previously tested this hypothesis by exposing yeast to the amino acid starvation-mimicking drug, 3-amino-1,2,4-triazole (3-AT), and measuring levels of total mRNA, pre-mRNA, and mature mRNA for intron-containing genes. We found that splicing was inhibited, specifically for a subset of the ribosomal protein genes, causing a transient accumulation of the pre-mRNA species of these transcripts (Pleiss *et al.*, 2007). We further showed that this response was elicited in a number of amino acid-limiting stresses, but that more stringent stresses cause nuclear degradation of the RPG pre-mRNAs, and that both of these responses require the activity of casein kinase 2 (CK2) (see chapter 3). However, very little is known about the mechanism by which the splicing inhibition occurs.

Splicing is dynamic and complex, requiring 5 snRNAs and over 100 proteins (Staley & Guthrie, 1998; Wahl *et al.*, 2009). It is believed to occur by stepwise assembly of spliceosomal complexes on a nascent pre-mRNA, followed by massive rearrangements of the RNA and protein interactions within the megadalton active spliceosome, leading

to splicing catalysis by a two-step trans-esterification reaction. The U1 snRNP is the first sub-complex to be recruited to the nascent pre-mRNA, and recognizes the 5' splice site. Subsequently, the U2 snRNP recognizes the branch point within the pre-mRNA intron. The U4/U6·U5 tri-snRNP is then recruited, and the assembling RNP machine undergoes massive rearrangements leading to the release of the U1 and U4 snRNAs (along with many of their associated proteins) and the establishment of the catalytically active spliceosome. At this point the first catalytic step takes place, in which the adenosine at the branch point attacks the 5' splice, cleaving the 5' exon and generating the lariat intermediate. In the second catalytic step, the 5' splice site attacks the 3' splice site, resulting in the ligation of the 5' and 3' exons and the release of the intron (Fabrizio *et al.*, 2009).

The many dynamic rearrangements of the spliceosome are orchestrated by the activities of several RNA-dependent ATP helicases, and it is becoming clear that the activities of these proteins are delicately regulated by post-translational modifications, protein-protein interactions within spliceosomal sub-complexes, and interactions with GTP (Bellare *et al.,* 2008; Maeder & Guthrie, 2008; Maeder *et al.*, 2009; Small *et al.*, 2006). Furthermore, it is becoming clear that the assembly of the spliceosome, and in many cases, splicing catalysis itself, occurs co-transcriptionally, affording the opportunity for regulatory interactions between the spliceosome, RNA polymerase II, and the chromatin environment (Perales & Bentley, 2009). It had been thought that the short terminal exons of the ribosomal protein genes would be too short to allow splicing catalysis to be completed co-transcriptionally, but recent studies by the Beggs and Neugebauer labs

have suggested that the rate of elongation of RNA polymerase II may be modulated in a splicing dependent way, such that splicing is allowed to finish co-transcriptionally. (Alexander *et al.,* 2010; Carrillo Oesterreich *et al.*, 2010). This suggests a high degree of coordination between splicing and transcription, and in this context, chromatin modifications, transcription factors, and 3' end processing factors could all contribute significantly to the regulation of splicing.

We took advantage of the fact that the 3-AT induced splicing inhibition is specific to a subset of RPGs by making chimeric contructs that swapped introns and promoters between 3-AT responsive RPGs and non-responsive non-RPGs. This allowed us to determine that the promoter is required for the response. We further showed that the co-transcriptional dynamics of spliceosome recruitment and RNA polymerase elongation are altered at RPG loci in response to amino acid starvation, and that unspliced pre-mRNAs are exported to the cytoplasm. Many questions still remain, but these findings begin to elucidate the mechanism by which splicing can be modulated in a transcript-specific manner in response to stress in budding yeast.

Results

RPG promoters and not their introns contain elements important for mediating the splicing response to 3-AT

In order to determine which *cis*- elements might contribute to the transcript specificity of the 3-AT response, and also to gain some insight into the point in the splicing cycle that is affected in 3-AT, we generated chimeric genes that swapped introns or

promoters between 3-AT responsive and non-responsive transcripts (Fig. 1A). We precisely replaced the intron of *NMD2*, which does not accumulate pre-mRNA in response to 3-AT, with that of *RPS9B*, which strongly accumulates pre-mRNA after 3-AT treatment. The introns of most RPGs are large (approximately 300-600 bases) compared to the size of the average non-RPG intron in yeast (approximately 100 bases), while the RPG open reading frames are generally quite short, and the *RPS9B* transcript conforms to these general trends. The *NMD2* transcript, on the other hand, is quite large at over three kilobases, and its intron is short. Thus, in the chimeric construct, the *RPS9B* intron is located within an open reading frame much longer than that of its native gene, and the *NMD2* gene contains a much larger intron than it normally contains. We also precisely replaced the intron of RPS26A, which strongly accumulates pre-mRNA in response to 3-AT, with that of ARF2, which does not accumulate. In this case, the sizes of both introns are similar, and both are normally contained in the 5' untranslated regions (UTRs) of their native genes, which also contain similarly sized open reading frames.

We also replaced the promoter of RPL24B, which strongly accumulates pre-mRNA in response 3-AT, with two other promoters that could drive similarly high levels of expression, both from non intron-containing genes. We used the promoter of the RPS5 gene, which drives constitutive high expression under favorable growth conditions. The promoters of both RPS5 and RPL24B are very broadly defined here as the entire genomic region upstream of the transcript of interest and downstream of the neighboring transcript, with the transcript boundaries determined by inspection of

published tiling microarray, EST analysis, or RNA seq data sets (David *et al.*, 2006). We also used the CUP1 promoter, which can be induced by adding copper sulfate to the culture media, and can drive expression to similar levels as seen with the native RPL24B promoter. This strain was grown in the presence of copper for approximately six hours before the start of any experiments. In mid-log phase growth, total expression levels of the RPL24B transcript are similar to each other when driven by the native RPL24B promoter, the RPS5 promoter, or the CUP1 promoter in the presence of copper (Fig. 1B).

In order to determine how the chimeric constructs behaved in response to 3-AT, we grew cells to mid-log phase in synthetic media lacking histidine (plus copper in the case of the strain carrying the CUP1 promoter), removed a 15 ml aliquot to serve as the zero time point, and then added 3-AT. Aliquots of culture were taken at 2.5, 5 and 10 minutes following the addition of 3-AT. Total RNA was extracted and cDNA was synthesized for measurement by qRT-PCR. For each relevant transcript, the amount of pre-mRNA was determined using primers specific to exon sequence, and the total amount of RNA was determined using primers against sequence in the second exon (including the 3' UTR in many cases, to distinguish between highly similar paralogous copies of the ribosomal protein genes). The efficiency of splicing of each transcript is represented by the percent unspliced transcript (Fig. 2).

The results of swapping introns between RPG transcripts that respond to 3-AT and non-RPG transcripts that fail to respond suggested that the identity of the intron does not

contribute substantially to the 3-AT response. The behavior of the chimeric transcript containing the RPS9B intron in the NMD2 locus was much more similar to that of the wild-type NMD2 transcript than to the behavior of the wild-type RPS9B transcript (Fig. 2, top). Likewise, the behavior of the chimeric transcript containing the ARF2 intron in the RPS26A locus was much more similar to that of the wild-type RPS26A transcript than to the behavior of the ARF2 transcript (Fig. 2, middle). Additional swaps (the RPS26A intron in the ARF2 transcript and the NMD2 intron in the RPL24B transcript) were made and yielded similar results (data not shown).

The results of replacing the RPL24B promoter with other high-level promoters from non-intron-containing genes suggested that elements in the promoter do indeed contribute to the splicing efficiency of a ribosomal protein gene, both constitutively and in response to 3-AT (Fig.2, bottom). Firstly, although all three promoters drove expression of the RPL24B transcript to similar levels, constitutive splicing efficiency of this transcript was much lower in the cases where expression was driven by a non-native promoter, leading to higher levels of unspliced pre-mRNA at the zero time point in this experiment. Furthermore, these transcripts failed to accumulate increased amounts of pre-mRNA in response to treatment with 3-AT. Thus, an element in the promoter of an RPG appears to be required for both constitutive efficient splicing of the RPG, and for 3-AT responsiveness of the splicing of the RPG. Attempts to determine the sufficiency of the RPL24B promoter to confer the splicing response to a non-RPG transcript were inconclusive (data not shown).

Chromatin immunoprecipitations reveal that recruitment and or retention of both U1 splicing factors and RNA polymerase II are affected in response to 3-AT

The requirement for an RPG promoter element in mediating the accumulation of RPG pre-mRNA in response to amino acid starvation suggested that the response was likely occurring co-transcriptionally. Mounting evidence has suggested that splicing factors are at least recruited to many intron-containing transcripts co-transcriptionally, and that in many cases splicing catalysis also occurs while the nascent transcript is still associated with RNA polymerase II (Carrillo Oesterreich *et al.,* 2010; Gornemann *et al.*, 2005; Moore *et al.*, 2006; Tardiff *et al.*, 2006). Chromatin immunoprecipitation has been widely used to assess co-transcriptional association of splicing factors with nascent transcripts at their genomic loci(Kotovic *et al.,* 2003; Lacadie & Rosbash, 2005), and we applied this technique to determine whether the distributions along intron-containing genes of either a U1 snRNP associated protein (Prp42), or RNA polymerase II itself, were affected by treatment with 3-AT.

Cells carrying a C-terminally HA-tagged version of Prp42, integrated at its genomic locus, were fixed with formaldehyde before, and at two and four minutes after treatment with 3-AT, and the tagged Prp42 and RNA polymerase II were immunoprecipitated in parallel from each sample. After reversing the crosslinks between the protein and DNA in both the immunoprecipitated samples and samples representing the input material for each immunoprecipitation, a small portion of each sample was analyzed by qRT-PCR for an

intergenic locus not expected to interact specifically with either Prp42 or RNA polymerase II and or by western blot, and roughly equivalent amounts of each sample, by these metrics, were carried forward to the next steps of the experiment (Supplemental Fig. S1). DNA from each sample was amplified by three rounds of Klenow reactions, and then each input sample was fluorescently labeled with Cy3 fluorophore and each immunoprecipitated sample was labeled with Cy5 fluorophore. Each immunoprecipitated input sample was competitively hybridized against the corresponding sample on a custom microarray containing probes tiling across the genomic loci of all intron-containing genes, and the ratios of immunoprecipitated (Cy5) to input (Cy3) signal for each probe were measured and then visualized plotted along their genomic loci, using the MochiView genome browser (Homann & Johnson, 2010). Because the samples were initially normalized to contain equivalent amounts of DNA at a locus not expected to be specifically associated with either Prp42 or RNA polymerase II, the ratio values measured were nearly all positive. Normalization to loading control sequences that were spiked in prior to the amplification steps were therefore used, rather than the more commonly used global loess normalization methods.

The results of this experiment showed that the distributions of both RNA polymerase II and Prp42 changed rapidly and substantially across many intron-containing genes, and that different patterns of change could be observed for different genes (Fig. 3). For example, the BMH2 gene rapidly lost association of both RNA polymerase II and Prp42 following treatment with 3-AT (Fig. 3A), suggesting that it may be transcriptionally down-regulated in this stress. BMH2 encodes one of two yeast 14-3-3 proteins, which

have differential roles in the responses to a wide variety of stresses, and are tightly regulated at the level of transcription (van Heusden, 2009). RNA polymerase II association dropped evenly and rapidly, across the gene, with both the 2- and 4-minute time points showing similar levels of association, much lower than the levels seen at the 0-minute time point. Prp42-HA association dropped more slowly, but also appeared to decrease evenly across the length of the gene, with the shape of the plot of its association remaining the same and just decreasing in magnitude.

In contrast to the BMH2 gene, the DBP2 gene is strongly and rapidly induced in response to 3-AT (Fig. 3B). Our previous microarray studies showed that the total levels of this transcript increase rapidly and strongly upon treatment with 3-AT (Pleiss *et al.*, 2007) (Supplemental Fig. 2). Not surprisingly, the association of both RNA polymerase II and Prp42-HA increased dramatically over the length of the gene following treatment with 3-AT. As with BMH2, the RNA polymerase II association appeared to change more rapidly than Prp42-HA association. Interestingly, in this case the shapes of the plots of association, especially of Prp42-HA, along the length of the gene also changed at different time points after 3-AT treatment. While both RNA polymerase II and Prp42 both showed increased association across the entire length of the gene at the 2- and 4-minute time points compared to the 0-minute time point, the increase was most dramatic at the 3' end of the gene. Especially for Prp42-HA, a strong peak of association was seen over the (unusually) short 3' exon of the gene at the 4-minute time point after 3-AT treatment. These observations are perhaps consistent with the pausing of RNA polymerase II near the 3' splice sites of intron-containing genes, especially after

transcription has been strongly induced, that has recently been reported (Alexander *et al.*, 2010).

A very interesting pattern of changes to the associations of RNA polymerase II and Prp42-HA with the genomic loci of many intron-containing RPGs was observed following treatment with 3-AT (examples in Fig. 3C-E). We were surprised to observe a strong increase in the association of RNA polymerase II with most RPG loci, particularly at the 3' ends of these genes. This was a surprise because we showed previously that the levels of most RPG transcripts (measured by microarray probes to the second exons of the transcripts) do not increase in response to 3-AT, but instead show mild decreases, especially at later time points after treatment (Pleiss *et al.*, 2007) (Supplemental Fig. S2). The chromatin immunoprecipitation assay cannot distinguish between actively elongating polymerase and polymerase that is stalled, but instead presents a "snapshot" of polymerase association at the time of crosslinking. Because the increased association of polymerase with the genomic loci of the RPGs observed upon 3-AT treatment does not correlate with increased expression, it seems likely that this association represents an increase in stalling or slowing rather than an increase in recruitment of polymerase. Several aspects of the patterns of association of polymerase with RPG loci following 3-AT treatment are consistent with this model. Firstly, although very large increases were observed at the 3' end of the gene, much smaller increases were observed at the 5' ends of the genes. Secondly, the pattern of association along the gene changed over time. At the zero time point, high levels of association were already observed for many of the RPGs. At the 2-minute time point, strong increases were seen at the loci that

showed the peak of association for the 0-minute time point, but at the 4-minute time point, the peak of association had shifted toward the 3' end of the gene (see especially RPS16B in Fig. 3C and RPS9B in Fig. 3D). The increase in association of Prp42-HA also had interesting kinetics. As was observed for the non-RPG loci, the change in Prp42-HA association appeared delayed compared to the change in association of polymerase, with the plot of the 2-minute time point much closer to that of the 0-minute time point than that of the 4-minute time point. And like the association of polymerase, the association of Prp42-HA appeared to become more 3' along the gene after treatment with 3-AT. This can be seen most dramatically by comparing the 2-minute time point to the 0-minute time point (see red arrows in Fig. 3C-E). Because the accumulation of unspliced pre-mRNA for these RPGs is evidence of decreased splicing efficiency, it seems likely that the increase in association of Prp42-HA does not represent an increase in productive U1 snRNP recruitment, but rather a failure of U1 release. In fact, the mild decrease in Prp42-HA association with the 5' end of RPG introns seen transiently at the 2-minute time point may be the result of decreased recruitment of new U1 snRNP.

Unspliced pre-mRNAs that accumulate in 3-AT are exported to the cytoplasm.

The changes in distribution of RNA polymerase II and Prp42-HA along the genomic loci of RPGs, as measured by chromatin immunoprecipitation, suggested that both polymerase and U1 snRNP were accumulating at the 3' ends of RPGs, as the pre-mRNAs for these genes were beginning to accumulate following treatment with 3-AT. We wished to gain further insight into the fates of the nascent transcripts that were

presumably associated with the accumulating polymerase and splicing factor, so we used single molecule RNA fluorescence in-situ hybridization to determine the localization of the intron for two different RPGs that accumulate pre-mRNA in response to 3-AT, RPS9B and RPL24B. Four to five oligonucleotide probes, each derivatized with four fluorescent Cy3 or Cy3.5 molecules, were used for each RNA to be imaged. This large amount of fluorescent signal allows single RNA molecules to be visualized as diffraction-limited spots by epi-fluorescent microscopy (Zenklusen & Singer, 2010).

Untreated yeast and yeast treated with 3-AT for 15 minutes were fixed with paraformaldehyde, spheroplasted, affixed to microscope cover slips, and labeled with probes to an RPG intron (red), the ITS region of the rRNA (to visualize the nucleolus, green) and DAPI (to visualize the nucleus, blue) (Fig. 4A). In untreated yeast, most cells contained 0-2 RPG introns, for both RPS9B (top panels) and RPL24B (middle panels). The introns were primarily found in the body of the nucleus, at the nuclear periphery, or at the boundary between the nucleus and the nucleolus. Following treatment with 3-AT for 15 minutes, the number of introns increased dramatically, consistent with increased levels of pre-mRNA detected previously by microarray (Supplemental Fig. S2, for examples). Strikingly, the additional introns were localized primarily in the cytoplasm. Most cells still contained 0-2 introns in their nuclei, but additionally contained up to seven introns in their cytoplasms. These results clearly indicated that the unspliced pre-mRNAs that accumulated in response to 3-AT were exported to the cytoplasm.

This result led us to ask where introns localized in mutants that cause accumulation of RPG pre-mRNA. We repeated the RNA FISH experiment with cells carrying deletions of *IST3* and *SNU66*, grown in rich media. Ist3 is a component of the RES complex (Wang *et al.*, 2005), which has been shown to participate in the retention of unspliced pre-mRNA in the nucleus. Snu66 is a component of the triple snRNP complex, consisting of the U4, U5, and U6 snRNAs and numerous proteins, which is believed to join the assembled U1 and U2 snRNPs on a pre-mRNA substrate just prior to catalytic activation of the spliceosome (Wahl *et al.*, 2009). The deletion of *IST3* or *SNU66* causes an accumulation of RPG pre-mRNA. We were not surprised to see that unspliced pre-mRNA accumulating in the *Δist3* strain localized to the cytoplasm, as this strain has previously been shown by a reporter assay to have a pre-mRNA leakage defect (Dziembowski *et al.*, 2004) (Fig. 4B, left panel). However, we also observed that the accumulated RPS9B intron in the *Δsnu66* strain localized to the cytoplasm. Thus it appears that a variety of different perturbations to splicing can result in leakage of unspliced pre-mRNA to the cytoplasm.

Discussion

Here we have shown that the previously observed accumulation of RPG pre-mRNA in response to 3-AT treatment depends on *cis*- elements present in an RPG promoter, and that both RNA polymerase II and a U1 snRNP protein accumulate at the 3' ends of RPG genomic loci as part of the response. Furthermore, we have shown that the accumulated RPG pre-mRNAs are largely exported to the cytoplasm. While there are

many questions still to be answered regarding the details of the mechanism by which 3-AT elicits a block to splicing of many of the RPG transcripts, these findings suggest that the changes to splicing in 3-AT are co-transcriptional, and in fact may reflect changes in the coordinated behaviors of both RNA polymerase II and splicing factors. The fact that the accumulated pre-mRNAs are found primarily in the cytoplasm suggests that they likely fail to engage the later-associating components of the splicing machinery and thus fail to commit to catalytic activation of the spliceosome. The observation of these changes in response to treatment with 3-AT offers some insight not only into the potential mechanisms for regulation at the level of splicing in response to environmental stresses, but also into the ways in which transcription and splicing may be coordinated constitutively.

The recent findings that RNA polymerase II slows its elongation rate in the terminal exons of efficiently spliced genes, that a 3' splice site proximal pause of RNA polymerase II requires active splicing, and that the 3' splice site proximal pause of RNA polymerase II is associated with the appearance of Ser2 phosphorylation in the CTD of the largest subunit of the polymerase suggest a high degree of coordination between transcription and splicing, at least for some intron-containing transcripts in yeast (Alexander *et al.,* 2010; Carrillo Oesterreich *et al.*, 2010). Our findings are very consistent with this view, and give some additional insights into the dynamics of the interaction between spliceosome assembly and RNA polymerase pausing in the 3' region of efficiently spliced genes.

Firstly, we show that elements in the promoter of an efficiently spliced RPG contribute both to the constitutive efficiency of its splicing and to the capacity of its splicing to be perturbed by treatment with 3-AT. It has been suggested on the basis of *in* vitro experiments that co-transcriptional splicing is more efficient than post-transcriptional splicing , and recent work showed that for the most efficiently spliced transcripts *in vivo (*Das *et al.*, 2007*)*, most splicing catalysis was completed co-transcriptionally (Carrillo Oesterreich *et al.*, 2010). The genes comprising the efficiently spliced category were predominantly ribosomal protein genes, and the characteristics that distinguished them from the less efficiently spliced genes were higher abundances and (paradoxically) shorter terminal exons. These two characteristics are general characteristics of ribosomal protein genes. We have shown here that high levels of expression do not by themselves cause high levels of splicing efficiency, as high levels of expression can be driven by the *CUP1* promoter or the promoter of the intronless *RPS5*, but splicing efficiency is much lower than that observed when transcription is driven by the native promoter of the intron-containing RPL24B. This result suggests that an important characteristic of efficiently spliced genes may in fact be the presence of a promoter element. More work will be required to precisely describe the nature of the promoter element(s) that is/are necessary for efficient splicing of the RPL24B gene, and likely contribute(s) to efficient splicing for the majority of the RPGs.

An apparent requirement for the co-transcriptional splicing of efficiently spliced genes, which tend to have short terminal exons, is that RNA polymerase II must slow down in the terminal exon to allow time for splicing catalysis to occur (Carrillo Oesterreich *et al.*,

2010). Our results, showing that both polymerase and the U1 snRNP factor Prp42 accumulate to high levels at the 3' ends of RPGs under 3-AT treatment conditions leading to the accumulation of their pre-mRNAs, agree well with this model. If the rate of elongation in the terminal exon is tuned to allow splicing catalysis to be completed co-transcriptionally, then a delay in splicing catalysis might be expected to elicit more dramatic pausing of polymerase, which would be consistent with our observation of high levels of polymerase accumulation at the 3' ends of genes following 3-AT treatment. This observation suggests a high degree of dynamic coordination between the behavior of RNA polymerase II and that of splicing factors under conditions in which splicing becomes inhibited. Further, our results suggest that the tendency for splicing to finish co-transcriptionally in efficiently spliced RPGs, which is accomplished by polymerase slowing in the terminal exon, is imposed by an element in the promoter. There are several possible mechanisms that could allow a promoter element to affect the behavior of the polymerase in the terminal exon of an intron-containing ribosomal protein gene. One is that a promoter element could affect the chromatin environment in the vicinity of the gene such that polymerase slows in the region downstream of the promoter. In higher eukaryotes, specific histone modifications have been shown to be associated with promoters, introns, and exons (Huff *et al.*, 2010). Another possibility is that a factor recruited to the promoters of efficiently spliced ribosomal protein genes associates with the elongating polymerase over the length of the gene and is capable of modulating polymerase speed in the terminal exon in response to the splicing status of the transcript. A similar model has been proposed to explain the influence of promoter

elements on alternative splicing in higher eukaryotes (Kornblihtt, 2005). A third possibility is that direct interactions between the promoters and 3' ends of efficiently spliced RPGs allow for elements in the promoters to affect the behavior of the polymerase at the 3' ends of these gene. "Gene looping", or interaction in three-dimensional space between the 5' and 3' ends of genes to allow for efficient recycling of polymerase at transiently repressed genes has been proposed to explain observations in yeast and in higher eukaryotes, and it seems possible that it could occur at the highly transcribed ribosomal protein genes under stressful conditions (Laine *et al.,* 2009; Tan-Wong *et al.*, 2009).

The elucidation of the exact cause and effect relationships that control the coordinated behavior of RNA polymerase II and splicing factors will require further experimentation, but it is interesting to note in our experiments that the accumulation of polymerase appears to precede the accumulation of U1 snRNP at the 3' ends of genes, following treatment with 3-AT. If indeed polymerase is slowing in response to some signal of delayed splicing catalysis, the kinetics of the response make it seem unlikely that the relevant signal is failure to release U1. Instead, perhaps a delay in the recruitment of U2 or U4/U5/U6, or subsequent rearrangements, steps in the splicing cycle that are believed to occur prior to U1 release (Fabrizio *et al.*, 2009), are detected by the elongating polymerase and elicits more dramatic slowing.

Our results showing that the accumulated unspliced pre-mRNA is exported to the cytoplasm after 3-AT treatment suggests that the fate of normally very efficiently

spliced transcripts that fail to complete splicing catalysis co-transcriptionally is to fail completely to assemble catalytically active splieosome, and to escape to the cytoplasm. The high accumulation of U1 snRNP at the 3' ends of RPG loci following 3-AT treatment suggests that nascent transcripts are recruiting U1 during the 3-AT response, but failing to either recruit or rearrange other splicing factors that are necessary for U1 release and splicing catalysis. It would be interesting to determine the fate of these transcripts that seem to have recruited U1 but failed to finish splicing catalysis. The appearance of unspliced transcripts in the cytoplasm suggests that they eventually finish being transcribed and undergo termination, cleavage, and polyadenylation. This suggests that association of a pre-mRNA with U1 is not sufficient to promote its retention in the nucleus. The fact that deletion of both *IST3* and *SNU66* also cause accumulation of pre-mRNA in the cytoplasm is potentially consistent with this model – both Ist3 and Snu66 act subsequent to the recruitment of U1. It is possible that in all cases we have examined, the pre-mRNAs that are exported to the cytoplasm are a distinct population that have failed to ever interact with U1, and that the perturbation to splicing that occurs after the recruitment of U1 in each case has the indirect effect of reducing the available population of U1 snRNP complexes that can interact with new nascent transcripts. It has been shown that mutations to the 5' splice site of a reporter transcript that could be detected by bulk RNA FISH caused its export to the cytoplasm, but mutations to the 3' splice site caused the retention of the transcript in the nucleus (Long *et al.*, 1995). Thus it appears that the start of splicing catalysis is sufficient to retain a pre-mRNA in the nucleus, but further experimentation will be required to

determine the precise step in the splicing cycle at which a transcript is sufficiently committed to splicing to be retained in the nucleus.

The results presented here suggest that the mechanism by which splicing is blocked in response to 3-AT occurs co-transcriptionally, and involves dynamic interactions between RNA polymerase and the splicing machinery. Many mechanistic questions still remain. While our results are consistent with the model that RNA polymerase slows at the 3' end of RPGs that accumulate unspliced transcript in response to delays in their splicing, it is unclear what factors lead directly to the delays in splicing. It remains possible that the slowing of RNA polymerase in fact causes the observed delay in splicing, although this seems less likely. The mechanism by which the slowing of polymerase occurs also remains unknown, as does the mechanism by which a promoter element contributes to the response. However, the results presented here suggest that further investigation of this system, in which an environmental stress imposes a rapid change to co-transcriptional splicing of the highly expressed and efficiently spliced ribosomal protein genes, could continue to yield important insights into both the constitutive coordination of transcription and splicing and the capacity of this coordination to allow for multiple layers of regulation of intron-containing genes.

Materials and Methods

Strain construction:

Promoter swaps: The CUP1 promoter marked by kan-MX was amplified from the pYM-N1 plasmid (Janke *et al.*, 2004) using the following primers to direct homologous recombination upstream of the RPL24B locus:

forward: CCT AAT ATG CCT GGT GTG CTG GAT AAG ATA TTA TGT TAA TGA AAT ATT TGC GTA CGC TGC AGG TCG AC

reverse: TGT TGA CCA CCC AAA AAT TTA AAC GCC TAT AAT TTA GTT AAT CAA TAT AGC ATC GAT GAA TTC TCT GTC G

The PCR product was purified and transformed into the yMB1 strain using standard methods, and transformants were verified by sequencing.

553 base pairs of sequence upstream of the RPS5 gene was amplified using the following primers, which introduce a SacI and a SpeI restriction site respectively:

forward: GCGGCGGAGCTCAAGAAACAATGAACAGCCTTGA

reverse: GCGGCGACTAGTTGGTCGGTTATTTCTAGTCTCTTTT

The purified PCR product was digested and cloned into pYM-N1, replacing the CUP1 promoter. The following primers were then used to amplify the kan-MX marked RPS5 promoter and direct its homologous recombination upstream of RPL24B:

forward: CCT AAT ATG CCT GGT GTG CTG GAT AAG ATA TTA TGT TAA TGA AAT ATT TGC GTA CGC TGC AGG TCG AC

reverse:TGTTGACCACCCAAAAATTTAAACGCCTATAATTTAGTTAATCAATATAGACTATAGGG
AGACCGGCAGAT

Intron swaps were performed using a modification of the delitto perfetto method (Storici & Resnick, 2006). Briefly, fusion PCR was used to generate a construct in which the CORE cassette (containing the kanMX marker, the URA3 gene, and the site cleaved by the ISce1 endonuclease) was flanked on its 5' end by sequence upstream of the native intron, joined precisely to the new intron, and then joined precisely to sequence downstream of the native intron; and on its 3' end by sequence within the native intron. This construct was transformed into a yeast strain carrying the ISce1 endonuclease under the control of the gal promoter, introduced into the ADE2 locus (strain yAP?). Colonies in which the construct had been successfully integrated were induced in galactose media and then plated on 5-FOA to select for a homologous recombination event in which the native intron and the CORE cassette have been removed and precisely replaced by the new intron.

Fusion PCR: Piece A was amplified from yeast genomic DNA, and piece B was amplified from the CORE plasmid. Then the pieces were mixed together with the forward primer from A and the reverse primer from B to generate the full construct. PCR was performed with ExTaq (TaKaRa) under standard conditions.

To introduce the RPS9B intron into the NMD2 locus:

forward primer for fusion piece A:

aatattgtatctgcattgataatacattggacagaaattatggacGTACGTATTAGACTATATCGAAGAG

reverse primer for fusion piece A:

ccaagctcgggtgttcaaatcatgcaattctttttccgtccatcCTAAAAAAAAAAAAGTAAAATTGGA

forward primer for fusion piece B:

gatggacggaaaaaagaattgcatgatttgaacacccgagcttggGTATTACCCTGTTATCCCTA

reverse primer for fusion piece B:

aacgatcaataaaagaagttagtataaaaccttagaagtactgaaTCCTTACCATTAAGTTGATC

To introduce the ARF2 intron into the RPS26A locus:

forward primer for fusion piece A:

cgctattacagataaaagaaccatagtcttaagtaGTATGTAACGAGTTTCATTAGGAGG

reverse primer for fusion piece A:

ttgtttctaccgttggaagctctcttctttggcattttgaatgatCTATTGGTTGGCTGATGTTAGTAAT

forward primer for fusion piece B:

ATCATTCAAAATGCCAAAGAAGAGAGCTTCCAACGGTAGAAACAAGTATTACCCTGTTATCCCT

A

reverse primer for fusion piece B:

aaagagttaaaataattagttagtaacttctcaatttttttTCCTTACCATTAAGTTGATC

A 3XHis tag was introduced to the C-terminus of Prp42 by amplifying the tag and a kanMX6 marker using primers to direct homologous recombination to the C-terminus of

Prp42, from plasmid pFA6a-3HA-kanMX6 (Longtine *et al.*, 1998). Primers used were as follows:

forward:

GGAGATGGATACATTAGAGGAAATGTTTACTGAAGAACCTCGGATCCCCGGGTTAATTAA

reverse:

TATTTATACCTTTTAATAAATGACAATGCCTTTTGGGAATTCGAGCTCGCTCGTTTAAAC

Table 1. Strains used in this study:

Strain	Genotype	Source
yMB1	MATα his3Δ1 leu2Δ0 lys2Δ0 ura3Δ0	(Pleiss *et al.*, 2007)
yMB3	MATa leu2Δ0 ura3Δ0 ade2::Gal_Isce1 (derived by crossing yAP53 with yMB1, and selecting spores with the above genotype)	This study
yMB4	The Intron from RPS9B precisely replaces the NMD2 intron, in its genomic locus. Otherwise the same as yMB3.	This study
yMB5	The intron from ARF2 precisely replaces the RPS26A intron, in its genomic locus. Otherwise the same as yMB3.	This study

yMB6	kanMX-RPS5 promoter replaces the RPL24B promoter. Otherwise the same as yMB1	This study
yMB7	kanMX-CUP1 promoter replaces the RPL24B promoter. Otherwise the same as yMB1	This study
yMB8	PRP42 c-terminally tagged with 3HA, marked with kanMX6. Otherwise the same as yMB1	This study
Δ*snu66*	MATa his3Δ1 leu2Δ0 met15Δ0 ura3Δ0 *snu66::kanMX*	(Giaever *et al.*, 2002)
Δ*ist3*	MATa his3Δ1 leu2Δ0 met15Δ0 ura3Δ0 *ist3::kanMX*	(Giaever *et al.*, 2002)

Growth conditions: For most experiments, yeast were grown in synthetic media lacking histidine prior to treatment with 3-AT. To induce an amino acid starvation response, 3-AT was added to a final concentration of 50mM from a 1M stock solution for the times indicated. For the CUP1 promoter experiments, $CuSO_4$ was added to the media to a final concentration of 250 uM. For the microscopy of the Δ*snu66* and Δ*ist3* strains, cultures were grown in YPD. All growth was at 30°C.

Expression analysis: To measure the accumulation of pre-mRNAs following treatment with3-AT, 15 ml culture aliquots were collected prior to treatment and at 2.5, 5, and 10 minutes after treatment by vacuum filtration onto a nitrocellulose filter. The cells and

filter were placed in a 15 ml conical tube and frozen immediately in liquid nitrogen. RNA was isolated by hot acid phenol extraction as previously described (Schmitt *et al.*, 1990), and then treated with DNase (Fermentas). 2.5ug of total RNA was used in a cDNA synthesis reaction primed by a mixture of all reverse primers at a final concentration of 250nM each. The cDNAs were diluted 25- to 750-fold and 10 ul were used per QPCR reaction.

qRT-PCR: qRT-PCR was performed in a BioRad CFX machine using a standard PCR buffer (Fermentas) with an annealing temperature of 57°C. Primers were as follows:

RPL24B intron forward: AAATCAGGACCGTCGAAAGA

RPL24B intron reverse: AAGCCGACAACGAGAACAGT

RPL24B second exon forward: AAAAGGCTAAGTCCGCTGGT

RPL24B second exon reverse: GTTAATTATCTTAACGGGAAGTGG

RPS9B intron forward (used in WT strains): AAATTCCATAATAGTATACCTTCAT

RPS9B intron reverse (used in WT strains): TCTAATGTATCCCTGTTTAACTGAA

RPS9B intron forward (used in chimera strain): GCCCTTGCAGACTTTTGTTC

RPS9B intron reverse (used in chimera strain, actually near the 5' end of NMD2 second exon): AGACTTCTTCGCCATTCCAA

RPS9B second exon forward: GAGTTGCTAGAAGAAACGCTGC

RPS9B second exon reverse: ATTATACAGTTATGAAATCAGCG

NMD2 intron forward:

GTATGTTTGATTTATCTTACTGTGGCCAGATCGGCCTTTCAGTACTTCTAAGGTTTTATA

NMD2 intron reverse:

CTAACTTCTTTTATTGATCGTTGTAAACTACGGTAACAATTATGTATCAACAG

NMD2 second exon forward: AGATATTGCCACCCAACCAA

NMD2 second exon reverse: TTGTGGCTTTGTTGTCCAAA

ARF2 intron forward (used in WT strain): CGGTGGGATGAGTTCCTAAA

ARF2 intron reverse (used in WT strain): GCTCGACTCCCCACAATTAG

ARF2 intron forward (used in chimera strain): GGTCTTACCGGCACCATCTA

ARF2 intron reverse (used in chimera strain, actually near the 5’ end of the RPS26A second exon): CTTCTTTGGCATTTTGAATGAT

ARF2 second exon forward: ACCGTCCATGGTTTATCCAG

ARF2 second exon reverse: GATTAGGATTGATTCTTCAAGTTGTTG

RPS26A intron forward: AAAGAAGGAAGTCGCCCATC

RPS26A intron reverse: TGGCAAAAAGGGAAGGAGAT

RPS26A second exon forward: CGCCAGAATTGTCAGAGTCA

RPS26A second exon reverse: ATCAGCAGGGGAAACCTTGT

Intergenic region forward (for normalizing chromatin IP samles):

GGCTGTCAGAATATGGGGCCGTAGTA

Intergenic region reverse: CACCCCGAAGCTGCTTTCACAATAC

Intergenic primers from (Komarnitsky *et al.*, 2000)

At least two biological replicates were performed for each experiment. Plotted data represent technical replicates from a representative biological replicate.

Chromatin immunoprecipitations followed by microarray analysis: Chromatin immunoprecipitations were performed as previously described with minor modifications (Kress *et al.,* 2008; Strahl-Bolsinger *et al.*, 1997; Tuch *et al.*, 2008). Briefly: 50 ml aliquots of mid-log phase cultures were fixed by adding 37% formaldehyde to a final concentration of 1%. Cells were incubated in formaldehyde for 15 minutes at room temperature, and then crosslinking was quenched by adding glycine to a final concentration of 125 mM. Cells were washed in cold TBS, then pelleted and frozen in liquid nitrogen. The pellet was resuspended in 500 ul lysis buffer supplemented with protease inhibitors and cells were disrupted by vigorous mixing in the presence of glass beads. The lysate was separated from the glass beads by centrifugation at low speed after puncturing the bottom of the tube containing the mixture. The low speed spin causes the chromatin to form a loose pellet, which was resuspended in 350 ul lysis buffer and transferred to a microfuge tube. The chromatin was sheared by sonication in

an ice water bath sonicator using two rounds of 15 minutes of cycling between 30 seconds of sonication at high frequency and 1 minute of rest. Cellular debris was pelleted by centrifugation at top speed in a mircocentrifuge and discarded. The total volume of the clarified lysate was brought to 500 ul. Five percent (25 ul) was added to 200 ul TE and retained for use as the "input" sample, and the remainder was split into two tubes. A monoclonal antibody to the HA tag (antibody 12CA5, Roche, at a 1:1000 dilution) was used to bind the HA-tagged Prp42 in one half of the lysate, and a monoclonal antibody to the Rpb3 subunit of RNA polymerase II (Neoclone, Madison WI, 1:1000) was used to bind polymerase in the other half of the lysate. After two hours of antibody binding at 4°C, 30 ul of a 50% slurry of protein G-sepharose beads were added and incubated overnight at 4°C. The beads were then washed twice with lysis buffer, twice with lysis buffer plus 500 mM NaCl, once with a high stringency LiCl buffer, and once with TE. Bound proteins and DNA were then eluted first by incubation for 15 minutes at 65°C in elution buffer and additionally with TE plus .67% SDS. The two elutions were pooled and the crosslinks were reversed in these samples and also in the input samples by incubation in a 65°C oven for 6 hours. 25 ul of each sample was retained for use in a western blot to ensure that roughly equivalent amounts of protein had been recovered in each sample, and the remainder of the samples were treated with proteinase K for 2 hours. DNA was purified from the samples by phenol-chloroform extraction and ethanol precipitation. Input samples were then additionally treated with RNAse A to remove RNA.

QPCR was performed to normalize input and immunoprecipitated sample such that each had equivalent amounts of an intergenic region not expected to be associated with either polymerase or splicing factors. At this point equal amounts of exogenous fragments of DNA derived by PCR from the *Candida albicans* genome were spiked into each sample to allow for normalization of the Cy3 and Cy5 channels during scanning (probes against these sequences were included in the array design). The DNA samples were amplified by successive reactions with Klenow enzyme (NEB) lacking exonuclease activity, primed with random nonamers. In the first two rounds of Klenow amplification, dNTPs were used as substrate for the amplification, while the third round introduced amino-allyl-modified dUTPs in a 3:2 ratio with dTTP. Following amplification to a final amount of 1-2 ug DNA per sample, samples were conjugated to either Cy3 fluorescent dye (input samples) or Cy5 fluorescent dye (immunoprecipitated sample) as has been previously described (DeRisi *et al.*, 1997). Each immunoprecipitated sample was then competitively hybridized against the relevant input sample to a custom tiling microarray (Agilent). The hybridization was carried out according to Agilent's recommendations, at 65°C in a rotisserie oven for 24-30 hours. Arrays were washed according to Agilent's recommendations (Wolber *et al.*, 2006) and then scanned using an Axon 4000B scanner and GenePix software (Molecular Devices). PMT values were selected such that the intensities of the spots corresponding to the spiked-in exogenous control DNA were equivalent in the Cy3 and Cy5 channels. No further normalization was performed on the ratio values from the microarray; the ratio of the median pixel intensities in the two channels for each spot was used directly for subsequent analysis. Further analysis was

performed using the MochiView software package for visualizing genomic scale data plotted along genome tracks (Homann & Johnson, 2010). The ratio value for each array probe was plotted according to the genomic locus of the probe sequence, for each of the immunoprecipitation samples, and then a smoothing algorithm was applied to generate the figures shown in this manuscript. The custom array used in these experiments was Agilent's 8X15K format custom array, and contained probes tiling across the genomic loci of all intron-containing genes, as well as non-intron-containing genes that have previously been reported to associate with splicing factors, and loci between the intron-containing genes in a few chromosomal regions that were rich in intron-containing genes. Files describing the complete set of probes included in the array, and the full chromatin immunoprecipitation array datasets are available in electronic format.

Primers to amplify exogenous loading control DNA from *Candida albicans:*

lc1 forward: gcttgtagtgattctggtctcaa

lc1 reverse: ggcaattatcactcctttacttgc

lc2 forward: TCATCTAAAGGGAATATCGACTCT

lc2 reverse: ttgaacggaatcatccctaaa

lc3 forward: tcccttctgaaaaactacaataaacc

lc3 reverse: CGACAACAGCAAACCGTCTA

lc4 forward: agaaATGCCCCATTTACGTG

lc4 reverse: aaaagtttattcttggggaaataat

Single molecule RNA fluorescence in-situ hybridization: Fluorescence in-situ hybridization to determine the localization of pre-mRNAs accumulating in response to amino acid starvation was carried in the laboratory of Robert Singer, with mentorship and assistance from Daniel Zenklusen, according to his published protocol (Zenklusen & Singer, 2010). Briefly: Four to five 50mer probes were synthesized to both the intronic and exonic sequences of the RPL24B and RPS9B transcripts. Probes were chosen to ideally have at least 45% GC content, and were synthesized to include approximately five amino-allyl modified bases per probe for conjugation to fluorescent dyes. Sequences of these probes are as follows:

RPL24A e-1 TCTGAAGATTTTGGAGTCACCACGGACAAACAAGGTACCTCTGCCTGGGT

RPL24A e-2 CGGTGATACCCTTCTTGTGATGCTTTCTGAATAAGACAGTCCAAGCGATTC

RPL24A e-3 GAAGCACCGGTAATTGGTCTTTGGGCCTTAACGGTTTTTCTAGATCTCTTC

RPL24A e-4 CCAGCAGACTTAGCCTTTTCAGCCTTTCTAGCAGCCTTTTCAGCCTTCTT

RPL24A e-5 TCGAGCATAAATCTTAACGAGAAGTAGCAGCAACCTTTTGGAAAGCACCCTT

RPL24B i-1 CACTGCGAAGCTCCTCGTTGTCCTCAATATTCTCTCATTTCCTAATGGGC

RPL24B i-2 CGCCTTTATCGTGGGCCTCTTATTAACCTCAGCATTGTTCAAATGGTCGCtt

RPL24B i-3 CCAATGATGTTCCGTACGTCTTTCGACGGTCCTGATTTATTCGCATGTACtt

RPL24B i-4 cgaCAACGAGAACAGTATTTCATCACGACAAGCATATCCAACAGATCCCGATG

RPS9B i-1 atgagGACCCGAACCTCTTTCAAAATCAACGAGTCAGAGTGAAGAATTTCCCTCC

RPS9B i-2 gaTCACCTTGATCTCTAATGTATCCCTGTTTAACTGAAGTGTCGGGAGTTCAgtg

RPS9B i-3 ggtatCCGCCTTGGAAAATAAAATACTGTCCCATTGTTACGAGAGAGATGTTCCC

RPS9B i-4 ttCTTGTTAGTCAAAAGTTTTCCCGGAACAAAAGTCTGCAAGGGCCCAAGTAag

RPS9B e-1 tTCACCGGCCAACTTCAATTCTGCGTCCAAACGAGAAGATTCGTAAGGTCTc

RPS9B e-2 tctTTGGGTCCTTTTCGTCTCTAGTTAACAAGTCTCTGGCAGCACGACGAATT

RPS9B e-3 gCAATGTGTCTTTGAGTGATTAAAACTCTGGCGTGGTGGACAGACTTGGCC

RPS9B e-4 GGTCTAGCACCACCGAATGGAGAAGTTGGAGCGAAGTCAATGTGCTTTTC

Probes against the intronic sequences were labeled by conjugation with the NHS ester derivative of the Cy3 fluorophore, and probes against the exonic sequences were labeled with the NHS ester derivative of Cy3.5 (GE Healthcare). One vial of dye intended to label 1 mg of protein was used to label 5 ug of DNA, and the labeling was carried out in 100mM sodium bicarbonate pH 9.0 as described. Equimolar amounts of all probes against the same sequence (eg. the RPS9B intron) were pooled and labeled in the same reaction. Cy5 labeled probes against the ITS region of the ribosomal RNA were included in hybridizations to identify the region occupied by the nucleolus, a portion of the nucleus that is not efficiently stained by DAPI.

Cells to be visualized were grown to mid-log phase in synthetic media lacking histidine and were treated with 3-AT for 15 minutes (or not, for untreated samples), and then were fixed with paraformaldehyde for 30 minutes at room temperature. Cells were then washed with sorbitol-containing buffer, spheroplasted using lyticase, and affixed to poly-L-lysine coated microscope coverslips placed in 12-well culture dishes.

Spheroplasting was monitored visually and stopped for each sample at the point in time when the cells began to appear darker, usually after approximately 15-20 minutes. Once the spheroplasted cells were fixed to the poly-L-lysine coated slides, the appropriate mixtures of fluorescently-labeled oligonucleotide probes were hybridized to the fixed cells overnight. Approximately 0.5 ng of each probe was used, along with a vast excess of unlabeled competitor nucleic acid, in a hybridization mix containing 40% formamide. The next day, cells were washed and stained with DAPI, then the cover slips were mounted to microscope slides using a mounting medium containing an anti-photobleaching agent (ProLong Gold, Invitrogen). Cover slips were sealed with nail polish. Cells were visualized by epi-fluorescence microscopy (Olympus BX61 microscope with Olympus UPlanApo 100x, 1.35 NA oil-immersion objective) using narrow bandpass filters to distinguish Cy3 and Cy3.5 fluorophores (Chroma). Images were captured as Z-stacks (CoolSNAP HQ camera) that were subsequently flattened by displaying the maximum projection, and channels collected with different filter sets were merged and false-colored using the ImageJ software. Although Cy3-labeled RPG exons were visualized, only the Cy3.5 signal derived from the intron probes are shown, as the extreme abundance of RPG exons in the cytoplasm of yeast cells can obscure intronic spots in the cytoplasm.

Acknowledgments

I received technical assistance from many people in carrying out these experiments, without whom much of this work would not have been possible. Alex Plocik assisted in

the design of the method for precisely swapping introns between different transcripts. Gregg Whitworth assisted in the design of the microarray for analyzing chromatin immunoprecipitations. Members of the Alexander Johnson lab, especially Aaron Hernday and Oliver Homann, were of great help in the execution and analysis of the chromatin immunoprecipitation experiments. Daniel Zenklusen and Robert Singer were extremely generous in sharing reagents, time, and expertise in the RNA FISH experiments. I am extremely grateful for the contributions of these people. I would also like to thank members of the Guthrie lab for helpful discussions. This work was supported by NIH grant GM21119. MB was supported by an HHMI pre-doctoral fellowship. CG is an American Cancer Society Research Professor of Molecular Genetics.

References

Alexander RD, Innocente SA, Barrass JD, Beggs JD (2010) Splicing-dependent RNA polymerase pausing in yeast. Mol Cell 40: 582-593.

Bellare P, Small EC, Huang X, Wohlschlegel JA, Staley JP et al. (2008) A role for ubiquitin in the spliceosome assembly pathway. Nat Struct Mol Biol 15: 444-451.

Carrillo Oesterreich F, Preibisch S, Neugebauer KM (2010) Global analysis of nascent RNA reveals transcriptional pausing in terminal exons. Mol Cell 40: 571-581.

Das R, Yu J, Zhang Z, Gygi MP, Krainer AR et al. (2007) SR proteins function in coupling RNAP II transcription to pre-mRNA splicing. Mol Cell 26: 867-881.

David L, Huber W, Granovskaia M, Toedling J, Palm CJ et al. (2006) A high-resolution map of transcription in the yeast genome. Proc Natl Acad Sci U S A 103: 5320-5325.

DeRisi JL, Iyer VR, Brown PO (1997) Exploring the metabolic and genetic control of gene expression on a genomic scale. Science 278: 680-686.

Dziembowski A, Ventura A, Rutz B, Caspary F, Faux C et al. (2004) Proteomic analysis identifies a new complex required for nuclear pre-mRNA retention and splicing. EMBO J 23: 4847-4856.

Fabrizio P, Dannenberg J, Dube P, Kastner B, Stark H et al. (2009) The evolutionarily conserved core design of the catalytic activation step of the yeast spliceosome. Mol Cell 36: 593-608.

Giaever G, Chu AM, Ni L, Connelly C, Riles L et al. (2002) Functional profiling of the Saccharomyces cerevisiae genome. Nature 418: 387-391.

Gornemann J, Kotovic KM, Hujer K, Neugebauer KM (2005) Cotranscriptional spliceosome assembly occurs in a stepwise fashion and requires the cap binding complex. Mol Cell 19: 53-63.

Homann OR, Johnson AD (2010) MochiView: versatile software for genome browsing and DNA motif analysis. BMC Biol 8: 49.

Huff JT, Plocik AM, Guthrie C, Yamamoto KR (2010) Reciprocal intronic and exonic histone modification regions in humans. Nat Struct Mol Biol 17: 1495-1499.

Janke C, Magiera MM, Rathfelder N, Taxis C, Reber S et al. (2004) A versatile toolbox for PCR-based tagging of yeast genes: new fluorescent proteins, more markers and promoter substitution cassettes. Yeast 21: 947-962.

Komarnitsky P, Cho EJ, Buratowski S (2000) Different phosphorylated forms of RNA polymerase II and associated mRNA processing factors during transcription. Genes Dev 14: 2452-2460.

Kornblihtt AR (2005) Promoter usage and alternative splicing. Curr Opin Cell Biol 17: 262-268.

Kotovic KM, Lockshon D, Boric L, Neugebauer KM (2003) Cotranscriptional recruitment of the U1 snRNP to intron-containing genes in yeast. Mol Cell Biol 23: 5768-5779.

Kress TL, Krogan NJ, Guthrie C (2008) A single SR-like protein, Npl3, promotes pre-mRNA splicing in budding yeast. Mol Cell 32: 727-734.

Lacadie SA, Rosbash M (2005) Cotranscriptional spliceosome assembly dynamics and the role of U1 snRNA:5'ss base pairing in yeast. Mol Cell 19: 65-75.

Laine J, Singh BN, Krishnamurthy S, Hampsey M (2009) A physiological role for gene loops in yeast. Genes Dev 23: 2604-2609.

Long RM, Elliott DJ, Stutz F, Rosbash M, Singer RH (1995) Spatial consequences of defective processing of specific yeast mRNAs revealed by fluorescent in situ hybridization. RNA 1: 1071-1078.

Longtine MS, McKenzie A3, Demarini DJ, Shah NG, Wach A et al. (1998) Additional modules for versatile and economical PCR-based gene deletion and modification in Saccharomyces cerevisiae. Yeast 14: 953-961.

Maeder C, Guthrie C (2008) Modifications target spliceosome dynamics. Nat Struct Mol Biol 15: 426-428.

Maeder C, Kutach AK, Guthrie C (2009) ATP-dependent unwinding of U4/U6 snRNAs by the Brr2 helicase requires the C terminus of Prp8. Nat Struct Mol Biol 16: 42-48.

Moore MJ, Schwartzfarb EM, Silver PA, Yu MC (2006) Differential recruitment of the splicing machinery during transcription predicts genome-wide patterns of mRNA splicing. Mol Cell 24: 903-915.

Perales R, Bentley D (2009) "Cotranscriptionality": the transcription elongation complex as a nexus for nuclear transactions. Mol Cell 36: 178-191.

Pleiss JA, Whitworth GB, Bergkessel M, Guthrie C (2007) Rapid, transcript-specific changes in splicing in response to environmental stress. Mol Cell 27: 928-937.

Schmitt ME, Brown TA, Trumpower BL (1990) A rapid and simple method for preparation of RNA from Saccharomyces cerevisiae. Nucleic Acids Res 18: 3091-3092.

Small EC, Leggett SR, Winans AA, Staley JP (2006) The EF-G-like GTPase Snu114p regulates spliceosome dynamics mediated by Brr2p, a DExD/H box ATPase. Mol Cell 23: 389-399.

Staley JP, Guthrie C (1998) Mechanical devices of the spliceosome: motors, clocks, springs, and things. Cell 92: 315-326.

Storici F, Resnick MA (2006) The delitto perfetto approach to in vivo site-directed mutagenesis and chromosome rearrangements with synthetic oligonucleotides in yeast. Methods Enzymol 409: 329-345.

Strahl-Bolsinger S, Hecht A, Luo K, Grunstein M (1997) SIR2 and SIR4 interactions differ in core and extended telomeric heterochromatin in yeast. Genes Dev 11: 83-93.

Tan-Wong SM, Wijayatilake HD, Proudfoot NJ (2009) Gene loops function to maintain transcriptional memory through interaction with the nuclear pore complex. Genes Dev 23: 2610-2624.

Tardiff DF, Lacadie SA, Rosbash M (2006) A genome-wide analysis indicates that yeast pre-mRNA splicing is predominantly posttranscriptional. Mol Cell 24: 917-929.

Tuch BB, Galgoczy DJ, Hernday AD, Li H, Johnson AD (2008) The evolution of combinatorial gene regulation in fungi. PLoS Biol 6: e38.

Wahl MC, Will CL, Luhrmann R (2009) The spliceosome: design principles of a dynamic RNP machine. Cell 136: 701-718.

Wang Q, He J, Lynn B, Rymond BC (2005) Interactions of the yeast SF3b splicing factor. Mol Cell Biol 25: 10745-10754.

Wolber PK, Collins PJ, Lucas AB, De Witte A, Shannon KW (2006) The Agilent in situ-synthesized microarray platform. Methods Enzymol 410: 28-57.

Zenklusen D, Singer RH (2010) Analyzing mRNA expression using single mRNA resolution fluorescent in situ hybridization. Methods Enzymol 470: 641-659.

van Heusden GPH (2009) 14-3-3 Proteins: insights from genome-wide studies in yeast. Genomics 94: 287-293.

A

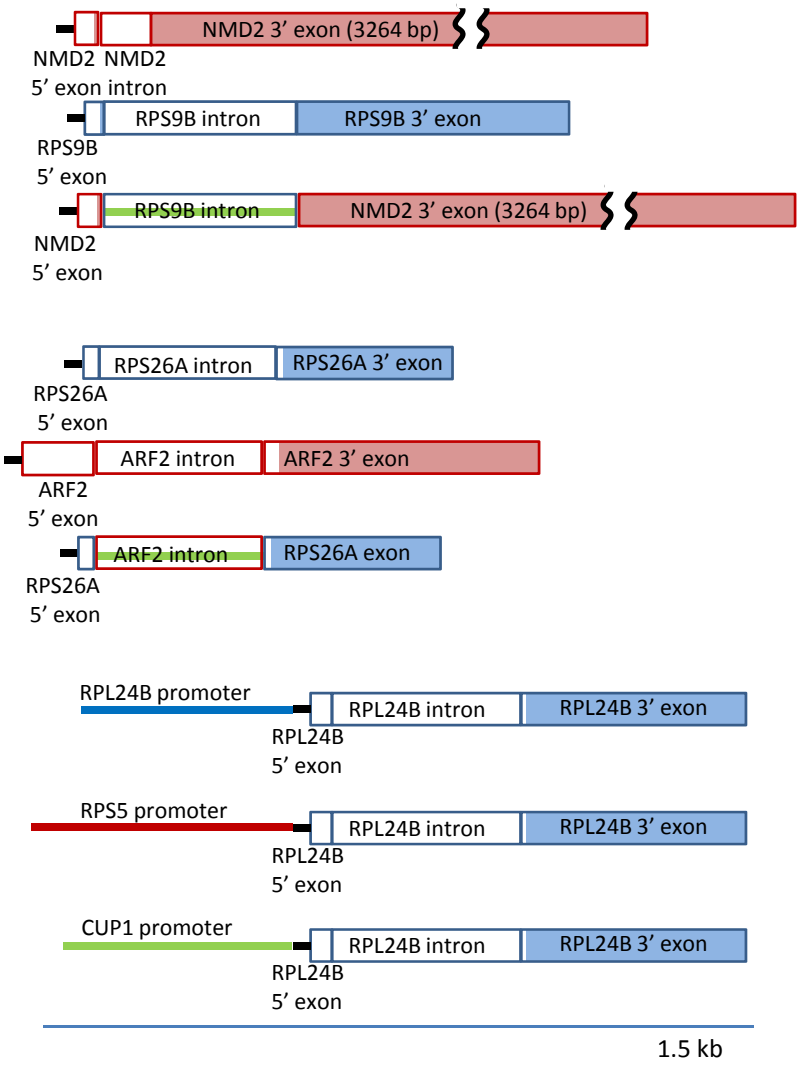
NMD2 3’ exon (3264 bp)
NMD2
5’ exon
NMD2
intron
RPS9B intron
RPS9B 3’ exon
RPS9B
5’ exon
RPS9B intron
NMD2 3’ exon (3264 bp)
NMD2
5’ exon
RPS26A intron
RPS26A 3’ exon
RPS26A
5’ exon
ARF2 intron
ARF2 3’ exon
ARF2
5’ exon
ARF2 intron
RPS26A exon
RPS26A
5’ exon
RPL24B promoter
RPL24B intron
RPL24B 3’ exon
RPL24B
5’ exon
RPS5 promoter
RPL24B intron
RPL24B 3’ exon
RPL24B
5’ exon
CUP1 promoter
RPL24B intron
RPL24B 3’ exon
RPL24B
5’ exon
1.5 kb

B

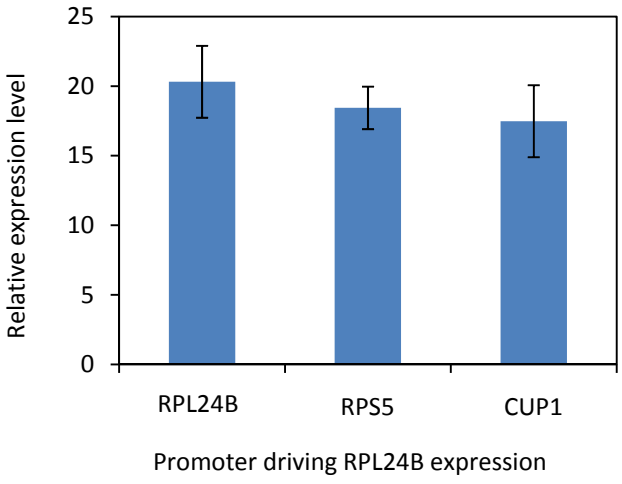
25
20
15
10
5
0
Relative expression level
RPL24B
RPS5
CUP1
Promoter driving RPL24B expression

Figure 1. Chimeric constructs to determine *cis*- contributions to the 3-AT splicing response. A. Schematics of genes involved in chimeric constructs tested in this study. Block regions represent transcribed sequence, while lines represent untranscribed sequences. Colored lines correspond to sequence defined as promoter sequence for the purposes of this study. Shaded block regions represent coding sequence, while white block regions represent untranslated sequence – either part of the 5' UTR or the intron (or both). The 3' untranslated regions are not depicted – the end of the block in each case represents the end of the coding sequence for the transcript. All constructs are integrated at their genomic loci. Promoter swaps are marked by the kanMX drug resistance cassette upstream of the promoter. B. Non-native promoters can drive expression of RPL24B to similar levels as the native promoter. Error bars represent the standard deviation from three technical replicates.

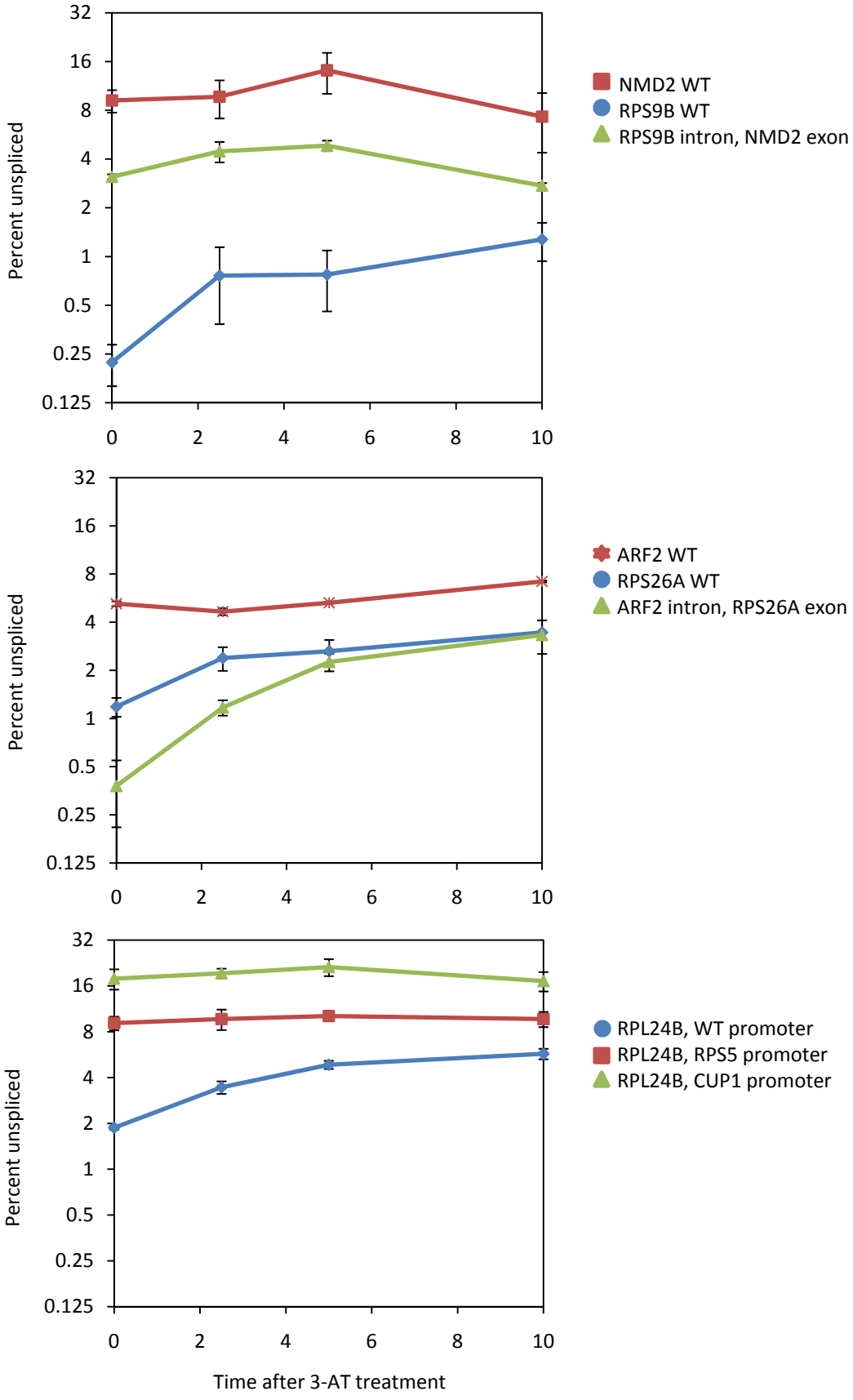
Percent unspliced
32
16
8
4
2
1
0.5
0.25
0.125
0
2
4
6
8
10
NMD2 WT
RPS9B WT
RPS9B intron, NMD2 exon
ARF2 WT
RPS26A WT
ARF2 intron, RPS26A exon
RPL24B, WT promoter
RPL24B, RPS5 promoter
RPL24B, CUP1 promoter
Time after 3-AT treatment

Figure 2. Elements in the promoter, but not the intron, are important for the 3-AT response. The percentage of total transcript that was unspliced before and during treatment with 3-AT was measured by QPCR with intron-specific and second exon primers. Values are plotted on a $\log_2$ scale, and error bars represent standard deviations from 2-4 technical replicates.

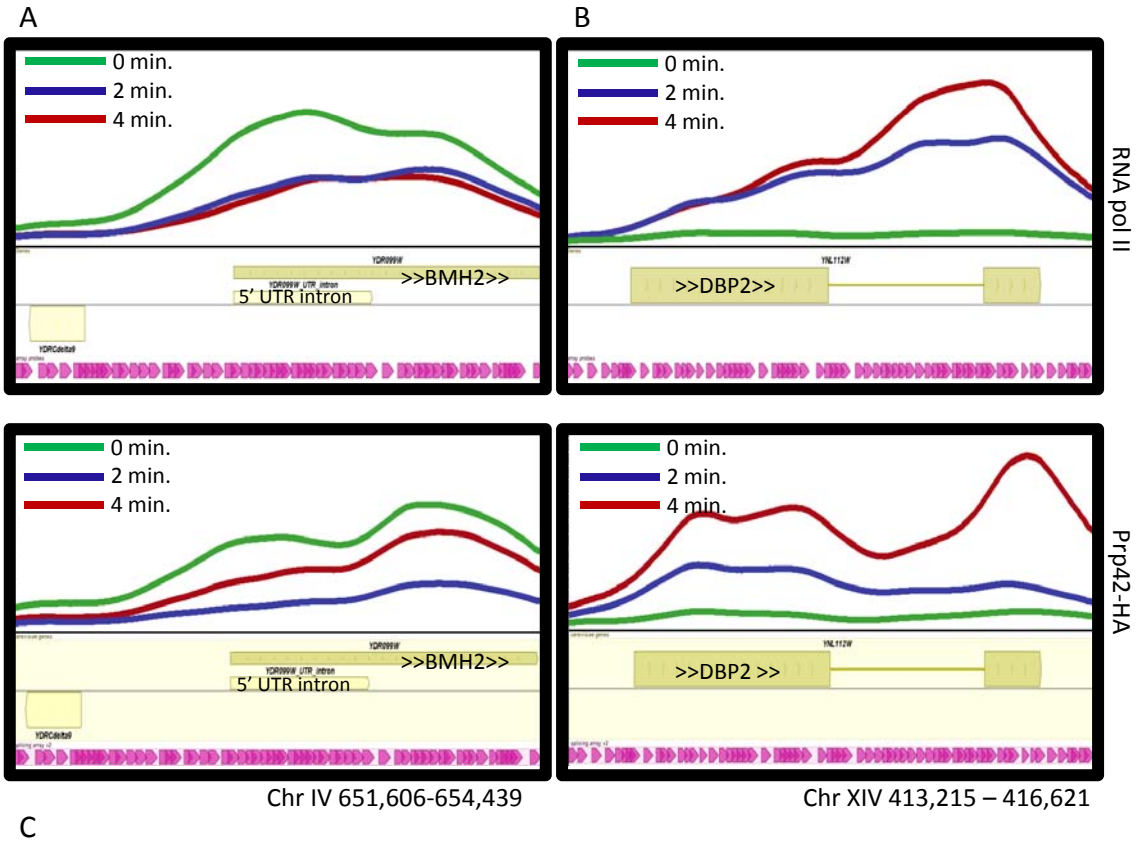
A
B
0 min.
2 min.
4 min.
>>BMH2>>
5' UTR intron
>>DBP2>>
RNA pol II
Prp42-HA
Chr IV 651,606-654,439
Chr XIV 413,215 – 416,621

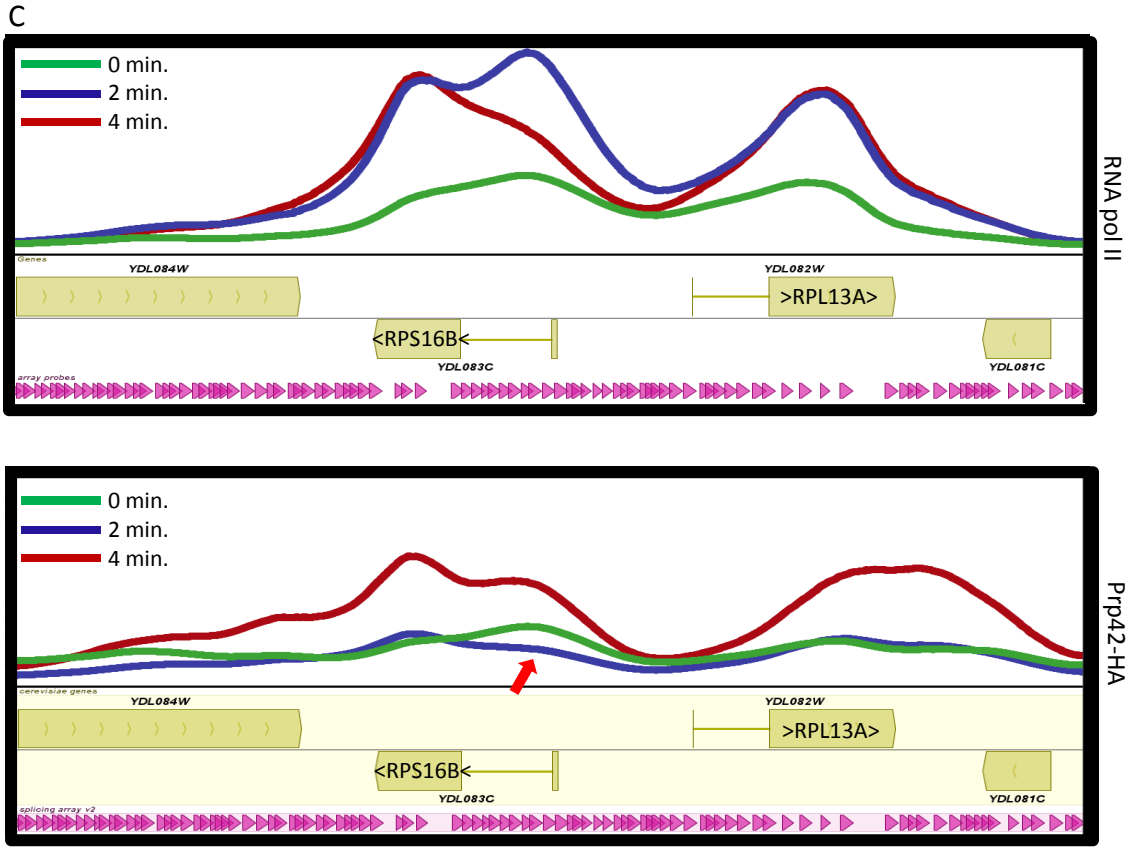
C
0 min.
2 min.
4 min.
YDL084W
YDL082W
>RPL13A>
<RPS16B<
YDL083C
YDL081C
RNA pol II
Prp42-HA
Chr IV 305223 - 310271

D

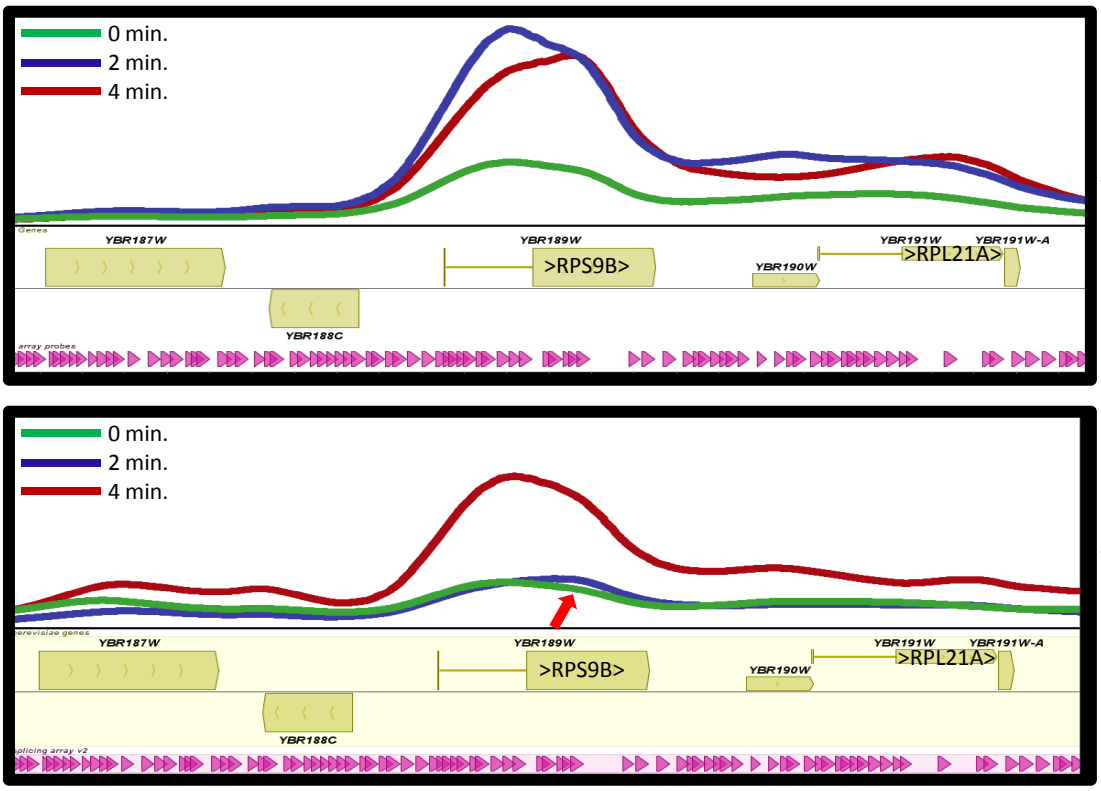

Chr II 602,479 – 607,527

E

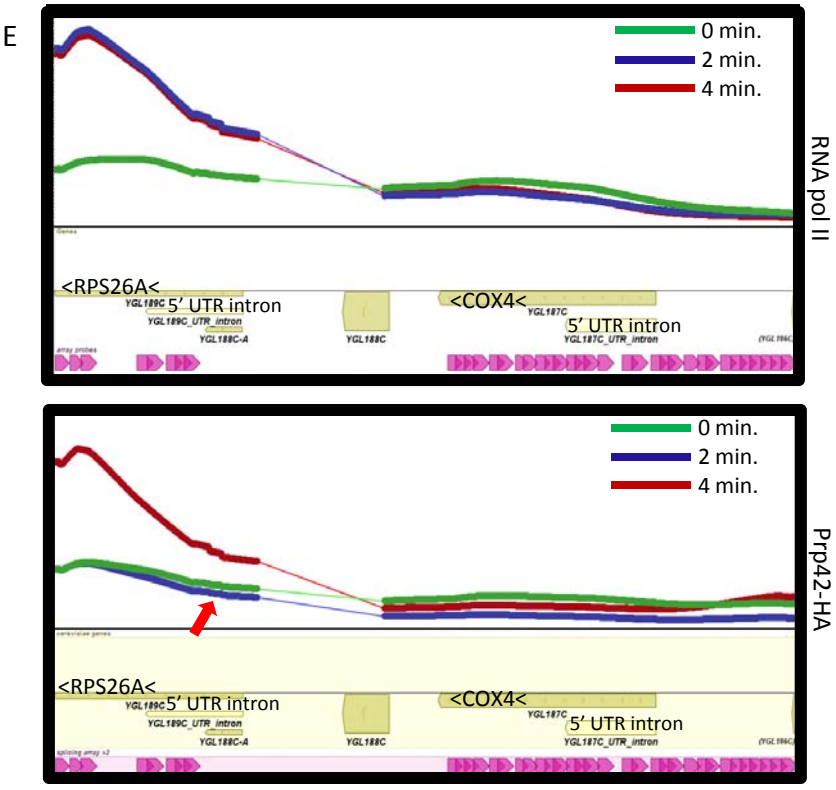

Chr VII 148,258 – 151,054

Figure 3. Association of RNA polymerase II and Prp42 with various genomic loci before and during 3-AT treatment. Ratio values from a microarray measuring DNA immunoprecipitated by either a monoclonal antibody to the Rpb3 subunit of RNA polymerase II or a monoclonal antibody to the HA tag introduced at the C-terminus of Prp42, compared to input DNA. DNA amounts and scanning parameters were normalized such that the two channels are equivalent at loci not expected to interact specifically with RNA polymerase II or Prp42. The y-axis represents relative association and absolute values are not the same in all plots. Likewise, the x-axis represents genomic coordinates, and the scale is not consistent between plots. The chromosomal regions represented are indicated below each plot. Raw values were subjected to a smoothing algorithm provided by the MochiView software before drawing the plots (see materials and methods for more details). A. The genomic locus containing BMH2. B. The genomic locus containing DBP2. C. The genomic locus containing RPS16B and RPL13A. D. The genomic locus containing RPS9B and RPL21A. E. The genomic locus containing RPS26A and COX4.

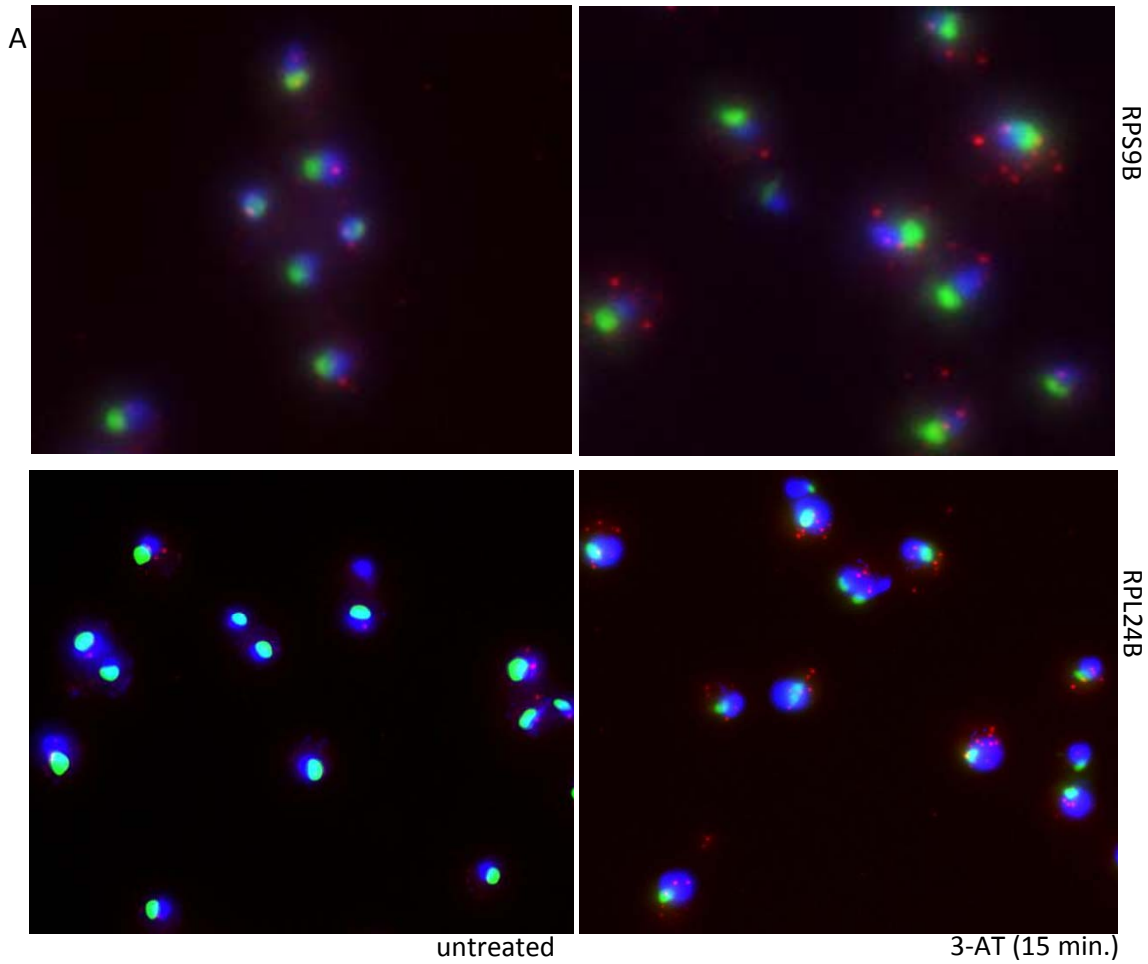
A
RPS9B
RPL24B
untreated
3-AT (15 min.)

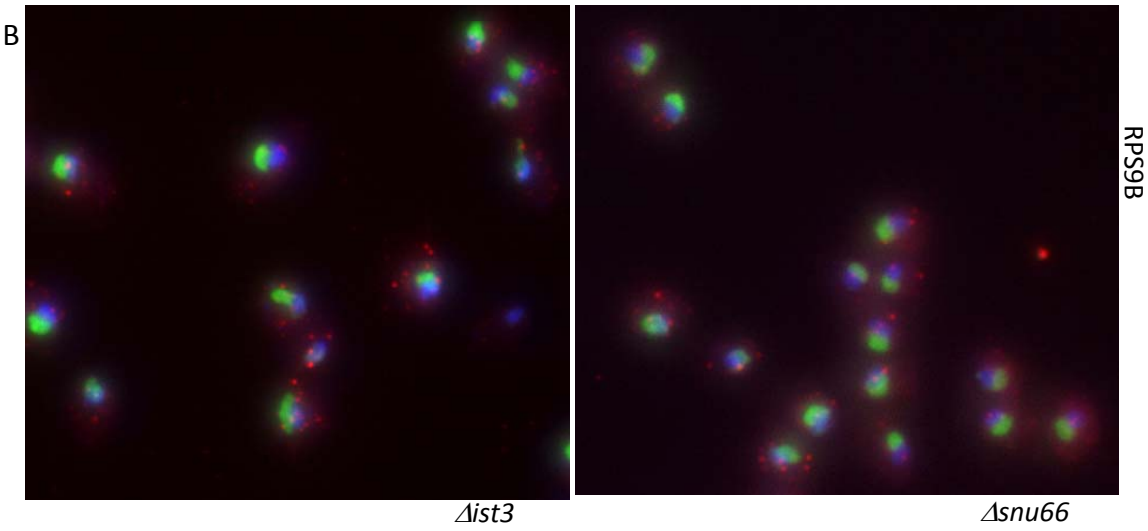
B
RPS9B
Δist3
Δsnu66

Figure 4. Unspliced pre-mRNAs are exported to the cytoplasm. Single molecule RNA fluorescence *in situ* hybridization was used to visualize the locations of individual RPG introns. A. Visualization of introns before and after treatment with 3-AT. Introns appear as diffraction-limited spots in red. The nucleus is stained with DAPI, represented with blue, and the nucleolus is stained with a fluorescently labeled probe against the ITS region of the rRNA, represented in green. B. Visualizations of individual RPS9B introns in two different mutant strains that have splicing defects. Colors are as in (A).

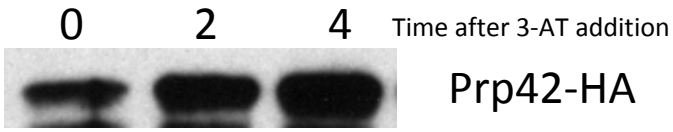

QPCR measurements of intergenic region

Time after 3-AT addition	Total intergenic	Rpb3 pulldown intergenic	Prp42-HA pulldown intergenic
0	0.14	0.40	0.19
2	0.27	1.10	1.05
4	0.81	1.30	1.02

Figure S1. Normalization of material for ChIP-chip experiment. Western blot showing immunoprecipitated amounts of Prp42-HA for each time point. The amount at 0-minute time point is less, but the amounts used in the experiment were normalized using QPCR values for an intergenic region displayed (displayed in table), which were correspondingly low for the 0-minute time point.

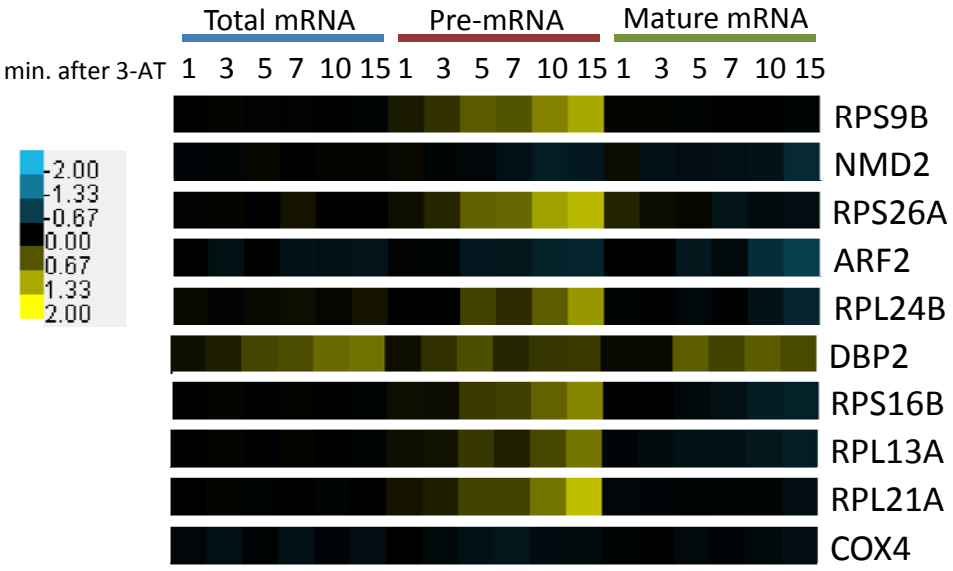

Figure S2. Levels of total mRNA, pre-mRNA, and mature mRNA for relevant transcripts following 3-AT treatment. Data are from Pleiss *et al,* 2007.

Epilogue

Future Directions

It has been very satisfying to watch the evolution of this project from a hypothesis that triggered strong skepticism among many members of the Guthrie lab to a rich problem with many avenues of further investigation to pursue. After more than seven years of work on the question of if and how splicing can be regulated in response to environmental stresses, I am left feeling that we have barely scratched the surface and that we have raised more questions than we have answered. I think that the answers to some of these new questions have the potential to offer important insights not only into the mechanism by which regulation at the level of pre-mRNA splicing can occur, but also more broadly into the ways in which mRNA processing activities are coordinated with transcription. The following describes what I see as the most pressing questions still to be answered, and future directions that I imagine could be very fruitful.

Modulation of the Co-transcriptional dynamics of spliceosome assembly and activation on RPGs in 3-AT stress

The recent demonstration that splicing of many RPGs is allowed to finish co-transcriptionally via slowing of RNA polymerase II at the 3' ends of their genomic loci (Carrillo Oesterreich *et al.*, 2010), coupled with our demonstration that RNA polymerase II accumulates even more dramatically at the 3' ends of ribosomal protein genes following treatment with 3-AT, raises many intriguing and accessible questions about the interactions between RNA polymerase II and the splicing machinery at the RPG loci.

We have shown that a component of the U1 snRNP (and presumably all of the U1 snRNP) accumulates along with RNA polymerase II at the 3' ends of genes following

treatment with 3-AT, but we have not investigated possible changes in the association of the other spliceosomal sub-complexes following 3-AT treatment. In initial studies, the mild decrease in U1 association observed at genomic loci near the 5' end of RPG introns was exaggerated due to difficulties in normalizing chromatin immunoprecipitation samples for quantitative comparison. We interpreted the data as suggesting a decrease and delay in U1 recruitment and imagined that subsequent spliceosomal sub-complexes would also be delayed in their recruitment. While our more recent data are still consistent with the possibility of a decrease in U1 recruitment to new transcripts following treatment with 3-AT, the more clear result is that U1 release is inhibited. This suggests that a step of spliceosome assembly or activation subsequent to U1 recruitment and prior to U1 release is likely to be perturbed following 3-AT treatment. A logical next set of experiments would be to determine the distribution of the U2 and U5 snRNPs along the genomic loci of intron-containing genes. These experiments are likely to be somewhat more technically difficult than determining the distribution of the U1 snRNP along the genomic loci of intron-containing genes, simply because the U2 and U5 snRNPs associate with the nascent transcript later and at further distances from the elongating polymerase and chromatin. U2 and U5 snRNPs have been successfully used to precipitate chromatin, but definitely do so less efficiently than U1 (Moore *et al.,* 2006; Tardiff *et al.*, 2006). The dynamic range for seeing a decrease in recruitment of U2 and U5 in response to 3-AT may be small, but a change in the position along an RPG at which these complexes appear should be apparent, as should a complete loss of recruitment. Determining whether it is

the recruitment of the U2 and U4/U6·U5 complexes, or the rearrangements that yield the catalytically active spliceosome, that causes U1 to be retained would be very helpful in narrowing the possibilities for the mechanism by which splicing is inhibited, and could provide some insight into which aspects of "splicing status" can be monitored by RNA polymerase II.

Another major mechanistic question raised by our result that an RPG promoter element is necessary for conferring constitutively efficient splicing and 3-AT responsiveness on RPGs is how precisely a promoter element affects the behavior of the elongating polymerase and assembling spliceosomal sub-complexes downstream. I think several experimental approaches could yield important insight into various aspects of this question.

Firstly, the finding that RNA polymerase and U1 accumulate near the 3' ends of RPGs suggests the possibility that *cis*- elements near the 3' ends of these genes could also contribute to the splicing response. This question could be tested by generating chimeric constructs juxtaposing the 3' UTR, cleavage and polyadenylation, and termination sites from non intron-containing, non-RPGs with the coding sequence of an RPG that responds strongly to 3-AT and measuring both constitutive splicing efficiency and the responsiveness of splicing to 3-AT.

Secondly, the contribution of the promoter to U1 recruitment and retention and RNA polymerase slowing at the 3' ends of RPGs could be tested directly by chromatin immunoprecipitation in a chimeric strain carrying RPL24B driven by the CUP1 or RPS5

promoters. It would be interesting to know whether the promoter element that appears to be required for the efficient splicing of RPL24B and its responsiveness to 3-AT is also required for the accumulation of RNA polymerase II at the 3' end of the gene, and the increase in this accumulation following treatment with 3-AT. If a *cis*- element at the 3' end of an RPG is also found to contribute to the 3-AT response, its contribution to the U1 and polymerase dynamics along the RPG genomic locus in 3-AT could also be tested.

A third question that could be tested using the assay of chromatin immunoprecipitation followed by microarray analysis is whether modifications of histones in the vicinity of RPGs change in response to 3-AT. Several lines of evidence suggest that histone modifications may contribute to the regulation of splicing, and to the regulation of RPGs. The histone acetylase Gcn5 interacts genetically with U2 snRNP proteins, and perturbations of Gcn5-mediated histone acetylation lead to changes in U2 recruitment and retention at some spliced genes, although the genes that were investigated were not RPGs (Gunderson & Johnson, 2009). In higher eukaryotes, different histone methylations have been shown to correlate with promoter, exon, and intron boundaries (Huff *et al.*, 2010). Also, histone ubiquitylation has been shown to be prevalent at RPG loci (A. Shilatifard, personal communication). Intriguingly, factors involved in the ubiquitylation and de-ubiquitylation of histones have strong genetic interaction with splicing factors (Collins *et al.*, 2007 and T. Kress, unpublished data). Finally, histone deacetylation has been implicated in the transcriptional down-regulation of RPGs in response to rapamycin (Rohde & Cardenas, 2003). Thus, it seems possible that a change

in a histone modification at RPG loci could contribute to the change in RPG splicing efficiency that we observe in response to amino acid starvation.

The search for protein factors that help mediate the 3-AT induced inhibition of splicing

I have spent a great deal of time and effort trying to identify protein factors that contribute to the inhibition of splicing in response to 3-AT. The search is complicated by the fact that cellular responses to 3-AT occur (apparently) at nearly every level of cellular metabolism, complicating the use of growth sensitivity to 3-AT as a screening tool. The things we have slowly learned about the response so far, and the findings of the experiments suggested above, should help facilitate the selection of promising candidates to test. In particular, it seems likely that post-translational modifications of RNA polymerase, splicing factors, and chromatin will play important roles.

The response we observe is very fast – the distribution of polymerase and U1 along the genomic loci of RPGs changes within one or two minutes after exposure to 3-AT. It seems unlikely that it depends on the synthesis of new protein factors. On the other hand, post-translational modifications are known to influence the behaviors of many transcription and splicing factors. The evidence suggesting that post-translational modifications of histones could be involved in this response is detailed above. In addition, it seems likely that changes in phosphorylation state of one or more splicing and transcription factors could be involved. We showed that both the activity and proper regulation of CK2 are required for the 3-AT response. CK2 has dozens of substrates with roles in transcription and splicing, so determining which of these are

relevant for the splicing inhibition in 3-AT will not be an easy task. It seems likely that coordinated changes in the phosphorylation states of multiple factors, orchestrated by CK2, could lead to the observed changes in the co-transcriptional dynamics of polymerase elongation and spliceosome recruitment. A more detailed understanding of the changes in these dynamics in response to 3-AT, as outlined above, should help narrow the pool of CK2 substrates that may be relevant in the 3-AT response. Another key series of phosphorylation events that could be relevant are the phosphorylations and dephosphorylations of the RNA polymerase carboxy-terminal domain (CTD). It has recently been shown that a splicing-dependent polymerase pause at the 3' splice site of both a splicing reporter construct and at least some endogenous genes is associated with the appearance of phosphorylation on Ser2 of the CTD heptad repeat (Alexander *et al.*, 2010). It would be interesting to investigate whether this phosphorylation event is altered in response to 3-AT. Finally, methylation and ubiquitylation have both been detected on splicing factors, and shown to have functional consequences in splicing activity (Bellare *et al.,* 2008; Chen *et al.*, 2010). The full range of post-translational modifications of splicing factors, their functions in the splicing mechanism, and their dynamics are only beginning to be understood. Elucidating a role for one or more of these modifications in the 3-AT induced inhibition of splicing would be very exciting indeed.

Previous unbiased (or at least broad) screens for factors involved in the 3-AT response at the level of splicing have failed due to the fact that the read-out in these screens was simply growth inhibition in the presence of 3-AT – far too unspecific a read-out for a

very specific question (see appendix 1). But a more specific screen could be done, and is being devised, to be carried out by Jaclyn Greimann in collaboration with Jeff Pleiss. Jeff has developed high-throughput methods for isolating RNA, synthesizing cDNA, and making qRT-PCR measurements of pre-mRNA and total mRNA for specific transcripts. Using these techniques, he has assayed splicing efficiencies in a collection of deletions or mutations of nearly all yeast genes. These techniques will be applied to assay splicing efficiency for an RPG following treatment of the collection of mutants with sulfometuron methyl, a drug that induces an amino acid starvation response very similar to that induced by 3-AT. The results of this screen will be very useful, especially in conjunction with the more focused lines of investigation described above.

The fate of unspliced RPG pre-mRNAs

The finding that the unspliced RPG pre-mRNA accumulate primarily in the cytoplasm raises some interesting questions. Conventional wisdom would suggest that they are likely to be degraded my NMD, but they persist at least long enough to be robustly detected by us in the absence of mutations to the NMD machinery. We have seen that they accumulate to higher levels in NMD mutants (and also in a strain carrying a deletion of the nuclear exosome component RRP6) (unpublished data), suggesting that they are subjected to some decay by both of these pathways. However, we have also seen that the cell can very efficiently degrade RPG pre-mRNAs in the nucleus, as it does following rapamycin treatment.

The question remains whether the export of the unspliced RPG pre-mRNAs to the cytoplasm is merely a consequence of the mechanism by which splicing and transcription are coordinately affected in response to 3-AT, or whether they may actually function in the cytoplasm. Interestingly, several of the RPG pre-mRNAs that accumulate in amino acid starvation contain their introns within the 5' UTR, such that the intron does not disrupt the coding sequence of the gene. The introns of all RPGs are very biased toward the 5' ends of their transcripts; even for coding sequences that are interrupted by the intron, a possibly functional protein could be translated from the unspliced transcript thorough the use of an in-frame start codon near the 3' end of the intron, in many cases. The main obstacle to translation of unspliced RPG transcripts, then, would be the presence of short upstream open reading frames in what would become a very long 5'UTR in the unspliced RPG transcripts. Short upstream open reading frames have been shown generally to target messages to NMD, but one condition in which the translation apparatus is better suited to scanning through them is amino acid starvation, where phosphorylation of eIF2α by Gcn2 has been shown to facilitate the translation of the upstream open reading frame-containing GCN4 transcript (Hinnebusch, 2005). Thus it could be interesting to determine whether the unspliced RPG pre-mRNAs that escape to the cytoplasm after 3-AT treatment are ever found associated with polysomes, indicating that they are being translated. A similar experiment to this has been done beautifully by Nick Ingolia, who isolated ribosomes under conditions of complete amino acid depletion and the purified and sequenced the mRNA fragments that were protected from nuclease digestion by the ribosome (Ingolia

et al., 2009). Unfortunately, his conditions of shifting yeast from rich media to synthetic media lacking all amino acids for 20 minutes before isolating ribosomes were likely too stringent to elicit the RPG pre-mRNA accumulation we see in 3-AT. When we shift yeast from synthetic complete media to media lacking all amino acids for 20 minutes, we see substantial decreases in the amounts of RPG pre-mRNA (chapter 3). Furthermore, we would be interested not only in the positions on a message of the ribosomes, but in whether a message associated with a polysome contained an intron, regardless of how ribosomes were distributed along it. Isolating polysomes following treatment with 3-AT and assaying the associated mRNAs for the presence of RPG pre-mRNAs by microarray would be an interesting and straightforward experiment. The translation of unpliced RPG transcripts could be a mechanism to continue translating some, but reduced numbers of ribosomal proteins under conditions when translation is generally inhibited but favors transcripts with upstream open reading frames. Additionally or alternatively, it could result in the translation of an array of ribosomal proteins that differ by a few amino acids at their N-termini, possibly allowing for slight differences in function when incorporated into ribosomes.

Other examples of splicing regulation

While there is plenty of work left to do to understand the splicing response to 3-AT, it seems like this is just the beginning of understanding how dynamic behavior of splicing (and mRNA processing in general) in different conditions can contribute to regulation of gene expression. Our epistasis mini-array profile (EMAP) of factors involved in RNA

processing revealed genetic interactions between the spliceosome and components of the COP9 signalosome, which removes the RUB1 post-translational modification (homologous to neddylation in higher eukaryotes) (See chapter 2). Interestingly, RUB1 itself contains an intron, and two of the four other genes involved in neddylation also contain introns. Recent proteomic analysis in humans has revealed that multiple splicing factors and ribosomal proteins are neddylated, suggesting that neddylation and deneddylation could be part of a feedback loop affecting splicing activity. I think the investigation of splicing regulation in yeast should be a rich source of interesting questions and intriguing answers for a long time to come.

References

Alexander RD, Innocente SA, Barrass JD, Beggs JD (2010) Splicing-dependent RNA polymerase pausing in yeast. Mol Cell 40: 582-593.

Bellare P, Small EC, Huang X, Wohlschlegel JA, Staley JP et al. (2008) A role for ubiquitin in the spliceosome assembly pathway. Nat Struct Mol Biol 15: 444-451.

Carrillo Oesterreich F, Preibisch S, Neugebauer KM (2010) Global analysis of nascent RNA reveals transcriptional pausing in terminal exons. Mol Cell 40: 571-581.

Chen Y, Milliman EJ, Goulet I, Cote J, Jackson CA et al. (2010) Protein arginine methylation facilitates cotranscriptional recruitment of pre-mRNA splicing factors. Mol Cell Biol 30: 5245-5256.

Collins SR, Miller KM, Maas NL, Roguev A, Fillingham J et al. (2007) Functional dissection of protein complexes involved in yeast chromosome biology using a genetic interaction map. Nature 446: 806-810.

Gunderson FQ, Johnson TL (2009) Acetylation by the transcriptional coactivator Gcn5 plays a novel role in co-transcriptional spliceosome assembly. PLoS Genet 5: e1000682.

Hinnebusch AG (2005) Translational regulation of GCN4 and the general amino acid control of yeast. Annu Rev Microbiol 59: 407-450.

Huff JT, Plocik AM, Guthrie C, Yamamoto KR (2010) Reciprocal intronic and exonic histone modification regions in humans. Nat Struct Mol Biol 17: 1495-1499.

Ingolia NT, Ghaemmaghami S, Newman JRS, Weissman JS (2009) Genome-wide analysis in vivo of translation with nucleotide resolution using ribosome profiling. Science 324: 218-223.

Moore MJ, Schwartzfarb EM, Silver PA, Yu MC (2006) Differential recruitment of the splicing machinery during transcription predicts genome-wide patterns of mRNA splicing. Mol Cell 24: 903-915.

Rohde JR, Cardenas ME (2003) The tor pathway regulates gene expression by linking nutrient sensing to histone acetylation. Mol Cell Biol 23: 629-635.

Tardiff DF, Lacadie SA, Rosbash M (2006) A genome-wide analysis indicates that yeast pre-mRNA splicing is predominantly posttranscriptional. Mol Cell 24: 917-929.

Appendix 1

Genetic Screens for Factors Involved in the Amino Acid Starvation Response

Early in my graduate career, part of the motivation for looking at amino acid starvation as a stress that might elicit a response at the level of pre-mRNA splicing was a series of genetic interactions that were uncovered between splicing factors and the kinase involved in signaling amino acid starvation to the translation machinery, Gcn2. Deletions of multiple splicing factors were found to suppress the 3-AT sensitivity of a Δgcn2 strain. This motivated the construction of a strain that carried a mutation in the phosphorylation site of the substrate of Gcn2, eIF2α (rendering it non-phosphorylatable) and also carried the "magic markers" required for high-throughput double mutant strain construction in an EMAP setting (Hinnebusch, 2005). This strain was crossed to the RNA processing, chromatin biology, and kinase/phosphatase EMAP collections (Collins *et al.,* 2007; Fiedler *et al.*, 2009; Wilmes *et al.*, 2008), and the resultant double mutant haploid strains were assayed for growth on 3-AT. The hope was that, in the context of the hypersensitized background imposed by the eIF2α phosphorylation site mutant, double mutants that exacerbated 3-AT sensitivity might reveal factors in pathways for responding to 3-AT that were parallel to the Gcn2-imposed inhibition of translation (i.e. the inhibition of ribosomal protein gene splicing!). This screen yielded some interesting candidates. For example, splicing factors were identified that exacerbated the sensitivity of the eIF2α strain to 3-AT, in contrast to the splicing factors that suppressed the sensitivity of the Gcn2 mutant. Additionally, several components of a pathway that sequentially phosphorylates inositol polyphosphates to yield a range of different small molecules believed to have roles in intracellular signaling, either strongly exacerbated or strongly suppressed the sensitivity of the eIF2α

strain to 3-AT suggesting that specific InsP molecules may have roles in modulating the response. Sadly, I failed to find any evidence that these roles directly impinged upon the splicing response (although intriguingly, $InsP_6$ has been shown to play a role in mRNA export, and could conceivably affect the export of unspliced pre-mRNA to the nucleus following 3-AT treatment). Likewise, microarray analysis of the splicing factor mutations that conferred sensitivity were inconclusive – many of them showed accumulations of pre-mRNA both before and after 3-AT treatment that were different than that seen in the wild type, but in complex ways. These microarray results are available in electronic format. I include here the early evidence for genetic interactions between GCN2 and splicing factors, and the results of the screen with the eIF2α phosphorylation site mutant, in case they might be of interest to anyone in the future.

References

Collins SR, Miller KM, Maas NL, Roguev A, Fillingham J et al. (2007) Functional dissection of protein complexes involved in yeast chromosome biology using a genetic interaction map. Nature 446: 806-810.

Fiedler D, Braberg H, Mehta M, Chechik G, Cagney G et al. (2009) Functional organization of the S. cerevisiae phosphorylation network. Cell 136: 952-963.

Hinnebusch AG (2005) Translational regulation of GCN4 and the general amino acid control of yeast. Annu Rev Microbiol 59: 407-450.

Wilmes GM, Bergkessel M, Bandyopadhyay S, Shales M, Braberg H et al. (2008) A genetic interaction map of RNA-processing factors reveals links between Sem1/Dss1-containing complexes and mRNA export and splicing. Mol Cell 32: 735-746.

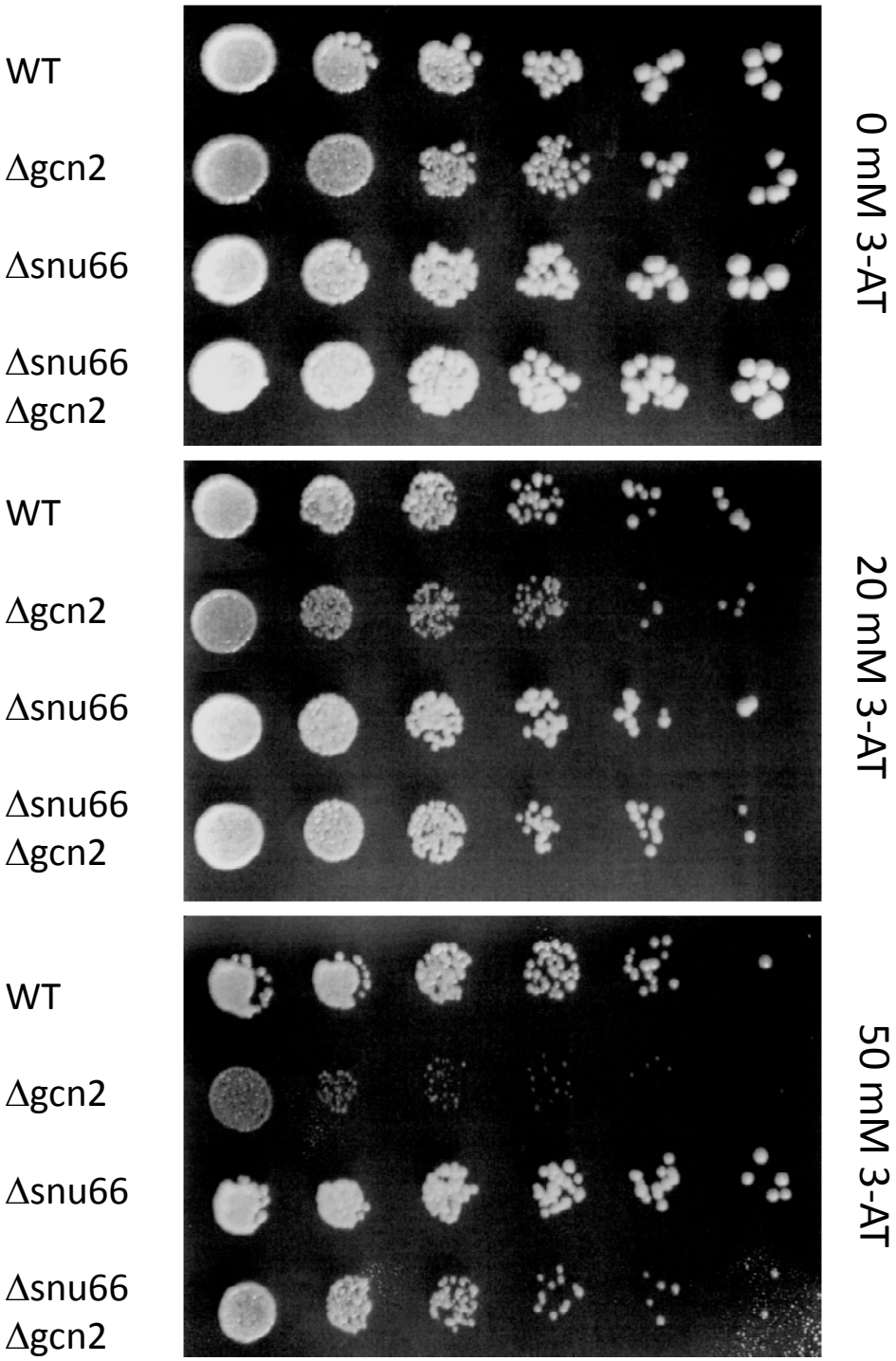
WT
Δgcn2
Δsnu66
Δsnu66
Δgcn2
0 mM 3-AT
WT
Δgcn2
Δsnu66
Δsnu66
Δgcn2
20 mM 3-AT
WT
Δgcn2
Δsnu66
Δsnu66
Δgcn2
50 mM 3-AT

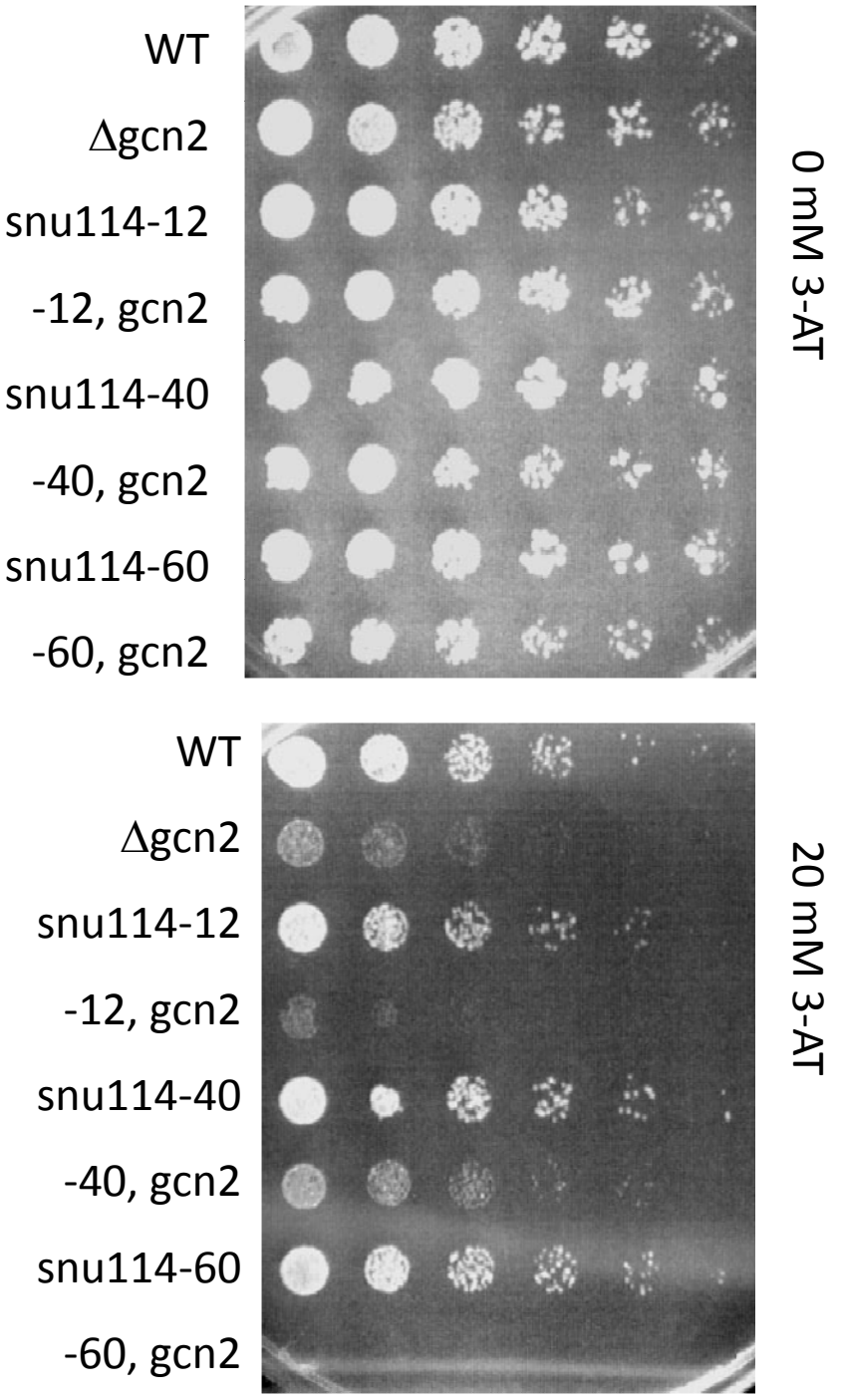

Figure 1. Genetic interactions between *GCN2* and splicing factors. Double mutant strains carrying a deletion of *GCN2* and a mutation or deletion in either *SNU66 or SNU114* were constructed and serial dilutions of a log phase culture were spotted either on SC –HIS plates or on SC –His plates containing 3-AT.

mutation	Spliceosome association	Effect on gcn2 3-AT sensitivity
Δsnu66	triple snRNP	suppresses
snu114-12	triple snRNP	mildly exacerbates
snu114-40	triple snRNP	suppresses
snu114-60	triple snRNP	strongly exacerbates
prp4-1	triple snRNP	mild suppression (?)
prp6-1	triple snRNP	none
prp28-1	triple snRNP	none
Gal-Aar2	16S U5 snRNP	none
Δmud1	U1 snRNP	mild suppression (?)
Gal-Utp21	??	none

mutation	Relationship to GCN2 or splicing	Effect on gcn2 3-AT sensitivity
Δpsr1	2-hybrid interaction with Snu66	none
Δoca1	2-hybrid interaction with Snu66	suppresses
Δyih1	overexpression causes a Gcn- phenotype that is suppressed by overexpression of GCN2	Very strongly suppresses
Δasc1	Deletion previously published to suppress 3-AT sensitivity of gcn2, gene has an intron with a snoRNA	Strongly suppresses

Table 1. Summary of genetic interactions with *GCN2*

Table 2. Growth of chromosome biology e-map strain double mutants. Single mutant strains from the chromosome biology e-map were crossed to the eIF2α S51A phosphorylation site mutant and the double mutant strains were pinned onto media containing 2 mM 3-AT. Mutations from the chromosome biology e-map are ordered by their average colony size in this assay, from smallest to largest. Averages were calculated from three replicates.

avg.colony size on 2mM 3AT	ORF	gene name	mutation
0	YOR038C	HIR2	Deletion
0	YNL294C	RIM21	Deletion
0	YMR138W	CIN4	Deletion
0	YML062C	MFT1	Deletion
0	YLR015W	BRE2	Deletion
0	YFL001W	DEG1	Deletion
2	YPL129W	TAF14	DAmP
4	YMR127C	SAS2	Deletion
13	YNL299W	TRF5	Deletion
21	YLR233C	EST1	Deletion
24	YGL066W	SGF73	Deletion
26	YLR095C	IOC2	Deletion
27	YPL055C	LGE1	Deletion
33	YOR368W	RAD17	Deletion
46	YML094W	GIM5	Deletion
50	YBR009C	HHF1	Deletion
65	YCL010C	SGF29	Deletion
66	YDR146C	SWI5	Deletion
70	YDL033C	SLM3	Deletion
72	YNR051C	BRE5	Deletion
77	YBL088C	TEL1	Deletion
88	YIL139C	REV7	Deletion
90	YPL254W	HFI1	Deletion
96	YJR053W	BFA1	Deletion
104	YMR075W	RCO1	Deletion
106	YLR102C	APC9	Deletion
109	YBR114W	RAD16	Deletion
113	YKL053C-A	MDM35	Deletion
116	YLR350W	ORM2	Deletion
118	YGR108W	CLB1	Deletion
125	YNL246W	VPS75	Deletion
127	YNL307C	MCK1	Deletion
127	YBR103W	SIF2	Deletion
128	YML071C	COG8	Deletion
129	YCL011C	GBP2	Deletion
132	YDR059C	UBC5	Deletion
134	YER007W	PAC2	Deletion

139	YDL074C	BRE1	Deletion
140	YDR477W	SNF1	Deletion
142	YMR199W		Deletion
143	YHR151C		Deletion
149	YGR252W		DAmP
150	YBL103C		Deletion
159	YBR255W		Deletion
159	YBR107C		Deletion
160	YBR094W		Deletion
160	YKL118W		Deletion
162	YER161C		Deletion
163	YJL168C		Deletion
164	YOR005C		Deletion
165	YNL224C		Deletion
165	YBR073W		Deletion
166	YCL037C		Deletion
166	YML124C		Deletion
170	YBR082C		Deletion
171	YLR085C		Deletion
171	YNL059C		Deletion
171	YBL016W		Deletion
174	YPR076W		Deletion
174	YBR171W		Deletion
175	YGL086W		Deletion
176	YDR225W		Deletion
178	YFR009W		Deletion
181	YER016W		Deletion
181	YJL148W		Deletion
183	YLR032W		Deletion
183	YAL011W		Deletion
184	YDR075W		Deletion
185	YJL030W		Deletion
186	YGR270W		Deletion
187	YBR173C		Deletion
187	YNL097C		Deletion
188	YNL153C		Deletion
188	YDR443C		Deletion
189	YGL173C		Deletion
191	YIL040W		Deletion
191	YHR191C		Deletion
193	YDR386W		Deletion
194	YGL019W		Deletion
194	YLR135W		Deletion
196	YBR095C		Deletion
196	YHR154W		Deletion
197	YPL022W		Deletion
197	YEL056W		Deletion
199	YDR488C		Deletion
203	YAL040C		Deletion
203	YDR257C		Deletion
204	YBR245C		Deletion
204	YBR278W		Deletion

206	YLR306W	Deletion
209	YPL129W	Deletion
210	YLR234W	Deletion
211	YDR440W	Deletion
211	YNL030W	Deletion
211	YBL093C	Deletion
212	YBL008W	Deletion
212	YGL174W	Deletion
212	YJL183W	Deletion
213	YHR207C	Deletion
213	YJR087W	Deletion
214	YLR262C	Deletion
218	YGR184C	Deletion
218	YOR014W	Deletion
219	YDR191W	Deletion
220	YBR010W	Deletion
221	YER173W	Deletion
221	YKL213C	Deletion
222	YMR038C	Deletion
223	YLR052W	Deletion
224	YGL087C	Deletion
227	YOR308C	Deletion
227	YJL098W	Deletion
227	YGR181W	Deletion
228	YER177W	Deletion
228	YNL025C	Deletion
229	YBR081C	Deletion
229	YJR104C	Deletion
230	YJL124C	Deletion
231	YER155C	Deletion
233	YBR098W	Deletion
233	YNL297C	Deletion
234	YKL010C	Deletion
236	YML102W	Deletion
236	YNL107W	Deletion
237	YEL044W	Deletion
239	YPL018W	Deletion
240	YOL067C	Deletion
241	YBR289W	Deletion
241	YKR101W	Deletion
242	YPL241C	Deletion
243	YPR018W	Deletion
243	YOR023C	Deletion
244	YPR031W	Deletion
245	YLR024C	Deletion
247	YOL051W	DAmP
247	YMR055C	Deletion
248	YML034W	Deletion
248	YBL052C	Deletion
249	YNL031C	Deletion
249	YLR210W	Deletion
249	YDR127W	Deletion

252	YGL244W	Deletion
253	YCR009C	Deletion
253	YDR092W	Deletion
254	YKL113C	Deletion
255	YDR469W	Deletion
255	YMR284W	Deletion
255	YBR195C	Deletion
256	YFL013C	Deletion
257	YEL012W	Deletion
259	YBR111W-A	Deletion
260	YKR028W	Deletion
261	YBR175W	Deletion
263	YNL273W	Deletion
263	YNL215W	Deletion
265	YBR057C	Deletion
265	YER095W	Deletion
266	YDR176W	Deletion
267	YHR090C	DAmP
267	YCR086W	Deletion
267	YHR041C	Deletion
268	YPR023C	Deletion
268	YBL058W	Deletion
268	YKR010C	Deletion
272	YOR144C	Deletion
272	YGR134W	Deletion
273	YCL016C	Deletion
274	YGR078C	Deletion
275	YHR066W	Deletion
275	YDR451C	Deletion
276	YDR363W	Deletion
276	YGL150C	DAmP
277	YLR381W	Deletion
277	YGR208W	Deletion
278	YPL226W	Deletion
279	YDR318W	Deletion
280	YLR373C	Deletion
281	YLL002W	Deletion
281	YDR334W	Deletion
283	YGL168W	Deletion
284	YDR217C	Deletion
284	YCR033W	Deletion
284	YGR135W	Deletion
287	YIL035C	Deletion
287	YOR089C	Deletion
288	YIL076W	Deletion
289	YFR010W	Deletion
289	YER116C	Deletion
291	YNL235C	Deletion
292	YOR195W	Deletion
292	YDR485C	Deletion
292	YGL020C	Deletion
292	YOL050C	Deletion

293	YMR022W	Deletion
293	YGL043W	Deletion
294	YEL003W	Deletion
295	YJL169W	Deletion
296	YOR349W	Deletion
296	YPL194W	Deletion
296	YML041C	Deletion
297	YNL136W	Deletion
297	YBL086C	Deletion
298	YIL084C	Deletion
299	YGL194C	Deletion
299	YPL180W	Deletion
299	YOL054W	Deletion
300	YMR179W	Deletion
300	YDR004W	Deletion
301	YER151C	Deletion
301	YDR159W	Deletion
301	YIL128W	Deletion
302	YCR077C	Deletion
305	YJL197W	Deletion
306	YBR231C	Deletion
310	YJL047C	Deletion
310	YPL139C	Deletion
310	YPL114W	Deletion
310	YCR065W	Deletion
311	YLR039C	Deletion
312	YMR201C	Deletion
313	YBR215W	Deletion
314	YNL236W	DAmP
314	YGL133W	Deletion
314	YGL151W	Deletion
314	YDR156W	Deletion
315	YOR106W	Deletion
316	YLR055C	Deletion
319	YPR120C	Deletion
319	YOR141C	Deletion
319	YGR200C	Deletion
320	YDR378C	Deletion
321	YLR398C	Deletion
321	YLR044C	Deletion
323	YDL155W	Deletion
325	YEL031W	Deletion
325	YDR392W	Deletion
331	YKL017C	Deletion
331	YDR289C	Deletion
332	YDL013W	Deletion
332	YDR108W	Deletion
332	YDL005C	Deletion
334	YPR141C	Deletion
334	YCL061C	Deletion
335	YBL093C	DAmP
335	YPR052C	Deletion

337	YFL023W	Deletion
337	YBR279W	Deletion
337	YLR200W	Deletion
337	YPR189W	Deletion
337	YDR181C	Deletion
338	YPR068C	Deletion
338	YKL101W	Deletion
340	YOR297C	Deletion
341	YOR191W	Deletion
342	YMR015C	Deletion
342	YNL199C	Deletion
342	YDR363W-A	Deletion
345	YKL160W	Deletion
347	YDR254W	Deletion
347	YDL020C	Deletion
348	YGL213C	Deletion
349	YPR119W	Deletion
351	YDR448W	DAmP
351	YPR046W	Deletion
352	YLR357W	Deletion
352	YFR038W	Deletion
360	YOR351C	Deletion
360	YOL004W	Deletion
362	YJR126C	Deletion
362	YPL086C	Deletion
363	YOR026W	Deletion
363	YNL206C	Deletion
365	YOL006C	Deletion
366	YER019W	Deletion
366	YDR153C	Deletion
368	YLR079W	Deletion
368	YPR070W	Deletion
368	YMR219W	Deletion
370	YPL047W	Deletion
371	YIL038C	Deletion
372	YMR224C	Deletion
373	YOL148C	Deletion
377	YGL195W	Deletion
377	YMR263W	Deletion
377	YML119W	Deletion
377	YPL253C	Deletion
378	YNL147W	Deletion
380	YPL057C	Deletion
386	YNL288W	Deletion
387	YNL253W	Deletion
388	YDL099W	Deletion
393	YOL017W	Deletion
395	YOR346W	Deletion
396	YLR190W	Deletion
398	YER111C	Deletion
400	YPL269W	Deletion
400	YER164W	Deletion

400	YOR304W	Deletion
404	YPL138C	Deletion
405	YNL218W	Deletion
406	YML090W	Deletion
407	YJL175W	Deletion
408	YLR087C	Deletion
408	YKL020C	Deletion
409	YGL163C	Deletion
411	YGL025C	Deletion
411	YOR001W	Deletion
413	YOL081W	Deletion
413	YEL018W	Deletion
420	YPL008W	Deletion
422	YOR124C	Deletion
424	YMR048W	Deletion
425	YOR213C	Deletion
427	YMR312W	Deletion
427	YOL108C	Deletion
427	YMR106C	Deletion
431	YOR058C	Deletion
432	YOR123C	Deletion
435	YFR040W	Deletion
435	YER092W	Deletion
435	YOL145C	Deletion
438	YMR100W	Deletion
441	YOR061W	Deletion
444	YDR014W	Deletion
445	YOR189W	Deletion
445	YOL012C	Deletion
446	YOL051W	Deletion
447	YPR164W	Deletion
448	YNL238W	Deletion
450	YJR035W	Deletion
453	YML008C	Deletion
454	YGR071C	Deletion
458	YAL002W	Deletion
460	YNL298W	Deletion
464	YOR043W	Deletion
468	YPL248C	Deletion
470	YHR200W	Deletion
473	YPL167C	Deletion
475	YAR003W	Deletion
476	YKR029C	Deletion
487	YGR104C	Deletion
488	YML028W	Deletion
490	YPL024W	Deletion
495	YGL115W	Deletion
500	YMR198W	Deletion
505	YJL013C	Deletion
522	YJR082C	Deletion
524	YDR369C	Deletion
547	YDL002C	Deletion

573	YJR140C	Deletion
580	YER162C	Deletion
584	YPR135W	Deletion
584	YHR178W	Deletion
596	YBR194W	Deletion
602	YPL256C	Deletion
610	YJR043C	Deletion
612	YPL214C	Deletion
614	YMR190C	Deletion
615	YAR002W	Deletion
648	YLR421C	Deletion
658	YDR200C	Deletion
671	YER178W	Deletion
676	YMR223W	Deletion
686	YPL101W	Deletion
705	YJL115W	Deletion
708	YNL072W	Deletion
715	YJR073C	Deletion
741	YDR073W	Deletion
751	YOR025W	Deletion
758	YOR039W	Deletion
781	YMR003W	Deletion
781	YKR048C	Deletion
790	YOR269W	Deletion
792	YJL092W	Deletion
871	YOL072W	Deletion
952	YNL201C	Deletion
971	YOR184W	Deletion
1014	YNL236W	Deletion
1043	YDR245W	Deletion
1049	YLR268W	Deletion
1052	YPL181W	Deletion
1117	YHR031C	Deletion
1161	YMR304W	Deletion
1293	YFR036W	Deletion

Table 3. Growth of kinase/phosphatase e-map double mutant strains on 3-AT. Single mutant strains from the kinase/phosphatase e-map were crossed to the eIF2α S51A phosphorylation site mutant and the double mutant strains were pinned onto media containing either 0mM, 2 mM, or 8 mM 3-AT. The ratio of the colony size on 2mM or 8mM 3-AT to the colony size on 0 mM 3-AT was calculated for each kinase/phosphatase mutation in this assay. Colony sizes were the averages of three replicates. The list is ordered by the ratio of colony size on 2 mM 3-AT to the colony size on 0 mM 3-AT, as a measure of sensitivity to 3-AT.

ratio 2 mM	ratio 8mM	ORF	gene name
0.07	0.16	YMR287C	MSU1
0.21	0.15	YKL048C	ELM1
0.24	0.13	YPL256C	CLN2
0.26	0.27	YJL183W	MNN11
0.27	0.20	YJL095W	BCK1
0.28	0.24	YBR095C	RXT2
0.29	0.24	YDR245W	MNN10
0.33	0.31	YPL181W	CTI6
0.34	0.26	YBR126C	TPS1
0.35	0.28	YDR075W	PPH3
0.35	0.32	YNR051C	BRE5
0.36	0.29	YJL057C	IKS1
0.36	0.36	YGL127C	SOH1
0.38	0.66	YBR095C	RXT2
0.38	0.39	YGL174W	BUD13
0.38	0.34	YIR005W	IST3
0.38	0.33	YHR082C	KSP1
0.39	0.37	YKL074C	MUD2
0.40	0.37	YDR315C	IPK1
0.40	0.33	YNL153C	GIM3
0.40	0.28	YCR027C	RHB1
0.41	0.51	YDL230W	PTP1
0.41	0.32	YHR030C	SLT2
0.41	0.34	YDR156W	RPA14
0.41	0.42	YNL289W	PCL1
0.43	0.40	YNL154C	YCK2
0.44	0.40	YIL050W	PCL7
0.44	0.35	YDL116W	NUP84
0.44	0.30	YGL215W	CLG1
0.45	0.33	YDR122W	KIN1
0.45	0.46	YOL001W	PHO80
0.45	0.47	YKL168C	KKQ8
0.45	0.45	YDR466W	PKH3
0.45	0.44	YDL056W	MBP1
0.45	0.35	YPR120C	CLB5
0.45	0.42	YDR363W-A	SEM1

0.45	0.30	YOL011W	PLB3
0.46	0.45	YDL025C	
0.46	0.36	YER129W	SAK1
0.46	0.30	YJL047C	RTT101
0.46	0.36	YJL128C	PBS2
0.46	0.44	YLR386W	VAC14
0.46	0.44	YGR203W	
0.46	0.29	YPL214C	THI6
0.47	0.53	YPL109C	
0.47	0.47	YOL045W	PSK2
0.48	0.47	YNL068C	FKH2
0.48	0.52	YNL201C	PSY2
0.48	0.45	YPR119W	CLB2
0.48	0.35	YKL166C	TPK3
0.49	0.43	YGL067W	NPY1
0.49	0.32	YNL325C	FIG4
0.49	0.50	YJL155C	FBP26
0.49	0.31	YCL024W	KCC4
0.49	0.52	YMR068W	AVO2
0.49	0.37	YPL180W	TCO89
0.49	0.48	YAR002W	NUP60
0.49	0.33	YOR267C	HRK1
0.50	0.30	YGR081C	SLX9
0.50	0.36	YHR031C	RRM3
0.50	0.44	YDR072C	IPT1
0.50	0.35	YEL042W	GDA1
0.50	0.54	YGR052W	
0.50	0.40	YHR079C	IRE1
0.50	0.48	YDL155W	CLB3
0.50	0.50	YDR127W	ARO1
0.51	0.42	YER062C	HOR2
0.51	0.55	YKL051W	SFK1
0.51	0.43	YPL115C	BEM3
0.51	0.40	YER052C	HOM3
0.51	0.49	YKL198C	PTK1
0.51	0.43	YLR016C	PML1
0.51	0.39	YER027C	GAL83
0.51	0.46	YNL298W	CLA4
0.51	0.39	YMR291W	
0.51	0.47	YNR034W	SOL1
0.51	0.40	YIL153W	RRD1
0.51	0.35	YER095W	RAD51
0.51	0.40	YGR036C	CAX4
0.51	0.38	YOL113W	SKM1
0.51	0.45	YDR147W	EKI1
0.51	0.45	YAR014C	BUD14
0.52	0.51	YGL253W	HXK2
0.52	0.36	YBL056W	PTC3
0.52	0.36	YGL059W	
0.52	0.40	YDL179W	PCL9
0.52	0.46	YDR318W	MCM21
0.52	0.39	YLR006C	SSK1
0.52	0.40	YPR073C	LTP1

0.52	0.48	YJL115W	ASF1
0.52	0.51	YDR096W	GIS1
0.53	0.47	YPL004C	LSP1
0.53	0.45	YJR066W	TOR1
0.53	0.48	YER123W	YCK3
0.53	0.51	YFR019W	FAB1
0.53	0.56	YJR105W	ADO1
0.53	0.45	YDR173C	ARG82
0.53	0.43	YPL203W	TPK2
0.53	0.43	YML124C	TUB3
0.53	0.40	YEL016C	NPP2
0.53	0.50	YDR481C	PHO8
0.53	0.44	YHR043C	DOG2
0.53	0.44	YCR026C	NPP1
0.53	0.39	YKR053C	YSR3
0.53	0.47	YDR503C	LPP1
0.53	0.43	YER089C	PTC2
0.53	0.52	YBR092C	PHO3
0.54	0.49	YJR110W	YMR1
0.54	0.48	YHR075C	PPE1
0.54	0.50	YJL187C	SWE1
0.54	0.48	YDR247W	VHS1
0.54	0.48	YLR377C	FBP1
0.54	0.50	YNL054W	VAC7
0.54	0.46	YDL006W	PTC1
0.54	0.47	YOR231W	MKK1
0.54	0.43	YGR123C	PPT1
0.54	0.43	YBL088C	TEL1
0.54	0.48	YHR191C	CTF8
0.54	0.49	YDL134C	PPH21
0.54	0.37	YPR152C	URN1
0.55	0.38	YBR022W	POA1
0.55	0.39	YDR485C	VPS72
0.55	0.43	YLR151C	PCD1
0.55	0.60	YMR048W	CSM3
0.55	0.41	YGL019W	CKB1
0.55	0.44	YKL161C	
0.55	0.45	YJL106W	IME2
0.55	0.47	YDL236W	PHO13
0.55	0.49	YMR006C	PLB2
0.55	0.44	YER170W	ADK2
0.55	0.32	YIL095W	PRK1
0.55	0.30	YPL120W	VPS30
0.56	0.45	YMR273C	ZDS1
0.56	0.57	YIL045W	PIG2
0.56	0.41	YOR233W	KIN4
0.56	0.44	YNR047W	
0.56	0.52	YLR096W	KIN2
0.56	0.46	YCR073W-A	SOL2
0.56	0.45	YKL171W	
0.56	0.50	YPL150W	
0.56	0.51	YBL046W	PSY4
0.56	0.45	YJL148W	RPA34

0.56	0.46	YJL058C	BIT61
0.56	0.60	YDR334W	SWR1
0.57	0.50	YCR079W	
0.57	0.57	YLR260W	LCB5
0.57	0.50	YGL126W	SCS3
0.57	0.50	YHR115C	DMA1
0.57	0.57	YIL113W	SDP1
0.57	0.59	YMR139W	RIM11
0.57	0.51	YPL219W	PCL8
0.57	0.48	YOL100W	PKH2
0.57	0.46	YKL001C	MET14
0.57	0.51	YPL213W	LEA1
0.57	0.41	YGL083W	SCY1
0.57	0.57	YNL116W	DMA2
0.57	0.55	YLR253W	
0.57	0.50	YDR523C	SPS1
0.57	0.50	YLR248W	RCK2
0.58	0.48	YBR175W	SWD3
0.58	0.46	YDR284C	DPP1
0.58	0.37	YJL165C	HAL5
0.58	0.44	YDR501W	PLM2
0.58	0.51	YNR031C	SSK2
0.58	0.51	YNL041C	COG6
0.58	0.54	YMR261C	TPS3
0.58	0.65	YLR210W	CLB4
0.58	0.51	YDL079C	MRK1
0.58	0.52	YJL100W	LSB6
0.58	0.50	YJL168C	SET2
0.58	0.52	YDL214C	PRR2
0.58	0.53	YDR436W	PPZ2
0.58	0.42	YHR135C	YCK1
0.58	0.51	YER134C	
0.58	0.54	YGL208W	SIP2
0.58	0.59	YAL040C	CLN3
0.58	0.45	YLR183C	TOS4
0.58	0.51	YCL061C	MRC1
0.58	0.55	YNL183C	NPR1
0.59	0.41	YER019W	ISC1
0.59	0.55	YNL233W	BNI4
0.59	0.47	YJL083W	TAX4
0.59	0.42	YJL098W	SAP185
0.59	0.57	YBL085W	BOI1
0.59	0.52	YGL180W	ATG1
0.59	0.54	YNL309W	STB1
0.59	0.51	YHR076W	PTC7
0.59	0.52	YDR378C	LSM6
0.59	0.45	YMR156C	TPP1
0.59	0.41	YOR227W	
0.59	0.39	YGL227W	VID30
0.59	0.39	YGL115W	SNF4
0.59	0.55	YDL101C	DUN1
0.60	0.62	YGR109C	CLB6
0.60	0.57	YBR276C	PPS1

0.60	0.58	YLR273C	PIG1
0.60	0.63	YDL127W	PCL2
0.60	0.54	YPL241C	CIN2
0.60	0.55	YBR128C	ATG14
0.60	0.56	YPR111W	DBF20
0.60	0.50	YBL016W	FUS3
0.60	0.51	YDR287W	
0.61	0.54	YPL152W	RRD2
0.61	0.59	YDR507C	GIN4
0.61	0.58	YER114C	BOI2
0.61	0.56	YOR090C	PTC5
0.61	0.59	YDR490C	PKH1
0.61	0.53	YGR080W	TWF1
0.61	0.63	YBR020W	GAL1
0.61	0.80	YMR267W	PPA2
0.61	0.48	YML109W	ZDS2
0.61	0.55	YIL002C	INP51
0.61	0.56	YKR019C	IRS4
0.61	0.53	YBL068W	PRS4
0.61	0.43	YER075C	PTP3
0.61	0.61	YNL128W	TEP1
0.61	0.53	YML057W	CMP2
0.61	0.58	YFL031W	HAC1
0.61	0.42	YOR208W	PTP2
0.61	0.61	YJL124C	LSM1
0.61	0.57	YFL033C	RIM15
0.62	0.52	YOL016C	CMK2
0.62	0.47	YNL025C	SSN8
0.62	0.48	YNL020C	ARK1
0.62	0.46	YHL032C	GUT1
0.62	0.59	YPL137C	GIP3
0.62	0.44	YDR074W	TPS2
0.62	0.56	YER059W	PCL6
0.62	0.46	YAL017W	PSK1
0.62	0.45	YPL140C	MKK2
0.62	0.57	YAR018C	KIN3
0.62	0.62	YDR422C	SIP1
0.62	0.48	YOL128C	YGK3
0.62	0.47	YLR433C	CNA1
0.63	0.56	YKL190W	CNB1
0.63	0.43	YFR053C	HXK1
0.63	0.43	YLR113W	HOG1
0.63	0.54	YGR086C	PIL1
0.63	0.57	YML070W	DAK1
0.63	0.58	YOR039W	CKB2
0.63	0.51	YKL067W	YNK1
0.63	0.56	YCR073C	SSK22
0.63	0.56	YNR012W	URK1
0.63	0.54	YKL116C	PRR1
0.63	0.59	YML094W	GIM5
0.63	0.51	YML100W	TSL1
0.63	0.56	YBR059C	AKL1
0.63	0.59	YNL051W	COG5

0.63	0.43	YDR099W	BMH2
0.64	0.53	YNL106C	INP52
0.64	0.58	YMR219W	ESC1
0.64	0.53	YKL208W	CBT1
0.64	0.49	YPR054W	SMK1
0.64	0.56	YJL141C	YAK1
0.64	0.59	YJL157C	FAR1
0.64	0.42	YIL040W	APQ12
0.64	0.60	YIL107C	PFK26
0.64	0.63	YKL101W	HSL1
0.64	0.59	YDR475C	JIP4
0.64	0.54	YER151C	UBP3
0.65	0.57	YGR194C	XKS1
0.65	0.53	YML041C	VPS71
0.65	0.53	YKR031C	SPO14
0.65	0.61	YMR311C	GLC8
0.65	0.49	YCR065W	HCM1
0.65	0.48	YOL136C	PFK27
0.65	0.55	YKL126W	YPK1
0.65	0.57	YFR040W	SAP155
0.65	0.62	YPL042C	SSN3
0.65	0.61	YBR274W	CHK1
0.66	0.59	YPL236C	
0.66	0.59	YGL179C	TOS3
0.66	0.47	YOL012C	HTZ1
0.66	0.51	YOR349W	CIN1
0.66	0.59	YIL042C	PKP1
0.66	0.42	YLR423C	ATG17
0.66	0.60	YOR351C	MEK1
0.66	0.57	YKR028W	SAP190
0.66	0.40	YKL212W	SAC1
0.67	0.65	YAR003W	SWD1
0.67	0.58	YGL020C	GET1
0.67	0.52	YFL053W	DAK2
0.67	0.53	YPR106W	ISR1
0.67	0.63	YGR108W	CLB1
0.67	0.56	YCR008W	SAT4
0.67	0.50	YLR079W	SIC1
0.67	0.69	YML059C	NTE1
0.67	0.59	YNL053W	MSG5
0.68	0.50	YPL179W	PPQ1
0.68	0.64	YBL009W	
0.68	0.60	YGR161C	RTS3
0.68	0.62	YOL006C	TOP1
0.68	0.56	YPL141C	
0.68	0.55	YOR109W	INP53
0.68	0.48	YEL003W	GIM4
0.68	0.60	YNL129W	NRK1
0.68	0.55	YCR091W	KIN82
0.68	0.55	YGL229C	SAP4
0.68	0.67	YIL131C	FKH1
0.68	0.64	YLR019W	PSR2
0.69	0.64	YLL019C	KNS1

0.69	0.57	YFL010C	WWM1
0.69	0.62	YMR036C	MIH1
0.69	0.56	YBR028C	
0.69	0.64	YPL026C	SKS1
0.69	0.55	YBR125C	PTC4
0.69	0.51	YGL213C	SKI8
0.69	0.61	YMR008C	PLB1
0.70	0.52	YOR101W	RAS1
0.70	0.49	YIR026C	YVH1
0.70	0.59	YOR076C	SKI7
0.70	0.56	YCL016C	DCC1
0.70	0.60	YGR040W	KSS1
0.70	0.70	YML016C	PPZ1
0.70	0.54	YDR028C	REG1
0.70	0.66	YKL113C	RAD27
0.70	0.51	YPR189W	SKI3
0.71	0.62	YPR046W	MCM16
0.71	0.68	YML032C	RAD52
0.71	0.63	YLL010C	PSR1
0.72	0.55	YOR171C	LCB4
0.72	0.58	YJR059W	PTK2
0.72	0.67	YOR014W	RTS1
0.72	0.55	YBR200W	BEM1
0.72	0.66	YDL188C	PPH22
0.72	0.75	YCL040W	GLK1
0.72	0.50	YHR081W	LRP1
0.72	0.75	YHR200W	RPN10
0.73	0.60	YNR032W	PPG1
0.73	0.72	YHR044C	DOG1
0.73	0.67	YFR014C	CMK1
0.74	0.70	YGL158W	RCK1
0.74	0.73	YER177W	BMH1
0.75	0.60	YLR238W	FAR10
0.75	0.65	YDR477W	SNF1
0.76	0.68	YMR199W	CLN1
0.76	0.70	YHR046C	INM1
0.77	0.59	YIL035C	CKA1
0.77	0.62	YMR120C	ADE17
0.77	0.71	YNL032W	SIW14
0.77	0.67	YPR023C	EAF3
0.78	0.67	YCR095C	OCA4
0.79	0.60	YLR268W	SEC22
0.79	0.56	YGR092W	DBF2
0.79	0.70	YBR030W	
0.80	0.73	YLR133W	CKI1
0.80	0.60	YMR205C	PFK2
0.81	0.68	YMR104C	YPK2
0.81	0.61	YHL020C	OPI1
0.82	0.76	YPL031C	PHO85
0.83	0.72	YJL164C	TPK1
0.83	0.65	YGR200C	ELP2
0.84	0.53	YAL016W	TPD3
0.84	0.81	YOL065C	INP54

0.84	0.65	YML112W	CTK3
0.84	0.84	YDR162C	NBP2
0.84	0.63	YNL217W	
0.86	0.75	YNL099C	OCA1
0.86	0.77	YMR180C	CTL1
0.87	0.60	YDR067C	OCA6
0.87	0.71	YHL029C	OCA5
0.88	0.73	YNL056W	OCA2
0.88	0.66	YGR240C	PFK1
0.89	0.72	YJL006C	CTK2
0.89	0.66	YLR410W	VIP1
0.89	0.64	YLR262C	YPT6
0.92	0.70	YLR052W	IES3
0.93	0.69	YCL032W	STE50
0.94	0.56	YHL007C	STE20
0.96	0.75	YDR017C	KCS1
0.96	0.74	YOL061W	PRS5
0.98	0.65	YER092W	IES5
1.00	0.89	YKL213C	DOA1
1.04	0.73	YDL047W	SIT4
1.05	0.78	YLR039C	RIC1
1.05	0.71	YER083C	GET2
1.09	0.64	YLR240W	VPS34
1.13	0.78	YDR293C	SSD1
1.13	0.87	YPL268W	PLC1
1.16	0.91	YMR207C	HFA1
1.30	1.05	YPL086C	ELP3
1.42	1.34	YKL139W	CTK1
1.54	0.95	YMR216C	SKY1
1.58	1.33	YHR025W	THR1

Table 4. Growth of RNA processing e-map double mutant strains on 3-AT. Single mutant strains from the RNA processing e-map were crossed to the eIF2α S51A phosphorylation site mutant and the double mutant strains were pinned onto media containing either 0mM, 2 mM, or 8 mM 3-AT. The ratio of the colony size on 2mM or 8mM 3-AT to the colony size on 0 mM 3-AT was calculated for each RNA processing mutation in this assay. Colony sizes were the averages of three replicates. The list is ordered by the ratio of colony size on 2 mM 3-AT to the colony size on 0 mM 3-AT, as a measure of sensitivity to 3-AT.

ratio 2mM	ratio 8mM	ORF	gene name	mutation
0.31	0.23	YGR003W	CUL3	DELETION
0.32	0.26	YGL127C	SOH1	DELETION
0.33	0.20	YMR287C	MSU1	DELETION
0.35	0.32	YBR175W	SWD3	DELETION
0.36	0.31	YKL149C	DBR1	DELETION
0.37	0.23	YJR082C	EAF6	DELETION
0.38	0.25	YML041C	VPS71	DELETION
0.39	0.29	YLR139C	SLS1	DELETION
0.39	0.26	YCR073W-A	SOL2	DELETION
0.40	0.32	YNL286W	CUS2	DELETION
0.40	0.32	YDL175C	AIR2	DELETION
0.40	0.31	YER127W	LCP5	DAMP
0.41	0.45	YJR074W	MOG1	DELETION
0.42	0.40	YLR069C	MEF1	DELETION
0.42	0.52	YPR057W	BRR1	DELETION
0.43	0.36	YDL224C	WHI4	DELETION
0.44	0.26	YGR126W	YGR126W	DELETION
0.44	0.24	YMR312W	ELP6	DELETION
0.44	0.39	YGR072W	UPF3	DELETION
0.44	0.31	YDL219W	DTD1	DELETION
0.45	0.30	YER095W	RAD51	DELETION
0.45	0.36	YGR129W	SYF2	DELETION
0.46	0.34	YHR121W	LSM12	DELETION
0.46	0.36	YDR458C	YDR458C	DELETION
0.46	0.35	YPL213W	LEA1	DELETION
0.46	0.40	YPL090C	RPS6A	DELETION
0.46	0.31	YHR216W	IMD2	DELETION
0.46	0.38	YNL189W	SRP1	DAMP
0.47	0.40	YGL232W	TAN1	DELETION
0.48	0.41	YGR081C	SLX9	DELETION
0.48	0.34	YDL040C	NAT1	DELETION
0.48	0.35	YHR034C	PIH1	DELETION
0.48	0.29	YHR015W	MIP6	DELETION
0.48	0.43	YDR139C	RUB1	DELETION
0.48	0.43	YBR141C	YBR141C	DELETION
0.50	0.45	YOR243C	PUS7	DELETION
0.50	0.44	YHR077C	NMD2	DELETION
0.50	0.44	YLL039C	UBI4	DELETION

0.50	0.41	YGL241W	KAP114	DELETION
0.50	0.38	YGL174W	BUD13	DELETION
0.50	0.39	YPL119C	DBP1	DELETION
0.50	0.46	YPR045C	MNI2	DELETION
0.50	0.39	YDR159W	SAC3	DELETION
0.50	0.37	YCL011C	GBP2	DELETION
0.51	0.35	YKR036C	CAF4	DELETION
0.51	0.37	YPL047W	SGF11	DELETION
0.51	0.44	YHR152W	SPO12	DELETION
0.51	0.44	YDR432W	NPL3_S411A	Mutation
0.52	0.38	YPL127C	HHO1	DELETION
0.52	0.39	YBL104C	YBL104C	DELETION
0.52	0.45	YDR334W	SWR1	DELETION
0.52	0.40	YLR039C	RIC1	DELETION
0.52	0.43	YJL124C	LSM1	DELETION
0.52	0.51	YER110C	KAP123	DELETION
0.53	0.34	YNL072W	RNH201	DELETION
0.53	0.43	YAR002W	NUP60	DELETION
0.53	0.35	YOL006C	TOP1	DELETION
0.53	0.51	YCR019W	MAK32	DELETION
0.53	0.42	YGL014W	PUF4	DELETION
0.53	0.49	YDL213C	NOP6	DELETION
0.53	0.47	YIL016W	SNL1	DELETION
0.54	0.49	YOR039W	CKB2	DELETION
0.54	0.42	YMR012W	CLU1	DELETION
0.54	0.41	YMR273C	ZDS1	DELETION
0.54	0.53	YMR255W	GFD1	DELETION
0.54	0.26	YAL003W	EFB1	DAMP
0.54	0.39	YGL019W	CKB1	DELETION
0.54	0.44	YLR192C	HCR1	DELETION
0.55	0.42	YOL125W	TRM13	DELETION
0.55	0.44	YBR212W	NGR1	DELETION
0.55	0.40	YPR042C	PUF2	DELETION
0.55	0.46	YOR076C	SKI7	DELETION
0.55	0.38	YMR087W	YMR087W	DELETION
0.55	0.47	YOR061W	CKA2	DELETION
0.56	0.44	YCR077C	PAT1	DELETION
0.56	0.43	YLR405W	DUS4	DELETION
0.56	0.44	YLR384C	IKI3	DELETION
0.56	0.38	YPL029W	SUV3	DELETION
0.56	0.44	YGL136C	MRM2	DELETION
0.56	0.33	YMR283C	RIT1	DELETION
0.57	0.44	YFL001W	DEG1	DELETION
0.57	0.46	YLR363C	NMD4	DELETION
0.57	0.51	YGR054W	YGR054W	DELETION
0.58	0.50	YDR457W	TOM1	DELETION
0.58	0.41	YGL063W	PUS2	DELETION
0.58	0.53	YDR429C	TIF35	DAMP
0.58	0.34	YBL079W	NUP170	DELETION
0.58	0.43	YDL167C	NRP1	DELETION
0.58	0.58	YLR200W	YKE2	DELETION
0.58	0.40	YPL009C	YPL009C	DELETION
0.58	0.40	YDR156W	RPA14	DELETION
0.59	0.45	YGL236C	MTO1	DELETION
0.59	0.48	YDR463W	STP1	DELETION
0.59	0.39	YGR173W	RBG2	DELETION

0.59	0.42	YJR132W	NMD5	DELETION
0.59	0.54	YER032W	FIR1	DELETION
0.59	0.46	YAL024C	LTE1	DELETION
0.59	0.47	YGR030C	POP6	DAMP
0.59	0.39	YKL057C	NUP120	DELETION
0.59	0.57	YML107C	PML39	DELETION
0.59	0.36	YKL074C	MUD2	DELETION
0.59	0.50	YOL023W	IFM1	DELETION
0.60	0.48	YPR163C	TIF3	DELETION
0.60	0.50	YML014W	TRM9	DELETION
0.60	0.51	YBR065C	ECM2	DELETION
0.60	0.54	YDR335W	MSN5	DELETION
0.60	0.38	YIL008W	URM1	DELETION
0.60	0.41	YFR004W	RPN11	DAMP
0.60	0.51	YEL037C	RAD23	DELETION
0.60	0.41	YOR123C	LEO1	DELETION
0.60	0.45	YBR048W	RPS11B	DELETION
0.60	0.43	YOR295W	UAF30	DELETION
0.60	0.53	YPL104W	MSD1	DELETION
0.60	0.38	YKR095W	MLP1	DELETION
0.60	0.46	YBL028C	YBL028C	DELETION
0.60	0.49	YKL025C	PAN3	DELETION
0.60	0.46	YLR087C	CSF1	DELETION
0.60	0.41	YBL018C	POP8	DAMP
0.61	0.52	YHR086W	NAM8	DELETION
0.61	0.50	YBR103W	SIF2	DELETION
0.61	0.43	YOL004W	SIN3	DELETION
0.61	0.38	YPR174C	YPR174C	DELETION
0.61	0.49	YDR235W	PRP42	DAMP
0.61	0.43	YGR283C	YGR283C	DELETION
0.61	0.40	YOL093W	TRM10	DELETION
0.61	0.44	YLR270W	DCS1	DELETION
0.61	0.52	YOR308C	SNU66	DELETION
0.61	0.44	YLR287C	YLR287C	DELETION
0.61	0.55	YAR003W	SWD1	DELETION
0.61	0.45	YDR025W	RPS11A	DELETION
0.61	0.56	YAR073W	IMD1	DELETION
0.62	0.43	YGL043W	DST1	DELETION
0.62	0.45	YER002W	NOP16	DELETION
0.62	0.52	YMR223W	UBP8	DELETION
0.62	0.48	YJR066W	TOR1	DELETION
0.62	0.42	YKL214C	YRA2	DELETION
0.62	0.59	YDR439W	LRS4	DELETION
0.62	0.42	YOR276W	CAF20	DELETION
0.62	0.50	YBL013W	FMT1	DELETION
0.62	0.48	YEL015W	EDC3	DELETION
0.62	0.46	YMR129W	POM152	DELETION
0.62	0.41	YMR080C	NAM7	DELETION
0.62	0.51	YIL071C	PCI8/CSN11	DELETION
0.62	0.41	YFR023W	PES4	DELETION
0.62	0.42	YGR271W	SLH1	DELETION
0.62	0.55	YGL029W	CGR1	DELETION
0.63	0.43	YMR285C	NGL2	DELETION
0.63	0.47	YDR289C	RTT103	DELETION
0.63	0.34	YDR496C	PUF6	DELETION
0.63	0.39	YDR138W	HPR1	DELETION

0.63	0.47	YNR024W	YNR024W	DELETION
0.63	0.54	YLR438C-A	LSM3	DAMP
0.63	0.54	YMR025W	CSI1	DELETION
0.63	0.38	YER068W	MOT2	DELETION
0.63	0.54	YHL034C	SBP1	DELETION
0.63	0.45	YIR001C	SGN1	DELETION
0.63	0.48	YGR276C	RNH70	DELETION
0.63	0.51	YOR133W	EFT1	DELETION
0.63	0.66	YML005W	TRM12	DELETION
0.63	0.46	YGL016W	KAP122	DELETION
0.63	0.59	YPR129W	SCD6	DELETION
0.63	0.46	YGR178C	PBP1	DELETION
0.63	0.45	YNL073W	MSK1	DELETION
0.63	0.44	YCR016W	YCR016W	DELETION
0.63	0.51	YHR156C	LIN1	DELETION
0.63	0.46	YKL130C	SHE2	DELETION
0.64	0.46	YBR181C	RPS6B	DELETION
0.64	0.46	YGR171C	MSM1	DELETION
0.64	0.51	YPL055C	LGE1	DELETION
0.64	0.55	YDR165W	TRM82	DELETION
0.64	0.46	YMR023C	MSS1	DELETION
0.64	0.51	YDR469W	SDC1	DELETION
0.64	0.52	YJL138C	TIF2	DELETION
0.64	0.52	YKR060W	UTP30	DELETION
0.64	0.51	YMR275C	BUL1	DELETION
0.64	0.41	YER105C	NUP157	DELETION
0.64	0.50	YPL157W	TGS1	DELETION
0.64	0.52	YDR101C	ARX1	DELETION
0.65	0.41	YHR200W	RPN10	DELETION
0.65	0.41	YER035W	EDC2	DELETION
0.65	0.45	YFR010W	UBP6	DELETION
0.65	0.55	YBR130C	SHE3	DELETION
0.65	0.60	YDL201W	TRM8	DELETION
0.65	0.65	YOR185C	GSP2	DELETION
0.65	0.59	YDR083W	RRP8	DELETION
0.65	0.45	YGR134W	CAF130	DELETION
0.65	0.67	YDR172W	SUP35	DAMP
0.65	0.56	YNL255C	GIS2	DELETION
0.65	0.58	YKL081W	TEF4	DELETION
0.65	0.48	YJL140W	RPB4	DELETION
0.66	0.46	YCR087C-A	YCR087C-A	DELETION
0.66	0.41	YLR221C	RSA3	DELETION
0.66	0.45	YMR302C	PRP12	DELETION
0.66	0.65	YBR095C	RXT2	DELETION
0.66	0.46	YLR128W	DCN1	DELETION
0.66	0.45	YOL124C	TRM11	DELETION
0.66	0.49	YIL038C	NOT3	DELETION
0.66	0.47	YKL213C	DOA1	DELETION
0.66	0.50	YKL208W	CBT1	DELETION
0.66	0.48	YIR005W	IST3	DELETION
0.66	0.55	YOL041C	NOP12	DELETION
0.67	0.65	YLR018C	POM34	DELETION
0.67	0.71	YNR010W	CSE2	DELETION
0.67	0.49	YOR274W	MOD5	DELETION
0.67	0.59	YKR056W	TRM2	DELETION
0.67	0.49	YPL123C	RNY1	DELETION

0.67	0.45	YBR165W	UBS1	DELETION
0.67	0.63	YMR269W	YMR269W	DELETION
0.67	0.49	YDR037W	KRS1	DAMP
0.67	0.52	YHR006W	STP2	DELETION
0.67	0.51	YPL048W	CAM1	DELETION
0.67	0.59	YDL043C	PRP11	DAMP
0.67	0.44	YDL014W	NOP1	DAMP
0.67	0.57	YDR432W	NPL3-longtine	oex mutation
0.67	0.52	YGR250C	YGR250C	DELETION
0.67	0.55	YNL136W	EAF7	DELETION
0.67	0.47	YDR026C	YDR026C	DELETION
0.68	0.58	YKL068W	NUP100	DELETION
0.68	0.56	YGL194C	HOS2	DELETION
0.68	0.62	YNR004W	YNR004W	DELETION
0.68	0.54	YNL147W	LSM7	DELETION
0.68	0.44	YHR163W	SOL3	DELETION
0.68	0.69	YHR087W	YHR087W	DELETION
0.68	0.50	YLR432W	IMD3	DELETION
0.68	0.54	YHR081W	LRP1	DELETION
0.68	0.63	YDL088C	ASM4	DELETION
0.68	0.53	YDL216C	RRI1	DELETION
0.68	0.63	YLR335W	NUP2	DELETION
0.68	0.51	YNR032C-A	HUB1	DELETION
0.68	0.58	YNL175C	NOP13	DELETION
0.69	0.51	YIL079C	AIR1	DELETION
0.69	0.59	YGR162W	TIF4631	DELETION
0.69	0.51	YDR192C	NUP42	DELETION
0.69	0.50	YJR091C	JSN1	DELETION
0.69	0.50	YKR029C	SET3	DELETION
0.69	0.48	YNL153C	GIM3	DELETION
0.69	0.48	YLR316C	TAD3	DAMP
0.69	0.47	YLR375W	STP3	DELETION
0.69	0.50	YGL064C	MRH4	DELETION
0.69	0.50	YDR005C	MAF1	DELETION
0.70	0.46	YDR120C	TRM1	DELETION
0.70	0.51	YNL278W	CAF120	DELETION
0.70	0.47	YDL051W	LHP1	DELETION
0.70	0.56	YDR381W	YRA1	DAMP
0.70	0.49	YIL030C	SSM4	DELETION
0.70	0.55	YKR026C	GCN3	DELETION
0.70	0.71	YOR046C	DBP5	DAMP
0.71	0.51	YLL013C	PUF3	DELETION
0.71	0.63	YLR067C	PET309	DELETION
0.71	0.45	YJR007W	SUI2	DAMP
0.71	0.70	YDL089W	YDL089W	DELETION
0.71	0.59	YML068W	ITT1	DELETION
0.72	0.50	YDL013W	HEX3	DELETION
0.72	0.55	YPR046W	MCM16	DELETION
0.72	0.52	YBR022W	POA1	DELETION
0.72	0.50	YGR169C	PUS6	DELETION
0.72	0.57	YML029W	USA1	DELETION
0.72	0.51	YDR363W-A	SEM1	DELETION
0.72	0.54	YPL125W	KAP120	DELETION
0.72	0.49	YPL212C	PUS1	DELETION
0.72	0.67	YER125W	RSP5	DAMP

0.72	0.58	YDR198C	YDR198C	DELETION
0.73	0.72	YPR152C	YPR152C	DELETION
0.73	0.48	YBR094w	YBR094W	DELETION
0.73	0.67	YJL125C	GCD14	DAMP
0.73	0.63	YER116C	SLX8	DELETION
0.73	0.57	YBL024W	NCL1	DELETION
0.73	0.48	YBR111W-A	SUS1	DELETION
0.73	0.51	YLR435W	TSR2	DELETION
0.73	0.51	YHR066W	SSF1	DELETION
0.74	0.58	YJR084W	CSN12	DELETION
0.74	0.49	YBR034C	HMT1	DELETION
0.74	0.57	YFL028C	CAF16	DELETION
0.74	0.52	YDR395W	SXM1	DELETION
0.75	0.59	YNL097C	PHO23	DELETION
0.75	0.57	YPL101W	ELP4	DELETION
0.75	0.53	YOR195W	SLK19	DELETION
0.75	0.71	YLR016C	PML1	DELETION
0.75	0.62	YPR047W	MSF1	DELETION
0.75	0.68	YML103C	NUP188	DELETION
0.75	0.64	YJL148W	RPA34	DELETION
0.75	0.75	YIL096C	YIL096C	DELETION
0.75	0.51	YOL117W	RRI2	DELETION
0.75	0.55	YKL143W	LTV1	DELETION
0.76	0.55	YKL139W	CTK1	DELETION
0.76	0.65	YDR432W	NPL3	DELETION
0.76	0.59	YLR298C	YHC1	DAMP
0.76	0.74	YMR153W	NUP53	DELETION
0.76	0.58	YDR312W	SSF2	DELETION
0.76	0.58	YPR134W	MSS18	DELETION
0.77	0.72	YPL086C	ELP3	DELETION
0.77	0.59	YLR136C	TIS11	DELETION
0.77	0.67	YLL002W	RTT109	DELETION
0.77	0.74	YAL029C	MYO4	DELETION
0.77	0.60	YNR015W	SMM1	DELETION
0.77	0.63	YPR178W	PRP4	DAMP
0.77	0.55	YOR006C	YOR006C	DELETION
0.78	0.69	YIL040W	APQ12	DELETION
0.78	0.47	YJL006C	CTK2	DELETION
0.78	0.48	YAR003W	SWD1	DELETION
0.78	0.63	YDL048C	STP4	DELETION
0.79	0.50	YOR001W	RRP6	DELETION
0.80	0.80	YDL020C	RPN4	DELETION
0.80	0.55	YBR167C	POP7	DAMP
0.80	0.71	YGL222C	EDC1	DELETION
0.80	0.61	YLR401C	DUS3	DELETION
0.80	0.62	YMR276W	DSK2	DELETION
0.81	0.53	YPR023C	EAF3	DELETION
0.81	0.69	YGR135W	PRE9	DELETION
0.81	0.64	YDL210W	UGA4	DELETION
0.81	0.54	YER143W	DDI1	DELETION
0.81	0.78	YHR167W	THP2	DELETION
0.82	0.57	YOR187W	TUF1	DELETION
0.82	0.75	YOR179C	SYC1	DELETION
0.82	0.92	YML080W	DUS1	DELETION
0.82	0.69	YMR180C	CTL1	DELETION
0.83	0.69	YLR285W	NNT1	DELETION

0.83	0.72	YNR034W	SOL1	DELETION
0.83	0.78	YLR059C	REX2	DELETION
0.83	0.70	YDR179C	CSN9	DELETION
0.83	0.49	YMR125W	STO1	DELETION
0.83	0.66	YPR101W	SNT309	DELETION
0.84	0.76	YML034W	SRC1	DELETION
0.84	0.71	YOL080C	REX4	DELETION
0.84	0.69	YJL122W	ALB1	DELETION
0.84	0.72	YOR078W	BUD21	DELETION
0.85	0.67	YGR200C	ELP2	DELETION
0.85	0.79	YOL012C	HTZ1	DELETION
0.85	0.57	YDR482C	CWC21	DELETION
0.85	0.56	YDR385W	EFT2	DELETION
0.85	0.77	YMR216C	SKY1	DELETION
0.86	0.54	YOR201C	MRM1	DELETION
0.86	0.67	YGL213C	SKI8	DELETION
0.86	0.90	YDR152W	GIR2	DELETION
0.86	0.62	YML094W	GIM5	DELETION
0.86	0.65	YPR070W	MED1	DELETION
0.87	0.55	YGR093W	YGR093W	DELETION
0.87	0.66	YKL204W	EAP1	DELETION
0.87	0.68	YBR061C	TRM7	DELETION
0.87	0.74	YDL112W	TRM3	DELETION
0.87	0.69	YKL205W	LOS1	DELETION
0.87	0.76	YPL064C	CWC27	DELETION
0.87	0.59	YLR107W	REX3	DELETION
0.88	0.82	YJR047C	ANB1	DELETION
0.88	0.71	YFR009W	GCN20	DELETION
0.89	0.65	YBL057C	PTH2	DELETION
0.90	0.65	YKR059W	TIF1	DELETION
0.90	0.62	YPL005W	AEP3	DELETION
0.91	0.66	YIL035C	CKA1	DELETION
0.91	0.74	YGL078C	DBP3	DELETION
0.91	0.64	YKR092C	SRP40	DELETION
0.91	0.64	YNL016W	PUB1	DELETION
0.92	0.84	YLR003C	YLR003C	DELETION
0.93	0.79	YCR060W	TAH1	DELETION
0.94	0.88	YML032C	RAD52	DELETION
0.95	0.78	YKR096W	YKR096W	DELETION
0.95	0.86	YGR119C	NUP57	DAMP
0.95	0.65	YKL183W	LOT5	DELETION
0.96	0.85	YDL074C	BRE1	DELETION
0.97	0.59	YGL173C	KEM1	DELETION
0.97	0.73	YBL072C	RPS8A	DELETION
0.98	0.62	YJR050W	ISY1	DELETION
0.99	0.96	YLR398C	SKI2	DELETION
0.99	0.77	YNL288W	CAF40	DELETION
0.99	1.02	YDR163W	CWC15	DELETION
0.99	1.24	YLR165C	PUS5	DELETION
1.02	1.07	YOL077C	BRX1	DAMP
1.03	0.69	YNL004W	HRB1	DELETION
1.04	0.71	YIL149C	MLP2	DELETION
1.04	1.19	YBR119W	MUD1	DELETION
1.05	0.72	YJL047C	RTT101	DELETION
1.05	0.87	YHR013C	ARD1	DELETION
1.09	1.03	YGL195W	GCN1	DELETION

1.09	0.71	YOR038C	HIR2	DELETION
1.10	0.94	YGL049C	TIF4632	DELETION
1.13	0.96	YDR240C	SNU56	DAMP
1.16	0.97	YOL072W	THP1	DELETION
1.17	0.78	YNL135C	FPR1	DELETION
1.21	1.17	YML056C	IMD4	DELETION
1.22	1.00	YOL115W	PAP2	DELETION
1.23	1.08	YMR116C	ASC1	DELETION
1.25	1.15	YBR188C	NTC20	DELETION
1.49	1.34	YKL009W	MRT4	DELETION
1.56	1.16	YLR262C	YPT6	DELETION

Appendix 2

Cover Art

I had the honor to be able to submit artwork for the covers of the journals in which Chapters 1 and 2 were published. Figure 1 appeared on the cover of the issue in which Chapter 1 appeared (Molecular Cell, September 21 2007), and Figure 2 appeared on the cover of the issue in which Chapter 2 appeared Molecular Cell, December 5 2008).

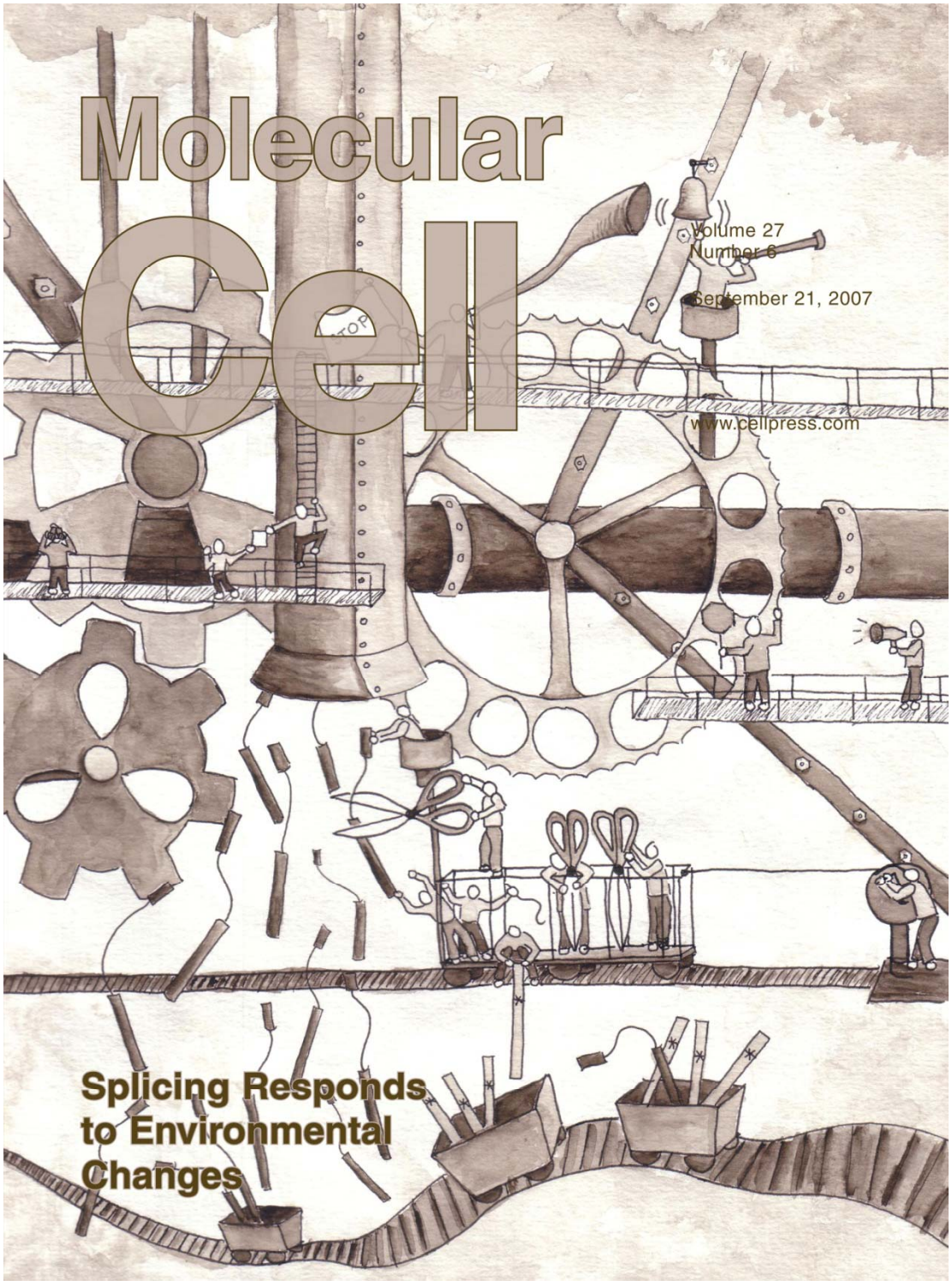
Molecular
Cell
Volume 27
Number 6
September 21, 2007
www.cellpress.com
Splicing Responds
to Environmental
Changes

Figure 1. Splicing responds to trouble on the horizon. The cover image depicts a whimsical interpretation of the gene expression machinery in *Saccharomyces cerevisiae*. An alarm is raised as a stress is detected. One part of the subsequent response is a change in splicing, represented by the platform of scissors-wielding workers, which is being reeled away from many of its intron-containing substrates. The result of this response to stress, as reported by Pleiss et al. in this issue, is a rapid accumulation of pre-mRNA for many intron-containing transcripts, detectable by intron-specific microarray probes. The response to a different stress affects a different subset of intron-containing transcripts, suggesting that splicing contributes in a complex way to the dynamic behavior of the gene expression machine.

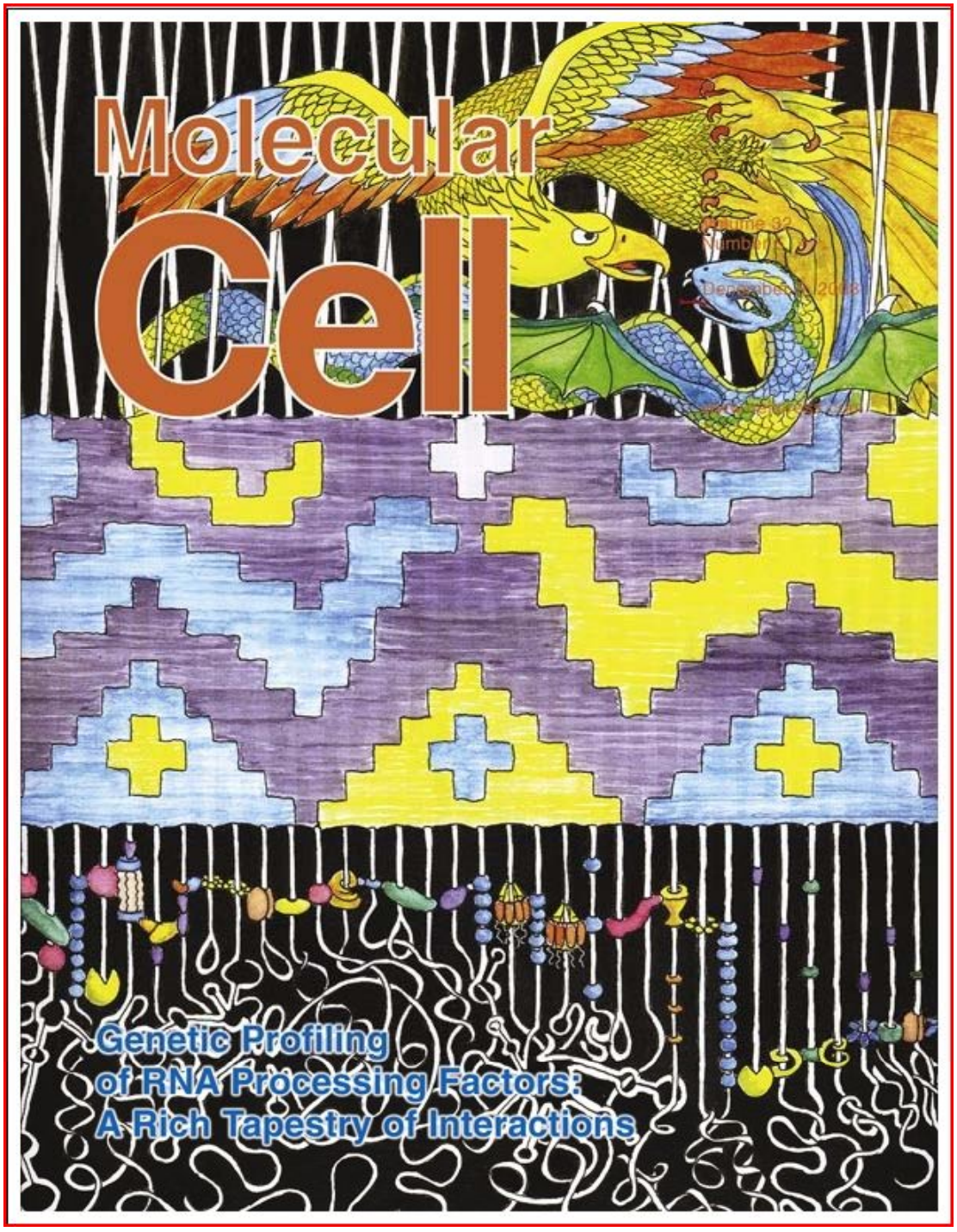
Molecular
Cell
Genetic Profiling
of RNA Processing Factors:
A Rich Tapestry of Interactions

Figure 2. Genetic profiling of RNA processing factors: a rich tapestry of interactions. The high-density genetic interaction map of factors involved in RNA processing described in this issue begins to untangle a complex network of functional relationships. As described by Wilmes et al. and also in the accompanying manuscript by Kress et al., this genetic interaction map aided in the elucidation of new functions for previously described factors and also suggests roles for previously uncharacterized factors. Furthermore, as represented by the bird and serpent emerging from the tapestry depicted in the cover image, systems level analysis of the dataset gives rise to some insight into the global interactions among complexes and pathways that contribute to the dynamic cycle of creation and destruction of RNA molecules within the cell.

Publishing Agreement

It is the policy of the University to encourage the distribution of all theses, dissertations, and manuscripts. Copies of all UCSF theses, dissertations, and manuscripts will be routed to the library via the Graduate Division. The library will make all theses, dissertations, and manuscripts accessible to the public and will preserve these to the best of their abilities, in perpetuity.

Please sign the following statement:

I hereby grant permission to the Graduate Division of the University of California, San Francisco to release copies of my thesis, dissertation, or manuscript to the Campus Library to provide access and preservation, in whole or in part, in perpetuity.

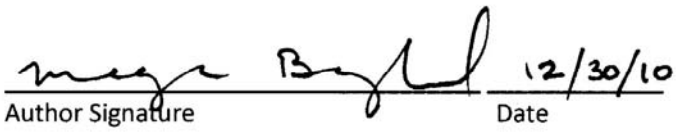

Author Signature Date